Volume 72A
Number 4
July–Aug. 1968

Physics and Chemistry

U.S. DEPARTMENT OF COMMERCE

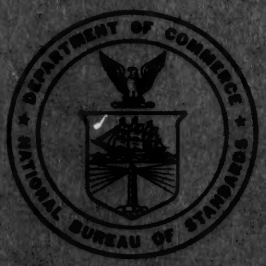

SECTION A

JOURNAL OF RESEARCH

NATIONAL BUREAU OF STANDARDS

Journal of Research

of the

National Bureau of Standards

A. Physics and Chemistry

July–Aug. • 1968

VOLUME • 72A

NUMBER • 4

Editor: C. W. Beckett

Associate Editors: D. D. Wagman

Publication dates:
Feb. 1, Apr. 1, June 1, Aug. 1, Oct. 1, Dec. 1, 1968

JOURNAL OF RESEARCH

The National Bureau of Standards Journal of Research reports research and development in the fields of activity shown at right. Also included from time to time are survey articles on topics closely related to the Bureau's scientific and technical program.

The Journal is published in three separate sections as follows:

A. Physics and Chemistry

Contains papers of interest primarily to scientists working in these fields. Issued six times a year. Annual subscription: domestic, $5.00; foreign, $6.00. Single copy, $1.00.

B. Mathematical Sciences

Presents studies and compilations designed mainly for the mathematician and the theoretical physicist. Issued quarterly. Annual subscription: domestic, $2.25; foreign, $2.75. Single copy, 75c.

C. Engineering and Instrumentation

Reports research and development results of interest chiefly to the engineer and the applied scientist. Issued quarterly. Annual subscription: domestic, $2.75; foreign, $3.50. Single copy, 75c.

The National Bureau of Standards[1] was established by an act of Congress March 3, 1901. Today, in addition to serving as the Nation's central measurement laboratory, the Bureau is a principal focal point in the Federal Government for assuring maximum application of the physical and engineering sciences to the advancement of technology in industry and commerce. To this end the Bureau conducts research and provides central national services in three broad program areas and provides central national services in a fourth. These are: (1) basic measurements and standards, (2) materials measurements and standards, (3) technological measurements and standards, and (4) transfer of technology.

The Bureau comprises the Institute for Basic Standards, the Institute for Materials Research, the Institute for Applied Technology, and the Center for Radiation Research.

THE INSTITUTE FOR BASIC STANDARDS provides the central basis within the United States of a complete and consistent system of physical measurement, coordinates that system with the measurement systems of other nations, and furnishes essential services leading to accurate and uniform physical measurements throughout the Nation's scientific community, industry, and commerce. The Institute consists of an Office of Standard Reference Data and a group of divisions organized by the following areas of science and engineering:

Applied Mathematics—Electricity—Metrology—Mechanics—Heat—Atomic Physics—Cryogenics[2]—Radio Physics[2]—Radio Engineering[2]—Astrophysics[2]—Time and Frequency.[3]

THE INSTITUTE FOR MATERIALS RESEARCH conducts materials research leading to methods, standards of measurement, and data needed by industry, commerce, educational institutions, and government. The Institute also provides advisory and research services to other government agencies. The institute consists of an Office of Standard Reference Materials and a group of divisions organized by the following areas of materials research:

Analytical Chemistry—Polymers—Metallurgy—Inorganic Materials—Physical Chemistry.

THE INSTITUTE FOR APPLIED TECHNOLOGY provides for the creation of appropriate opportunities for the use and application of technology within the Federal Government and within the civilian sector of American industry. The primary functions of the Institute may be broadly classified as programs relating to technological measurements and standards and techniques for the transfer of technology. The Institute consists of a Clearinghouse for Scientific and Technical Information,[3] a Center for Computer Sciences and Technology, and a group of technical divisions and offices organized by the following fields of technology:

Building Research—Electronic Instrumentation—Technical Analysis—Product Evaluation—Invention and Innovation—Weights and Measures—Engineering Standards—Vehicle Systems Research.

THE CENTER FOR RADIATION RESEARCH engages in research, measurement, and application of radiation to the solution of Bureau mission problems and the problems of other agencies and institutions. The Center for Radiation Research consists of the following divisions:

Reactor Radiation—Linac Radiation—Applied Radiation—Nuclear Radiation.

[1] Headquarters and Laboratories at Gaithersburg, Maryland, unless otherwise noted; mailing address Washington, D.C. 20234.
[2] Located at Boulder, Colorado 80302.
[3] Located at 5285 Port Royal Road, Springfield, Virginia 22151.

U.S. DEPARTMENT OF COMMERCE
C. R. Smith, Secretary

NATIONAL BUREAU OF STANDARDS
A. V. Astin, Director

Order all publications from the Superintendent of Documents
U.S. Government Printing Office, Washington, D.C. 20402

Use of funds for printing this publication approved by the Director of the Bureau of the Budget (June 22, 1966).

JOURNAL OF RESEARCH of the National Bureau of Standards—A. Physics and Chemistry
Vol. 72A, No. 4, July–August 1968

Mass Spectrometric Study of Photoionization. X. Hydrogen Chloride and Methyl Halides

Morris Krauss, James A. Walker, and Vernon H. Dibeler

Institute for Basic Standards, National Bureau of Standards, Washington, D.C. 20234

(March 12, 1968)

Photoionization efficiency curves are obtained for hydrogen chloride and several methyl halides, both ordinary and deuterated, from ionization threshold to 600 Å. Discussion is given on electronic structure of ions, autoionizing Rydberg states, and line-shape behavior. Ionization energies, heats of formation of ions, and bond dissociation energies are tabulated without regard to distribution of energy in internal modes, in relative kinetic energy, or other possible modes.

Key Words: Dissociation energies; HCl; ionization; mass spectrometry; methyl halides; vacuum ultraviolet spectroscopy.

1. Introduction

The purpose of this paper is to analyze the photoionization efficiency (PE) curves of HCl, CH_3F, CD_3Cl, CH_3Cl, CH_2DCl, CHD_2Cl, and CH_3Br measured from their thresholds to 600 Å. Analysis of such a series is usually undertaken in the expectation of the similarities that are revealed. Such a motive is clearly revealed in early studies of the Rydberg series in the hydrogen [1] [1] and methyl [2] halides. Understanding of the electronic structure of these molecules is clearly aided by studying trends in the series. Up to a point the same philosophy will hold for photoionization studies.

However, the ion production channels are not always dominant and the regularities in electronic behavior are not always mirrored in the PE curves. In particular, the ion-pair production yields very unusual qualitative behavior. The structure of the ion-pair PE curve [3] for CH_3Cl is so rich that further investigation into this process was instituted by examining the deuterated methyl chloride molecules and by searching for ion-pair processes in the fluoride and bromide. Methyl iodide has previously been studied [4]. In order to complete the investigation, all ions from the methyl halides were studied and HCl was also examined to assist the interpretation of the CH_3Cl spectra. The HCl PE curves were found to possess a rich autoionization structure interesting in itself.

At present, experimental resolution is insufficient to warrant quantitative spectroscopic analysis. However, sufficient results are available to warrant a comprehensive qualitative analysis of hydrogen chloride and the methyl halides. The analysis will report and speculate on the following:

1. Electronic structure of the ions and autoionizing states.
2. Bond energies and ionization thresholds.
3. Line-shape behavior especially in neighborhood of the $^2\Sigma^+$ HCl threshold.

2. Experimental Procedure

Photoionization efficiency curves were obtained by means of the combined vacuum ultraviolet monochromator and mass spectrometer described in detail in the first paper of this series [5], but including minor modifications reported in more recent studies [6]. Data were obtained with an optical resolution of about 1 Å, with an uncertainty in the absolute wavelength of 1 Å, or less over all wavelengths. In the absence of systematic error, the uncertainty in the reported relative ionization efficiency (ions per photon transmitted through the ion source) is of the order of 3 percent. It is ascribed principally to the uncertainty in measuring the numbers of electrons photoejected from a tungsten photon detector.

The hydrogen chloride and the ordinary methyl halides were reagent gases [2] obtained from the Matheson Company. The minimum purity as stated by the supplier was generally better than 99 percent. Mass

[1] Figures in brackets indicate the literature references at the end of this paper.

[2] Certain commercial materials are identified in this paper in order to adequately specify the experimental procedure. In no case does such identification imply recommendation or endorsement by the National Bureau of Standards, nor does it imply that the material identified is necessarily the best available for the purpose.

spectrometric analysis showed no significant amounts of interfering impurities. The deuteromethyl halides were obtained from Merck, Sharp, and Dohme, Ltd. Isotopic purities were stated to be better than 98 atom percent D, and these were confirmed by mass spectra. Chemical purities were apparently comparable.

The following conversion factors are used in this report:

$$1 \text{ eV molecule}^{-1} = 96.4870 \text{ kJmol}^{-1}, 1 \text{ kcal mol}^{-1} = 4.1840 \text{ kJmol}^{-1}.$$

3. HCl

Electronic Structure and PE Curves. Mulliken [7] first described the electronic structure of HCl in terms of molecular orbitals (MO). He noted that one-electron ionization would yield two ion states that are in the energy range of the present investigation. The electronic structure is given as

KL	$4\sigma^2$	$5\sigma^2$	π^4
	30.39	16.26	12.70

where the ionization energies in eV (theoretical estimate for 4σ [8]) are given below the orbital symbol. Transitions between the $^2\Sigma^+$ and $^2\Pi$ levels of the ion states were analyzed by Norling [9] and the asymptotic behavior and spectroscopic constants given [10]. The inner ionization energy was thus determined quite accurately relative to the ion ground-state energy and the doublet splitting, $^2\Pi_{3/2} - {}^2\Pi_{1/2}$, was also determined.

Although a Rydberg series has not been analyzed for HCl, Price [1] deduced a value of 12.84 eV for the ionization onset. Electron impact values have been somewhat lower. Morrison [11] determined values of 12.53 ± 0.09 eV and 12.78 ± 0.03 eV using the linear extrapolation and critical slope methods, respectively; whereas Fox [12] reports 12.56 ± 0.1 eV. Considerable curvature in the threshold ionization curve was attributed by Fox to the doublet electronic structure. He then estimated the doublet splitting to be 0.3 eV which is much larger than the value of 0.08 eV determined spectroscopically. There is also disagreement between the spectroscopic and electron impact values for the energy of the first excited state of HCl^+. Fox and Morrison find indications of a second ionization limit 1.5 eV above threshold and Norling reports a value of 3.56 eV for the interval. These discrepancies are reminiscent of similar problems that have been traced to autoionization contributions and this is apparently the case here. As we shall see below, autoionization is the dominant feature of the photoionization efficiency curve below 20 eV.

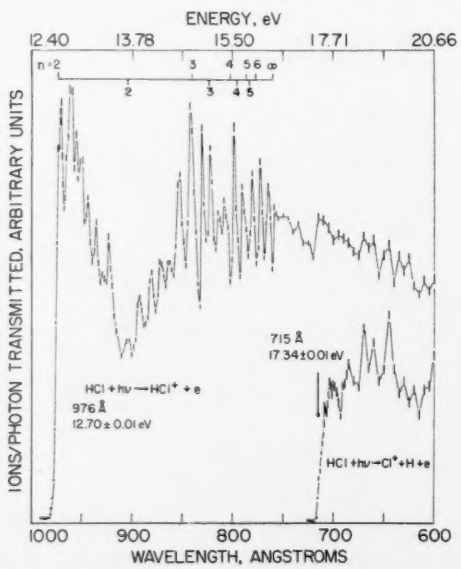

FIGURE 1. *Photoionization yield curves for the* HCl^+ *and* Cl^+ *ions of hydrogen chloride.*

As rotational transitions are not resolved and vibrational bands are probably superimposed, the assignment of transitions is, at best, speculative. Intensities are not a sure guide to selecting a given vibrational band accompanying Rydberg excitation. However, we can use the known ionization energy for the $^2\Sigma^+$ state to estimate quantum defects and Rydberg energies. Selected wavelengths of the peak maxima are given in table 1. As can be seen in figure 1, several series of peaks seem to be connected and are probably vibrational progressions accompanying either one Rydberg transition or several closely spaced ones. We particularly have in mind the progressions beginning at 971 Å, the one at 904 Å, and finally the one at 854 Å. Assuming that the peaks at 904 and 971 represent the 0–0 vibrational bands to electronic states to two separate Rydberg series, we can use the known ionization energy to fit quantum defects. A list of the estimated energies of the other members in

TABLE 1A. *Selected wavelengths of peak maxima in HCl* [a]

Peak wavelength (Å)	Peak separation (eV)	Effective quantum number	Peak wavelength (Å)	Peak separation (eV)	Effective quantum number
971.5	0.12	~1.9	904	0.17	~2.3
962	.08		893	.17	
956	.04		882	.15	
952.5	.10		872	.15	
945	.13		863	.15	
936	.05		854	.21	~2.8
932	.10		842	.19	
925			831	.15	
			823		

[a] Peak wavelengths are estimated from figure 1 for apparent vibrational series originating at 971.5, 904, and 854 Å. The effective quantum number at the origin is estimated from the known $^2\Sigma^+$ ionization potential.

TABLE 1B. *Estimate of higher Rydberg levels in HCl* [a]

971 Å Series n^*	Rydberg wavelength (Å)	904 Å Series n^*	Rydberg wavelength (Å)
1.94	971	2.28	904
2.94	841	3.28	824
3.94	803	4.28	796
4.94	787	5.28	783

[a] Estimate of band origins for two Rydberg series with constant quantum defects of 0.06 and 0.72 respectively.

table 1B shows how difficult it is to separate and to assign states in the 815 Å region and beyond. Primarily, the difficulty is due to the large number of vibrational states that are excited.

Franck-Condon factors have been reported [13] for the transitions to the $^2\Sigma^+$ ion and we will assume that the Rydberg behavior is similar. The $^2\Sigma^+\omega_e$ is about 1605 cm^{-1} with a fairly large $\omega_e x_e$ of 40 cm^{-1}. The levels beginning at 904 Å are spaced at about 0.15 eV and those beginning at 854 Å average a little larger, closer to 0.20 eV. There seems little doubt that these two states are Rydbergs with the $^2\Sigma^+$ ion as the limit. The 904 Å progression may be the basis of the second break in the electron-impact ionization efficiency curve found by Fox and by Morrison.

Speculative assignments can be made now by considering Rydberg orbitals in the field of the $^2\Sigma^+$ core and the molecular states that correlate with appropriate asymptotic atom states. In the molecular orbital scheme the $^2\Sigma^+$ ion state arises from a single-electron ionization from the bonding 5σ orbital. This state correlates asymptotically with the $H^+ + Cl(^2P)$ atoms rather than the $H(^2S) + Cl^+(^3P)$ as does the $^2\Pi$ ion ground state. Superficially one would expect that the $^2\Sigma^+$ Rydberg states would correlate with the atomic hydrogen Rydberg states and ground state atomic chlorine. The noncrossing rule technically forbids this but near the molecular equilibrium position a catalog of possible molecular states can be made from the attachment of atom-like Rydberg orbitals with considerable hydrogen character that correlate to the asymptotic hydrogen Rydbergs. Since the ground state electronic distribution is well represented by the ionic formula H^+Cl^-, excitation of hydrogenic Rydbergs results in large transition moments of the charge transfer type.

The 971 Å system is found to have an effective quantum number less than 2. Autoionization between the $^2\Pi_{1/2}$ and $^2\Pi_{3/2}$ doublet analogous to that in the rare gas atom is probably not observed because of the disparity that will be shown in the magnitude of the cross sections to the direct $^2\Pi$ and $^2\Sigma^+$ ionization continua. Curvature found by Fox is probably unrelated to the doublet splitting. It is due more likely to the autoionization peaks at threshold. Using peak maxima positions as the band origins, the energy separations in the 971 Å system are not found to fit any regular pattern. Peaks are evidently not resolved and may be due to more than one electronic state. The $np\sigma^*$-series first member would locate at this energy for a primarily $n=2$ hydrogen Rydberg. The MO designation is KL $4\sigma^2 5\sigma\pi^4 6\sigma$ and overall symmetry is $^1\Sigma^+$.

Table 2 shows the correlation rules and energies of the lowest asymptotic atom states. The ion-pair state yields a $^1\Sigma^+$ state but this correlates ultimately with the $V^1\Sigma^+$ state some 5 eV lower in energy. This V state is the first Rydberg state (which will probably not fit the series well) for a series KL $4\sigma^2\ 5\sigma^2\ 2\pi^3\ n\pi$. It has been connected to the $4\sigma^2\ 5\sigma\ 2\pi^4\ 6\sigma$ state [14] but we prefer to assign this MO configuration to the Rydberg observed at 971 Å. Note that there will be considerable configuration mixing at equilibrium

TABLE 2. *Correlation of asymptotic atom states for HCl* [a]

Atom states [b]		Molecular correlation	Energy (eV)
Cl, $^2P^o$	H, ^2S		
H, ^2S	Cl, $^2P^o$	Σ^+, Π	0
	$4s(^3P)^2P$	Σ^-, Π	9.20
$H^+ + Cl^-$		Σ^+	9.98
$n=2$ ^2S			10.20
$n=2$ $^2P^o$		$\Sigma^+(2), \Sigma^-, \Pi(2), \Delta$	
	$4s(^1D)^2D$	Σ^+, Π, Δ	10.43
	$4p(^3P)^2D^o$	Σ^-, Π, Δ	10.49
	$4p(^3P)^2S^o$	Σ^-	10.57
	$4p(^3P)^2P^o$		10.59
	$4p(^1D)^2P^o$		11.69
	$4p(^1D)^2F^o$	$\Sigma^+, \Pi, \Delta, \Phi$	11.79
	$5p(^3P)^2D^o$		11.83
. . . . .	. . . . .	. . . . .	. . . . .
	$4d(^3P)^3F$	$\Sigma^-, \Pi, \Delta, \Phi$	12.00
. . . . .	. . . . .	. . . . .	. . . . .
$n=3$ ^2S			
$n=3$ $^2P^o$			12.09
$n=3$ ^2D			

[a] Asymptotic excited atom states are combined with either ground state hydrogen or chlorine atoms except for the $H^+ + Cl^-$ ion-pair state. The excited orbital is noted and the parent ion state is given in parentheses. Relative energies are given for the lowest multiplet level. Note that the dissociation energy of HCl is $D_0(HCl) = 4.33$ eV.

[b] Correlation states are not repeated for similar pairs of atom states. A number of levels are deleted as the density of levels increases but the positions of the Cl $4d$ and $H(n=3)$ states are given.

positions as well as at large internuclear separations. If there is considerable ionic character to this state the dissociation energy would exceed that of the $^2\Sigma^+$ ion and the vibrational spacing would also be smaller than that of the ion. The lower (infinity of) $^1\Sigma^+$ Rydberg states go asymptotically to the chlorine and hydrogen Rydberg asymptotic states producing complicated interactions at large R distances. However, the $(5\sigma\ 6\sigma)_s$ configuration should dominate in the neighborhood of the first ionization threshold. Note that a direct calculation [14] of the oscillator strength yields about 1.5 for this transition and 0.005 for the $2\pi \rightarrow 6\sigma$ transition explaining the relative insignificance of the direct $^2\Pi$ ionization and the $\Pi_{3/2}-\Pi_{1/2}$ autoionization.

Comparison of the effective quantum number in table 1A with those for the Rydberg states of H_2 are quite suggestive. Effective quantum numbers for the $np\sigma^*$ series in H_2 are 1.79, 2.80, . . . and the values 2.08, 3.08, 4.08, . . . fit the $np\pi^*$ series. Evidently the 971 and 854 Å progressions arise from the same Rydberg series but either the $2p\sigma$ ($v=0$) bands must be below the ionization limit or the $v=0$ band is obscured for the $3p\sigma$ progression in order that the quantum defect decrease as a function of increasing n. The structure of HCl Rydbergs does not seem to differ from that of H_2. Two series, $np\sigma$ and $np\pi$, are suggested with the very approximate band origins given in table 1B.

The asymptotic dissociation fragments for these Rydbergs cannot easily be inferred. If the progression for the $2p\pi$ state really begins at 904 Å, then the dissociation energy into $H(n=2)$ is only 0.9 eV which is inconsistent with the observed vibrational spacing. Fortunately, the asymptotic behavior of the electronic energy curve is of little importance in this experiment as long as the bands cannot be resolved.

The vibrational progression at 854 Å can be associated with a quantum-number three state which would primarily consist of $3p$ hydrogenic orbitals. If the peaks at 854, 842, 831, and 823 Å are attributed to vibra-

tional bands of one electronic state then the vibrational spacings of about 0.21, 0.19, and 0.15 eV are quite consistent with vibrational spacing for the $^2\Sigma^+$ ion. However, the density of resonance states is high in this region and assignments are difficult to make. The 854 Å series apparently belongs to the same series as the one at threshold and the two smaller peaks just below 800 Å could fit the series with the first member at 904 Å. Speculation on the remainder of the peaks before the $^2\Sigma^+$ threshold would be fruitless except to note that if only hydrogen Rydbergs play an important role then there would only be the two dominant HCl ($^2\Sigma^+$) Rydberg series. It is possible that Rydbergs which lead to a bound ion state or states which go asymptotically to the Cl^+ $3p^4$ ^1D state may be present with small probability but sufficient to disturb the regularity of the vibrational progressions.

The poorly resolved peaks that begin at about 714 Å are found in both the parent ion and the Cl^+ PE curves. The resonance states contribute to both channels and all the open channels appear to have resonances at the same energy. The resonance states are probably Rydberg states leading to bound-ion states that correlate with both the $Cl^+(3s^23p^4$ ^1D and $^1S)$ atoms. Predissociation into the ion state may be enhanced by the $^2\Sigma^-$ state that arises from ground state $Cl^+(^3P)$.

The last feature of interest is the *lack of structure* just beyond the second ionization threshold. At least at this level of optical resolution there is a sudden break in the PE curve as the autoionizing peaks have apparently reached their limit. This is unusual since the Franck-Condon factors would lead one to expect structure beyond the ionization limit. Speculation on this feature is deferred to the section on autoionization.

4. Line-Shape Behavior

The theory of the configuration interaction of a single resonance with many continua has been given by Fano [15]. The basic result is that configuration interaction of a single discrete state with two or more continua is shown to be equivalent to interaction of a single discrete level with one continuum. This continuum is a linear combination of uncoupled standing-wave continua weighted by the discrete state-continuum interaction. If coupling is considered, the results are somewhat more complicated but have been considered by Fano and Prats [16] and Mies [17]. The only parameter that will concern us here is q. This is defined as

$$q = \frac{(\Phi|z|\Psi_0)}{\pi\Sigma_j(\phi|H|\Psi_{jE})\,(\Psi_{jE}|z|\Psi_0)} \qquad (1)$$

If we ignore the principal-part integral in (1) then the numerator is just the transition probability to the unperturbed embedded bound-Rydberg electronic state. To a good approximation this integral is the product of an electronic integral and a vibrational overlap integral.

As we can see from figure 1, the autoionization is most apparent as absorption-like peaks. This is associated with a large q. Calculation indicates that the electronic transition probability to the $^2\Sigma^+$ Rydbergs is large and the Franck-Condon calculations suggest that at least five vibrational resonance states should contribute. The denominator is more complicated but it is likely that the integral $(\Psi_{\pi E}|z|\Psi_0)$ is small as the transition integral of the first Rydberg to this state has been found to be small in a virtual Hartree-Fock calculation [14]. At an energy lower than the $^2\Sigma^+$ threshold we have only one ionization continuum although there are predissociation and fluorescence channels that contribute to the width.

When the $^2\Sigma^+$ channel is open, there are effectively two terms in the denominator of (1). The direct transition integral to the $^2\Sigma^+$ continuum is probably large but because the coupling is due to Born-Oppenheimer breakdown, is offset to some extent by reduction in coupling to the continua from the resonance state, a high vibrational state of a $^2\Sigma^+$ Rydberg. Nonetheless, we can speculate that the q in a vibrational progression changes quite drastically on passing through the $^2\Sigma^+$ threshold since the denominator suddenly increases while the numerator is effectively unchanged. A small q is associated with structure that does not give the appearance of absorption peaks. In fact for an extremely small q the structure in the neighborhood of the resonance appears as a "window" in the absorption. This region of the spectrum should be reexamined with higher resolution to determine whether this speculation has some basis or the qualitative change in the PE curve is due either to experimental line width resolution problems or to an incorrect value for the $^2\Sigma^+$ threshold.

5. Methyl Halides

Electronic Structure and PE Curves. The molecular orbital (MO) structure of the lowest energy orbitals in the halides was represented by Mulliken [7] as follows:

$$(CHe)^4(CXa)^2(Xe)^4$$

The CH*e* MO is very similar to the bonding CH orbital in CH_4 and will have an ionization threshold slightly less than that for CH_4; i.e., < 12.7 eV. The *Xe* orbital is considered essentially the *np* atomic orbital of the halogen atom. The ionization threshold of the C*Xa* MO is not so easily estimated. It is the bonding C*X* orbitals and the ionization threshold should be higher than the mean of the dominant valence orbitals that make up the MO.

Mulliken noted that in the case of the fluoride the CH*e* orbital has the lowest ionization energy; whereas, for the bromide it is the *Xe* orbital. Although he indicated that the chloride most likely behaves like the bromide and iodide, it was noted that this case is more ambiguous. Price [2a] analyzed the Rydberg states of CH_3Cl and concluded that it was the *Xe* electron that was ionized. He also determined the doublet splitting in the degenerate ^2E ion to be 800 cm^{-1}.

The only mass-analyzed photoionization work on the methyl halides is a study of CH_3I which exhibited autoionization peaks which could be correlated with the spectroscopically observed Rydbergs converging to the $^2E_{1/2}$ ion limit. A preliminary communication on the ion-pair process in CH_3Cl [3] showed that configuration interaction was important in this process. Comparison of the CH_3Cl mass-analyzed ionization threshold also agreed with previous photoionization data and was somewhat lower than electron impact results.

Inspection of the parent-ion PE curves of the methyl halides (figs. 2 to 6) shows the difficulty in deducing electronic structure directly from structure in the PE curve. Autoionization or configuration interaction is prominent in the fluoride, chloride, and bromide PE curves. However, in only one case, the ion-pair curves for CH_3Cl, are lines sufficiently resolved to permit comparison with previous spectroscopic results [2a]. Dibeler and Walker have already noted that the structure in this case is due to at least two series with the CH_3Cl^+ ground-state as a limit.

In order to assist in the discussion of the results it is helpful to have estimates of the inner ionization energies. Approximate Hartree-Fock calculations were obtained for CH_3F and CH_3Cl for this purpose. A brief description of these calculations has already been given [18] but for completeness eigenvalues are given in table 3. These results will be used to assist a detailed analysis of all aspects of the PE curves excepting the chloride ion-pair process.

TABLE 3. *Orbital and ionization energies for* CH_3F *and* CH_3Cl [a]

Molecule	Symmetry	Energy	Ionization energy
CH_3F			
	$2e$	14.3	12.50
	$5a_1$	17.8	
	$1e$	18.8	
CH_3Cl			
	$3e$	11.7	11.28
	$7a_1$	14.4	
	$2e$	16.8	

[a] All energies are in eV.

6. CH_3F

The onset of the parent PE curve (fig. 2) resembles that of CH_4 as the ionized orbitals are similar. However, there are apparently five steps at intervals of 7 to 4 Å. The Hartree-Fock calculation would indicate that this progression includes excitation of the symmetric C–F stretch as well as C–H modes since the orbital is bonding with respect to C–H and antibonding with respect to C–F. The autoionization noted by Chupka [19] for CH_4 is also found in CH_3F. However, it is not clear if all the features are analogous. The highest peak in the neighborhood of 925 Å is at an energy where $n=3$ Rydbergs to the $5a_1^{-1}$ ion are expected. In CH_4, the inner ionization energy is much too high so that all autoionization is due to Born-Oppenheimer breakdown in high vibrational states of $1t_1^{-1}$ Rydbergs or, in the case of CH_3F, from $1e^{-1}$ Rydbergs.

There is a striking indication of the dominance of configuration interaction at threshold and a caution on the attribution of peak-like structure to autoionization and of step-like structure to vibrational progressions in direct ionization. Examination of the CH_3^+ and F^- ion-pair PE curves shows a remarkable resemblance to the parent PE curve. A common precursor resonant-state must be assumed to contribute significantly to both ionization and ion-pair production. The ion-pair curves extend over some 2 eV and the resonance states must change in character over this range. In particular, we note clear evidence of configuration interaction between 875 to 900 Å with the Rydberg states leading to inner ionization thresholds.

The ionization of the $5a_1$ electron is predicted to br 3.5 eV above the first onset. This orbital is primarily the C–F bonding orbital and the onset of the CH_3^+ evidently occurs from this excited ion surface. The ion ground state is bonding with respect to C–F and the probability of exciting vibrational levels directly into the $CH_3^+ + F$ channel is very small. Evidently the autoionizing higher $5a_1^{-1}$ Rydbergs also do not contribute appreciably.

7. CH_3Cl

Several steps are evident at threshold in the CH_3Cl^+ PE curves shown in figure 3. The first step interval is 0.09 eV which is of the order of the spectroscopically deduced doublet splitting. However, no obvious autoionization structure appears in this interval for either CH_3Cl^+ or CD_3Cl^+ curves (figs. 3 and 4). Of probable significance is the observation that in the photoionization of argon obtained with the same apparatus used in this research, the doublet is not observed due to a lack of resolution.

Excitation of a CH_3 deformation mode accompanies the transitions to the lower Rydberg states [2a]. The structure observed below 1090 Å has energy separations of the order of 0.07 eV or about one-half that observed in the Rydbergs. Of course, the second step in CH_3Cl beyond the initial doublet could correlate with the vibrational excitation observed by Price. This transition would occur for a smaller energy in CD_3Cl and the steps are not resolved in CD_3Cl. The $3e$ orbital is primarily occupied by the chlorine lone-pair electrons but there is significant Cl–H antibonding and C–H bonding character. Deformation of the ^2E Jahn-Teller state should be appreciable and excitation of all the C–H modes is expected.

The Hartree-Fock threshold for $7a_1^{-1}$ is 2.7 eV above the first ionization energy. The $7a_1$ orbital is primarily the C–Cl bonding orbital and thus long vibrational progressions are expected in the Rydbergs and the ion state. The ionization threshold region for $7a_1^{-1}$ will also be overlapped by the autoionizing Rydbergs with the $2e^{-1}$ limit. Since the $2e_1$ orbital is the C–H bonding orbital, the Rydberg and ion transitions will be accompanied by long vibrational progressions and it is

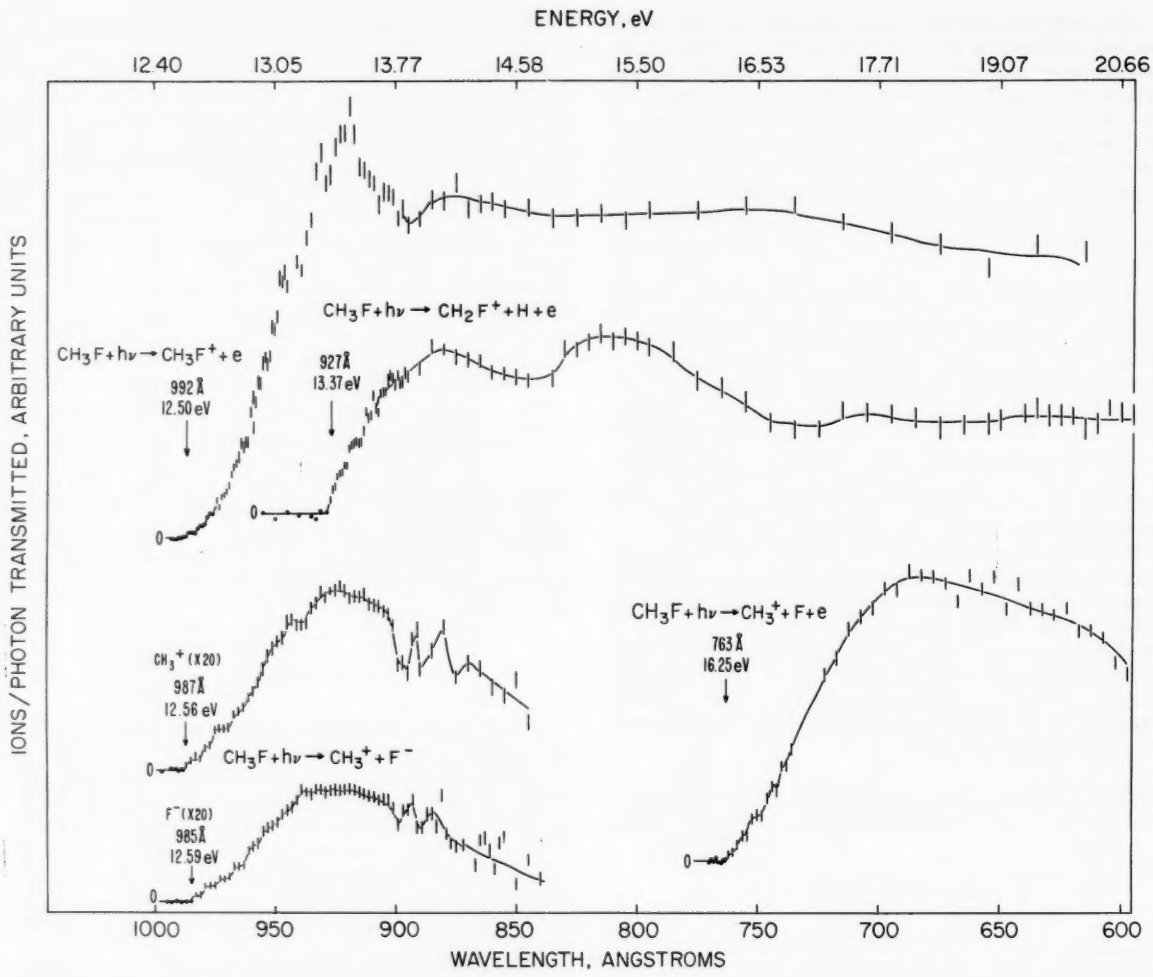

FIGURE 2. *Photoionization yield curves for the molecule and some fragment ions of methyl fluoride.*

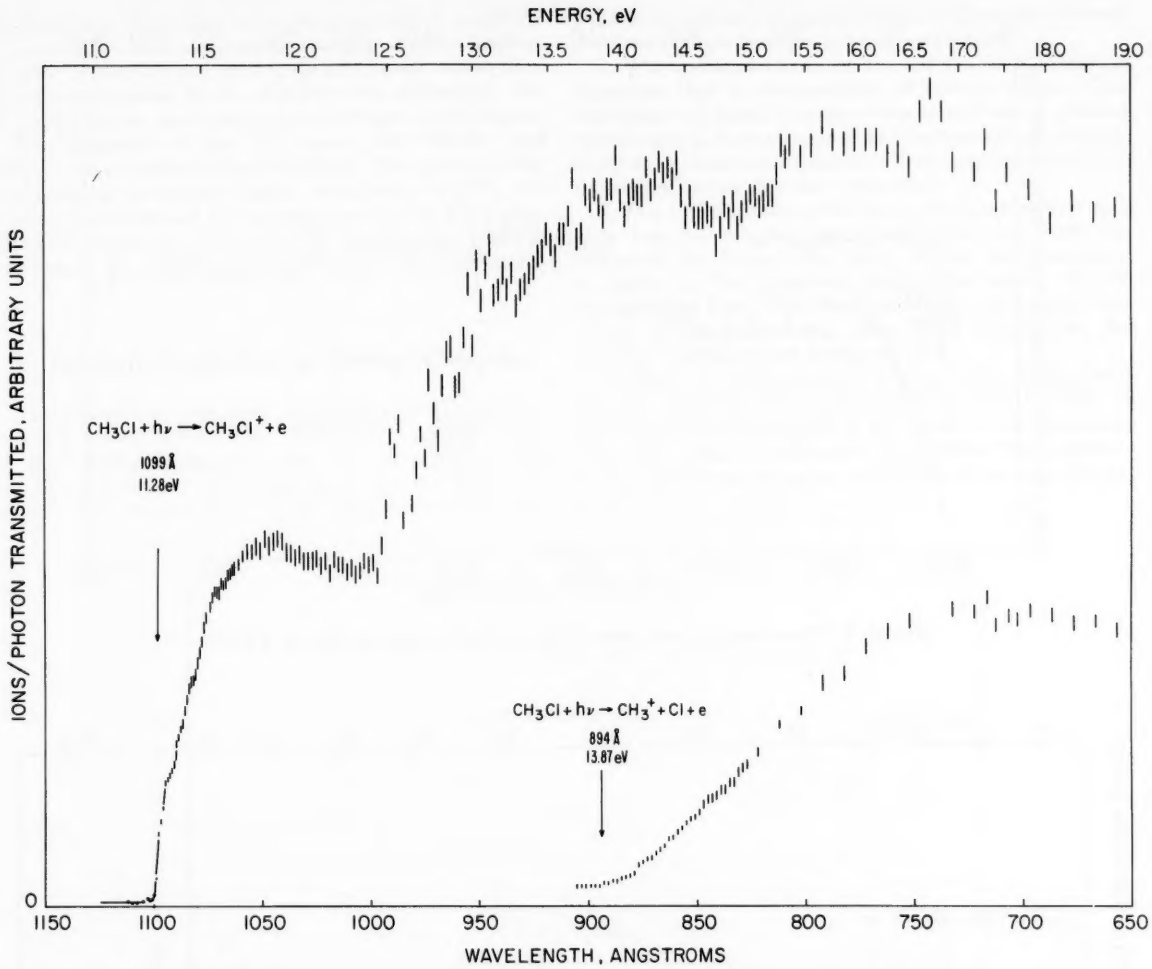

FIGURE 3. *Photoionization yield curves of the* CH_3Cl^+ *and the* CH_3^+ *ions of methyl chloride.*

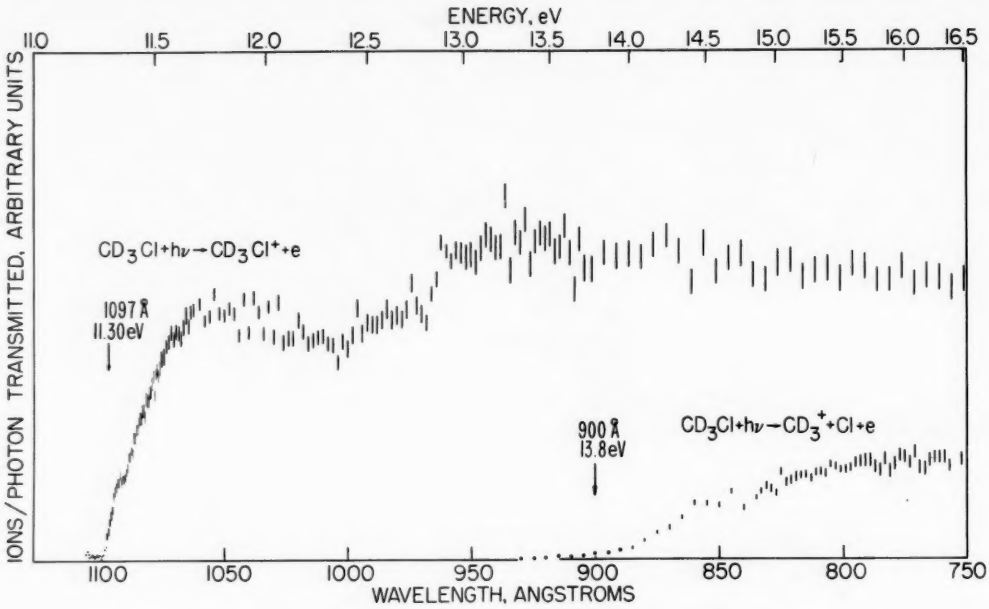

FIGURE 4. *Photoionization yield curves for the molecule ion and the* CD_3^+ *ion of* CD_3Cl.

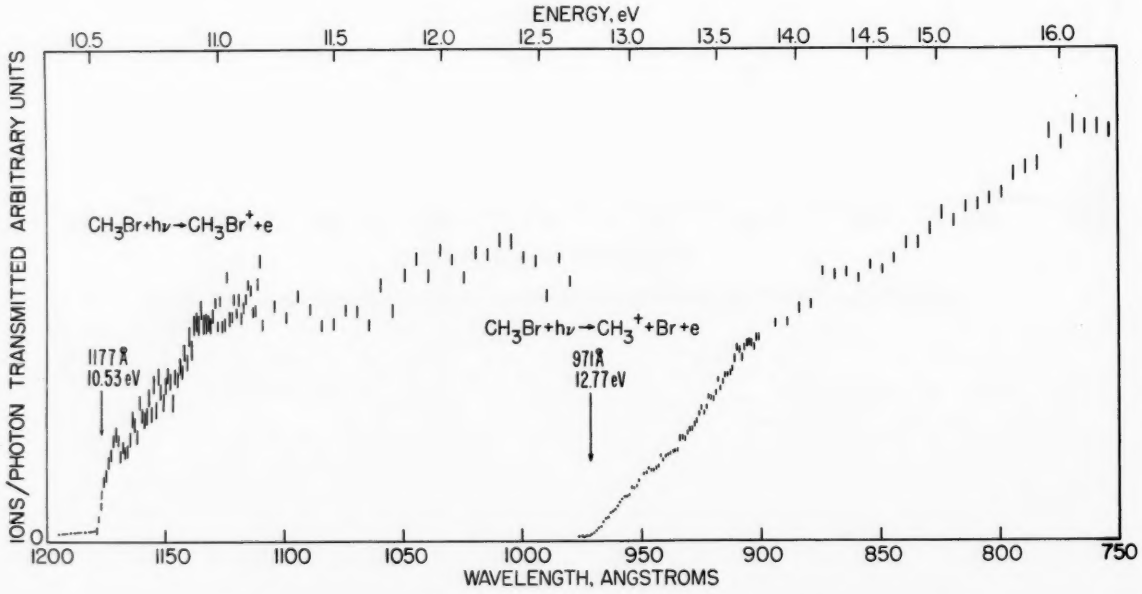

FIGURE 5. *Photoionization yield curves for the molecule and methyl ions of methyl bromide.*

not surprising that the ionization thresholds are obscured. It is also to be expected that the CH_3^+ ion is produced on the $7a_1^{-1}$ surface but there is no evidence for the contributions of the autoionization of levels to this process.

8. CH_3Br

The methyl bromide results (fig. 5) confirm Price's conclusion that the nonbonding Br orbital is ionized and that no vibrational levels of the ion are excited.

Contrary to the iodide or to photoionization measurements on Kr, however, the Rydberg levels that lead up to $\Omega = 1/2$ level do not appear as prominent absorption-like autoionization levels. Whether this difference, too, is significant or an experimental artifact is not known.

The behavior of the PE curves for CH_3Br^+ and CH_3^+ is very similar to that of CH_3Cl. The premise that autoionizing resonance states contribute to CH_3^+ formation is evidenced by the structure in the PE curve. The level spacing in the CH_3^+ PE curve would point to excitation of vibrational modes involving hydrogens.

9. Ion-Pair Production in Methyl Chloride

The ion-pair curves were verified by obtaining identical PE curves for the CH_3^+ and the Cl^- ions. In order to provide some insight into the mechanism, the ion-pair results of all deuterated species were obtained. The results for ordinary and deuterated compounds are shown in figures 6 and 7. There are several features of these curves that draw attention.

1. The general shape of the curves is a distorted Gaussian that is independent of isotope effect. This indicates a Franck-Condon transition from a ground vibrational polyatomic state to a continuum vibrational state in at least one degree of freedom for which the hydrogen atoms are not important.

2. The interference structure on the long wavelength side can be roughly correlated with the Rydbergs observed by Price. The peak values are compared in table 4. The structure disappears about 0.1 eV beyond the first ionization threshold indicating that either excited Rydberg vibrational bands or the doublet splittings are being excited.

3. There is a pronounced isotope shift on the total ion-pair current. The ratio for $CH_3:CH_2D:CHD_2$ is 1.0:0.9:0.6 as measured at the peak of the Gaussian. The CD_3^+ peak is observed but cannot be quantitatively measured because of the signal-to-noise limitation.

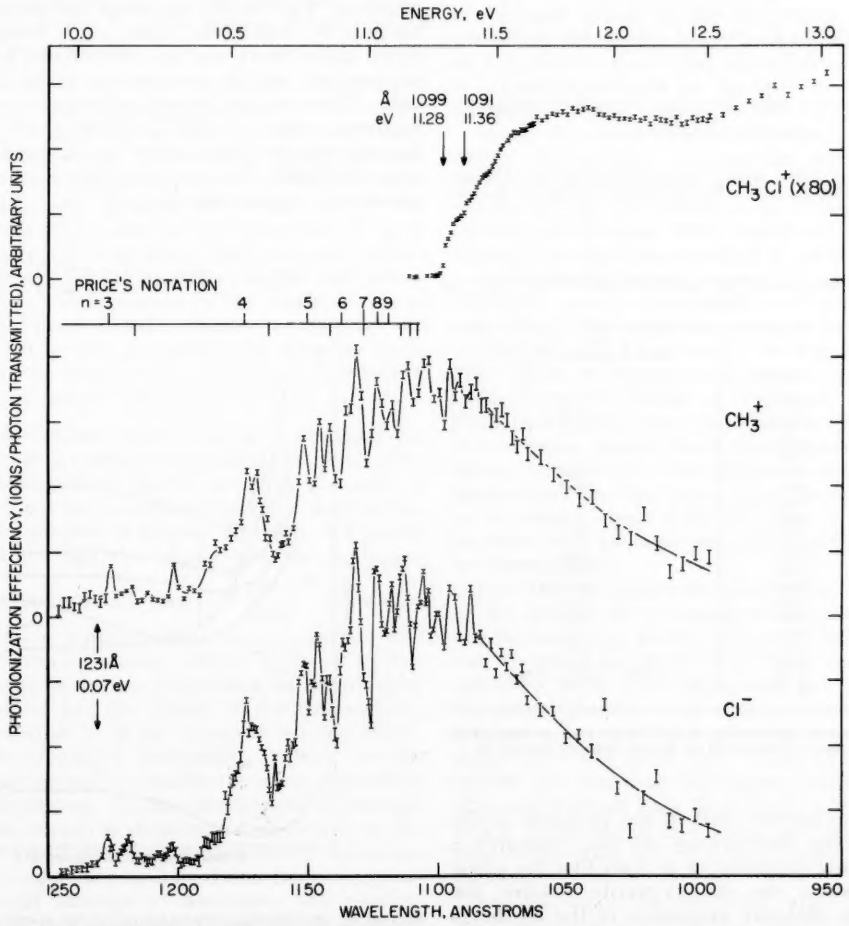

FIGURE 6. *Photoionization yield curves for the methyl and halogen ions of methyl chloride formed by the ion-pair process.*

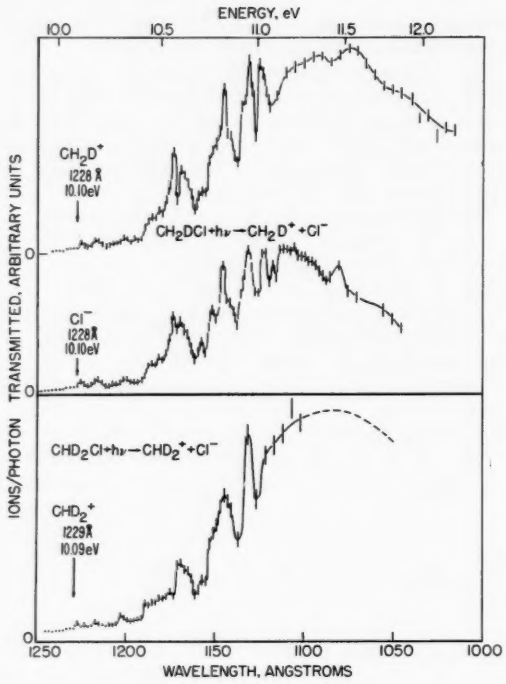

FIGURE 7. *Photoionization yield curves for the methyl and halogen ions of* CH_2DCl *and the methyl ion of* CHD_2Cl *formed by the ion-pair process.*

TABLE 4. *Comparison of ion-pair structure with* CH_3Cl *Rydberg bands*

Ion-pair peaks		Rydberg band energy (eV) [a]
Angstroms	*eV*	
1227.	10.10	10.10
1219.5	10.17	10.18
1201.5	10.32	
1185.	10.46	
1174.	10.56	10.55
1170.	10.60	10.63
1163.5	10.65	
1159.5	10.69	
1152.5	10.76	10.77
1148.	10.80	
1143.	10.85	10.86
1137.	10.90	10.90
1132.5	10.95	10.98(2)
1124.5	11.02	11.03
1119.	11.08	11.07
1106.5	11.20	11.11
1104.5	11.22	11.15
1101.5	11.25	11.18
1095.	11.32	Limits: ~11.22, 11.30
1088.	11.39	

[a] Rydberg band energies are obtained from ref. 2a. They are compared with approximate peak values from figure 6. The limits of the Rydberg series are from ref. 2a.

4. There is no isotope shift in the positions of the observed Rydberg interference so this indicates a lack of vibrational structure or at least that the vibrational progressions do not primarily involve the hydrogen atoms. Relative intensities of the Rydbergs do not vary much with isotopic substitution. It is possible that the observed variation is due to line-width and noise problems.

The interpretation of these results can only be speculative as a calculation of the electronic structures of the excited states of methyl chloride is beyond our means. A very simplified diatomic model will be adopted and is schematically given in figure 8. The only repulsive curve that is rapidly rising in the ion-pair energy region is presumed to arise from the interaction of the unobserved $CH_3(^2E)$ state with the ground-state Cl. The Rydberg states to the $3e_1^{-1}$ ion intersect this state and the configuration interaction is apparent up to the $3e_1$ ionization limit. The Franck-Condon factor associated with the direct transition would be only slightly dependent on isotopic substitution. In order to provide for such an effect there is the final configuration interaction with the curve that connects asymptotically with the ion pair.

This model can be expressed more precisely in terms of the results of Mies [17]. His modification of the Fano continuum configuration theory includes the effect of direct inelastic coupling between the continua. The model we adopt for production of the ion-pair is dependent upon such coupling. As we noted above there are two continua to be considered, the ion-pair and the one leading to the $CH_3(^2E)$ molecule. There is an infinity of resonance states, the Rydberg states of CH_3Cl. Other continua involving fluorescence or dissociation are ignored. The transition amplitude for photoabsorption into the ion-pair channel is approximately given by

$$t_{\bar{\alpha}} = A^{\circ *}_{\alpha,\beta}(1 - i\mathbf{K}_{\beta\beta})^{-1}\left(t^c_\beta + \sum_n \frac{V_{n,\beta}}{E - E_n}\, t^b_n\right)$$

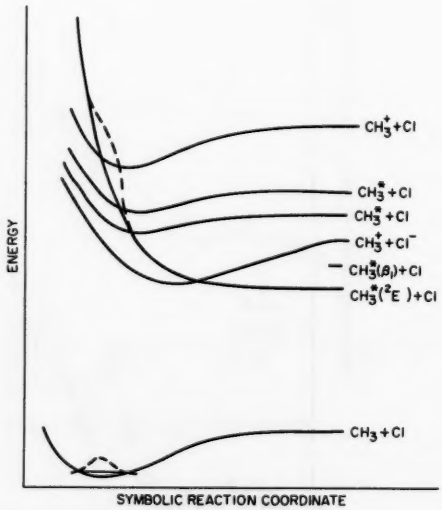

FIGURE 8. *Schematic representation of the energy levels for a simplified model of* CH_3Cl.

The precise mathematical definition of these terms is given by Mies but we will try to explain their significance to the problem at hand. **K** is the reactance matrix and $(1-i\mathbf{K})^{-1}$ is a normalization term which conserves flux. The matrix element $V_{n,\beta}$ is a measure of the coupling of the continuum β to the nth resonance state. The transition amplitudes t_β° and t_n^b are the dipole matrix elements coupling the ground state to the $CH_3(^2E)_\beta$ continuum and the nth resonance state, respectively. $A_{\alpha,\beta}^\circ$ is the amplitude of inelastic scattering from the β continuum to the α or ion-pair continuum.

It is our contention that there are no appreciable dipole couplings directly to the α continuum and in addition the resonance states do not couple to this continuum. Since the hydrogen vibrational modes are not excited there is no appreciable isotope effect in t_β°, t_n^b and, as required by the experimental results, in $V_{n,\beta}$. The fundamental resonance structure is not primarily related to the ion-pair state. As the β continuum packet develops, there is a coupling to the α continuum given by $A_{\alpha,\beta}^\circ$. This amplitude is proportional to V, where V is the matrix element which couples the two continua.

The radiationless transition converts translational into vibrational and electronic energy. In this model there is only a small isotope effect in the electronic-translational conversion. Under very simple assumptions V^2 is proportional to the Franck-Condon factor for the N−1 vibrational degrees of freedom that are assumed not to participate in the transition. A large isotope effect is expected here. The transition occurs at large CH_3 and Cl separations so that the subsequent couplings are neglected as the fragments go to infinity. The Franck-Condon factor of greatest importance is that for the pyramidal CH_3 bending mode to the planar one since at the crossing it is assumed that almost free planar CH_3^+ is produced.

The Franck-Condon factor can be calculated for an oscillator that is primarily displaced. Siebrand [20] has provided numerical results for such a model. It can be shown that for a constant energy E and excitation of a large number of quanta, the ratio of Franck-Condon factors for the deuterium to hydrogen molecules is proportional to $\exp\left[-k\left(\frac{\mu_D}{\mu_H}\right)^{1/2}E\right]$ where μ is the effective reduced mass for the normal frequency. The reduced masses can be replaced by the ratio of frequencies ω_H/ω_D. Depending on the number of quanta excited and the details of the frequencies, it would be possible to fit the observed isotope effect. Obviously the transition probability is less for the deuterated species and is smaller the more deuterium atoms are substituted. As the distribution of translation-vibrational energy is determined by details in the force constants and equilibrium positions of which we are ignorant, it can only be hoped that further experimentation would attempt to determine the relative kinetic energy. A knowledge of the distribution of kinetic energies for a given frequency, ω, would go a long way toward establishing the validity of this model and make quantitative work meaningful.

This model predicts the production of the first excited $CH_3(^2E)$ state with the same resonance structure that is found for the ion-pair. The continuum shown by Price [2a] as starting at about 10 eV can be attributed to this excited state. Transitions from the pyramidal excited state are not forbidden to the ground state and could be observed. In figure 8 we have assumed that the ^2E state is lower than all observed [21] Rydbergs of CH_3. This may not be true but the ^2E asymptote should be less than that for the ion-pair. The relative position with respect to the Rydberg β_1 state would have an important bearing on the production of the β_1 state by a transition to the β continuum.

10. Thermodynamic Properties

The simplest use of the data is to determine bond energies and ionization thresholds. The experimental data on the ionization thresholds are summarized in table 5. Where possible, calculated heats of formation of ions are given. In the two cases where accurate ionization thresholds have been obtained by analysis of a Rydberg series [2a] the values of the PE onset is in good agreement for the bromide and is about 0.1 eV greater in the case of the chloride.

When threshold values for fragment ions are used uncritically without concern for the distribution of energy in either internal modes or in relative kinetic energy, or for the transition probabilities to a given vibrational-rotational level, bond energies can be deduced. These are summarized in table 6. The required atomic halogen ionization energies are obtained from Huffman's recent report [22] and the NBS compilation [23]. The ionization energy for CH_3, $I(CH_3)=9.843$ eV (227.0 kcal mol^{-1}) is that due to Herzberg [21]. Heats of formation of neutral species are taken from "Selected Values of Chemical Thermodynamic Properties" [24]. Note that Chupka [19] has evidence that in some simple bond dissociations the rotational energy distribution contributes to the threshold ion production. On this basis bond energies would have to be raised about 0.02 eV. This is not done here because with present resolution such effects cannot be distinguished.

For HCl, the threshold value of the Cl^+ ion is taken as the ΔH_0 for the reaction shown in table 5. Subtracting the ionization energy, $I(Cl)=12.967$ eV (299.0 kcal mol^{-1}) gives $\Delta Hf_0^\circ(Cl)=27.2$ kcal mol^{-1}. Thus, we calculate $D_0(H-Cl)=100.8$ kcal mol^{-1} (4.37 eV). To the extent that this is an accurate value of the heat of formation, we may also obtain an improved value for $D_0(Cl-Cl)=54.4$ kcal mol^{-1} (2.36 eV). Our $D_0(H-Cl)$ is 0.06 eV less than the values quoted by Herzberg [25] and Cottrell [26]. The $D_0(H-Cl^+)$ is greatly different from Herzberg's value but this is due to the inaccurate value of $I(HCl)$ used in the thermochemical cycle.

Unfortunately, the threshold values of the observed fragmentations of the methyl halides (possibly excepting CH_3Br) apparently do not yield direct bond dis-

TABLE 5. *Summary of threshold energies for hydrogen chloride and methyl halides*

Molecule	Ion	Threshold (eV)	Process	ΔHf_0° (ion) (kcal mol^{-1})
HCl	HCl^+	12.70	$HCl + h\nu \rightarrow HCl^+ + e$	270.9
	Cl^+	17.34	$\rightarrow Cl^+ + H + e$	326.2
CH_3F	CH_3F^+	12.50	$CH_3F + h\nu \rightarrow CH_3F^+ + e$	[a] 233.
	CH_2F^+	13.37	$\rightarrow CH_2F^+ + H + e$	
	CH_3^+	12.56	$\rightarrow CH_3^+ + F^-$	
		16.25	$\rightarrow CH_3^+ + F + e$	
	F^-	12.59	$\rightarrow F^- + CH_3$	
CH_3Cl	CH_3Cl^+	11.28	$CH_3Cl + h\nu \rightarrow CH_3Cl^+ + e$	242.7
	CH_3^+	10.07	$\rightarrow CH_3^+ + Cl^-$	
		13.87	$\rightarrow CH_3^+ + Cl + e$	
	Cl^-	10.07	$\rightarrow Cl^- + CH_3$	
CH_2DCl	CH_2DCl^+	11.29	$CH_2DCl + h\nu \rightarrow CH_2DCl^+ + e$	242.9
	CH_2D^+ / Cl^-	10.10	$\rightarrow CH_2D^+ + Cl^-$	
CHD_2Cl	CHD_2Cl^+	11.30	$CHD_2Cl + h\nu \rightarrow CHD_2Cl^+ + e$	243.1
	CHD_2^+	10.09	$CHD_2^+ + Cl^-$	
CD_3Cl	CD_3Cl^+	11.30	$CD_3Cl + h\nu \rightarrow CD_3Cl^+ + e$	243.1
	CD_3^+	13.8	$\rightarrow CD_3^+ + Cl + e$	
CH_3Br	CH_3Br^+	10.53	$CH_3Br + h\nu \rightarrow CH_3Br^+ + e$	238.1
		(10.81)		
	CH_3^+	12.77	$\rightarrow CH_3^+ + Br + e$	261.6

[a] Assuming $\Delta Hf(CH_3F) = -55$ kcal mol^{-1} from ref. 27.

TABLE 6. *Summary of observed and calculated bond dissociation energies*

Bond	Dissociation energy (eV)	
	Observed	Calculated [a]
$D_0(H-Cl)$	4.37	[b] 4.43
$D_0(H-Cl^+)$	4.64	[b] 4.48
$D_0(CH_3-F)$	6.30 (ion-neutral) 6.17 (ion-pair)	[c] 4.66
$D_0(CH_3^+-F)$	3.75	2.00
$D_0(CH_2F^+-H)$	0.87	
$D_0(CH_3-Cl)$	4.03 (ion-neutral) 3.84 (ion-pair)	3.49
$D_0(CH_3^+-Cl)$	2.59	1.96
$D_0(CH_3-Br)$	2.93	2.90
$D_0(CH_3^+-Br)$	2.24	2.22

[a] Calculated from usual summation of heats of formation given in ref. 24.
[b] Reported in ref. 25.
[c] $\Delta Hf_0^\circ(CH_3F) = -55$ kcal mol^{-1} from ref. 27.

sociation energies. The heats of formation of the molecules, and of the related radicals and ions are generally established well within the uncertainties in the present measurements. A comparison of the observed CH_3–X bond dissociation energies summarized in the second column of table 6 with values calculated from heats of formation or obtained by spectroscopic means indicate that excess energy is included in most of the dissociative ionization processes. We had previously noted that the dissociation occurs from the excited ion state. The excess energy decreases from 1.7 eV in CH_3F to about 0.5 eV in CH_3Cl and is probably insignificant in CH_3Br. The excess energy is observed in ion-pair as well as in ion-neutral processes. The appearance of kinetic energy with the formation of CH_3^+ ions in the fluoride and chloride compounds was reported in an earlier electron-impact study [28]. the magnitude decreased from fluoride to chloride and was immeasurable (< 0.2 eV) in the bromide and iodide. However, in the case of the fluoride, a lower-energy threshold was also observed in both the ion-neutral and ion-pair processes that resulted in a H_3C–F bond dissociation energy of 4.7 eV. This lower-energy threshold is not observed in the present study.

11. Conclusion

The behavior of the homologous series is disappointingly specific. The fluoride ion-pair production is from a resonance state which also branches into the ion-neutral process. Neutral predissociation probably dominates the resonances below ionization threshold as ion and Rydberg bond energies are very low. This is completely analogous to the methane case. In neither the fluoride nor the bromide cases, though, is the direct repulsive transition observed.

The significance of autoionization in these systems is undeniable. However, the data emphasize the need for caution in the interpretation of this autionization. If no observation of the ion-pair process had been made, the threshold would be considered a direct process and no thought of resonance states would arise. As it is, resonance neutral states would appear to contribute over the entire threshold region not only at the positions where peak-like structure is apparent.

Autoionization between the doublets also behaves in an unusual manner. Structure is apparent in the bromide which can be correlated with Rydberg levels reported by Price. However, the chloride gives no evidence of such autoionization. In the analogous argon curve at the same resolution, the doublet splitting is not observable. However, for the chloride there is a step at about the right energy. Perhaps, this

is a vibrationally excited state superimposed on the doublet structure.

The thermochemical results more closely bound the ionization and bond energies although the role of rotational energy must still be considered. But as always, certain processes can be shown to occur from excited states and lead to excited states. This is the case for $D(CH_3-F)$ and $D(CH_3-Cl)$. To assist in interpreting such bond energy deductions or in determining inner ionization energies all ancillary information is required. In particular, approximate Hartree-Fock calculations of the electronic structure and inner ionization thresholds are very helpful especially as such calculations are essentially routine. From the data and the ionization threshold extremes, it is apparent that experimental determination of the inner onsets is not possible, at least at this resolution.

12. References

[1] Price, W. C., Proc. Roy. Soc. (London) **167,** 216 (1938).
[2] (a) Price, W. C., J. Chem. Phys. **4,** 539 (1936); (b) Stokes, S., and Duncan, A. B. F., J. Amer. Chem. Soc. **80,** 6177 (1958); (c) Kimura, K., and Nagakura, S., Spectrochimica Acta **17,** 166 (1961).
[3] Dibeler, V. H., and Walker, J. A., J. Chem. Phys. **43,** 1842 (1965).
[4] Morrison, J. D., Hurzeler, H., Inghram, M. G., and Stanton, H. E., J. Chem. Phys. **33,** 821 (1960).
[5] Dibeler, V. H., and Reese, R. M., J. Res. NBS **68A,** 409 (1964).
[6] Dibeler, V. H., and Walker, J. A., J. Opt. Soc. Am. **57,** 1007 (1967).
[7] Mulliken, R. S., Revs. Mod. Phys. **4,** 6 (1932).
[8] Cade, P. E., and Huo, W. M., J. Chem. Phys. **47,** 649 (1967).
[9] Norling, F., Z. Physik **104,** 638 (1937).
[10] Norling, F., Z. Physik **106,** 177 (1937).
[11] Morrison, J. D., J. Chem. Phys. **19,** 1305 (1951).
[12] Fox, R. E., J. Chem. Phys. **32,** 385 (1960).
[13] Halmann, M., and Laulicht, I., J. Chem. Phys. **43,** 1503 (1965).
[14] Nesbet, R. K., J. Chem. Phys. **41,** 100 (1964).
[15] Fano, U., Phys. Rev. **124,** 1866 (1961).
[16] Fano, U., and Prats, F., J. Natl. Acad. Sci. India **A33,** 553 (1963).
[17] Mies, F., private communication.
[18] Krauss, M., International Mass Spectrometry Conference, Berlin (1967). The eigen functions are available upon reasonable request.
[19] Chupka, W. A., J. Chem. Phys. **48,** 2337 (1968).
[20] Siebrand, W., J. Chem. Phys. **46,** 440 (1967).
[21] Herzberg, G., Proc. Roy. Soc. (London) **A262,** 291 (1961).
[22] Huffman, R. E., Larrabee, J. C., and Tanaka, Y., J. Chem. Phys. **47,** 856 (1967).
[23] Moore, C. E., NBS Circ. 467 (1952).
[24] Wagman, D. D., Evans, W. H., Parker, V. B., Halow, I., Bailey, S. M., and Schumm, R. H., NBS Tech. Note 270–3 (1968).
[25] Herzberg, G., Molecular Spectra and Molecular Structure I. Spectra of Diatomic Molecules (D. Van Nostrand Co., Inc., New York, 1950).
[26] Cottrell, T. L., The Strengths of Chemical Bonds (Academic Press Inc., New York, 1958).
[27] Benson, S. W., J. Chem. Educ. **42,** 502 (1965).
[28] Dibeler, V. H., and Reese, R. M., J. Res. NBS **54,** 127 (1955) RP2573.

(Paper 72A4–502)

JOURNAL OF RESEARCH of the National Bureau of Standards—A. Physics and Chemistry
Vol. 72A, No. 4, July–August 1968

The Fourth and Fifth Spectra of Vanadium (V IV and V V)

Laura Iglesias*

(April 26, 1968)

The V IV spectrum has been extended by using as light sources a condensed spark and a hollow cathode discharge. With the new data, the experimental interpretation of levels of the $3d^2$, $3d\,4d$, $3d\,5s$, $3d\,5p$, $3d\,4f$, $3d\,5d$ and $3d\,6s$ configurations has been completed with the exception of three levels of the $3d\,4f$ and $3d\,5d$ configurations. Four levels of the $3d\,5g$ electron configuration have also been found. These levels account for 340 of the 360 lines assigned to V IV in the region 675 Å–5940 Å.

Three members of the $3d\,ns$ series give an ionization potential of 376730 ± 40 cm^{-1} = 46.70 volts. The $4d\,^2$D term of V V has also been located in the course of this work. With the aid of the new observations between 675 Å and 2200 Å the value of some levels already known has been improved.

Key Words: Atomic spectra, V IV and V V; classified lines, V IV and V V spectra; spectra, V IV and V V; terms, V IV and V V spectra; vanadium, the fourth and fifth spectra of.

1. Introduction

The fourth spectrum of vanadium was analyzed by White [1][1] in 1929, who found the terms of the main configurations, $3d^2$, $3d\,4s$, $3d\,4p$, and two terms of the $3d\,4d$ configuration. From a study of related spectra, B. Edlén deduced (see A.E.L. [2]), that the singlet term ^{1}S of the $3d^2$ configuration was incorrect and that the energy level values of all singlet terms should be decreased by 698 cm^{-1}.

As a result of new observations a complete revision and extension of the V IV spectrum has been made, and the results are presented in this paper, together with some new levels of V V.

2. Experimental Details

The analyses are based on two sets of spectrograms. The first set was obtained by the author during a stay at Princeton University, and covers the region 675 to 2200 Å. The plates were taken with the 2 meter-grating spectrograph at Palmer Physical Laboratory, by using as light source a condensed spark in helium, under the same conditions used by A. G. Shenstone to excite Ni III [3]. In the present case V I, V II, V III, V IV and V V were excited; by observation of the polarity of the lines it was not difficult to differentiate among the lines corresponding to the various stages of ionization. (See fig. 1.)

The second set of plates, from 2200 to 5940 Å, was obtained by Velasco in Lund in 1953. The light source was a pulsed hollow cathode discharge used under the conditions described in a paper on V III [4]; the spectral instruments used were a 21-ft grating spectrograph in a Wadsworth mounting and a quartz prism spectrograph Hilger–E478. More than one thousand lines were then attributed to V III but it was pointed out that some of them might belong to V IV. In most of the grating spectrograms, it was impossible to distinguish V III from V IV lines. Other spectrograms obtained with the prism spectrograph permitted, however, an unambiguous distinction between V III and V IV lines. The analysis of V IV could thus be substantially extended.

On the vacuum spectrograph the plate factor was about 4.2 Å/mm in the first order. From 675 to 800 Å all but the weakest lines were measured in the second order. In the hollow cathode spectrograms the plate factor varied from 2.0 Å/mm in the prism spectrograms to about 5 Å/mm in those taken in the first order.

Most of the wavelength values given in table 3 are averages of measurements made on two or more plates. To distinguish between the accuracy of different measurements three decimal places have been retained for the lines with an estimated probable error not higher than ±0.01 Å. When only two decimal places are given in the wavelength, the error may range from 0.01 to 0.03 Å, depending on the character of the line. Correspondingly the number of significant figures in the wave number column (table 3) has been adjusted to the assumed accuracy of the wavelengths. The symbols used in the "Intensity" column in table 3 are those recommended by the Joint Commission for Spectroscopy [5].

About 360 lines in all were assigned to V IV.

*An invited paper. Present address: Instituto de Optica, Madrid 6, Spain.

[1] Figures in brackets indicate the literature references at the end of this paper.

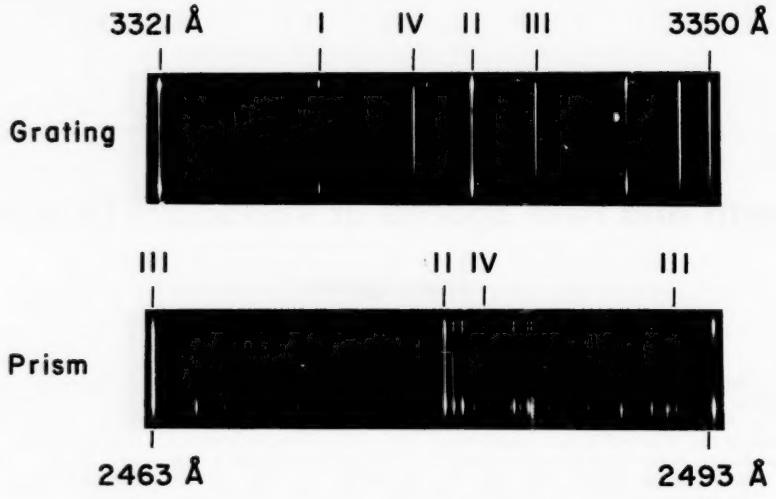

FIGURE 1. *Hollow Cathode Spectra of Vanadium. The lines belonging to each spectrum are indicated by the corresponding roman numeral.*
On the prism spectrum V IV lines are clearly shorter and wider than V III lines of similar intensity.

3. Analysis

Within the main configurations only the term $3d^2\ {}^1S$ was missing. The only remaining unclassified line in the region of the $3d^2-3d\,4p$ transitions, $\lambda = 884.146$ Å, was, therefore, designated as the ${}^1S-{}^1P^\circ$ combination, giving a value of 42462.1 cm^{-1} for the ${}^1S$ level. New transitions between the even and odd levels confirm the reality of the energy levels given in A.E.L. [2], with exception of the $3d({}^2D)4d\ {}^3F$ term.

With the present observations the values of the energy levels already known have been improved. An asterisk in tables 1 and 2 indicates that a slight change in the level value has been made as a result of this revision.

The determination of levels and their grouping into terms in the higher configurations did not offer special difficulties. The search for new energy levels has been made by the usual method of recurring differences. The assignment of levels to terms and electron configurations, takes into account the relative intensities of lines in multiplets, the intervals, and the relative positions of terms and configurations deduced from comparisons with such related spectra as Ti III and Ti IV. In the case of the $4f$ electron configuration the theoretical calculations for Fe VII by Y. Shadmi were used as a guide [6].

The limit of the $3d\,nx$ configurations being a ${}^2D$ term of V V and the coupling nearly *LS* for low values of "x", the designation of the levels was rather straightforward. In the case of the $4f$ electron configuration there are a few levels that share the same *LS* character. The designation is, therefore, not so conclusive, and the assignment has been made by comparison with Ti III [7] and Fe VII [8, 6], as stated above. The $3d\,5g$ configuration is expected to show a high percentage of pair coupling. Only four levels have been found with certainty, which, accordingly, are presented in table 1 with pair-coupling notation.

As a result of this analysis, all the terms belonging to $3d\,4d$, $3d\,5s$, $3d\,5p$, $3d\,4f$, $3d\,5d$ and $3d\,6s$ have been found with the exception of three levels of the $3d\,4f$ and $3d\,5d$ configurations (tables 1 and 2). The total number of classified lines has now been extended to 340 lines of the V IV spectrum. Their wavelengths, visual intensities, wave numbers and classifications are given in table 3. Only twenty of the observed lines still remain unclassified, and very probably they correspond to $4f-5g$ transitions.

Ionization Potential.—By using a Ritz formula $n^* = n + a + bT$ on the three observed members of the $3d({}^2D)ns$ series an ionization potential of 376730 ± 40 cm^{-1} or 46.70 volts has been calculated. The levels and series used for the calculations of this limit are collected in table 4.

TABLE 1. *Even levels of* V IV

Config.	Desig.	J	Level	Interval
$3d^2$	$3d\,^3F$	2	0.0*	
				325.4
		3	325.4*	
				409.3
		4	734.7*	
$3d^2$	$3d\,^1D$	2	10959.3*	
$3d^2$	$3d\,^3P$	0	13122.8*	
				116.4
		1	13239.2*	
				219.1
		2	13458.3*	
$3d^2$	$3d\,^1G$	4	18391.2*	
$3d^2$	$3d\,^1S$	0	42462.1	
$3d(^2D)4s$	$4s\,^3D$	1	96196.1*	
				216.0
		2	96412.1*	
				385.7
		3	96798.0*	
$3d(^2D)4s$	$4s\,^1D$	2	100200.7*	
$3d(^2D)4d$	$4d\,^1F$	3	215957.7	
$3d(^2D)4d$	$4d\,^3D$	1	216905.0	
				203.0
		2	217108.0	
				242.0
		3	217350.0	
$3d(^2D)4d$	$4d\,^3G$	3	217836.3*	
				263.7
		4	218100.0*	
				363.6
		5	218463.6*	
$3d(^2D)4d$	$4d\,^1P$	1	217990.7	
$3d(^2D)4d$	$4d\,^3S$	1	220343.5	

TABLE 1. *Even levels of* V IV—Continued

Config.	Desig.	J	Level	Interval
$3d(^2D)4d$	$4d\,^3F$	2	222794.6	
				238.4
		3	223033.0	
				271.6
		4	223304.6	
$3d(^2D)4d$	$4d\,^1D$	2	225804.1	
$3d(^2D)4d$	$4d\,^3P$	0	226521.6	
				95.5
		1	226617.1	
				179.2
		2	226796.3	
$3d(^2D)4d$	$4d\,^1G$	4	227712.5	
$3d(^2D)4d$	$4d\,^1S$	0	234121.8	
$3d(^2D)5s$	$5s\,^3D$	1	236148.6	
				173.8
		2	236322.4	
				444.5
		3	236766.9	
$3d(^2D)5s$	$5s\,^1D$	2	237638.8	
$3d(^2D)5d$	$5d\,^1F$	3	283459.4	
$3d(^2D)5d$	$5d\,^3D$	1	283722.7	
				217.7
		2	283940.4	
				286.3
		3	284226.7	
$3d(^2D)5d$	$5d\,^3G$	3	284101.1	
				239.0
		4	284340.1	
				359.2
		5	284699.3	
$3d(^2D)5d$	$5d\,^1P$	1	284365.7?	
$3d(^2D)5d$	$5d\,^3S$	1	285298.6	
$3d(^2D)5d$	$5d\,^3F$	2	285798.9	
				258.0
		3	286056.9	
				229.6
		4	286286.5	

TABLE 1. *Even levels of* V IV—Continued

Config.	Desig.	J	Level	Interval
$3d(^2D)5d$	$5d\ ^1D$	2	287221.4	
$3d(^2D)5d$	$5d\ ^3P$	2	287733.4	
$3d(^2D)5d$	$5d\ ^1G$	4	288127.6	
$3d(^2D)6s$	$6s\ ^3D$	1	291796.0	
				122.1
		2	291918.1	
				499.5
		3	292417.6	
$3d(^2D)6s$	$6s\ ^1D$	2	292766.7	
$3d(^2D)5g$	$5g\ [3\frac{1}{2}]$	3	306323.1	
				4.6
		4	306327.7	
$3d(^2D)5g$	$5g\ [4\frac{1}{2}]$	5	306871.0	
				−5.3
		4	306876.3	

TABLE 2. *Odd levels of* V IV

Config.	Desig.	J	Level	Interval
$3d(^2D)4p$	$4p\ ^1D°$	2	*144273.1**	
$3d(^2D)4p$	$4p\ ^3D°$	1	*146117.7**	
				311.6
		2	*146429.3**	
				425.8
		3	*146855.1**	
$3d(^2D)4p$	$4p\ ^3F°$	2	*147135.2**	
				521.3
		3	*147656.5**	
				712.7
		4	*148369.2**	
$3d(^2D)4p$	$4p\ ^3P°$	0	*151449.1**	
				−22.1
		1	*151427.0**	
				140.3
		2	*151567.3**	

Table 2. *Odd levels of* V IV—Continued

Config.	Desig.	J	Level	Interval
$3d(^2D)4p$	$4p\ ^1F°$	3	*153918.7**	
$3d(^2D)4p$	$4p\ ^1P°$	1	*155565.5**	
$3d(^2D)5p$	$5p\ ^1D°$	2	*254468.8*	
$3d(^2D)5p$	$5p\ ^3D°$	1	*254824.1*	
				322.7
		2	*255146.8*	
				298.7
		3	*255445.5*	
$3d(^2D)5p$	$5p\ ^3F°$	2	*255463.3*	
				284.3
		3	*255747.6*	
				504.1
		4	*256251.7*	
$3d(^2D)5p$	$5p\ ^3P°$	0	*256739.9*	
				41.9
		1	*256781.8*	
				361.4
		2	*257143.2*	
$3d(^2D)5p$	$5p\ ^1F°$	3	*257690.8*	
$3d(^2D)5p$	$5p\ ^1P°$	1	*258288.8*	
$3d(^2D)4f$	$4f\ ^1G°$	4	*263111.4*	
$3d(^2D)4f$	$4f\ ^3F°$	2	*263593.0*	
				15.3
		3	*263608.3*	
				504.8
		4	*264113.1*	
$3d(^2D)4f$	$4f\ ^3H°$	4	*263822.4*	
				339.4
		5	*264161.8*	
				683.9
		6	*264845.7*	
$3d(^2D)4f$	$4f\ ^3G°$	3	*263902.3*	
				499.6
		4	*264401.9*	
				190.0
		5	*264591.9*	

Table 2. *Odd levels of* V IV—Continued

Config.	Desig.	J	Level	Interval
$3d(^2D)4f$	$4f\ ^1D^\circ$	2	*264482.8*	
$3d(^2D)4f$	$4f\ ^1F^\circ$	3	*264902.2*	
$3d(^2D)4f$	$4f\ ^3D^\circ$	1	*265019.7*	47.7
		2	*265067.4*	204.2
		3	*265271.6*	
$3d(^2D)4f$	$4f\ ^3P^\circ$	1, 2	*265879.2*	
$3d(^2D)4f$	$4f\ ^1H^\circ$	5	*266600.3*	

TABLE 3. *Classified lines of* V IV

λ vac.	Intensity	Wave number	Classification	λ vac.	Intensity	Wave number	Classification
675.469	30	148045.2	$3d\ ^3F_3-4p\ ^3F^\circ_4$	722.912	40	138329.4	$3d\ ^3P_1-4p\ ^3P^\circ_2$
677.345	200	147635.2	$3d\ ^3F_4-4p\ ^3F^\circ_4$	723.045	40	138303.9	$3d\ ^3P_0-4p\ ^3P^\circ_1$
678.740	60	147331.8	$3d\ ^3F_3-4p\ ^3F^\circ_3$	723.537	40	138209.9	$3d\ ^3P_1-4p\ ^3P^\circ_0$
679.647	50	147135.2	$3d\ ^3F_2-4p\ ^3F^\circ_2$	723.652	40	138188.0	$3d\ ^3P_1-4p\ ^3P^\circ_1$
680.632	40	146922.2	$3d\ ^3F_4-4p\ ^3F^\circ_3$	724.068	40	138108.5	$3d\ ^3P_2-4p\ ^3P^\circ_2$
681.145	40	146811.6	$3d\ ^3F_3-4p\ ^3F^\circ_2$	724.809	5	137967.3	$3d\ ^3P_2-4p\ ^3P^\circ_1$
682.455	40	146529.8	$3d\ ^3F_3-4p\ ^3D^\circ_3$	734.344	20	136175.9	$3d\ ^1D_2-4p\ ^3F^\circ_2$
682.923	40	146429.3	$3d\ ^3F_2-4p\ ^3D^\circ_2$	737.854	400	135528.1	$3d\ ^1G_4-4p\ ^1F^\circ_3$
684.368	500	146120.2	$3d\ ^3F_4-4p\ ^3D^\circ_3$ $3d\ ^3F_2-4p\ ^3D^\circ_1$	745.165	20	134198.4	$3d\ ^3P_2-4p\ ^3F^\circ_3$
				749.641	40	133397.1	$3d\ ^3P_2-4p\ ^3D^\circ_3$
684.450	100	146102.7	$3d\ ^3F_3-4p\ ^3D^\circ_2$	750.110	150	133313.7	$3d\ ^1D_2-4p\ ^1D^\circ_2$
691.530	100	144606.8	$3d\ ^1D_1-4p\ ^1P^\circ_1$	750.809	40	133189.6	$3d\ ^3P_1-4p\ ^3D^\circ_2$
693.128	50	144273.4	$3d\ ^3F_2-4p\ ^1D^\circ_2$	751.908	30	132995.0	$3d\ ^3P_0-4p\ ^3D^\circ_1$
699.497	30	142959.8	$3d\ ^1D_2-4p\ ^1F^\circ_3$	752.038	30	132972.0	$3d\ ^3P_2-4p\ ^3D^\circ_2$
702.035	1	142443.0	$3d\ ^3P_0-4p\ ^1P^\circ_1$	752.568	20	132878.3	$3d\ ^3P_1-4p\ ^3D^\circ_1$
711.911	20	140467.0	$3d\ ^1D_2-4p\ ^3P^\circ_1$	778.433	tr	128463.2	$3d\ ^1G_4-4p\ ^3D^\circ_3$

TABLE 3. *Classified lines of* V IV—Continued

λ vac.	Intensity	Wave number	Classification	λ vac.	Intensity	Wave number	Classification
884.146	30	113103.4	$3d\,^1S_0-4p\,^1P^\circ_1$	1326.807	5	75368.9	$4p\,^3P^\circ_1-4d\,^3P_2$
1071.054	20	93366.0	$4p\,^1D^\circ_2-5s\,^1D_2$	1329.288	10	75228.2	$4p\,^3P^\circ_2-4d\,^3P_2$
1086.382	5	92048.6	$4p\,^1D^\circ_2-5s\,^3D_2$	1329.968	10	75189.8	$4p\,^3P^\circ_1-4d\,^3P_1$
1096.375	2	91209.7	$4p\,^3D^\circ_2-5s\,^1D_2$	1330.355	10	75167.9	$4p\,^3P^\circ_0-4d\,^3P_1$
1110.720	2	90031.7	$4p\,^3D^\circ_1-5s\,^3D_1$	1331.665	tr	75094.0	$4p\,^3P^\circ_1-4d\,^3P_0$
1112.199	5	89912.0	$4p\,^3D^\circ_3-5s\,^3D_3$	1332.459	3	75049.2	$4p\,^3P^\circ_2-4d\,^3P_1$
1112.436	5	89892.8	$4p\,^3D^\circ_2-5s\,^3D_2$	1334.493	( )	74934.8	$4p\,^3F^\circ_4-4d\,^3F_4$
1127.836	20	88665.4	$4p\,^3F^\circ_3-5s\,^3D_2$	1339.335	5	74663.9	$4p\,^3F^\circ_4-4d\,^3F_3$
1131.255	20	88397.4	$4p\,^3F^\circ_4-5s\,^3D_3$	1344.493	tr	74377.5	$4p\,^3P^\circ_1-4d\,^1D_2$
1194.462	20	83719.7	$4p\,^1F^\circ_3-5s\,^1D_2$	1347.030	1	74237.4	$4p\,^3P^\circ_2-4d\,^1D_2$
1226.523	60	81531.3	$4p\,^1D^\circ_2-4d\,^1D_2$	1355.131	80	73793.6	$4p\,^1F^\circ_3-4d\,^1G_4$
1242.248	3	80499.2	$4p\,^3D^\circ_1-4d\,^3P_1$	1356.529	10	73717.6	$4p\,^1D^\circ_2-4d\,^1P_1$
1243.718	10	80404.1	$4p\,^3D^\circ_1-4d\,^3P_0$	1391.105	20	71885.3	$4p\,^1F^\circ_3-4d\,^1D_2$
1244.287	2	80367.3	$4p\,^3D^\circ_2-4d\,^3P_2$	1395.001	60	71684.5	$4p\,^1D^\circ_2-4d\,^1F_3$
1247.069	30	80188.0	$4p\,^3D^\circ_2-4d\,^3P_1$	1400.416	5	71407.3	$4p\,^3D^\circ_2-4d\,^3G_3$
1250.918	20	79941.3	$4p\,^3D^\circ_3-4d\,^3P_2$	1403.618	8	71244.4	$4p\,^3D^\circ_3-4d\,^3G_4$
1271.153	2	78668.7	$4p\,^3F^\circ_2-4d\,^1D_2$	1408.639	8	70990.5	$4p\,^3D^\circ_1-4d\,^3D_2$
1272.972	30	78556.3	$4p\,^1P^\circ_1-4d\,^1S_0$	1410.018	8	70921.1	$4p\,^3D^\circ_3-4d\,^3D_2$
1273.529	10	78522.0	$4p\,^1D^\circ_2-4d\,^3F_2$	1412.686	20	70787.1	$4p\,^3D^\circ_1-4d\,^3D_1$
1304.173	30	76676.9	$4p\,^3D^\circ_1-4d\,^3F_2$	1414.409	50	70700.9	$4p\,^3F^\circ_2-4d\,^3G_3$
1305.420	40	76603.7	$4p\,^3D^\circ_2-4d\,^3F_3$	1414.842	20	70679.3	$4p\,^3D^\circ_2-4d\,^3D_2$
1308.061	50	76449.0	$4p\,^3D^\circ_3-4d\,^3F_4$	1418.533	30	70495.4	$4p\,^3D^\circ_3-4d\,^3D_3$
1309.502	10	76364.9	$4p\,^3D^\circ_2-4d\,^3F_2$	1418.921	10	70476.1	$4p\,^3D^\circ_2-4d\,^3D_1$
1312.717	20	76177.9	$4p\,^3D^\circ_3-4d\,^3F_3$	1419.580	80	70443.4	$4p\,^3F^\circ_3-4d\,^3G_4$
1317.566	5	75897.5	$4p\,^3F^\circ_2-4d\,^3F_3$	1423.420	10	70253.3	$4p\,^3D^\circ_3-4d\,^3D_2$
1321.719	10	75659.0	$4p\,^3F^\circ_2-4d\,^3F_2$	1423.719	30	70238.6	$4p\,^1P^\circ_1-4d\,^1D_2$
1321.917	10	75647.7	$4p\,^3F^\circ_3-4d\,^3F_4$	1424.197	tr	70215.0	$4p\,^3F^\circ_2-4d\,^3D_3$
1326.666	5	75376.9	$4p\,^3F^\circ_3-4d\,^3F_3$	1424.916	10	70179.4	$4p\,^3F^\circ_3-4d\,^3G_3$

TABLE 3. *Classified lines of* V IV—Continued

λ vac.	Intensity	Wave number	Classification	λ vac.	Intensity	Wave number	Classification
1426.654	100	70094.1	$4p\ ^3F^\circ_4-4d\ ^3G_5$	1963.103	300	50939.8	$4s\ ^3D_1-4p\ ^3F^\circ_2$
1429.114	10	69973.4	$4p\ ^3F^\circ_2-4d\ ^3D_2$	1966.244	20	50858.4	$4s\ ^3D_3-4p\ ^3F^\circ_3$
1433.276	1	69770.2	$4p\ ^3F^\circ_2-4d\ ^3D_1$	1971.471	40	50723.5	$4s\ ^3D_2-4p\ ^3F^\circ_2$
1434.092	15	69730.5	$4p\ ^3F^\circ_4-4d\ ^3G_4$	1982.422	15	50443.3	$4s\ ^3D_2-4p\ ^3D^\circ_3$
1434.842	15	69694.1	$4p\ ^3F^\circ_3-4d\ ^3D_3$	1990.712	40	50233.3	$4s\ ^3D_1-4p\ ^3D^\circ_2$
1439.834	1	69452.5	$4p\ ^3F^\circ_3-4d\ ^3D_2$	1997.722	500	50057.0	$4s\ ^3D_3-4p\ ^3D^\circ_3$
1447.120	tr	69102.8	$4p\ ^3D^\circ_3-4d\ ^1F_3$	1999.320	200	50017.0	$4s\ ^3D_2-4p\ ^3D^\circ_2$
1449.681	20	68980.7	$4p\ ^3F^\circ_4-4d\ ^3D_3$	λ air			
1451.042	30	68916.0	$4p\ ^3P^\circ_1-4d\ ^3S_1$	2002.480	100	49921.9	$4s\ ^3D_1-4p\ ^3D^\circ_1$
1451.496	10	68894.5	$4p\ ^3P^\circ_0-4d\ ^3S_1$	2011.180	40	49706.0	$4s\ ^3D_2-4p\ ^3D^\circ_1$
1454.000	40	68775.8	$4p\ ^3P^\circ_2-4d\ ^3S_1$	2014.199	40	49631.5	$4s\ ^3D_3-4p\ ^3D^\circ_2$
1520.142	60	65783.3	$4p\ ^3P^\circ_2-4d\ ^3D_3$	2027.144	1	49314.6	$4d\ ^1F_3-4f\ ^3D^\circ_3$
1522.493	40	65681.7	$4p\ ^3P^\circ_1-4d\ ^3D_2$	2042.454	20 *H*	48945.0	$4d\ ^1F_3-4f\ ^1F^\circ_3$
1525.756	10	65541.3	$4p\ ^3P^\circ_2-4d\ ^3D_2$	2060.113	tr *H*	48525.5	$4d\ ^1F_3-4f\ ^1D^\circ_2$
1527.223	15	65478.3	$4p\ ^3P^\circ_1-4d\ ^3D_1$	2063.563	2 *H*	48444.4	$4d\ ^1F_3-4f\ ^3G^\circ_4$
1527.721	15	65457.0	$4p\ ^3P^\circ_0-4d\ ^3D_1$	2079.300	30	48077.8	$4s\ ^3D_1-4p\ ^1D^\circ_2$
1601.915	80	62425.3	$4p\ ^1P^\circ_1-4d\ ^1P_1$	2084.433	20 *H*	47959.4	$4d\ ^3D_2-4f\ ^3D^\circ_2$
1611.879	80	62039.4	$4p\ ^1F^\circ_3-4d\ ^1F_3$	2086.073	30 *H*	47921.7	$4d\ ^3D_3-4f\ ^3D^\circ_3$
1806.184	80	55365.3	$4s\ ^1D_1-4p\ ^1P^\circ_1$	2088.737	50 *h*	47860.6	$4s\ ^3D_2-4p\ ^1D^\circ_2$
1809.854	60	55253.1	$4s\ ^3D_1-4p\ ^3P^\circ_0$	2105.709	tr	47474.9	$4s\ ^3D_3-4p\ ^1D^\circ_2$
1810.566	30	55231.3	$4s\ ^3D_1-4p\ ^3P^\circ_1$	2106.560	2	47455.7	$4s\ ^1D_2-4p\ ^3F^\circ_3$
1813.050	50	55155.7	$4s\ ^3D_2-4p\ ^3P^\circ_2$	2120.052	40 *H*	47153.7	$4d\ ^1F_3-4f\ ^1G^\circ_4$
1817.676	100	55015.3	$4s\ ^3D_2-4p\ ^3P^\circ_1$	2129.934	30	46935.0	$4s\ ^1D_2-4p\ ^3F^\circ_2$
1825.836	200	54769.4	$4s\ ^3D_3-4p\ ^3P^\circ_2$	2136.330	10 *h*	46794.5	$4d\ ^3D_2-4f\ ^3G^\circ_3$
1861.558	300	53718.4	$4s\ ^1D_2-4p\ ^1F^\circ_3$	2137.741	20 *h*	46763.6	$4d\ ^3D_3-4f\ ^3F^\circ_4$
1939.065	500	51571.2	$4s\ ^3D_3-4p\ ^3F^\circ_4$	2141.199	40 *H*	46688.1	$4d\ ^3D_1-4f\ ^3F^\circ_2$
1946.772	5	51367.1	$4s\ ^1D_2-4p\ ^3P^\circ_2$	2146.828	50 *H*	46565.7	$4d\ ^3G_3-4f\ ^3G^\circ_4$
1951.432	400	51244.4	$4s\ ^3D_2-4p\ ^3F^\circ_3$	2149.852	20 *H*	46500.2	$4d\ ^3D_2-4f\ ^3F^\circ_3$

TABLE 3. *Classified lines of* V IV—Continued

λ air	Intensity	Wave number	Classification	λ air	Intensity	Wave number	Classification
2150.231	40 *H*	46492.0	$4d\,^3G_4-4f\,^3G^\circ_5$ $4d\,^1P_1-4f\,^1D^\circ_2$	2384.729	10 *H*	41920.7	$4f\,^3G^\circ_4-5g\,[3\frac{1}{2}]_3$
2151.087	20 *h*	46473.5	$4d\,^3D_3-4f\,^3H^\circ_4$	2387.663	3 *H*	41869.2	$4d\,^3F_3-4f\,^1F^\circ_3$
2155.336	100 *H*	46381.9	$4d\,^3G_5-4f\,^3H^\circ_6$	2395.450	10 *H*	41733.1	$4d\,^1F_3-5p\,^1F^\circ_3$
2159.055	10 *H*	46302.0	$4d\,^3G_4-4f\,^3G^\circ_4$	2402.855	5 *H*	41604.5	$4f\,^3D^\circ_3-5g\,[4\frac{1}{2}]_4$
2160.222	20 *H*	46277.0	$4d\,^3G_3-4f\,^3F^\circ_4$	2413.256	20 *H*	41425.2	$4f\,^3G^\circ_3-5g\,[3\frac{1}{2}]_4$
2162.498	30	46228.3	$4s\,^1D_2-4p\,^3D^\circ_2$	2413.524	5 *H*	41420.6	$4f\,^1F^\circ_3-5g\,[3\frac{1}{2}]_3$
2167.200	20 *H*	46128.0	$4d\,^3G_5-4f\,^3G^\circ_5$	2416.552	30 *h*	41368.7	$4d\,^3F_3-4f\,^3G^\circ_4$
2170.384	(40 *H*)	46060.4	$4d\,^3G_4-4f\,^3H^\circ_5$	2421.317	50 *h*	41287.3	$4d\,^3F_4-4f\,^3G^\circ_5$
2173.893	10 *H*	45986.0	$4d\,^3G_3-4f\,^3H^\circ_4$	2431.885	30 *h*	41107.9	$4d\,^3F_2-4f\,^3G^\circ_3$
2186.394	tr *H*	45723.1	$4d\,^3G_4-4f\,^3H^\circ_4$	2432.518	10 *h*	41097.2	$4d\,^3F_4-4f\,^3G^\circ_4$
2187.562	5 *H*	45698.7	$4d\,^3G_5-4f\,^3H^\circ_5$	2433.530	50 *h*	41080.1	$4d\,^3F_3-4f\,^3F^\circ_4$
2195.388	10 *H*	45535.8	$4d\,^3S_1-4f\,^3P^\circ_2$	2446.071	30 *h*	40869.5	$4d\,^3F_3-4f\,^3G^\circ_3$
2268.298	500	44072.3	$4s\,^1D_2-4p\,^1D^\circ_2$	2446.802	50 *h*	40857.3	$4d\,^3F_4-4f\,^3H^\circ_5$
2313.236	1 *H*	43216.2	$4f\,^1G^\circ_4-5g\,[3\frac{1}{2}]_4$	2449.404	40 *h*	40813.9	$4d\,^3F_2-4f\,^3F^\circ_3$
2321.962	1 *H*	43053.8	$4f\,^3H^\circ_4-5g\,[4\frac{1}{2}]_4$	2449.723	20 *h*	40808.6	$4d\,^3F_4-4f\,^3F^\circ_4$
2322.259	5 *H*	43048.3	$4f\,^3H^\circ_4-5g\,[4\frac{1}{2}]_5$	2450.329	20 *h*	40798.5	$4d\,^3F_2-4f\,^3F^\circ_2$
2326.291	3 *H*	42973.7	$4f\,^3G^\circ_3-5g\,[4\frac{1}{2}]_4$	2450.869	50 *h*	40789.5	$4d\,^3F_3-4f\,^3H^\circ_4$
2338.032	10 *H*	42757.9	$4f\,^3F^\circ_4-5g\,[4\frac{1}{2}]_5$	2463.796	10 *h*	40575.5	$4d\,^3F_3-4f\,^3F^\circ_3$
2339.548	20 *H*	42730.2	$4f\,^3F^\circ_2-5g\,[3\frac{1}{2}]_3$	2464.720	2 *h*	40560.3	$4d\,^3F_3-4f\,^3F^\circ_2$
2340.140	10 *H*	42719.4	$4f\,^3F^\circ_3-5g\,[3\frac{1}{2}]_4$	2467.287	20 *h*	40518.1	$4d\,^3F_4-4f\,^3H^\circ_4$
2340.704	5 *H*	42709.1	$4f\,^3H^\circ_5-5g\,[4\frac{1}{2}]_5$	2478.119	1 *H*	40341.0	$4d\,^3D_3-5p\,^1F^\circ_3$
2351.934	5 *H*	42505.2	$4f\,^3H^\circ_4-5g\,[3\frac{1}{2}]_4$	2480.739	30 *h*	40298.4	$4d\,^1P_1-5p\,^1P^\circ_1$
2353.639	3 *H*	42474.4	$4f\,^3G^\circ_4-5g\,[4\frac{1}{2}]_4$	2494.351	20 *h*	40078.5	$4d\,^3F_3-4f\,^1G^\circ_4$
2356.369	10 *H*	42425.2	$4f\,^3G^\circ_3-5g\,[3\frac{1}{2}]_4$	2497.049	10 *h*	40035.2	$4d\,^3D_2-5p\,^3P^\circ_2$
2356.624	5 *H*	42420.6	$4f\,^3G^\circ_3-5g\,[3\frac{1}{2}]_3$	2506.969	10 *h*	39876.8	$4d\,^3D_1-5p\,^3P^\circ_1$
2364.512	1 *H*	42279.1	$4f\,^3G^\circ_5-5g\,[4\frac{1}{2}]_5$	2509.606	5 *h*	39834.9	$4d\,^3D_1-5p\,^3P^\circ_0$
2378.290	1 *H*	42034.2	$4d\,^3F_3-4f\,^3D^\circ_2$	2511.377	1 *H*	39806.8	$4d\,^3F_4-4f\,^1G^\circ_4$
2381.712	10 *H*	41973.8	$4f\,^1F^\circ_3-5g\,[4\frac{1}{2}]_4$	2512.242	( )	39793.1	$4d\,^3D_3-5p\,^3P^\circ_2$

TABLE 3. *Classified lines of* V IV—Continued

λ air	Intensity	Wave number	Classification	λ air	Intensity	Wave number	Classification
2519.803	20 *h*	39673.7	$4d\,^3D_2-5p\,^3P^\circ_1$	2650.613	8 *h*	37715.9	$4d\,^3D_2-5p\,^3D^\circ_1$
2530.520	2 *h*	39505.7	$4d\,^1F_3-5p\,^3F^\circ_2$	2655.408	50 *H*	37647.8	$4d\,^3G_4-5p\,^3F^\circ_3$
2532.982	20 *h*	39467.3	$4d\,^1D_2-4f\,^3D^\circ_3$	2656.868	50 *H*	37627.1	$4d\,^3G_3-5p\,^3F^\circ_2$
2546.228	20 *h*	39262.0	$4d\,^3P_1-4f\,^3P^\circ_2$	2667.837	1 *h*	37472.4	$4d\,^1P_1-5p\,^3F^\circ_2$
2550.971	2 *H*	39189.0	$4d\,^1F_3-5p\,^3D^\circ_2$	2669.483	10 *h*	37449.3	$5p\,^1D^\circ_2-6s\,^3D_2$
2556.915	50 *h*	39097.9	$4d\,^1D_2-4f\,^1F^\circ_3$	2703.933	20 *H*	36972.2	$5p\,^3D^\circ_3-6s\,^3D_3$ $5p\,^3D^\circ_1-6s\,^3D_1$
2557.897	15 *h*	39082.9	$4d\,^3P_2-4f\,^3P^\circ_2$				
2569.812	10 *h*	38901.7	$4d\,^3D_3-5p\,^3F^\circ_4$	2716.594	20 *h*	36799.9	$4d\,^3S_1-5p\,^3P^\circ_2$
2570.724	80 *h*	38887.9	$4d\,^1G_4-4f\,^1H^\circ_5$	2718.722	2 *h*	36771.1	$5p\,^3D^\circ_2-6s\,^3D_2$
2584.636	40 *h*	38678.6	$4d\,^1D_2-4f\,^1D^\circ_2$	2727.780	1 *h*	36649.0	$5p\,^3D^\circ_2-6s\,^3D_1$
2587.258	10 *h*	38639.4	$4d\,^3D_2-5p\,^3F^\circ_3$	2740.545	5 *h*	36478.3	$4d\,^1P_1-5p\,^1D^\circ_2$
2592.747	( )	38557.6	$4d\,^3D_1-5p\,^3F^\circ_2$	2740.966	5 *h*	36472.7	$5p\,^3D^\circ_3-6s\,^3D_2$
2595.858	20 *H*	38511.4	$4d\,^1F_3-5p\,^1D^\circ_2$	2743.523	20 *h*	36438.7	$4d\,^3S_1-5p\,^3P^\circ_1$
2596.761	15 *h*	38498.0	$4d\,^3P_0-4f\,^3D^\circ_1$	2751.528	10 *h*	36332.7	$5p\,^3F^\circ_2-6s\,^3D_1$
2598.287	30 *h*	38475.4	$4d\,^3P_2-4f\,^3D^\circ_3$	2763.860	15 *h*	36170.6	$5p\,^3F^\circ_3-6s\,^3D_2$
2599.983	30 *h*	38450.3	$4d\,^3P_1-4f\,^3D^\circ_2$	2764.219	15 *h*	36165.9	$5p\,^3F^\circ_4-6s\,^3D_3$
2603.213	10 *h*	38402.6	$4d\,^3P_1-4f\,^3D^\circ_1$	2824.131	20 *h*	35398.7	$4d\,^1G_4-4f\,^1G^\circ_4$
2607.633	5 *h*	38337.5	$4d\,^3D_2-5p\,^3D^\circ_3$	2834.089	5 *H*	35274.3	$5p\,^3P^\circ_2-6s\,^3D_3$
2610.323	10 *h*	38298.0	$5p\,^1D^\circ_2-6s\,^1D_2$	2850.160	2 *H*	35075.4	$5p\,^1F^\circ_3-6s\,^1D_2$
2614.159	1 *h*	38241.8	$4d\,^3D_1-5p\,^3D^\circ_2$	2899.575	2 *h*	34477.7	$5p\,^1P^\circ_1-6s\,^1D_2$
2620.320	25 *h*	38151.9	$4d\,^3G_4-5p\,^3F^\circ_4$	3034.27	10	32947.3	$4d\,^3F_4-5p\,^3F^\circ_4$
2623.483	15 *h*	38105.9	$4d\,^3P_2-4f\,^1F^\circ_3$	3052.346	10	32752.16	$5p\,^1D^\circ_2-5d\,^1D_2$
2624.213	50 *h*	38095.3	$4d\,^3D_3-5p\,^3D^\circ_3$	3055.864	5	32714.46	$4d\,^3F_3-5p\,^3F^\circ_3$
2628.090	20 *h*	38039.1	$4d\,^3D_2-5p\,^3D^\circ_2$	3060.146	5	32668.68	$4d\,^3F_2-5p\,^3F^\circ_2$
2636.401	30 *h*	37919.2	$4d\,^3D_1-5p\,^3D^\circ_1$	3067.85	tr?	32586.6	$5p\,^3D^\circ_2-5d\,^3P_2$
2636.936	10 *h*	37911.5	$4d\,^3G_3-5p\,^3F^\circ_3$	3077.476	15	32484.72	$4d\,^1D_2-5p\,^1P^\circ_1$
2644.946	8 *h*	37796.7	$4d\,^3D_3-5p\,^3D^\circ_2$	3084.36	1	32412.2	$4d\,^3F_3-5p\,^3D^\circ_3$
2645.541	80 *H*	37788.2	$4d\,^3G_5-5p\,^3F^\circ_4$	3096.226	2	32288.01	$5p\,^3D^\circ_3-5d\,^3P_2$
				3110.416	30	32140.72	$4d\,^3F_4-5p\,^3D^\circ_3$

TABLE 3. *Classified lines of* V IV—Continued

λ air	Intensity	Wave number	Classification	λ air	Intensity	Wave number	Classification
3113.022	25	32113.81	$4d\,^3F_3-5p\,^3D^\circ_2$	3489.51	tr	28649.1	$4d\,^3P_2-5p\,^3D^\circ_3$
3121.304	10	32028.60	$4d\,^3F_2-5p\,^3D^\circ_1$	3490.913	30	28637.61	$5p\,^3F^\circ_2-5d\,^3G_3$
3135.192	20	31886.73	$4d\,^1D_2-5p\,^1F^\circ_3$	3496.419	50	28592.51	$5p\,^3F^\circ_3-5d\,^3G_4$
3227.507	15	30974.72	$5p\,^3D^\circ_1-5d\,^3F_2$	3500.57	1 *H*	28558.6	$5p\,^3P^\circ_0-5d\,^3S_1$
3229.92	tr	30951.6	$5p\,^3P^\circ_2-5d\,^3P_1$	3504.10	1 *H*	28529.8	$4d\,^3P_1-5p\,^3D^\circ_2$
3234.251	20	30910.14	$5p\,^3D^\circ_2-5d\,^3F_3$	3505.70	10	28516.8	$5p\,^3P^\circ_1-5d\,^3S_1$
3241.460	40 *H*	30841.40	$5p\,^3D^\circ_3-5d\,^3F_4$	3514.25	80 *h*	28447.4	$5p\,^3F^\circ_4-5d\,^3G_5$
3268.077	15 *h*	30590.22	$5p\,^3P^\circ_2-5d\,^3P_2$	3525.89	tr *H*	28353.5	$5p\,^3F^\circ_3-5d\,^3G_3$
3274.931	5 *H*	30526.20	$4d\,^3P_1-5p\,^3P^\circ_2$	3545.98	tr *h*	28192.9	$5p\,^3F^\circ_3-5d\,^3D_2$
3284.560	50	30436.71	$5p\,^1F^\circ_3-5d\,^1G_4$	3550.718	10	28155.27	$5p\,^3P^\circ_2-5d\,^3S_1$
3294.259	40	30347.10	$4d\,^3P_2-5p\,^3P^\circ_2$	3681.04	10	27158.5	$5p\,^3P^\circ_1-5d\,^3D_2$
3295.501	10	30335.66	$5p\,^3F^\circ_2-5d\,^3F_2$	3691.236	15	27083.46	$5p\,^3P^\circ_2-5d\,^3D_3$
3298.371	20	30309.27	$5p\,^3F^\circ_3-5d\,^3F_3$	3833.74	15 *H*	26076.8	$5p\,^1P^\circ_1-5d\,^1P_1$
3303.719	5	30260.21	$4d\,^3P_0-5p\,^3P^\circ_1$	4136.72	5 *H*	24166.9	$4d\,^1S_0-5p\,^1P^\circ_1$
3314.175	2	30164.74	$4d\,^3P_1-5p\,^3P^\circ_1$	4450.75	tr	22461.8	$4f\,^3D^\circ_3-5d\,^3P_2$
3318.788	5 *h*	30122.82	$4d\,^3P_1-5p\,^3P^\circ_0$	4479.195	2 *h*	22319.18	$4f\,^1F^\circ_3-5d\,^1D_2$
3328.527	30	30034.68	$5p\,^3F^\circ_4-5d\,^3F_4$	4505.17	1 *H*	22190.5	$4f\,^3F^\circ_3-5d\,^3F_2$
3333.986	15	29985.50	$4d\,^3P_2-5p\,^3P^\circ_1$	4508.67	2 *H*	22173.3	$4f\,^3F^\circ_4-5d\,^3F_4$
3334.79	60	29978.3	$4d\,^1G_4-5p\,^1F^\circ_3$	4518.58	8 *H*	22124.6	$4f\,^3H^\circ_5-5d\,^3F_4$
3385.336	1	29530.69	$5p\,^1F^\circ_3-5d\,^1D_2$	4565.63	tr *H*	21896.6	$4f\,^3G^\circ_3-5d\,^3F_2$
3433.52	tr	29116.3	$5p\,^3D^\circ_1-5d\,^3D_2$	4608.15	1 *H*	21694.6	$4f\,^3G^\circ_5-5d\,^3F_4$
3448.410	50	28990.57	$5p\,^1D^\circ_2-5d\,^1F_3$	4616.57	1 *H*	21655.0	$4f\,^3G^\circ_4-5d\,^3F_3$
3452.741	3 *H*	28954.20	$5p\,^3D^\circ_2-5d\,^3G_3$	4643.985	10 *H*	21527.20	$4f\,^1H^\circ_5-5d\,^1G_4$
3455.325	15	28932.55	$5p\,^1P^\circ_1-5d\,^1D_2$	4801.54	2 *H*	20820.8	$5s\,^3D_2-5p\,^3P^\circ_2$
3459.40	10 *h*	28898.5	$5p\,^3D^\circ_1-5d\,^3D_1$	4828.990	1 *H*	20702.48	$4d\,^1S_0-5p\,^3D^\circ_1$
3471.989	20	28793.69	$5p\,^3D^\circ_2-5d\,^3D_2$	4841.26	20 *h*	20650.0	$5s\,^1D_2-5p\,^1P^\circ_1$
3473.458	20	28781.51	$5p\,^3D^\circ_3-5d\,^3D_3$	4845.21	3 *h*	20633.2	$5s\,^3D_1-5p\,^3P^\circ_1$
3487.63	30	28664.6	$4d\,^1D_2-5p\,^1D^\circ_2$	4855.05	3 *H*	20591.3	$5s\,^3D_1-5p\,^3P^\circ_0$

TABLE 3. *Classified lines of* V IV—Continued

λ air	Intensity	Wave number	Classification	λ air	Intensity	Wave number	Classification
4886.36	20 *h*	20459.4	$5s\ ^3D_2-5p\ ^3P^\circ_1$	5175.950	30 *h*	19314.75	$5s\ ^3D_1-5p\ ^3F^\circ_2$
4891.52	tr *h*	20437.8	$4f\ ^3G_3-5d\ ^3G^\circ_4$	5222.93	5 *H*	19141.0	$5s\ ^3D_2-5p\ ^3F^\circ_2$
4899.56	tr *h*	20404.3	$4f\ ^3H^\circ_4-5d\ ^3D_3$	5227.89	10 *H*	19122.8	$5s\ ^3D_2-5p\ ^3D^\circ_2$
4906.280	40 *h*	20376.35	$5s\ ^3D_3-5p\ ^3P^\circ_2$	5262.164	50 *h*	18998.3	$5s\ ^3D_1-5p\ ^3D^\circ_2$
4913.083	10 *h*	20348.14	$4f\ ^1G^\circ_4-5d\ ^1F_3$	5267.045	10 *h*	18980.69	$5s\ ^3D_3-5p\ ^3F^\circ_3$
4916.94	2 *H*	20332.2	$4f\ ^3F^\circ_3-5d\ ^3D_2$	5310.77	20 *H*	18824.4	$5s\ ^3D_2-5p\ ^3D^\circ_2$
4954.408	1 *h*	20178.41	$4f\ ^3H^\circ_5-5d\ ^3G_4$	5352.320	60 *h*	18678.29	$5s\ ^3D_3-5p\ ^3D^\circ_3$
4966.38	2 *h*	20129.8	$4f\ ^3G^\circ_3-5d\ ^3F_2$	5353.090	25 *H*	18675.60	$5s\ ^3D_1-5p\ ^3D^\circ_1$
4970.348	3 *h*	20113.70	$4f\ ^3F^\circ_4-5d\ ^3D_3$	5387.210	3 *h*	18557.32	$4f\ ^1F^\circ_3-5d\ ^1F_3$
4971.941	1 *h*	20107.26	$4f\ ^3G^\circ_5-5d\ ^3G_5$	5496.67	1 *H*	18187.8	$4f\ ^3D^\circ_3-5d\ ^1F_3$
4985.653	50 *h*	20051.96	$5s\ ^1D_2-5p\ ^1F^\circ_3$	5509.19	30 *H*	18146.4	$5s\ ^3D_2-5p\ ^1D^\circ_2$
5035.460	10 *h*	19853.62	$4f\ ^3H^\circ_6-5d\ ^3G_5$	5520.63	2 *H*	18108.9	$5s\ ^1D_2-5p\ ^3F^\circ_3$
5074.90	5 *H*	19699.3	$4f\ ^3G^\circ_4-5d\ ^3G_3$	5608.71	20 *H*	17824.4	$5s\ ^1D_2-5p\ ^3F^\circ_2$
5130.78	50 *H*	19484.8	$5s\ ^3D_3-5p\ ^3F^\circ_4$	5710.10	8 *H*	17508.0	$5s\ ^1D_2-5p\ ^3D^\circ_2$
5146.502	40 *h*	19425.26	$5s\ ^3D_2-5p\ ^3F^\circ_3$	5940.12	40 *H*	16830.0	$5s\ ^1D_2-5p\ ^1D^\circ_2$

TABLE 4. *Energy levels and limits of the* ns *series of* V IV

Electron	Desig.	Energy level	Term value	n^*	Limit	I.P.
4*s*	$^3D_3$	96798.0	280538.0	2.50172		
5*s*	$^3D_3$	236766.9	140569.1	3.53419	377336	376716
6*s*	$^3D_3$	292417.4	84918.6	4.54709		
4*s*	$^3D_2$	96412.1	280353.9	2.50254		
5*s*	$^3D_2$	236322.4	140443.6	3.53577	376766	376766
6*s*	$^3D_2$	291918.1	84847.9	4.54898		
4*s*	$^3D_1$	96196.1	280515.9	2.50182		
5*s*	$^3D_1$	236148.6	140563.6	3.53426	376712	376712
6*s*	$^3D_1$	291796.0	84916.0	4.54716		
4*s*	$^1D_2$	100200.7	277134.3	2.51704		
5*s*	$^1D_2$	237638.8	139696.2	3.54522	377335	376715
6*s*	$^1D_2$	292766.7	84568.3	4.55651		

4. V v

As a by-product of the V IV analysis, 8 lines of the fifth spectrum of vanadium were identified in the region 675 to 2200 Å. With the present measurements, the levels published in A.E.L. [2] giving combinations in this part of the spectrum have been corrected and the ^{2}D term of the $4d$ configuration has been found. The new values based on the assumption that $4p\,^2P^\circ_{1\frac{1}{2}} = 207617.0\ cm^{-1}$ is correct, are the following:

New levels of V v

Config.	Desig.	J	Level
$4s$	^{2}S	$0\frac{1}{2}$	148100.1
$4p$	^{2}P°	$0\frac{1}{2}$	206350.6
$4d$	^{2}D	$1\frac{1}{2}$	293859.5
		$2\frac{1}{2}$	294004.3
$5s$	^{2}S	$0\frac{1}{2}$	328173.5
$4f$	^{2}F°	$3\frac{1}{2}$	349210.6

the observed combinations among them are as follows:

Newly classified lines of V v

λ	Int.	Wave number	Classification
820.866	15	121822.5	$4p\,^2P^\circ_{01/2} - 5s\,^2S_{01/2}$
829.483	20	120557.0	$4p\,^2P^\circ_{11/2} - 5s\,^2S_{01/2}$
1142.741	40	87508.9	$4p\,^2P^\circ_{01/2} - 4d\,^2D_{11/2}$
1157.577	50	86387.3	$4p\,^2P^\circ_{11/2} - 4d\,^2D_{21/2}$
1159.520	10	86242.6	$4p\,^2P^\circ_{11/2} - 4d\,^2D_{11/2}$
1680.199	100	59516.9	$4s\,^2S_{01/2} - 4p\,^2P^\circ_{11/2}$
1716.722	50	58250.5	$4s\,^2S_{01/2} - 4p\,^2P^\circ_{01/2}$
1811.388	40 *h*	55206.3	$4d\,^2D_{21/2} - 4f\,^2F^\circ_{31/2}$

The author is indebted to A. G. Shenstone for the many facilities placed at her disposal to carry out part of the experimental work on which this paper is based, and to R. Velasco for the use of his hollow cathode spectrograms and for many helpful discussions during the course of this investigation. Thanks are also due to Mrs. Charlotte Moore-Sitterly (NBS) for her kind cooperation in the correction of the English manuscript and during the editorial stages of this paper.

(Paper 72A4–503)

6. References

[1] White, H. E., Phys. Rev. **33,** 538 (1929).
[2] Edlén, B., See C. E. Moore, Atomic Energy Levels, NBS Circ. 467, Vol. **I** (1949).
[3] Shenstone, A. G., J. Opt. Soc. Am. **44,** 749 (1954).
[4] Iglesias, L. and Velasco, R., An. Soc. Esp. Fis. Quim. **54A,** 83 (1958).
[5] Joint Commission for Spectroscopy, J. Opt. Soc. Am. **43,** 410 (1953).
[6] Shadmi, Y., J. Opt. Soc. Am. **56,** 647 (1966).
[7] Edlén, B., unpublished material (1967).
[8] Edlén, B., See C. E. Moore, Atomic Energy Levels, NBS Circ. 467, Vol. **II** (1952).

JOURNAL OF RESEARCH of the National Bureau of Standards—A. Physics and Chemistry
Vol. 72A, No. 4, July–August 1968

Variation of Absorptance-Curve Shape With Changes in Pigment Concentration*

Gerald L. Howett

Institute for Basic Standards, National Bureau of Standards, Washington, D.C. 20234

(March 29, 1968)

A complete quantitative analysis is presented of changes in the shape of the spectral absorptance curve of any Beer's-law pigment solution (or other Bouguer's-law material) as concentration of the pigment, or thickness of the solution layer, is varied. The relative absorptance curve, normalized to unit maximum, is taken as defining the shape of the absolute absorptance curve, and the index of shape change is taken to be the difference between the normalized curves. All concentration changes from infinite decrease to infinite increase are covered, with some extreme cases requiring limit methods. Formulas and graphs are given for determining, as a function of concentration change and peak absolute absorptance of the original curve, where along the curve the shape change is greatest, and how large the maximum change is. Implications for color vision theory are discussed and it is shown that the assumption of low peak absorptances ($< 10\%$) for the visual photopigments accounts for the constancy of the color-matching functions for moderate luminances, but not, in itself, for the breakdown of matches at high luminances; while the assumption of high peak absorptances ($\approx 80\%$), although it contradicts recent microspectrophotometric measurements, seems to account for both phenomena.

Key Words: Absorption; adaptation; Beer's law; chromatic adaptation; color vision; concentration; cones; curve shape; high luminance; metameric matches; pigment; photopigment; vision.

1. Introduction

The theory that chromatic adaptation is explainable by changes in the concentrations of the visual photopigments has lost some adherents in recent years to the notion that adaptation is a neural or synaptic phenomenon [1, 2, 3].[1] One of the objections which has been raised [3] to the pigment-concentration theory is that a change in the concentration of a pigment in solution necessarily changes the shape of the absorptance curve of the pigment solution, because of the nonlinear (exponential) character of Beer's Law. A sufficient change in shape of the absorptance curves of the visual photopigments would be behaviorally detectable, since the color-matching functions would be altered. On the other hand, the empirical evidence indicates that the color-matching functions are independent of chromatic adaptation [4] over an unlimited range of chromaticities and a wide, but not unlimited [5, 6] range of luminances, the implication being that the shapes of the absorptance curves of the photopigments do *not* vary significantly with nonextreme changes in the adaptive state.

It appears to be generally understood [7] that the changes in shape of the absorptance curves are not significant if the initial (dark-adapted) concentrations of the photopigments are sufficiently low. The purpose of this paper is to specify quantitatively the nature and extent of the shape changes induced in the absorptance curve of a layer of pigment by changes in the concentration of the pigment (or the thickness of the layer). Although the final treatment will be completely

*A portion of this work (specifically, the single limiting case of complete bleaching) was presented orally at the Spring 1965 meeting of the Optical Society of America in Dallas, Texas [J. Opt. Soc. Am. **55**, 604A (1965)].

[1] Figures in brackets indicate the literature references at the end of this paper.

general and will apply to any real pigment, there are two basic decisions to be made in advance that are determined by the primary purpose of the study, which is investigation of visual photopigments.

The first decision is what is to be meant by the "shape" of a curve. The definition to be developed is based on the convention that multiplying the ordinates of a curve by a constant does not change its "shape." As applied to visual photopigment absorptance curves or the color-matching functions of a colorimetric system, this convention is the appropriate one, because the facts of metamerism (that is, which spectral radiance distributions match in color) would be left unchanged if the spectral absorptance curve of any of the visual photopigments were to be changed by multiplication by a constant factor; and, correspondingly, the predictions of metamers of a colorimetric system are invariant under any scale-factor change in any of the color-matching functions.

These same considerations determine the other basic decision as well: what specific measure of amount of light absorption by a pigment should be used. It is *absorptance* that counts directly in color vision, not any other measure, such as optical density, commonly used in other contexts.

2. Beer's Law

Given a layer of pigment in solution, Beer's Law [7a] permits us to calculate the spectral absorptance, α_λ,[2] of the layer. If c is the concentration of the pigment in the solvent, x is the thickness of the solution layer, and β_λ is the spectral absorption coefficient of the pigment, then the expression for α_λ is:

$$\alpha_\lambda = 1 - \exp(-\beta_\lambda cx), \tag{1}$$

provided we neglect surface reflections, scattering, and the absorptance of the solvent; in other words, if we assume that all light not transmitted by the layer is absorbed by the pigment. In the case of the visual photopigments, the solvent is presumably a clear gel and these simplifying assumptions probably do not introduce too much of a distortion in the analysis.

Now suppose that the action of a bleaching light reduces the concentration of the pigment (or, equivalently, the thickness of the pigmented layer)[3] to $1/n$ times its original value. Then the new absorptance, $\alpha_\lambda^{(n)}$, is given by:

$$\alpha_\lambda^{(n)} = 1 - \exp(-\beta_\lambda cx/n). \tag{2}$$

In the case of the visual photopigments, it is possible that significantly absorbing breakdown products are produced by bleaching, but this investigation will be confined to consideration only of the absorptance of the original pigment.

If we isolate the exponential term in eq (1) and raise both sides to the power $1/n$, the result is:

$$(1-\alpha_\lambda)^{1/n} = [\exp(-\beta_\lambda cx)]^{1/n} \equiv \exp(-\beta_\lambda cx/n); \tag{3}$$

and, from (2) and (3), we see that

$$\exp(-\beta_\lambda cx/n) = 1 - \alpha_\lambda^{(n)} = (1-\alpha_\lambda)^{1/n}. \tag{4}$$

---

[2] In current international practice, a subscript λ denotes a spectral concentration; a dimensionless function of wavelength like absorptance is properly denoted $\alpha(\lambda)$. However, in order to avoid complicating the many equations in this paper with another level of parentheses, the subscript notation will be used throughout. No ambiguity can arise, since no quantity referred to in the paper is a spectral concentration.

[3] This parenthetical alternative should be understood implicitly wherever "concentration" is referred to in the remainder of this paper. Although this paper is phrased in terms of a pigment solution, it should also be understood that all results apply to any pigment suspension, whether a true solution or not, as long as the suspension follows Beer's law; and also to any transmitting substance whatever that follows Bouguer's law.

Thus we conclude from (4) that

$$\alpha_\lambda^{(n)} = 1 - (1 - \alpha_\lambda)^{1/n}. \tag{5}$$

The transformation (5) from α_λ to $\alpha_\lambda^{(n)}$ is order-preserving. That is, if for wavelengths μ and ν,

$$\alpha_\mu > \alpha_\nu, \tag{6}$$

it is also true that

$$\alpha_\mu^{(n)} > \alpha_\nu^{(n)} \qquad (\text{all } n).^4 \tag{7}$$

The proof of this property is equivalent to proving that $\alpha_\lambda^{(n)}$ is a monotonically increasing function of α_λ, for any n, and this is in turn equivalent to showing that the derivative of $\alpha_\lambda^{(n)}$ with respect to α_λ is always positive.

Differentiating (5), we find that

$$\frac{\partial \alpha_\lambda^{(n)}}{\partial \alpha_\lambda} = \frac{(1 - \alpha_\lambda)^{\frac{1}{n} - 1}}{n}. \tag{8}$$

We see that the derivative (8) is indeed always positive, for any (positive) n and any $\alpha_\lambda < 1$. (The fact that the derivative reaches zero at $\alpha_\lambda = 1$, for $n < 1$, is irrelevant to the order-preserving property, since no α_λ can be greater than unity.)

The fact that the transformation preserves order implies in particular that at any wavelength at which α_λ has a maximum or a minimum, $\alpha_\lambda^{(n)}$ has a corresponding maximum or minimum. Thus we know that whatever distortions in the absorptance curve may be produced by a change of pigment concentration, there is no shifting of the wavelengths at which the peaks and valleys occur.

3. Normalized Absorptance Curves

The object of this analysis is to deal quantitatively with the "shapes" of functions.[5] In discussions of vision, and in other contexts where functions are known only to within a scale factor (or where the absolute size of the ordinates is irrelevant to the purpose at hand), it is commonly said that the shape of a function—let us say of wavelength—is unchanged if we multiply the function by a fixed constant at every wavelength. This convention can be used as the basis for formulating a definition of "shape." If we want to find out whether two given functions have the same shape, it is clear that what we want to do is to divide each function by some constant so that both sets of values are reduced to the same scale. The original curves have the same shape if the adjusted curves are identical.

A familiar way of reducing curves to the same scale is to divide each curve by its own maximum value. Another way of describing this procedure is to say that we are "normalizing" each curve so that it will have a maximum of unity.

---

[4] Naturally, negative values of n are excluded as meaningless. Normally, it should be understood that $n > 0$, but the limiting case $n = 0$ (an infinite *increase* in pigment concentration) will be considered where appropriate. It will prove helpful to keep in mind that n is the factor by which the original concentration is *divided*—not multiplied—so that reductions of concentration ("bleaching") are implied by the range $1 < n \leq \infty$ and increases of concentration by the range $0 \leq n < 1$. This choice of meaning for n was dictated by the relatively greater interest in bleaching than in concentration increase in the field of visual pigments.

[5] Technically speaking, it is the curves representing the functions that have shapes, but it is convenient to speak interchangeably of the shape of the curve or the function.

If we let M be the (or a) wavelength at which α_λ has its maximum value, α_M, then we have shown previously that the maximum value of $\alpha_\lambda^{(n)}$ is, for all n, the value of $\alpha_\lambda^{(n)}$ at that same wavelength M. In short, taking note of (5), we may write:

$$\max \alpha_\lambda^{(n)} = \alpha_M^{(n)} = 1-(1-\alpha_M)^{1/n}. \tag{9}$$

Now let us define a normalized function, $\hat{\alpha}_\lambda$, as the function α_λ divided by its maximum value:

$$\hat{\alpha}_\lambda = \alpha_\lambda/\alpha_M, \qquad \alpha_M \neq 0. \tag{10}$$

Similarly, we define a normalized function, $\hat{\alpha}_\lambda^{(n)}$, by:

$$\hat{\alpha}_\lambda^{(n)} = \alpha_\lambda^{(n)}/\max \alpha_\lambda^{(n)} = \frac{1-(1-\alpha_\lambda)^{1/n}}{1-(1-\alpha_M)^{1/n}}, \qquad \alpha_M \neq 0. \tag{11}$$

The case $\alpha_M = 0$ represents a pigment that does not absorb at all ($\alpha_\lambda \equiv 0$). There is little to be gained by defining the normalized functions in this degenerate situation (one can argue for choosing either a constant value of unity or of zero), and it will be assumed tacitly from here on that $\alpha_M > 0$. For the sake of completeness, however, we will consider later the limiting behavior of certain functions as α_M *approaches* zero.

The normalized functions $\hat{\alpha}_\lambda$ and $\hat{\alpha}_\lambda^{(n)}$ are equal to unity (and consequently to each other) at all wavelengths at which α_λ takes on its maximum value. Moreover, the functions are also equal (to zero) at all wavelengths at which $\alpha_\lambda = 0$. The question we are interested in pursuing is how different are $\hat{\alpha}_\lambda$ and $\hat{\alpha}_\lambda^{(n)}$ at other wavelengths?

Before developing an answer to this question, let us first investigate a few important properties of the normalized absorptance curve $\hat{\alpha}_\lambda^{(n)}$ defined by (11).

In Appendix A it is proved that

$$\hat{\alpha}_\lambda^{(p)} < \hat{\alpha}_\lambda^{(q)} \qquad \text{for } p > q \tag{12}$$

[except for wavelengths for which the absorptance, α_λ, is 0 or the maximal value, α_M, in which cases an equality sign replaces the less-than sign in (12)]. In other words, as n increases (concentration decreases), the values of $\hat{\alpha}_\lambda^{(n)}$ become smaller and smaller: the sequence of curves $\hat{\alpha}_\lambda^{(n)}$ is monotonically decreasing. Since all the curves of the sequence $\hat{\alpha}_\lambda^{(n)}$ have a common maximum of unity at the same wavelength(s), a simple statement of the situation is that the normalized absorptance curve (or the shape of the absorptance curve) "narrows" as pigment concentration decreases; or, more precisely, the half-peak width of the primary absorption band covers a smaller wavelength range.

No matter how much the concentration is reduced, the normalized absorptance curve continues to narrow, but the decreases in the values of $\hat{\alpha}^{(n)}$ become smaller and smaller as n grows larger. In fact, the sequence of curves $\hat{\alpha}_\lambda^{(n)}$ approaches a limiting curve, $\hat{\alpha}_\lambda^{(\infty)}$, as n becomes indefinitely larger (concentration approaches zero). If we try to evaluate this limit by letting n approach infinity in the expression (11) for $\hat{\alpha}_\lambda^{(n)}$, we are initially frustrated by the fact that both the numerator and denominator approach zero, the result being indeterminate. The limit can be evaluated, however, by an application of L'Hospital's rule, which says that in such an instance, the limit is unaffected by differentiation of both numerator and denominator. Thus:

$$\hat{\alpha}_\lambda^{(\infty)} = \lim_{n\to\infty} \hat{\alpha}_\lambda^{(n)} = \lim_{n\to\infty} \frac{1-(1-\alpha_\lambda)^{1/n}}{1-(1-\alpha_M)^{1/n}} = \lim_{n\to\infty} \frac{(1-\alpha_\lambda)^{1/n} \ln (1-\alpha_\lambda)}{(1-\alpha_M)^{1/n} \ln (1-\alpha_M)} \tag{13}$$

or

$$\hat{\alpha}_\lambda^{(\infty)} = \frac{\ln (1-\alpha_\lambda)}{\ln (1-\alpha_M)}; \qquad \alpha_M, \alpha_\lambda \neq 1. \tag{14}$$

If *any* amount of pigment is present, the normalized absorptance curve is broader and greater than the limiting curve defined in (14). For sufficiently low concentrations, however, the curves become insignificantly different from the $\hat{\alpha}_\lambda^{(\infty)}$ curve. It should be stressed that this conclusion applies to any absorptance curve whatever.

When any $\alpha_\lambda = 1$, it follows that also $\alpha_M = 1$, since no absorptance can be greater than unity. In that case, it is clear from (11) that

$$\hat{\alpha}_\lambda^{(n)} = 1, \qquad \text{for } \alpha_\lambda = 1 \text{ (all } n\text{);} \tag{15}$$

so that also the limit

$$\hat{\alpha}_\lambda^{(\infty)} = 1, \qquad \text{for } \alpha_\lambda = 1. \tag{16}$$

Finally, when $\alpha_M = 1$:

$$\hat{\alpha}_\lambda^{(n)} = 1 - (1 - \alpha_\lambda)^{1/n}, \qquad \text{for } \alpha_M = 1; \tag{17}$$

and

$$\hat{\alpha}_\lambda^{(\infty)} = 0, \qquad \text{for } \alpha_M = 1,\ \alpha_\lambda \neq 1. \tag{18}$$

Equations (16) and (18) together indicate that if there is any wavelength at which absorptance is complete—if $\alpha_M = 1$—then the limiting normalized absorptance curve, $\hat{\alpha}_\lambda^{(\infty)}$, takes on a discontinuous line or rectangular form which is unity where the original absorptance curve, α_λ, is unity, and is zero everywhere else. This is the ultimate in narrowing, and is not seen unless there is a wavelength at which absorptance is total.

It is also of interest to consider what happens when the concentration of the pigment becomes much greater than the initial value. Physically, the increase in concentration is limited by the solubility of the pigment in the solvent, but for theoretical purposes, we can consider the consequences of letting n approach 0. (If we consider the physical dimension being varied to be the thickness of the solution layer, rather than the concentration of the pigment in the solvent, the case of infinitesimal n becomes operationally meaningful.) We see from (11) that

$$\hat{\alpha}_\lambda^{(0)} = \lim_{n \to 0} \hat{\alpha}_\lambda^{(n)} = \lim_{n \to 0} \frac{1 - (1 - \alpha_\lambda)^{1/n}}{1 - (1 - \alpha_M)^{1/n}} = \frac{1}{1} = 1, \qquad \text{for } \alpha_\lambda \neq 0. \tag{19}$$

When $\alpha_\lambda = 0$, we have:

$$\hat{\alpha}_\lambda^{(0)} = \lim_{n \to 0} \hat{\alpha}_\lambda^{(n)} = \lim_{n \to 0} \frac{0}{1 - (1 - \alpha_M)^{1/n}} = \frac{0}{1} = 0, \qquad \text{for } \alpha_\lambda = 0. \tag{20}$$

Thus, as the pigment concentration is greatly increased, the normalized absorptance curve (in other words, the shape of the absorptance curve) approaches a rectangular, discontinuous function which is zero wherever $\alpha_\lambda = 0$, and is unity wherever $\alpha_\lambda > 0$. This is the ultimate in broadening, and is associated with infinitely dense layers of any pigment whatever.

Most of the relationships discussed above are illustrated in figure 1a, which represents the variation of the normalized spectral absorptance of macular pigment with concentration or thickness. Similar families of curves have been published previously for other visually significant pigments, such as visual purple, by Dartnall [8]; and the hypothetical cone pigments based on the Judd [9] primaries, by Terstiege [10].

The curve taken as the original α_λ [that is, $\alpha_\lambda^{(1)}$] for the construction of figure 1a is the equivalent of the macular pigment density curve given by Wyszecki and Stiles [11], with an arbitrary

extrapolation by the present author down to 340 nm, based on Wald's [12] indication that the absorptance of the macular pigment is essentially zero by 350 nm. Figure 1a confirms that as concentration increases, the absorptance curve broadens, progressively obscuring the fine structure, and approaches a rectangular form covering the entire wavelength range over which the pigment absorbs at all.

On the other hand, the most conspicuous aspect in figure 1a of the changes occurring with decreasing concentration is the quite limited extent of these changes. The curve for infinite decrease of concentration is indeed the narrowest and lowest of all, but it is not much narrower or lower than the original curve. The curve representing a mere halving of the concentration is already about half way from the curve for the original concentration toward the curve for an infinite decrease in concentration. Concentration decrease will be seen to cause some sharpening of the fine structure. Because the peak absorptance of the original absolute curve is only 0.684 (density = 0.5), the limiting curve for infinite concentration decrease does not even approach the line spectrum required by eqs (16) and (18) when the absorptance is 1.0 at one or more isolated wavelengths (or the rectangular curve resulting when the original absorptance is 1.0 over a continuous range of wavelengths).

Figure 1b illustrates the approach to a line spectrum for a fictitious pigment having as its *absolute* spectral absorptance curve the *normalized* curve for one layer of the macular pigment on which figure 1a is based. In other words, the new absorptance curve is simply the absolute curve for one layer of macular pigment divided by the constant 0.684 (actually, $1-10^{-0.5}$) so as to have a peak absorptance of 1 instead of 0.684.

Such an absorptance curve would be difficult to find in any real pigment. For one thing, an absorptance actually equal to 1 (infinite density) at any given concentration requires an absorptance of 1 at *all* concentrations, but all real pigment layers become quite transparent at all wavelengths if the concentration or thickness is made sufficiently small. Secondly, even if the peak absorptance is only near 1 (say 0.99999) instead of equal to 1, the absorptance would not drop off from the peak

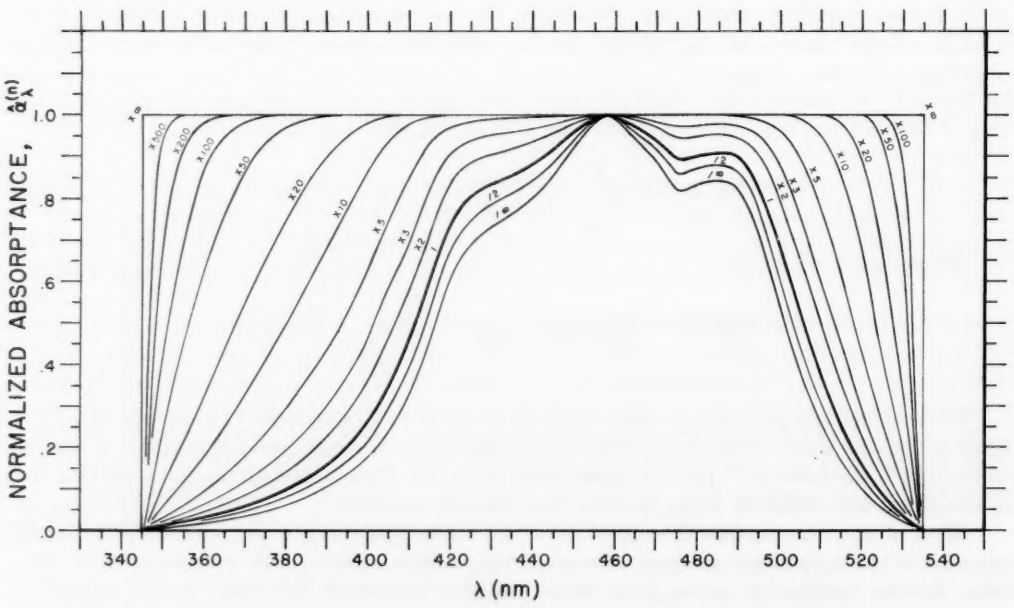

FIGURE 1a. *Variation in the shape of the spectral absorptance curve of macular pigment (normalized to unit maximum) as the pigment concentration changes.*

The curve labeled "1" is the original curve (peak absolute absorptance = 0.684), "×2" denotes a doubling of concentration (or thickness), and "/2" denotes a halving of concentration. The right sides of the ×200 and ×500 curves are omitted for clarity.

as rapidly as in our fictitious example. A real pigment layer with such a high absorptance anywhere within the interior of its absorption spectrum would have to either be very thick (compared to a layer that transmits substantially at all wavelengths) or contain an extremely high concentration of pigment. Therefore its absorptance curve would be of the flat, near-rectangular form characteristic of high concentration multiples. The curve for such a layer does not come close to reaching the "spike" form, no matter how much the concentration is reduced. In fact, the "×10" curve in figure 1a, corresponding to a layer of macular pigment 10 times thicker or more concentrated than the standard layer, does represent a peak absolute absorptance of 0.99999. Obviously the bleaching of such a layer would follow the course represented by the curves below it in figure 1a, and the limiting curve for infinite bleaching is the very same curve as the "/∞" curve in that graph. While the "/∞" curve is considerably more spiky than the "×10" curve, it is very far indeed from being a line spectrum.

Except for the limiting top ($n=0$) and bottom ($n=\infty$) curves in figures 1a and 1b, the other curves were generated by use of eq (11) in a computer program. In order to obtain a rough picture of how much the shape of any absorptance curve changes for any specified change in concentration of the pigment, it is sufficient to make use of figure 2, which is based on eq (5) and gives the relationship between the absolute absorptances $\alpha_\lambda^{(n)}$ and α_λ for various values of n. When the absolute absorptance curve has been sketched out through the use of figure 2, it is easy enough to divide by the maximum value to obtain the normalized curve.

The parameter numbers on the curves in figure 2 do not represent n, the concentration reduction factor, but instead represent P, the percentage bleach. The relationship between these quantities is given by the equations

$$P=100\left(1-\frac{1}{n}\right); \tag{21}$$

$$n=\frac{100}{100-P}. \tag{22}$$

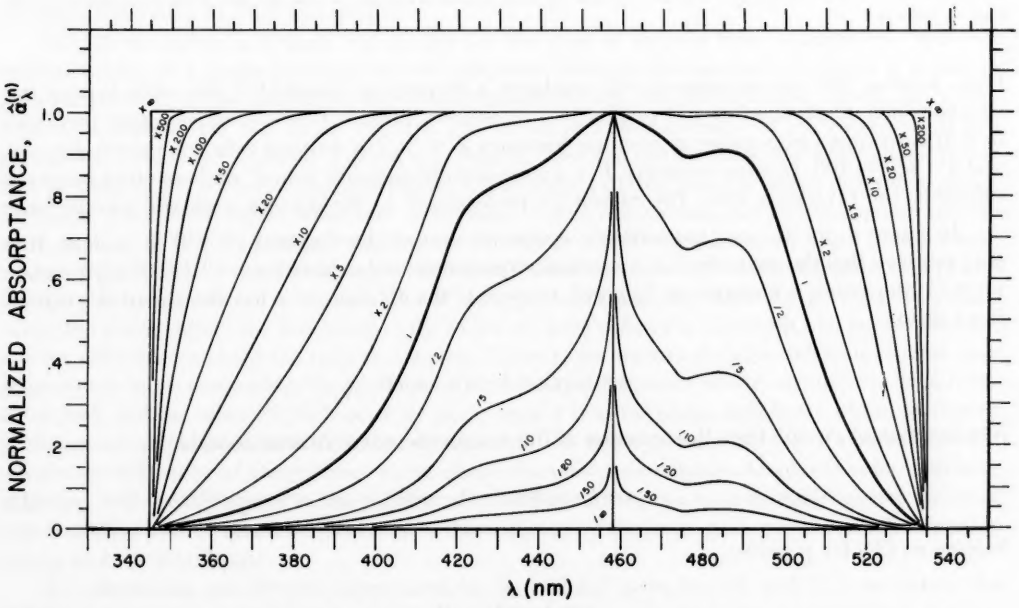

FIGURE 1b. *Same type of plot as figure 1a, but here the "1" curve (identical to that in fig. 1a) corresponds to a fictitious macular-like pigment with a peak absolute absorptance of 1.*

The right sides of the ×100 and ×500 curves are omitted for clarity.

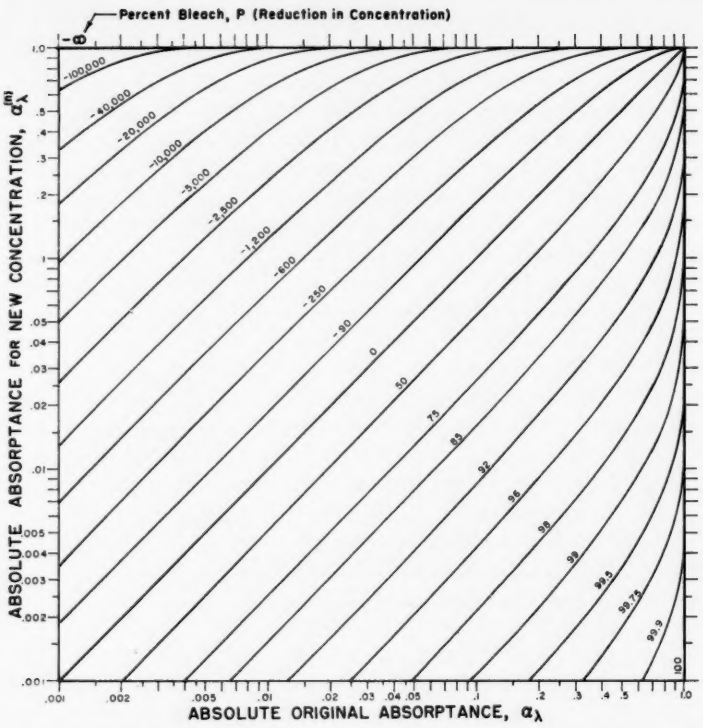

FIGURE 2. *Variation of (absolute) absorptance with pigment concentration (or thickness). This graph applies to any pigment solution layer that follows Beer's law, or to any material that follows Bouguer's law.*

Negative values of the parameter refer to percentage concentration increases. All the curves converge on and reach the point (1,1); despite appearances, none of the curves for $P \neq -\infty$ reaches $\alpha_\lambda^{(n)} = 1$ until $\alpha_\lambda = 1$. Also all the curves converge on and reach the point (0,0), although this is not evident because the graph is a log-log plot.

Thus, halving the concentration ($n=2$) produces a 50 percent bleach ($P=50$), while leaving the concentration unchanged ($n=1$) results in a 0 percent bleach ($P=0$). Concentration increases ($n<1$) correspond to negative percentage bleaches ($P<0$). The limiting values are $n=0$, $P=-\infty$; and $n=\infty$, $P=100$. In some contexts, P is a more natural measure than n, while in other frames of reference the reverse is true. The reason for preferring P in the present work will emerge later.

In figure 2, an at least approximate symmetry around the diagonal ($P=0$) is evident. It is easy to prove that the curve for $n=k$ is actually symmetric to the curve for $n=1/k$. For any function $y=f(x)$, the curve symmetric to $f(x)$ with respect to the 45° line $y=x$ has the equation $x=f(y)$. If we define

$$y=f_k(x) \equiv 1-(1-x)^{1/k} \tag{23}$$

[the function of eq (5)], then the equation of the symmetric curve is representable as

$$x=f_k(y) \equiv 1-(1-y)^{1/k}. \tag{24}$$

Solving eq (24) for y yields:

$$y=1-(1-x)^k, \tag{25}$$

and this is precisely $f_{(1/k)}(x)$, as was to be proved.

Since the curves for n and n' in figure 2 are symmetrical when

$$n=\frac{1}{n'}, \tag{26}$$

we know from (22) that the curves for P and P' are symmetrical when

$$\frac{100}{100-P}=\frac{100-P'}{100} \tag{27}$$

or

$$P'=\frac{-100P}{100-P}. \tag{28}$$

The curves in figure 2 were selected to have simple values of P, and the pairs of approximately symmetric curves are related according to (28) closely but, in most cases, not precisely. The symmetry is therefore not exact, although a perfectly symmetrical set of curves could be produced if desired.

4. Changes in Shape

We are now ready to deal with our basic problem: the extent of the difference between the shapes of α_λ and $\alpha_\lambda^{(n)}$. Definition of a quantitative index of shape difference is the first requirement, and since we identify the shapes of absolute absorptance curves with the corresponding normalized absorptance curves, it is tempting to define the index simply as:

$$\delta_\lambda^{(n)}=\hat{\alpha}_\lambda^{(n)}-\hat{\alpha}_\lambda. \tag{29}$$

This measure is not an overall index of shape difference between two curves, but rather a definition of shape difference at each wavelength.

In (29) the index is defined specifically for the case of interest here: namely, two different concentrations of a single pigment; but the difference between the normalized curves is meant to be a measure of shape difference applying generally to any two absorptance curves. Brief consideration reveals that this index behaves with intuitive reasonableness at the extremes. If two normalized curves are equal at a given wavelength, then the curves have the same shape there; that is, there is a 0 percent shape discrepancy. The most extreme possible shape difference at any particular wavelength exists when one absorptance curve has its maximum at that point and the other is zero. In terms of the normalized curves, this is a difference between 1 and 0, or a shape change of 1 (100%). It should be emphasized that if we are comparing two absorptance curves at a wavelength where one curve is 2 percent of its peak value and the other is 1 percent of its peak value, the shape difference according to the index we have defined is 1 percent and not 50 percent; it is the difference and not the ratio that counts. Clearly, the amount of shape difference in this case is intuitively more comparable in significance to the shape difference where one curve is 80 percent of its peak and the other 79 percent of its peak, than it is to the shape difference where one curve is 80 percent of its peak and the other 40 percent. The point of view here is of course directed toward the relevance of absorptance-curve shape changes to detectable changes in color-matching behavior, and the difference in the relative rates of light absorption by a receptor system with two different absorptance functions depends on the arithmetic difference in the normalized absorptance curves at each wavelength.

By substituting into (29) the expressions for $\hat{\alpha}_\lambda$ and $\hat{\alpha}_\lambda^{(n)}$ given by (10) and (11), we obtain the formula:

$$\delta_\lambda^{(n)}=\frac{1-(1-\alpha_\lambda)^{1/n}}{1-(1-\alpha_M)^{1/n}}-\frac{\alpha_\lambda}{\alpha_M}. \tag{30}$$

Various measures of overall shape difference between the curves α_λ and $\alpha_\lambda^{(n)}$ can be defined in terms of the index for shape difference at individual wavelengths specified in (29) or (30). If K and L are the lower and upper limits, respectively, of the wavelength range of interest, we might for different purposes be interested in any one of a number of measures such as the following:

$$\frac{1}{L-K}\int_K^L [\delta_\lambda^{(n)}]^2 d\lambda; \qquad \frac{1}{L-K}\int_K^L |\delta_\lambda^{(n)}| d\lambda; \qquad \max_\lambda |\delta_\lambda^{(n)}|. \tag{31}$$

Since our interest here is primarily in determining upper limits of change, let us choose the simple measure listed last in (31). Let

$$S^{(n)} = \max_\lambda |\delta_\lambda^{(n)}| = \max_\lambda |\hat{\alpha}_\lambda^{(n)} - \alpha_\lambda| \qquad (\lambda = K \text{ to } L). \tag{32}$$

In the remainder of the paper, any indication of a maximum over λ refers to the wavelength range $\lambda = K$ to L.

5. Location of the Maximum Discrepancy

Since $\delta_\lambda^{(n)} \geq 0$ for $n \leq 1$ and $\delta_\lambda^{(n)} \leq 0$ for $n \geq 1$, we can write the first equality in (32) as:

$$S^{(n)} = \max_\lambda [\pm \delta_\lambda^{(n)}], \tag{33}$$

the plus sign applying when $n \leq 1$ and the minus sign when $n \geq 1$. Since, in general, for any function f,

$$\max_\lambda [-f(\lambda)] = -\min_\lambda f(\lambda), \tag{34}$$

an equivalent of (33) is:

$$S^{(n)} = \max_\lambda \delta_\lambda^{(n)}, \qquad n \leq 1; \tag{35a}$$

$$S^{(n)} = -\min_\lambda \delta_\lambda^{(n)}, \qquad n \geq 1. \tag{35b}$$

For any n, then, the maximum absolute discrepancy, $S^{(n)}$, between the normalized curves, occurs at a critical point of the function $\delta_\lambda^{(n)}$, and hence in all cases we can find the value of α_λ yielding the greatest discrepancy by setting the derivative of $\delta_\lambda^{(n)}$ with respect to α_λ equal to zero.

We have from (18) that

$$\frac{\partial \delta_\lambda^{(n)}}{\partial \alpha_\lambda} = \frac{(1-\alpha_\lambda)^{\frac{1}{n}-1}}{n[1-(1-\alpha_M)^{1/n}]} - \frac{1}{\alpha_M}. \tag{36}$$

Setting the derivative equal to zero to obtain the critical point and solving for α_λ, we conclude that

$$\alpha_\lambda = 1 - \left\{\frac{\alpha_M}{n[1-(1-\alpha_M)^{1/n}]}\right\}^{\frac{n}{n-1}} \tag{37}$$

for maximum discrepancy between $\hat{\alpha}_\lambda^{(n)}$ and $\hat{\alpha}_\lambda$.

To convert the absolute absorptance in (37) to a normalized absorptance, we need only divide through by α_M, the result being:

$$A^{(n)}(\alpha_M) = \hat{\alpha}_\lambda \text{ for } \max_\lambda |\delta_\lambda^{(n)}| = \frac{1}{\alpha_M}\left\langle 1 - \left\{ \frac{\alpha_M}{n[1-(1-\alpha_M)^{1/n}]} \right\}^{\frac{n}{n-1}} \right\rangle. \tag{38}$$

Equation (38) tells us that at the wavelength(s) where the original absolute absorptance curve, α_λ, has dropped to that fraction, $A^{(n)}(\alpha_M)$, of its maximum value, α_M, specified by the right side of (38), the greatest discrepancy in shape between α_λ and $\alpha_\lambda^{(n)}$ exists; that is, the magnitude of the difference between the curves $\hat{\alpha}_\lambda$ and $\hat{\alpha}_\lambda^{(n)}$ is greatest. This result applies to any absorptance curve whatever, the normalized form of which contains the critical $\hat{\alpha}_\lambda$ value, $A^{(n)}(\alpha_M)$, defined by (38). For the treatment of exceptions—$\hat{\alpha}_\lambda$ curves that fail to contain the value $A^{(n)}(\alpha_M)$ over the wavelength range of interest—see appendix B. The actual wavelength where the maximum $|\delta_\lambda^{(n)}|$ occurs depends, of course, on the shape of the particular absorptance curve being considered.

The expression (38) is not defined for four special cases: $\alpha_M = 0$, $n = 0$, $n = 1$, and $n = \infty$. These cases, and their various combinations, have all been worked out by defining the value of (38) as the value of the limit of (38) as the special values are approached. In evaluating the limits for the three special n values, it emerges that $\alpha_M = 1$ is also a special case in combination with these n values only. To avoid circumlocution, further reference to the "special" or "limiting" values will include this fifth case of $\alpha_M = 1$.

The evaluation of the various limits is discussed in appendix C. Table 1 gives a complete summary of the formulas for all cases. A graphical representation of all the results is given in figure 3, which plots $A^{(n)}(\alpha_M)$, the $\hat{\alpha}_\lambda$ for maximum $|\delta_\lambda^{(n)}|$, as a function of the peak absolute absorptance, α_M, of the original curve, with percent bleach, P, as the parameter.

A number of significant features can be observed in the family of curves of figure 3. To begin with, a bleach of -100 percent—that is, a doubling of concentration—plays a unique role (although the case $n = \frac{1}{2}$ is not "special" in the sense of requiring the use of limit methods). The graph shows that if the concentration of any pigment is doubled, the maximum shape change occurs where the original absorptance curve has exactly half its maximum value, regardless of what that maximum absolute absorptance may be. For no other concentration change is the location of the point of maximum shape change independent of the peak absolute absorptance of the original curve.

TABLE 1. *Formulas for calculating* $A^{(n)}(\alpha_M)$, *the normalized absorptance* $(\hat{\alpha}_\lambda)$ *for which the greatest amount of shape change,* $|\delta_\lambda^{(n)}|$, *occurs when the pigment concentration is reduced by a factor of* n

The maximum absolute absorptance for the original pigment concentration is α_M.

	Increases of concentration				Decreases of concentration	
	$\lim_{n\to 0}$	$0 < n < 1$ [a]	$n = \frac{1}{2}$ [b]	$\lim_{n\to 1}$	$1 < n < \infty$ [a]	$\lim_{n\to\infty}$
$\lim_{\alpha_M\to 0}$	0.5	0.5	0.5	0.5	0.5	0.5
$0 < \alpha_M < 1$	0	$\frac{1}{\alpha_M}\left\langle 1 - \left\{ \frac{n[1-(1-\alpha_M)^{1/n}]}{\alpha_M} \right\}^{\frac{n}{1-n}} \right\rangle$	0.5	$\frac{1}{\alpha_M}\left[1 - \frac{1/e}{(1-\alpha_M)^{\frac{1-\alpha_M}{\alpha_M}}} \right]$ $1/e \approx 0.367879441$	$\frac{1}{\alpha_M}\left\langle 1 - \left\{ \frac{\alpha_M}{n[1-(1-\alpha_M)^{1/n}]} \right\}^{\frac{n}{n-1}} \right\rangle$	$\frac{1}{\alpha_M} - \frac{1}{-\ln(1-\alpha_M)}$
$\lim_{\alpha_M\to 1}$	0	$1 - n^{\frac{n}{1-n}}$ [c]	0.5	$1 - \frac{1}{e}$ ≈ 0.632120559	$1 - \frac{1}{n^{\frac{n}{n-1}}}$ [c]	1

[a] These are the ordinary ranges of values of n, and the same formulas apply in both cases. In each case, the formulas have been expressed in a form that makes the exponents positive, but either of the equivalent forms is valid over both ranges.

[b] The case $n = \frac{1}{2}$ is tabulated here because of its uniqueness, but it is not a limiting case.

[c] No limits are involved in these cases; simply set $\alpha_M = 1$ in the regular formula $(0 < \alpha_M < 1)$.

For concentration increases of less than 100 percent and for all concentration decreases—even infinite decrease—we see that $A^{(n)}(\alpha_M)$ is not much greater than 0.5, as long as the peak absolute absorptance, α_M, is not too great. When α_M is very close to 1 and the bleach is very severe, the critical $\hat{\alpha}_\lambda$ value approaches 1; that is, the greatest discrepancy occurs where the curve is close to its peak height. This result corresponds to either of two previously discussed situations: the absorptance curve of a pigment that absorbs *completely* at some wavelength approaches a spikelike form as bleaching is carried toward completion (see fig. 1b); or, if the limiting curve is not close to a spike, for an original curve with a peak absolute absorptance just less than 1, the original curve must be flat around the peak—that is, very close to its peak height over a considerable wavelength range (compare the "$\times 10$" and "$/\infty$" curves in fig. 1a).

For concentration increases of more than 100 percent, the critical $\hat{\alpha}_\lambda$ value, $A^{(n)}(\alpha_M)$, is seen from figure 3 to be always less than 0.5. For very great increases of concentration, $A^{(n)}(\alpha_M)$ approaches 0 for any except very low α_M values; that is, the greatest discrepancy occurs near the end of the absorption range. This result corresponds to the previously discussed fact that the absorptance curve of any pigment approaches a rectangular form as the concentration is increased enormously. Figure 1a provides a clear picture of why the greatest discrepancy occurs near where the curve drops to zero when the concentration increase is carried very far.

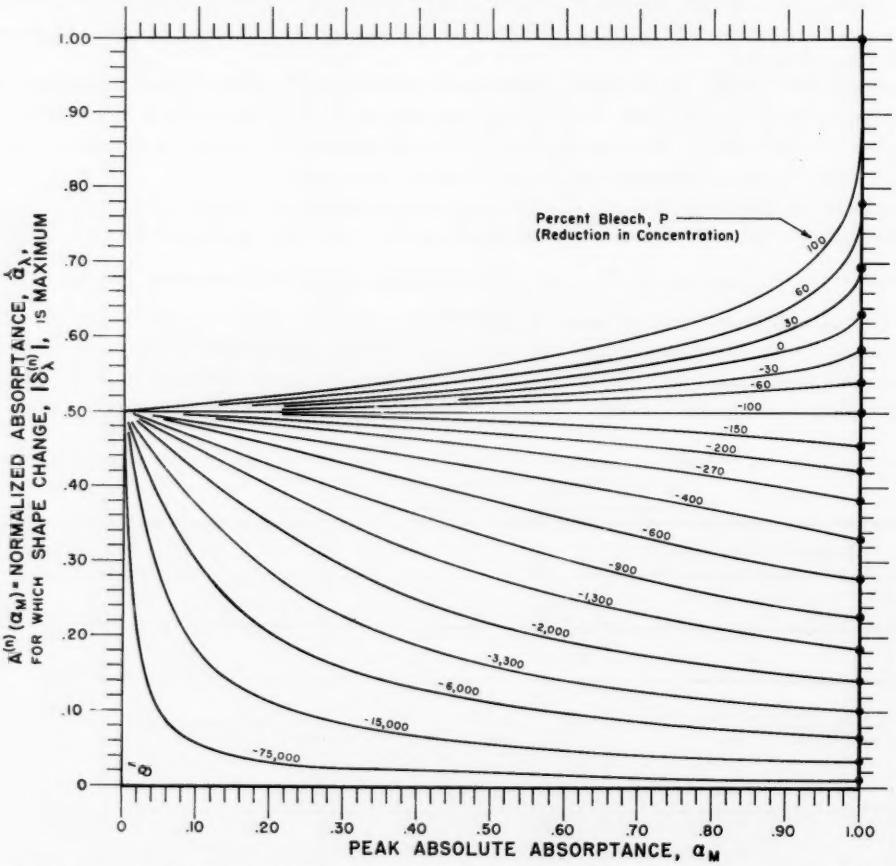

FIGURE 3. *Location of the point at which the shape of the spectral absorptance curve of a pigment solution layer changes most as concentration (or thickness) varies. These results apply to any pigment solution obeying Beer's law, or to any material obeying Bouguer's law.*

"Shape" change is defined as the difference between the normalized absorptance curves. The critical point is specified (ordinate) in terms of the normalized absorptance, $\hat{\alpha}_\lambda$, of the original pigment layer. The critical $\hat{\alpha}_\lambda$ is shown as a function of (abscissa) the peak absolute absorptance, α_M, of the original pigment layer. The circles along the right edge of the graph indicate the termination points of the curves.

One aspect of figure 3 is particularly non-intuitive: the curve for no bleaching at all ($P=0$; $n=1$) indicates that the location of the maximum discrepancy varies with the peak absolute absorptance, α_M, of the original pigment. Obviously, when there is no bleaching there is no discrepancy, so the maximum discrepancy, zero, occurs *everywhere* along the curve. In particular, it does occur at the $\hat{\alpha}_\lambda$ values indicated in the $P=0$ curve, so that the curve is not incorrect, only incompletely informative. (The true complete function for $P=0$ covers the entire area of the graph.) The reason for choosing the particular curve presented in figure 3 to represent $P=0$ is to preserve continuity: the curves for very slight bleaching and very slight concentration increase approach the $P=0$ curve as the amount of concentration change becomes smaller and smaller. The procedure of defining the function in (38) to be equal to the limit at those values of n and α_M for which the expression is not defined is the source of this continuity.

6. The Size of the Maximum Discrepancy

Since we now know where the maximum discrepancy, $S^{(n)}$, occurs, we need only substitute the expression for the critical α_λ given in (37) into eq (30) to obtain the amount of this largest shape difference. The result, which unfortunately does not seem to be expressible in an appreciably simpler form, is:

$$S^{(n)}=\max_\lambda|\delta_\lambda^{(n)}|=\left|\left\langle\frac{1-\left\{\frac{\alpha_M}{n\left[1-(1-\alpha_M)^{1/n}\right]}\right\}^{\frac{1}{n-1}}}{1-(1-\alpha_M)^{1/n}}\right\rangle-\left(\frac{1}{\alpha_M}\right)\left\langle1-\left\{\frac{\alpha_M}{n\left[1-(1-\alpha_M)^{1/n}\right]}\right\}^{\frac{n}{n-1}}\right\rangle\right| \tag{39}$$

The expression in (39), like that in (38), is not defined for the special cases $\alpha_M=0$, $n=0$, $n=1$, $n=\infty$, and, in combination with the latter three cases, $\alpha_M=1$. Here, too, the function approaches a limit in each special case, and can conveniently be defined as equal to the limiting value in each of these cases. The evaluation of these limits is discussed in appendix C. Table 2 provides a complete summary of the formulas for all cases, but the functions tabulated are not the

TABLE 2. *Formulas for calculating* $D^{(n)}(\alpha_M)$, *the shape change* $[\delta_\lambda^{(n)}]$ *of maximum size,*[a] *produced when the pigment concentration is reduced by a factor of* n

The maximum absolute absorptance for the original pigment concentration is α_M.

	Increases of concentration				Decreases of concentration	
	$\lim_{n\to0}$	$0<n<1$ [b]	$n=\frac{1}{2}$ [c]	$\lim_{n\to1}$	$1<n<\infty$ [b]	$\lim_{n\to\infty}$
$\lim_{\alpha_M\to0}$	0	0	0	0	0	0
$0<\alpha_M<1$	1	$\left\langle\frac{1-\left\{\frac{n[1-(1-\alpha_M)^{1/n}]}{\alpha_M}\right\}^{\frac{1}{1-n}}}{1-(1-\alpha_M)^{1/n}}\right\rangle-\left(\frac{1}{\alpha_M}\right)\left\langle1-\left\{\frac{n[1-(1-\alpha_M)^{1/n}]}{\alpha_M}\right\}^{\frac{n}{1-n}}\right\rangle$	$\frac{\alpha_M}{4(2-\alpha_M)}$	0	$\left\langle\frac{1-\left\{\frac{\alpha_M}{n[1-(1-\alpha_M)^{1/n}]}\right\}^{\frac{1}{n-1}}}{1-(1-\alpha_M)^{1/n}}\right\rangle-\left(\frac{1}{\alpha_M}\right)\left\langle1-\left\{\frac{\alpha_M}{n[1-(1-\alpha_M)^{1/n}]}\right\}^{\frac{n}{n-1}}\right\rangle$	$\frac{1-\ln\alpha_M+\ln[-\ln(1-\alpha_M)]}{-\ln(1-\alpha_M)}-\frac{1}{\alpha_M}$
$\lim_{\alpha_M\to1}$	1	$(1-n)n^{\frac{n}{1-n}}$ [d]	0.25	0	$-\frac{(n-1)}{n^{\frac{n}{n-1}}}$ [d]	-1

[a] Note that this table does not list $S^{(n)}=\max_\lambda|\delta_\lambda^{(n)}|$, but gives $D^{(n)}(\alpha_M)$, the corresponding $\delta_\lambda^{(n)}$ with the correct algebraic sign. The sign is negative for concentration decreases and positive for increases. (To obtain the absolute value, change the sign of all the formulas for concentration decreases.)

[b] These are the ordinary ranges of values of n, and because the algebraic sign has been retained, the same formulas apply in both cases. In each case, the formulas have been expressed in a form that makes the exponents positive, but either of the equivalent forms is valid over both ranges.

[c] The case $n=\frac{1}{2}$ is tabulated here because of its uniqueness, but it is not a limiting case.

[d] No limits are involved in these cases; simply set $\alpha_M=1$ in the regular formula ($0<\alpha_M<1$).

absolute values specified in (39); instead the algebraic sign is retained, so that the formulas for decreases of concentration produce immediately recognizable negative numbers. On those occasions that the absolute value is desired, it is only necessary to change the sign in all of the formulas for concentration decreases; the quantities generated by the concentration-increase formulas are already positive.

It will be convenient to have a separate symbol, $D^{(n)}(\alpha_M)$, to denote the signed $\delta_\lambda^{(n)}$ value of maximum absolute size, as listed in table 2. Thus,

$$S^{(n)} = |D^{(n)}(\alpha_M)|. \tag{40}$$

A warning is necessary concerning the numerical evaluation of the function in (39), or its limiting forms given in table 2. The two quantities between which the difference is taken in (39) are in many cases equal for the first several significant figures, so that the value of $S^{(n)}$ is determined by differences existing out as far (in the very worst instances) as the ninth or tenth significant figure. An attempt to evaluate $S^{(n)}$ by the use of tables of logarithms (to assess the exponential expressions) is almost certainly doomed to failure, unless a table with extraordinarily many places of both the argument and the function is available. If a particular n is chosen, and an attempt to evaluate $S^{(n)}$ for a number of values of α_M is made, the values obtained by the use of tables may form a reasonable, smooth curve, but the curve may deviate quite badly from the true curve, especially at the ends.

The only practical method of generating values directly from (39) is through the use of a digital computer. It was found that for extreme values of α_M (near 0 or 1), and extreme values of n (near 0, ∞, or the "special" value 1) even the 8-place arithmetic of an ordinary digital computer may generate significantly erroneous values of $S^{(n)}$, so that recourse to double-precision (16-place) computer arithmetic was required in some cases. To insure accuracy, therefore, the curves of figures 4 and 5, which graphically summarize the relationships embodied in eq. (39), were all obtained by means of such 16-significant-figure calculation. Analogous considerations, it must be pointed out, are applicable to the functions in (38), table 1, and figure 3.

Figure 4 is a plot of $S^{(n)}$, the maximum amount of shape change at any wavelength, against α_M, the peak absolute absorptance of the original α_λ curve, for bleaching ($n > 1$); figure 5 is the corresponding plot for concentration increases ($n < 1$). The numerical parameter identifying the curves on each graph is not n, but the percentage bleach, P, defined by (21). Because a wide range of P values is of interest for different purposes, as well as a wide range of α_M values, it seemed most useful to plot figures 4 and 5 on log-log coordinates, so that several orders of magnitude of each variable can be represented.

Nothing shown in figure 4 seems intuitively unreasonable. The maximum shape change increases with the degree of bleaching, and approaches a limiting value for total bleaching ($P = 100\%$; $n = \infty$). For any particular degree of bleaching, the maximum shape change is an increasing function of α_M, the initial peak absolute absorptance. Because the origin is at infinity in a log-log plot it is not clear in figure 4, but is nevertheless a fact, that all the curves pass through the point ($\alpha_M = 0$, $S^{(n)} = 0$). Thus, as is obvious, pigment that does not absorb at all undergoes no shape change whatever, no matter how much "bleaching" occurs. (This is again a matter of behavior in the limit, if we consider lower and lower densities of any pigment at all.) Finally, the greatest possible shape change—$S^{(n)} = 1$—occurs only for the single case of infinite bleaching of a pigment that absorbs completely at some wavelength ($\alpha_M = 1$), this case being again a matter of behavior in the limit. [The perfect absorber ($\alpha_\lambda \equiv 1$), as well as the other exceptional cases discussed in appendix B, of course are not covered by table 2 or figs. 4 or 5.]

For concentration increases, shown in figure 5, a few additional considerations arise. As expected, the maximum shape change increases with the extent of the concentration increase, and approaches a limiting value for infinite increase in concentration ($P = -\infty$; $n = 0$). The limiting value for $P = -\infty$ is the greatest possible value, $S^{(n)} = 1$, and is constant for any $\alpha_M > 0$. For

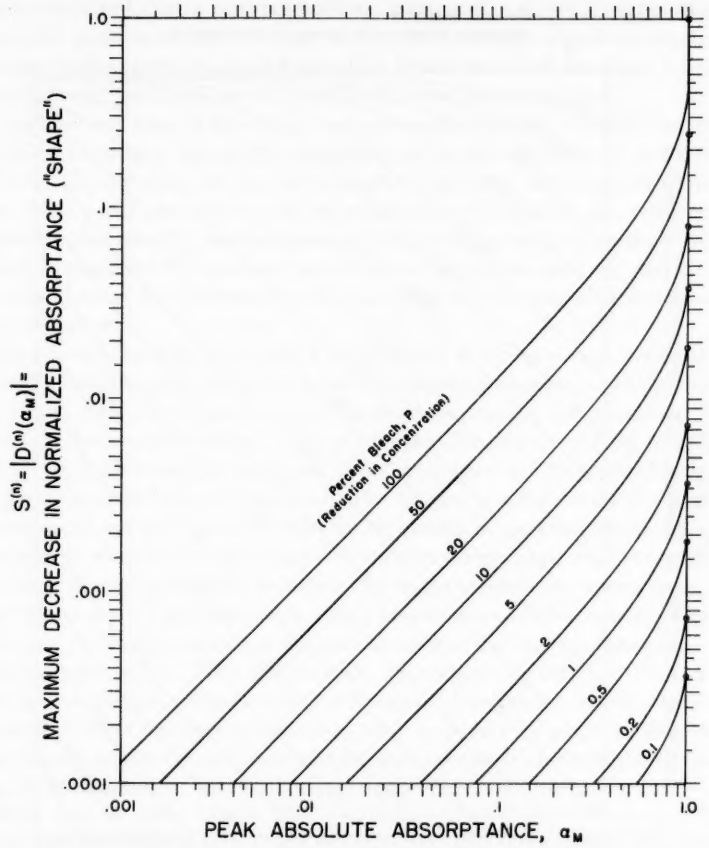

FIGURE 4. *The amount of the greatest change, as concentration (or thickness) is reduced, in the shape of the spectral absorptance curve of any pigment solution layer obeying Beer's law, or of any material obeying Bouguer's law.*

The maximum shape change is given (ordinate) in terms of the difference between the normalized absorptance curves for the original and reduced concentrations. The abscissa variable is the peak absolute absorptance, α_M, of the original pigment layer. The circles along the right edge of the graph indicate the points at which the curves terminate. All the curves reach the point (0,0), which is not shown because both scales are logarithmic.

anything less than infinite concentration increase, $S^{(n)}$ is an increasing function of α_M. All the curves in figure 5, as in figure 4, pass through the origin. The limiting curve for $P=-\infty$ is thus of a rectangular form, in linear coordinates, with the discontinuity at $\alpha_M=0$, just as the "$\times\infty$" curves in figures 1a and 1b are analogously discontinuous.

It can be observed in table 2 that the curve for $n=1/2$ ($P=-100\%$) in figure 5 is of unique form. In linear coordinates, this one curve is a portion of a rectangular hyperbola, but because the origin is not the center of this hyperbola, the use of log-log coordinates in figure 5 does not rectify the curve. If instead of plotting $S^{(n)}$ against α_M, as in figure 5, we had plotted $S^{(n)}+1/4$ against $2-\alpha_M$, in log-log coordinates, the curve for $n=1/2$ would have been a straight line (and the only straight line).

•The final aspect of figures 4 and 5 to which attention will be drawn here is the marked similarity between figure 4 and the diagonally lower half of figure 5 (the curves for $P\geqslant -100$). It will be found that the curve for P in figure 4 is virtually the same curve as that for $-P$ in figure 5, not merely in shape but in actual value. For small absolute values of P, the corresponding curves in the two figures appear to be quite identical, and even for large percentage changes in concentration (P), the lower parts of the curves ($\alpha_M \ll 1$) are indistinguishable. However, observation of the upper limits of the curves, for $\alpha_M=1$, reveals some discrepancy for the highest few curves,

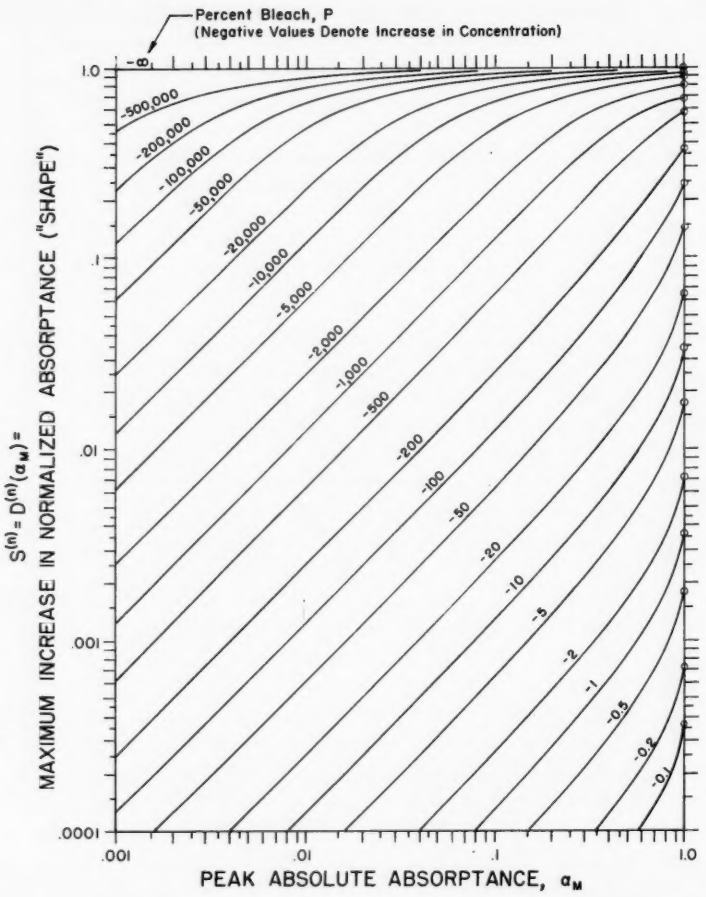

FIGURE 5. *Same type of plot as figure 4, but for increases in concentration.*

The terminations of the five curves for $-500\,000 \leq P \leq -20\,000$ are omitted for clarity; all of these terminal $S^{(n)}$ values are slightly less than 1, and only for $P = -\infty$ does $S^{(n)} = 1$.

and, in fact, the correspondence between P and $-P$ is really only approximate, the approximation being better for values of P or α_M near 0.

It was this close correspondence between the maximum shape changes for a given percentage bleach and for the same percentage increase in concentration (negative bleach) that dictated the choice of P as the most informative parameter for these curve families. It is interesting to observe in figure 3 that an approximate correspondence between P and $-P$ exists for the *locations* of the maximum shape changes as well. In figure 3, however, the correspondence does not involve an identity or a mirror symmetry of curve shape, but rather equal distances above and below the upward bending curve for $P = 0$.

7. Implications for Vision

The information summarized in figure 4 constitutes a set of restrictions to which any theory of color vision based on the idea of photopigments in solution must conform. The constancy of metameric matches under nonextreme levels of adaptation implies that within the applicable luminance range, the shape changes produced in the pigment absorptance curves by bleaching are so small as to be not behaviorally detectable. It is difficult to say how large a maximum shape change [$S^{(n)}$] in these absorptance curves would have been noticed in the various experiments

that have been conducted, but a maximum shape change of 1 percent seems likely to be safely below the threshold of detectability. In other words, the new color-matching functions determined by such a change in the pigments would not differ from the initial functions by amounts greater than the experimental uncertainties customary in color-matching data.

Figure 4 reveals that even if bleaching were virtually total ($P = 100\%$), the maximum shape change from the absorptance curves of the unbleached pigments can be kept below 1 percent provided the peak absorptances of the dark-adapted pigments are no greater than 7½ percent. As it happens, this is just about the order of magnitude of the peak absorptances found by the recent microspectrophotometric measurements of the absorptances of single cones [13, 14, 15]. Thus a *sufficient* explanation for metamer constancy is an upper limit of, say, 10 percent on the maximum absorptances of the photopigments, regardless of how much bleaching of the pigments occurs during adaptation.

On the other hand, the low-absorptance explanation is by no means *necessary*. If chromatic adaptation actually involves only limited degrees of pigment bleaching, over the constant-metamer range of luminance, then much higher initial peak absorptances are allowable. Rushton's work [16] with fundus reflectometry indicates that a considerable degree of light adaptation can occur in the cones with little bleaching of pigment. If no more than a 5 percent bleach occurs, for example, figure 4 indicates that shape changes can be limited to a maximum of 1 percent even when the peak absorptances are as high as 84 percent. It should be pointed out in this connection that there is a minority of workers in color who still support (or at least, until recently supported) the notion of high-absorptance pigments. Brindley [6] hypothesized an absorptance peak of nearly 70 percent and Walraven [17] estimates the peak absorptances at 80 percent. These researchers, and others [18], are evidently somewhat dubious about the low absorptance peaks claimed in the microspectrophotometric work. They presumably suspect some sort of artifact or misinterpretation leading to spuriously low estimates of the absolute absorptance levels of the curves, but no specific statement of their suspicions seems to have appeared in print. In any event, it is clear that high absorptance peaks are not inconsistent with metamer constancy if not much bleaching occurs during light adaptation within the applicable range of luminance.

An important fact of color vision, that has been stressed particularly by Walraven [19] in recent years, is the breakdown of metameric matches that does occur with very high retinal illuminances (above 10^4 trolands) [5, 6, 20]. It is not yet known what the cause of this breakdown is, but if it is shape changes in the pigment absorptance curves brought about by relatively extreme degrees of bleaching, figure 4 provides some quantitative restrictions. Walraven's [21] analysis of Brindley's [6] data on changes in the Rayleigh match with very high levels of adaptation led him to the conclusion that the spectral character of the changes in color-matching behavior are indeed what would be expected on the basis of bleaching of the photopigments: namely, a narrowing of the absorptance curves (particularly the red curve).

Just as we had to choose 1 percent more or less arbitrarily as an amount of maximum shape change that would almost surely be behaviorally nondetectable, we are also faced with choosing a figure to represent a degree of maximum shape change that would in all likelihood produce evident behavioral consequences; 10 percent seems a reasonable round number that is probably not much, if at all, above the minimum detectable level. The question now is: what is the *lowest* peak absorptance that will allow for shape changes at least as great as 10 percent?

Figure 4 tells us that if the pigments are nearly completely bleached ($P \approx 100\%$) when the metamer breakdowns occur, the peak absorptances of the photopigments must be at least 55 percent to allow for maximum shape changes of 10 percent or more. Rushton [22] regularly refers to "complete bleaching" after adaptation to very bright lights, so this estimate must be taken seriously. If, on the other hand, 5 percent bleaching were the most extreme attainable for even dazzling luminances (a seemingly unrealistic assumption), then we would have to abandon the hypothesis that the high-luminance breakdown of metameric matches is due simply to pigment bleaching, since the most extreme shape change possible for 5 percent bleaching is only 1.9 percent, no matter how high the initial peak absorptance (α_M) is. In fact, it is impossible to reach

a 10-percent shape change unless the bleach is greater than about 30 percent, and then only in the extreme case of $\alpha_M = 1$. Figure 4 indicates that if there are levels of adapting luminance high enough to produce a maximum photopigment shape change of 10 percent—that is, a clearcut disturbance of metameric matches—but which entail no more than a 50-percent bleaching of the pigments, then the pigments must have $\alpha_M \geq 0.82$.

The conclusion that must be drawn is that if the breakdown of metameric matches at high luminances is due to bleaching changes alone, and if a maximum shape change of at least 10 percent is necessary to make the breakdown experimentally evident, then the visual photopigments *must* have peak dark-adapted absorptances greater than 55 percent, and might possibly have peaks over 80 percent. If, therefore, any researcher's overall view of all the relevant evidence leads him to reject the hypothesis of high-absorptance pigments, it appears to be necessary also to reject the notion that the high-luminance breakdown of metameric matches can be attributed solely to changes in shape of the photopigment absorptance curves due to bleaching. An alternative explanation then becomes necessary and the most obvious candidate is the accumulation of significant quantities of one or more spectrally selective breakdown products.

One might imagine these products diffusing relatively uniformly over the retina and playing a role similar to that of the macular pigment; that is, acting as a filter in front of all the receptors. Brindley [6] interprets his data on high-luminance metamer breakdown as refuting this "screening pigment" model. Another possibility is that the breakdown products do not leave the receptors at all, but accumulate and regenerate in the individual cones in which they are formed. In that case, each of the three cone types can be thought of as covered by a filter the density of which is a direct function of the rate of absorption of the incident light by that class of cone. A still more complicated variant of this hypothesis allows for differences in the kinds of breakdown products formed from each of the cone pigments, so that the filters over the three types of cones vary not only in density but also in the gross spectral form of their absorptances.

Finally, there is even the possibility that it is not the products of the photopigment degenerations that accumulate, but that the extremely intense illumination of the eye causes spectrally selective changes in one of the normally photostable, nonvisual ocular pigments such as the macular or lens pigment. Brindley's [6] rejection of any "screening pigment" hypothesis of course applies to this explanation as well as to the hypothesis of photoproduct diffusion. Goldstein and Williams [6a], on the basis of extensive direct computations of the effect, also consider a significant role in human vision by screening pigments unlikely, provided the peak absorptances of the dark-adapted photopigments are sufficiently low. If in fact the breakdown of metameric matches at high luminances cannot be ascribed to any screening-pigment accumulation, the believers in low-absorptance photopigments face the challenge of providing a less obvious but more plausible hypothesis.

Those workers who believe in high-absorptance photopigments need not concern themselves with any of these alternative explanations for high-luminance breakdown of metamers; their belief is consistent with the simple bleaching model. One problem they do face is to show quantitative experimental evidence that the degree of pigment bleaching produced in the upper reaches of the constant-metamer range of luminance is low enough to produce shape changes of a size consistent with the nondetectability of the changes in the color-matching functions.

If we take 10^4 trolands as approximately the upper end of the constant-metameter range [4], and consult Rushton's measurements [16] of percentage cone pigment bleached as a function of the adapting retinal illuminance, we find that during steady-state adaptation to 10^4 trolands, only about 20 percent of the pigment is bleached away. We see in figure 4 that 20 percent bleaching of a pigment having a peak absolute absorptance of 80 percent yields a maximum shape change of only about 4 percent, a change quite possibly below the threshold of behavioral detectability.

Thus, if Rushton's data and his interpretation of them are substantially accurate, the assumption of photopigment absorptance curves with maxima of 80 percent accounts for both the constancy of metameric matches at moderate luminance levels and the breakdown of these matches at higher luminance levels. The most serious challenge to the high-absorptance theory, then,

would seem to be finding a flaw in the claimed absolute absorptance scales of the single-cone microspectrophotometric measurements that find low absorptance peaks for the pigments. Although parsimony makes the high-absorptance model logically attractive, it must be recognized that there is a definite possibility that in this case nature did not choose the simplest way. However, the very latest word available to the author as this article goes to press is encouraging for the high-absorptance theorists: MacNichol [23] has stated that the current estimate in his laboratory is that the peak absorptance of the cone pigments is of the order of at least 1.8 percent *per single micron of receptor length*. This measure would make the total absorptance of a cone with a pigmented length of 40 μm equal to nearly 52 percent at the peak [calculated from eq (5) with $n=1/40$], in marked contrast to the 3 to 6 percent peaks mentioned in the work from MacNichol's laboratory published in 1964 [13]. It remains to be seen whether similar re-evaluations emerge from the other two laboratories that have published [14, 15] this type of measurement.

8. Appendix A. Proof of Inequality (12)

Given $p > q$, we wish to show that

$$\hat{\alpha}_{\lambda}^{(p)} < \hat{\alpha}_{\lambda}^{(q)}, \tag{41}$$

in the range

$$0 < \alpha_{\lambda} < \alpha_{M} (\leqslant 1). \tag{42}$$

By formula (11), we can write (41) as:

$$\frac{1-(1-\alpha_{\lambda})^{1/p}}{1-(1-\alpha_{M})^{1/p}} < \frac{1-(1-\alpha_{\lambda})^{1/q}}{1-(1-\alpha_{M})^{1/q}}. \tag{43}$$

In order to simplify the analysis, let us introduce new variables v and b defined by:

$$e^{-v} = 1-\alpha_{\lambda};\ e^{-b} = 1-\alpha_{M}. \tag{44}$$

By virtue of (42), we can see that

$$0 \leqslant e^{-b} < e^{-v} < 1 \tag{45}$$

or

$$0 < v < b \leqslant \infty. \tag{46}$$

Substituting (44) into (43), we have:

$$\frac{1-e^{-v/p}}{1-e^{-b/p}} < \frac{1-e^{-v/q}}{1-e^{-b/q}}. \tag{47}$$

Because $p > q \geqslant 0$, it follows that

$$1/p < 1/q; \tag{48}$$

and it is therefore sufficient, for the purpose of establishing (47), to prove that the function

$$f(x) \equiv \frac{1-e^{-vx}}{1-e^{-bx}} \qquad (0<v<b) \tag{49}$$

is monotonically increasing for positive x.

To establish monotonic increase, we will demonstrate the positivity of $f'(x)$. Since $f(x)$ is obviously positive for positive x, we can choose equivalently to show the positivity of $f'(x)\cdot[x/f(x)]$, a maneuver that simplifies the algebra in the present case. From (49) we derive that

$$\frac{xf'(x)}{f(x)} \equiv \frac{vx}{e^{vx}-1} - \frac{bx}{e^{bx}-1} \qquad (0<v<b). \tag{50}$$

To show that the expression in (50) is positive, it is sufficient to demonstrate that the function

$$g(z) \equiv \frac{z}{e^z-1} \tag{51}$$

is monotonically decreasing for $z>0$, since the right side of (50) is $g(vx)-g(bx)$, with $0<vx<bx$.

We proceed by showing that $g'(z)$ is negative for positive z. Since

$$g'(z) \equiv \frac{e^z(1-z)-1}{(e^z-1)^2}, \tag{52}$$

we need to prove that

$$e^z(1-z)-1<0 \qquad (z>0); \tag{53}$$

or, defining

$$h(z) \equiv e^z(1-z), \tag{54}$$

we must establish that

$$h(z)<1 \qquad (z>0). \tag{55}$$

Since

$$h'(z) \equiv -ze^z<0 \qquad (z>0), \tag{56}$$

we know that $h(z)$ decreases monotonically from its value at $z=0$. Thus the proof of (55) is concluded by simply noting that $h(0)=1$.

9. Appendix B. Treatment of Special Cases: Discontinuous Absorptance Curves and Curves Maintaining High Absorptance to the Ends of the Spectral Range Considered

There are several situations in which the $\hat{\alpha}_\lambda$ curve fails to take on at *any* wavelength the value specified by the expression (38). Only two basic cases need be distinguished: (a) all $\hat{\alpha}_\lambda$ values in the interval $K \leq \lambda \leq L$ are greater than the critical value specified by (38) because the absorptance simply has not dropped off far enough at the ends of the specified wavelength interval; or (b) the $\hat{\alpha}_\lambda$ curve contains absorptance values both greater than and less than the critical value,

but not equal to it because the curve has discontinuities in the form of either absorption lines (zero bandwidth) or vertical edges representing jumps from one continuum level to another.

In case (a), the maximum $|\delta_\lambda^{(n)}|$ will occur at the wavelength(s) at which $\hat{\alpha}_\lambda$ is minimum—and hence closest to the critical value. This result follows because $|\delta_\lambda^{(n)}|$ has but a single maximum (over the $\hat{\alpha}_\lambda$ range 0 to 1) and decreases monotonically to zero as $\hat{\alpha}_\lambda$ progresses from the critical value toward either 0 or 1. It is irrelevant whether the $\hat{\alpha}_\lambda$ curve possesses discontinuities or not.

A unique example of this case deserves separate mention: the perfectly nonselective absorber. If, over the wavelength range K to L, $\alpha_\lambda \equiv c$, where $0 < c \leq 1$, then the flat curve has its maximum (and only) value everywhere, so that $\hat{\alpha}_\lambda \equiv 1$, $\hat{\alpha}_\lambda^{(n)} \equiv 1$ (all n), and $\delta_\lambda^{(n)} \equiv 0$ (all n). In short, as is obvious, the shape of the absorptance curve of a nonselective pigment does not change with concentration.

Case (b) is physically nonexistent, since all "lines," whether absorption, transmission, or emission, have finite width according to quantum theory; and no abrupt transition from one level of absorptance to another can be literally discontinuous. However, because real measurements cannot be made with infinite resolving power, one can be faced with effectively discontinuous curves. Mathematically, this situation can be treated by restricting attention to only two $\hat{\alpha}_\lambda$ values: the least upper bound[6] (l.u.b.) of the values less than the critical value and the greatest lower bound (g.l.b.)of the values greater than the critical value. Since in general the falloff of $|\delta_\lambda^{(n)}|$ from its maximum value is not symmetrical with respect to variation of $\hat{\alpha}_\lambda$ above and below the critical value, one cannot simply see which of the aforementioned two significant $\hat{\alpha}_\lambda$ values is closer to the critical value. It is necessary actually to evaluate $|\delta_\lambda^{(n)}|$ for both $\hat{\alpha}_\lambda$ values by use of eq (30). If the function values are sufficiently different, it may be possible to make the decision by using figure 2 appropriately.

Although in case (a) the location of the point on the curve for which $|\delta_\lambda^{(n)}|$ is maximum is simple, the evaluation of $\delta_\lambda^{(n)}$ at that point must also be accomplished by the use of eq (30), or, if a rough estimate is satisfactory, by the use of figure 2.

10. Appendix C. Evaluation of Limits

As was pointed out earlier, the fundamental expressions (38) (plotted in fig. 3) and (39) (plotted in figs 4 and 5) are indeterminate for several special values of the variables n and α_M. We have already made use of L'Hospital's rule [see eq (13)] to evaluate a limit that took the form 0/0. With appropriate rearrangements of terms, the same device is sufficient to evaluate the limits of (38) and (39) as all the special values are approached, with the exception of the limits as α_M approaches 0. In the latter case, it was found necessary to use the technique of replacing part of the function by its power series expansion; this procedure will be illustrated later.

As an example of the method of application of L'Hospital's rule, let us develop the limit of the expression for $A^{(n)}(\alpha_M)$ in (38) as n approaches infinity (complete bleaching). Let

$$B^{(\infty)} = \lim_{n \to \infty} \left\{ \frac{\alpha_M}{n[1-(1-\alpha_M)^{1/n}]} \right\}^{\frac{n}{n-1}}. \tag{57}$$

The exponent, $n/(n-1)$, approaches 1 as n approaches infinity. The part of the overall limit in (57) that requires manipulation is the limit of the denominator. Let

$$C^{(\infty)} = \lim_{n \to \infty} n[1-(1-\alpha_M)^{1/n}]. \tag{58}$$

The expression (58) approaches the indeterminate form $\infty \cdot 0$. Whenever L'Hospital's rule is to be used, the core of the problem is to rearrange the expression into a fraction to which the

[6] The use of the l.u.b. and the g.l.b. allows for open intervals of $\hat{\alpha}_\lambda$ values, which can arise if there is either a locally nonconstant absorptance continuum with a peak on which an absorptance line is superimposed or a jump discontinuity between locally nonconstant continua. Those not familiar with or interested in this fine point can read "largest" for "least upper bound" and "smallest" for "greatest lower bound."

rule can be successfully applied. The requirements are that the fraction approach a limit of the form 0/0 or ∞/∞ and be of such a form that differentiation simplifies, rather than complicates, the limit evaluation. In the case of the limit in (58), a suitable expression is:

$$C^{(\infty)}=\lim_{n\to\infty}\frac{1-(1-\alpha_M)^{1/n}}{1/n}, \tag{59}$$

which is of the form 0/0.

L'Hospital's rule yields:

$$C^{(\infty)}=\lim_{n\to\infty}\frac{-(1-\alpha_M)^{1/n}\ln(1-\alpha_M)\cdot(-1/n^2)}{-1/n^2}=\lim_{n\to\infty}-(1-\alpha_M)^{1/n}\ln(1-\alpha_M). \tag{60}$$

As long as $\alpha_M \neq 1$ (it being kept in mind, of course, that $0 \leqslant \alpha_M \leqslant 1$):

$$\lim_{n\to\infty}(1-\alpha_M)^{1/n}=(1-\alpha_M)^0=1; \tag{61}$$

so

$$C^{(\infty)}=-\ln(1-\alpha_M), \qquad \alpha_M \neq 1. \tag{62}$$

By applying (62) to the original limit (57), we conclude:

$$B^{(\infty)}=\frac{\alpha_M}{-\ln(1-\alpha_M)}, \qquad \alpha_M \neq 1. \tag{63}$$

Thus, finally, the limit of (38) as $n \to \infty$ is seen to be:

$$A^{(\infty)}(\alpha_M)=\hat{\alpha}_\lambda \text{ for } \max_\lambda |\delta_\lambda^{(\infty)}|=\frac{1}{\alpha_M}\left[1-\frac{\alpha_M}{-\ln(1-\alpha_M)}\right]$$

$$=\frac{1}{\alpha_M}-\frac{1}{-\ln(1-\alpha_M)}, \qquad \alpha_M \neq 0, 1. \tag{64}$$

The uppermost curve in figure 3 is a plot of the function given in (64).

Since the second term of (39), which corresponds to the critical $\hat{\alpha}_\lambda$, is given by (38), we know that once (38) has been evaluated for any of the special arguments, the problem of evaluating (39) reduces to evaluating the first term, which corresponds to the critical $\hat{\alpha}_\lambda^{(n)}$. In the case under consideration, $n \to \infty$, we have already found the general expression for $\hat{\alpha}_\lambda^{(\infty)}$ in eq (14). We could, therefore, obtain the critical α_λ by multiplying (64) by α_M and then simply substitute into (14) to obtain the critical $\hat{\alpha}_\lambda^{(\infty)}$ as a function of α_M. However, to prove that the single expression (39) really does give rise to all the special cases, let us evaluate the first term of (39) directly as a limit. Let

$$G^{(\infty)}=\lim_{n\to\infty}\frac{1-\left\{\frac{\alpha_M}{n[1-(1-\alpha_M)^{1/n}]}\right\}^{\frac{1}{n-1}}}{1-(1-\alpha_M)^{1/n}} \tag{65}$$

$$=\lim_{n\to\infty}\frac{1-\left\{\frac{\alpha_M}{C^{(\infty)}}\right\}^{\frac{1}{n-1}}}{1-(1-\alpha_M)^{1/n}}, \tag{66}$$

where $C^{(\infty)}$, defined by (58), is given explicitly by (62). Thus

$$G^{(\infty)}=\lim_{n\to\infty}\frac{1-\left\{\dfrac{\alpha_M}{-\ln(1-\alpha_M)}\right\}^{\frac{1}{n-1}}}{1-(1-\alpha_M)^{1/n}}. \tag{67}$$

As $n\to\infty$, the exponents in both the numerator and denominator of (67) approach 0, so that, as long as $\alpha_M\neq 0$ or 1, the exponential terms both approach 1. The expression in (67) therefore approaches the form

$$\frac{1-1}{1-1}=\frac{0}{0} \tag{68}$$

and is consequently eligible for direct application of L'Hospital's rule. The result of the differentiation of the numerator and denominator of (67) is:

$$G^{(\infty)}=\lim_{n\to\infty}\frac{-\left\{\dfrac{\alpha_M}{-\ln(1-\alpha_M)}\right\}^{\frac{1}{n-1}}\ln\left\{\dfrac{\alpha_M}{-\ln(1-\alpha_M)}\right\}\cdot\left[\dfrac{-1}{(n-1)^2}\right]}{-(1-\alpha_M)^{1/n}\ln(1-\alpha_M)\cdot\left(\dfrac{-1}{n^2}\right)} \tag{69}$$

$$=\frac{\ln\left\{\dfrac{\alpha_M}{-\ln(1-\alpha_M)}\right\}}{\ln(1-\alpha_M)}=\frac{\ln\alpha_M-\ln[-\ln(1-\alpha_M)]}{\ln(1-\alpha_M)},$$

$$\alpha_M\neq 0,\ 1. \tag{70}$$

The complete evaluation of (39) as $n\to\infty$ can now be obtained by combining (70) and (64), the result being:

$$S^{(\infty)}=|D^{(\infty)}(\alpha_M)|=\max_{\lambda}|\delta_\lambda^{(\infty)}|=\left|\frac{\ln\alpha_M-\ln[-\ln(1-\alpha_M)]}{\ln(1-\alpha_M)}-\left[\frac{1}{\alpha_M}-\frac{1}{-\ln(1-\alpha_M)}\right]\right|$$

$$=\left|\frac{1-\ln\alpha_M+\ln[-\ln(1-\alpha_M)]}{-\ln(1-\alpha_M)}-\frac{1}{\alpha_M}\right|,\qquad \alpha_M\neq 0,\ 1. \tag{71}$$

The function (71) is plotted as the uppermost curve in figure 4, and $D^{(\infty)}(\alpha_M)$ (the function with the absolute value signs omitted) is listed in table 2.

As has been mentioned, all of the limiting-case formulas were derived by methods similar to the L'Hospital's-rule manipulations employed above, except for the case $\alpha_M\to 0$, for which a different method was found necessary. It is possible that some sequence of imaginative rearrangements of terms could allow this case, too, to be treated solely by L'Hospital's rule, but in the absence of such a derivation, the proof to be given here is based on a series expansion, namely:

$$(1-x)^{1/n}=1-\frac{x}{n}-\left(\frac{n-1}{2n^2}\right)x^2+R_3(x)\qquad (x^2<1), \tag{72}$$

where the remainder series $R_3(x)$ is of order x^3 (that is, the leading term contains x^3 as a factor and all succeeding terms contain higher powers of x).

We apply the series (72) by letting $x=\alpha_M$, and replacing $(1-\alpha_M)^{1/n}$ in (38) by the resulting expression. With suitable regrouping of terms, the new form of (38) is then:

$$A^{(n)}(\alpha_M)=\frac{1}{\alpha_M}\left\langle 1-\left[\frac{1}{1+\left(\frac{n-1}{2n}\right)\alpha_M-R_2(\alpha_M)}\right]^{\frac{n}{n-1}}\right\rangle, \tag{73}$$

where $R_2(\alpha_M)$ is a series of order α_M^2.

Straightforward rearrangement allows (73) to be written in the form:

$$A^{(n)}(\alpha_M)=\frac{\left[1+\left(\frac{n-1}{2n}\right)\alpha_M-R_2(\alpha_M)\right]^{\frac{n}{n-1}}-1}{\alpha_M}\cdot\frac{1}{\left[1+\left(\frac{n-1}{2n}\right)\alpha_M-R_2(\alpha_M)\right]^{\frac{n}{n-1}}}. \tag{74}$$

We now make use of the fact that as α_M approaches 0, each term of $R_i(\alpha_M)$ (for any $i\geq 1$) approaches 0, so that the sum of the entire R_i series also approaches 0. Thus, letting α_M approach 0, we see that the second factor in (74) approaches $1/1=1$ (as long as $n\neq 0$ or 1), so that the overall limit is equal to the limit of the first factor. The first factor approaches $(1-1)/0=0/0$, so that L'Hospital's rule can be applied. Differentiating numerator and denominator, we obtain:

$$A^{(n)}(0)=\lim_{\alpha_M\to 0}A^{(n)}(\alpha_M)=\lim_{\alpha_M\to 0}\frac{\left(\frac{n}{n-1}\right)\left[1+\left(\frac{n-1}{2n}\right)\alpha_M-R_2(\alpha_M)\right]^{\frac{n}{n-1}-1}\left[\left(\frac{n-1}{2n}\right)-R_1(\alpha_M)\right]}{1}, \tag{75}$$

where $R_1(\alpha_M)$ is a series of order α_M.

Finally, letting α_M approach 0 in the numerator of (75), we find that the final limit is:

$$A^{(n)}(0)=\left(\frac{n}{n-1}\right)[1]\left[\frac{n-1}{2n}\right]\equiv\frac{1}{2}\qquad(n\neq 0,\ 1). \tag{76}$$

The invalidity of (76) for the two values $n=0$ and 1 is a reflection of the fact that the original expression (38) is not defined for those values. Since (76) does hold for all other values of n, however, we can evaluate the limit of (76) as n approaches 0 and 1, and also as n increases without limit $(n\to\infty)$, and define the function values as equal to these limits. Thus

$$A^{(0)}(0)=\lim_{n\to 0}A^{(n)}(0)=\lim_{n\to 0}\frac{1}{2}=\frac{1}{2} \tag{77}$$

$$A^{(1)}(0)=\lim_{n\to 1}A^{(n)}(0)=\lim_{n\to 1}\frac{1}{2}=\frac{1}{2} \tag{78}$$

$$A^{(\infty)}(0)=\lim_{n\to\infty}A^{(n)}(0)=\lim_{n\to\infty}\frac{1}{2}=\frac{1}{2}. \tag{79}$$

In other words, the value of $A^{(n)}(\alpha_M)$ as $\alpha_M\to 0$ may be taken as 1/2 for *any* value of n.

In order to find $D^{(n)}(0)$, the limit as α_M approaches 0 of the function in (39) with the absolute value signs omitted, we have to evaluate the limit of the first term only, since the second term is the same as (38), which we have just shown approaches 1/2. Let

$$L_0=\lim_{\alpha_M\to 0}\frac{1-\left\{\frac{\alpha_M}{n[1-(1-\alpha_M)^{1/n}]}\right\}^{\frac{1}{n-1}}}{1-(1-\alpha_M)^{1/n}}. \tag{80}$$

Again we use the device of series expansion, converting (80) to the form

$$G_0 = \lim_{\alpha_M \to 0} \frac{1 - \left\{ \dfrac{\alpha_M}{n\left\{1 - \left[1 - \dfrac{\alpha_M}{n} + \left(\dfrac{n-1}{2n^2}\right)\alpha_M^2 + R_3(\alpha_M)\right]\right\}} \right\}^{\frac{1}{n-1}}}{1 - \left[1 - \dfrac{\alpha_M}{n} + \left(\dfrac{n-1}{2n^2}\right)\alpha_M^2 + R_3(\alpha_M)\right]}. \tag{81}$$

After terms are combined in (81), it is clear that the expression approaches the limit $(1-1)/0 = 0/0$ ($n \neq 0, 1$), so that L'Hospital's rule can be applied. The result of differentiating the numerator and denominator and then allowing α_M to approach 0 is:

$$G_0 = \frac{\dfrac{1}{2n}}{\dfrac{1}{n}} \equiv \frac{1}{2} \qquad (n \neq 0, 1). \tag{82}$$

Thus as α_M approaches 0, both the first and second terms of $D^{(n)}(\alpha_M)$ in (39) approach 1/2, and hence the difference approaches 0, for any n other than 0 or 1. In short,

$$D^{(n)}(0) \equiv 0 \qquad (n \neq 0, 1). \tag{83}$$

Continuity considerations analogous to those leading to eqs (77) to (79) allow us to make the definitions

$$D^{(0)}(0) = \lim_{n \to 0} D^{(n)}(0) = \lim_{n \to 0} 0 = 0 \tag{84}$$

$$D^{(1)}(0) = \lim_{n \to 1} D^{(n)}(0) = \lim_{n \to 1} 0 = 0 \tag{85}$$

$$D^{(\infty)}(0) = \lim_{n \to \infty} D^{(n)}(0) = \lim_{n \to \infty} 0 = 0. \tag{86}$$

In other words, the value of $D^{(n)}(\alpha_M)$ as $\alpha_M \to 0$ may be taken as 0 for *any* value of n.

No further resort to series expansion will be necessary. Let us turn now to the case $n = 1$ and evaluate (38) as n approaches 1. Let

$$A^{(1)}(\alpha_M) = \lim_{n \to 1} \frac{1}{\alpha_M} \left\langle 1 - \left\{ \frac{\alpha_M}{n\left[1 - (1-\alpha_M)^{1/n}\right]} \right\}^{\frac{n}{n-1}} \right\rangle \tag{87}$$

$$= \frac{1}{\alpha_M} \langle 1 - B^{(1)} \rangle \qquad (\alpha_M \neq 0), \tag{88}$$

where

$$B^{(1)} = \lim_{n \to 1} \left\{ \frac{\alpha_M}{n\left[1 - (1-\alpha_M)^{1/n}\right]} \right\}^{\frac{n}{n-1}}. \tag{89}$$

In order to convert a limit of the form of (89) into a simple ratio form, it is only necessary to take the logarithms of both sides:

$$\ln B^{(1)} = \lim_{n \to 1} \left(\frac{n}{n-1}\right) \ln \left\{ \frac{\alpha_M}{n\left[1 - (1-\alpha_M)^{1/n}\right]} \right\} \tag{90}$$

$$= \lim_{n \to 1} \frac{n\{\ln \alpha_M - \ln n - \ln\left[1 - (1-\alpha_M)^{1/n}\right]\}}{n-1} \qquad (\alpha_M \neq 0). \tag{91}$$

The expression in (91) approaches 0/0 as $n \to 1$, so L'Hospital's rule is applicable. The result is, for $\alpha_M \neq 0$ or 1:

$$\ln B^{(1)} = \lim_{n \to 1} \frac{n\left\{-\frac{1}{n} + \frac{(1-\alpha_M)^{1/n} \ln (1-\alpha_M)\left(-\frac{1}{n^2}\right)}{1-(1-\alpha_M)^{1/n}}\right\} + \{\ln \alpha_M - \ln n - \ln [1-(1-\alpha_M)^{1/n}]\} \cdot 1}{1}. \tag{92}$$

As n approaches 1, the second term in (92) vanishes, while the first term approaches

$$-1 - \frac{(1-\alpha_M) \ln (1-\alpha_M)}{\alpha_M}. \tag{93}$$

Rearrangement of terms then allows us to write:

$$\ln B^{(1)} = \ln \left[e^{-1} \cdot (1-\alpha_M)^{-\left(\frac{1-\alpha_M}{\alpha_M}\right)}\right]. \tag{94}$$

Thus, taking antilogs and substituting for $B^{(1)}$ in (88), we have:

$$A^{(1)}(\alpha_M) = \frac{1}{\alpha_M}\left[1 - \frac{1/e}{(1-\alpha_M)^{\frac{1-\alpha_M}{\alpha_M}}}\right] \qquad (\alpha_M \neq 0, 1). \tag{95}$$

Evaluating (95) as α_M approaches 0 or 1 would complete the calculation of a double limit; that is, the limit as $\alpha_M \to 0$ (or $\alpha_M \to 1$) of the limit as $n \to 1$ of (38). Both double limits happen to be much easier to evaluate when the limits are taken in reverse order; that is, when the calculation is of the limit as $n \to 1$ of the limit as $\alpha_M \to 0$ (or $\alpha_M \to 1$) of (38). Such interchange of the order of limits does not change the final value for continuous functions, and, as a check, the limits were derived both ways to be sure (although the more difficult methods will not be shown here). The limit as $\alpha_M \to 0$ was already found, quite easily, in (78). The case $\alpha_M = 1$, for values of n other than 0, 1, or ∞, is not a limiting case, and simple substitution in (38) yields the expression:

$$A^{(n)}(1) = 1 - \frac{1}{n^{\frac{n}{n-1}}}. \tag{96}$$

Similarly, setting $\alpha_M = 1$ in (39) gives:

$$D^{(n)}(1) = -\frac{n-1}{n^{\frac{n}{n-1}}}. \tag{97}$$

Finding the limit of (96) as $n \to 1$ is equivalent to finding the limit as $\alpha_M \to 1$ of (95).

By taking the logarithms of both sides and then applying L'Hospital's rule, it is easy to derive that

$$\lim_{n \to 1} n^{\frac{n}{n-1}} = e. \tag{98}$$

With (98) established, it follows directly from (96) and (97) that

$$A^{(1)}(1) = 1 - \frac{1}{e} \tag{99}$$

and

$$D^{(1)}(1)=0. \tag{100}$$

We now complete the case $n\to 1$ by finding $D^{(1)}(\alpha_M)$ corresponding to $A^{(1)}(\alpha_M)$ in (95). We need only find the limit as $n\to 1$ of the first term in (39), the limit of the second term being equal to $A^{(1)}(\alpha_M)$. Let

$$G^{(1)}=\lim_{n\to 1}\frac{1-\left\{\dfrac{\alpha_M}{n[1-(1-\alpha_M)^{1/n}]}\right\}^{\frac{1}{n-1}}}{1-(1-\alpha_M)^{1/n}} \tag{101}$$

$$=\frac{1-\lim\limits_{n\to 1}\langle B^{(1)}\rangle^{1/n}}{\alpha_M}\qquad(\alpha_M\neq 0), \tag{102}'$$

where $B^{(1)}$ is defined by (89) and evaluated in (94). We conclude from (102) that

$$G^{(1)}=\frac{1}{\alpha_M}\langle 1-B^{(1)}\rangle\qquad(\alpha_M\neq 0); \tag{103}$$

and (88) establishes that

$$G^{(1)}=A^{(1)}(\alpha_M). \tag{104}$$

Thus, since

$$D^{(1)}(\alpha_M)=G^{(1)}-A^{(1)}(\alpha_M) \tag{105}$$

[a special case of eq (39)], (104) implies that

$$D^{(1)}(\alpha_M)\equiv 0\qquad(\alpha_M\neq 0). \tag{106}$$

We have now shown that for *any* value of α_M, there is no shape change at all for $n=1$. This conclusion is obviously correct, since with no change of concentration there is no change of shape. Although we have proved above by limit methods that eq (39) correctly implies this fact, a much more straightforward proof of (106) is obtained by simply setting $n=1$ in (30). [The restriction $\alpha_M\neq 0$ in (30) is tacit, as explained following (11)]. The resulting conclusion,

$$\delta_\lambda^{(1)}\equiv 0\qquad(\alpha_M\neq 0), \tag{107}$$

means that for $n=1$ there is no shape change anywhere along the curve, so that, in particular, the shape at the point where $\hat{\alpha}_\lambda=A^{(1)}(\alpha_M)$ (that is, the maximum change) is also zero.

Returning to formulas (96) and (97), we can now easily fill in the limits for the case $n\to\infty$ for $\alpha_M\to 1$. The same values could also have been obtained by the reverse ordering of the limits; that is, by letting $n\to\infty$ in (64) and (71); these latter derivations are omitted here. By (96), we have:

$$A^{(\infty)}(1)=\lim_{n\to\infty}A^{(n)}(1)=\lim_{n\to\infty}\left[1-\frac{1}{n^{\frac{n}{n-1}}}\right]=1-\frac{1}{\lim\limits_{n\to\infty}n^{\frac{n}{n-1}}}. \tag{108}$$

Let

$$H^{(\infty)} = \lim_{n \to \infty} n^{\frac{n}{n-1}}. \tag{109}$$

Then, taking logarithms and applying L'Hospital's rule, we find that

$$H^{(\infty)} = \infty, \tag{110}$$

and, substituting (110) into (108), we conclude:

$$A^{(\infty)}(1) = 1 - \frac{1}{\infty} = 1 - 0 = 1. \tag{111}$$

By (97), we have:

$$D^{(\infty)}(1) = \lim_{n \to \infty} D^{(n)}(1) = \lim_{n \to \infty} \frac{-1}{n^{\frac{1}{n-1}}} + \lim_{n \to \infty} \frac{1}{n^{\frac{n}{n-1}}}. \tag{112}$$

The second limit in (112) is the reciprocal of $H^{(\infty)}$, defined in (109) and evaluated in (110) as equal to ∞. Hence the second limit is $1/\infty = 0$.

The first limit in (112) is the negative reciprocal of

$$J^{(\infty)} = \lim_{n \to \infty} n^{\frac{1}{n-1}}. \tag{113}$$

Taking logarithms and applying L'Hospital's rule, we conclude that

$$J^{(\infty)} = 1. \tag{114}$$

Thus the first limit in (112) is the negative reciprocal of 1, which is -1. Therefore

$$D^{(\infty)}(1) = -1 + 0 = -1. \tag{115}$$

The last limits remaining to be worked out here are those for $n \to 0$. Let

$$A^{(0)}(\alpha_M) = \lim_{n \to 0} \frac{1}{\alpha_M} \left\langle 1 - \left\{ \frac{\alpha_M}{n[1 - (1 - \alpha_M)^{1/n}]} \right\}^{\frac{n}{n-1}} \right\rangle \tag{116}$$

$$= \frac{1}{\alpha_M} \langle 1 - B^{(0)} \rangle \qquad (\alpha_M \neq 0), \tag{117}$$

where

$$B^{(0)} = \lim_{n \to 0} \left\{ \frac{\alpha_M}{n[1 - (1 - \alpha_M)^{1/n}]} \right\}^{\frac{n}{n-1}} \tag{118}$$

or

$$\ln B^{(0)} = \lim_{n \to 0} \left\langle \left(\frac{n}{n-1} \right) \ln \left\{ \frac{\alpha_M}{n[1 - (1 - \alpha_M)^{1/n}]} \right\} \right\rangle \tag{119}$$

$$= \lim_{n \to 0.} \frac{n \ln \alpha_M}{n-1} - \lim_{n \to 0} \frac{n \ln n}{n-1} - \lim_{n \to 0} \frac{n \ln [1-(1-\alpha_M)^{1/n}]}{n-1} \qquad (\alpha_M \neq 0). \tag{120}$$

The first term in (120) is simply equal to 0 as it stands. To evaluate the second limit, we divide numerator and denominator by n and apply L'Hospital's rule, the result being a limit of 0.

To evaluate the last limit in (120) we observe that if

$$0 < \alpha_M < 1, \tag{121}$$

then also

$$0 < 1-\alpha_M < 1. \tag{122}$$

If a quantity properly between 0 and 1 is raised to a power that grows larger without limit, the result approaches 0. Hence

$$\lim_{n \to 0} (1-\alpha_M)^{1/n} = 0 \qquad (\alpha_M \neq 0, 1), \tag{123}$$

so that

$$\lim_{n \to 0} \ln [1-(1-\alpha_M)^{1/n}] = \ln [1-0] = \ln 1 = 0 \qquad (\alpha_M \neq 0, 1). \tag{124}$$

Thus all three limits in (120) are 0, and

$$\ln B^{(0)} = 0-0-0 = 0 \qquad (\alpha_M \neq 0, 1), \tag{125}$$

or

$$B^{(0)} = 1 \qquad (\alpha_M \neq 0, 1). \tag{126}$$

We conclude from (117) that

$$A^{(0)}(\alpha_M) = \frac{1}{\alpha_M} \langle 1-1 \rangle \equiv 0 \qquad (\alpha_M \neq 0, 1). \tag{127}$$

To evaluate $D^{(0)}(\alpha_M)$ we need the limit as $n \to 0$ of the first term of (39). Let

$$G^{(0)} = \lim_{n \to 0} \frac{1 - \left\{ \dfrac{\alpha_M}{n[1-(1-\alpha_M)^{1/n}]} \right\}^{\frac{1}{n-1}}}{1-(1-\alpha_M)^{1/n}} \tag{128}$$

$$= \lim_{n \to 0} \frac{1 - \left\{ \dfrac{n[1-(1-\alpha_M)^{1/n}]}{\alpha_M} \right\}^{\frac{1}{1-n}}}{1-(1-\alpha_M)^{1/n}}. \tag{129}$$

Taking note of (123), we see immediately that

$$G^{(0)} = \frac{1 - \left\{ \dfrac{0[1-0]}{\alpha_M} \right\}^{\frac{1}{1-0}}}{1-0} = \frac{1-0^1}{1} = \frac{1}{1} = 1 \qquad (\alpha_M \neq 0, 1). \tag{130}$$

Thus, from (127) and (130) we see that

$$D^{(0)}(\alpha_M) \equiv G^{(0)} - A^{(0)}(\alpha_M) \equiv 1 - 0 \equiv 1 \qquad (\alpha_M \neq 0, 1). \tag{131}$$

Obviously, by (127),

$$A^{(0)}(1) = \lim_{\alpha_M \to 1} A^{(0)}(\alpha_M) = \lim_{\alpha_M \to 1} 0 = 0; \tag{132}$$

and, by (131),

$$D^{(0)}(1) = \lim_{\alpha_M \to 1} D^{(0)}(\alpha_M) = \lim_{\alpha_M \to 1} 1 = 1. \tag{133}$$

Reassuring confirmations of these limits are easily obtained by reversing the order of the variables. We see from (96) that

$$A^{(0)}(1) = \lim_{n \to 0} A^{(n)}(1) = 1 - \frac{1}{\lim\limits_{n \to 0} n^{\frac{n}{n-1}}}. \tag{134}$$

Evaluation of the limit in (134) by the now-familiar procedure of taking logarithms and then applying L'Hospital's rule yields a limit of 1, and so we conclude that

$$A^{(0)}(1) = 1 - \frac{1}{1} = 1 - 1 = 0, \tag{135}$$

in confirmation of (132).

Similarly, (97) tells us that

$$D^{(0)}(1) = \lim_{n \to 0} D^{(n)}(1) = \lim_{n \to 0} \left[-\frac{n-1}{n^{\frac{n}{n-1}}} \right] \tag{136}$$

$$= \frac{-1}{\lim\limits_{n \to 0} n^{\frac{1}{n-1}}} + \frac{1}{\lim\limits_{n \to 0} n^{\frac{n}{n-1}}}. \tag{137}$$

The second limit in (137) is the same as that in (134) and is equal to 1. The first limit (denominator) requires no manipulation, and is directly equal to $0^{-1} = \infty$. Thus (137) becomes

$$D^{(0)}(1) = \frac{-1}{\infty} + \frac{1}{1} = 1, \tag{138}$$

in confirmation of (133).

Each of the six limits $A^{(\infty)}(0)$, $A^{(\infty)}(1)$, $A^{(1)}(0)$, $A^{(1)}(1)$, $A^{(0)}(1)$, and $A^{(0)}(0)$, and each of the six corresponding D limits, can be derived from two different more general formulas. These are the cases for which one can proceed by taking the n limit first and the α_M limit second, or the reverse. Only for the limits $A^{(0)}(1)$ and $D^{(0)}(1)$ that have just been discussed have we actually shown the consistency of the two possible evaluations of such limits, but consistency exists in all the other cases, too, *except for* $A^{(0)}(0)$ and $D^{(0)}(0)$.

If we define $A^{(0)}(0)$ as

$$\lim_{n \to 0} A^{(n)}(0),$$

as we in fact did in (77), we arrive at a limit value of 0.5, the value characterizing $\alpha_M = 0$ for all other n values. If, however, we define $A^{(0)}(0)$ as

$$\lim_{\alpha_M \to 0} A^{(0)}(\alpha_M),$$

it is clear from (127) that we would arrive at a limit of 0, the value characterizing $n = 0$ for all other α_M values. Thus, whether we choose to define $A^{(0)}(0)$ as 0.5 or 0, we will be violating continuity in one respect or another. The decision as to which definition to adopt must therefore be made on some basis other than the simple preservation of continuity.

Inspection of figure 3 reveals the basis for adopting the definition $A^{(0)}(0) = 0.5$. The alternative definition, $A^{(0)}(0) = 0$, would preserve the full continuity of the single curve for $n = 0$ ($P = -\infty$), but would destroy the continuity of the entire family of curves. It is obvious that as one moves downward in figure 3 ($n \to 0$), the vertical and horizontal legs of the curves become progressively straighter and the bend between these legs becomes progressively sharper. The limiting curve ought to have a vertical leg, just as all the others do, and the visual impression is compelling that the limiting curve is the right angle formed by the vertical and horizontal axes of the graph. It appears intuitively that it would constitute a more serious violation of the overall scheme to have the limiting curve of the family be of a grossly different character than all the other curves, than it would to have that one limiting curve possess a truly vertical leg—that is, a discontinuity. It is, in fact, precisely this vertical leg that makes the $n = 0$ curve fit in with the rest of the curve family.

As for $D^{(0)}(0)$, it could reasonably be defined either as 0, as it was in (84), or as 1, as it would be if it were calculated as

$$\lim_{\alpha_M \to 0} D^{(0)}(\alpha_M)$$

[see eq (131)]. Because figure 5 is a log-log plot, it does not provide a compelling geometrical impression of what the top limiting curve ($P = -\infty$) ought to be; an arithmetical plot would have shown that the limiting curve appears to be not the upper edge of the graph [the line $S^{(n)} = 1$], but the right angle formed by the upper and left edges [the horizontal line $S^{(n)} = 1$ and the vertical line $\alpha_M = 0$]. However, a consideration of the *meaning* of the case $\alpha_M = 0$, $n = 0$ leads to the inevitable conclusion that $D^{(0)}(0) = 0$ is the reasonable choice. If $\alpha_M = 0$, we are dealing with a pigment with a perfectly flat absorptance curve ($\alpha_\lambda \equiv 0$), and the shape of a flat curve stays the same—namely, flat—no matter how much the concentration of the pigment is changed. Thus the shape difference everywhere along the curve, and consequently the maximum difference $D^{(0)}(0)$ as well, is zero.

The argument for $D^{(0)}(0) = 1$ is wholly unconvincing; in fact it turns into an additional argument for $D^{(0)}(0) = 0$. When $n = 0$, we are dealing with an infinitely increased concentration (or thickness) of pigment. We know that wherever a pigment has any absorptance at all, it absorbs completely when infinitely concentrated, so the maximum shape change is infinitesimally different from 1 [7] for a pigment that contains a continuous range of absorptances including 0 and extending any finite amount above 0. However, at any wavelength where the original absorptance is actually 0, it remains 0 no matter how much the concentration is increased. Therefore, if an absorptance curve is 0 everywhere, the reasoning that leads to a maximum shape change of 1 for more ordinary curves breaks down, and the shape change is 0 everywhere.

[7] More precisely, the least upper bound (l.u.b.) of the shape changes is 1.

11. References

[1] Wolbarsht, M. L., in Ciba Foundation Symposium: Colour Vision: Physiological and Experimental Psychology, p. 279 (Little, Brown and Company, Boston, 1965). Refs. 1–3 are not meant by any means to be an exhaustive list, but only a sampling of three recent explicit statements of disaffection from the pigment-concentration theory of chromatic adaptation.

[2] Rushton, W. A. H., in Ciba Foundation Symposium: Colour Vision: Physiological and Experimental Psychology, p. 368 (Little, Brown and Company, Boston, 1965).

[3] Terstiege, H., Untersuchungen zum Persistenz- und Koeffizientensatz, doctoral dissertation, Technical University of Berlin (Musterschmidt-Verlag, Göttingen, 1966). Also in press in Farbe **16** (1967).

[4] Wright, W. D., Proc. Roy. Soc. (London) **B115,** 49 (1934).

[5] Wright, W. D., J. Physiol. (London) **87,** 23 (1936).

[6] Brindley, G. S., J. Physiol. (London) **122,** 332 (1953).

[6a] Goldstein, E. B., and Williams, T. P., Vision Res. **6,** 39 (1966).

[7] Hunt, R. W. G., Adaptation and the trichromatic theory, in Visual Problems of Colour, National Physical Laboratory Symposium No. 8 (Her Majesty's Stationery Office, London, 1958), Vol. **II,** p. 641. See p. 643; also statement by W. S. Stiles on p. 733.

[7a] For a discussion of Beer's and Bouguer's laws, see for example: Committee on Colorimetry of the Optical Society of America, The Science of Color, p. 180 (Thomas Y. Crowell Co., New York, 1953).

[8] Dartnall, H. J. A., The Visual Pigments, p. 16 (Methuen and Co., London, 1957).

[9] Judd, D. B., J. Opt. Soc. Am. **35,** 199 (1945).

[10] Ref. 3, p. 51 of the dissertation.

[11] Wyszecki, G., and Stiles, W. S., Color Science: Concepts and Methods, Quantitative Data and Formulas, p. 219 (John Wiley & Sons, Inc., New York, 1967).

[12] Wald, G., Science **101,** 653 (1945).

[13] Marks, W. B., Dobelle, W. H., and MacNichol, E. F., Jr., Science **143,** 1181 (1964).

[14] Brown, P. K., and Wald, G., Science **144,** 45 (1964).

[15] Liebman, P. A., and Entine, G., J. Opt. Soc. Am. **54,** 1451 (1964). This paper reports measurements on goldfish cones only, while Refs. 17 and 18 show data for humans and monkeys.

[16] Rushton, W. A. H., Ann. N.Y. Acad. Sci. **74,** 291 (1958).

[17] Walraven, P. L., in discussion of H. Terstiege, Der Einfluss von Sehstoff-Konzentrationsänderungen auf Farbgleichungen, in Internationale Farbtagung Luzern 1965: Tagungsbericht, Vol. **1,** p. 154 (Musterschmidt-Verlag, Göttingen, 1966).

[18] Weale, R. A., High light intensities and photochemical reactions of human visual pigments in situ, in Cold Spring Harbor Symposia on Quantitative Biology: Sensory Receptors (Cold Spring Harbor Laboratory of Quantitative Biology, Cold Spring Harbor, Long Island, N.Y., 1965), Vol. **30,** p. 335. See Weale's statement in the discussion of his paper, p. 343.

[19] See, for example, P. L. Walraven, in Recent Progress in Photobiology, Proceedings of the 4th International Photobiology Congress, Oxford, 1964, p. 128 (Blackwell Scientific Publications, Oxford, 1965).

[20] Brindley, G. S., Proc. Phys. Soc. (London) **68B,** 862.

[21] Walraven, P. L., On the mechanisms of colour vision, doctoral dissertation, University of Utrecht, p. 23 (Institute for Perception RVO–TNO, Soesterberg, Netherlands, 1962).

[22] Rushton, W. A. H., Nature **206,** 1087 (1965).

[23] MacNichol, E. F., Jr., personal communication.

(Paper 72A4–504)

JOURNAL OF RESEARCH of the National Bureau of Standards—A. Physics and Chemistry
Vol. 72A, No. 4, July–August 1968

Periodic Acid, a Novel Oxidant of Polycyclic, Aromatic Hydrocarbons*

Alexander J. Fatiadi

Institute for Materials Research, National Bureau of Standards, Washington, D.C. 20234

(April 1, 1968)

Certain polycyclic, aromatic hydrocarbons can be oxidized with periodic acid in aprotic solvents containing a small proportion of water. A unique, two-fold character of response to periodic acid by these hydrocarbons has been found: (1) production of a coupling reaction through a radical intermediate [conversion of pyrene into 1,1′-bipyrene, and fluorene into 1,2-bis(2,2′-biphenylylene)ethylene] or (2) conversion into quinones by a two-equivalent oxidation mechanism that does not involve a radical intermediate [acenaphthene, anthracene, anthrone, benz[*a*]anthracene, naphthacene, naphthalene, and phenanthrene]. Little or no reaction was observed when oxidation was attempted with sodium metaperiodate instead of periodic acid.

Electron-spin resonance revealed no radical intermediate in the oxidation of malonic acid with either periodic acid or sodium periodate.

Key Words: Aprotic solvents; aromatic hydrocarbons; malonic acid; periodic acid; pyrene radical; quinones; reaction mechanism; sodium metaperiodate.

1. Introduction

Recently in this laboratory [1],[1] the fate of certain of the polycyclic, aromatic hydrocarbons that have been identified as constituents of polluted air has been studied under conditions simulating those that these substances encounter as air pollutants; that is, (a) in the presence of ultraviolet irradiation, (b) exposure to air and slight heat, and (c) contact with powdered solids (particulates). Oxidation of many of the hydrocarbons studied occurs under such conditions. In order to identify the products, it was necessary to synthesize possible oxidation products for use as reference materials.

The main object of the present report is to describe the usefulness of periodic acid for the oxidation of polycyclic, aromatic hydrocarbons. Numerous reagents have been used to effect such oxidations, including the Milas reagent [2], the Fenton reagent [3], benzoyl peroxide [4, 5], benzyl radicals [6], phenyl radicals [7], and other free-radical reagents [8], lead tetraacetate [9, 10], ozone [11–14], and peroxy acids [15] including hydrogen peroxide in acetic acid [16], peroxyacetic acid [17, 18], and peroxytrifluoroacetic acid [19–21]. In addition, there are autooxidations [22], metabolic oxidation [23], peroxidase oxidation [24], photooxidation using solutions [25], photooxidation on solids [1], one-electron transfer oxidation [26], and various other methods [27].

Periodic acid (or its salts) has been used extensively for cleavage of 1,2-glycols, and α-hydroxy-aldehydes and -ketones [28–33]. In aprotic solvents containing some water, periodic acid has been used for the oxidative hydroxylation of an active methylene group [34–36], for oxidative cleavage of enols and reductones [37, 38], and for hydroxylation and further oxidation of compounds containing an isolated double bond, e.g., cinnamic acid [39] and cholesterol [40].

The application of periodic acid alone as an oxidant for polycyclic, aromatic hydrocarbons has not hitherto been reported [33, 41]. Sodium metaperiodate has, however, been used conjointly with such diol-forming agents as osmium tetraoxide or ruthenium tetraoxide [42]. The present study shows that, when it reacts with certain polycyclic, aromatic compounds, periodic acid has the ability to (1) produce radicals by abstraction of (a) electrons or (b) protons, (2) oxidize a methine group at an activated double bond of polycyclic, aromatic compounds, or (3) oxidize an activated methylene group.

2. Reaction Conditions

2.1. Solvent

The choice of a solvent in which to oxidize polycyclic, aromatic hydrocarbons with periodic acid appears to

*Preliminary communication: Chem. Commun. **1967**, 1087.

[1] Figures in brackets indicate the literature references at the end of this paper.

be very important. In the present work, glacial acetic acid was usually the first solvent investigated; sometimes, propionic acid could be used. In most cases, oxidations in formic acid afford lower yields than in acetic acid. A series of aprotic solvents, miscible with water and relatively stable in the presence of periodic acid at elevated temperature, was tried. These solvents, in the order of their decreasing stability to the oxidant are: *N,N*-dimethylformamide, *p*-dioxane, acetonitrile, acetone, tetrahydrofuran, methyl sulfoxide, and acetic anhydride. Methyl sulfoxide was used in the oxidation of anthracene with good results, but its application with other hydrocarbons has not yet been explored.

The stability of *N,N*-dimethylformamide in the presence of periodic acid has previously been indicated [43]. Such solvents as formamide, 2-methoxyethanol, bis(2-methoxyethyl) ether (diglyme), or 1,2-dimethoxyethane are not suitable as the reaction medium, because of instability in the presence of periodic acid at elevated temperature. When acetic anhydride was used in the oxidation of pyrene with periodic acid, with application of heat, a violent reaction occurred.

2.2. Temperature

To initiate oxidation of polycyclic, aromatic hydrocarbons with periodic acid, some degree of heating was found to be necessary. In the conversion of pyrene (**1**) into 1,1′-bipyrene (**2**) only mild warming (40 to 50 °C) was necessary; however, dimerization of fluorene (**20**) into 1,2-bis(2,2′-biphenylylene)ethylene (**24**) required a much higher temperature. The oxidations that resulted in quinone formation usually require 5 to 10 min of heating at 95 to 130 °C to start; then the temperature must be lowered to 60 to 80 °C to avoid vigorous and sometimes violent reaction. Usually, the beginning of the oxidation (and the end of the induction period) is noted by a change of the reaction medium from colorless to red or brown-red; sometimes, this is followed by evolution of iodine vapor.

2.3. Proportion of the Oxidant

Oxidative dimerization of pyrene (**1**) to 1,1′-bipyrene (**2**) was effected with a 1:1 mole ratio of periodic acid to hydrocarbon. In this reaction, it was possible to demonstrate stoichiometric consumption of the periodic acid. However, in the oxidation of the other hydrocarbons to quinones, approximately 4.2 moles of the oxidant were used per mole of hydrocarbon. This proportion was employed on the assumption that, in each hydrocarbon molecule, two methine or methylene groups become hydroxylated and then oxidized to the corresponding quinone.

2.4. Compounds Oxidized

Three kinds of polycyclic, aromatic hydrocarbons were used in the oxidations: (1) compounds having the acene structure with two active methine groups [naphthacene (**3**), anthracene (**4**), naphthalene (**7**), benz[*a*]anthracene (**12**), and pentacene (**17**)], (2) a compound having the phene structure and one active methine group [pyrene (**1**)], and (3) compounds having one or two active methylene groups [anthrone (**8**), acenaphthene (**15**), and fluorene (**20**)]. Malonic acid (**14**), which has an active methylene group, was also oxidized. In addition, the following condensed-ring, polycyclic, aromatic hydrocarbons were tested: biphenyl, chrysene, coronene, fluoranthene, perylene, picene, *p*-terphenyl, and triphenylene.

3. Results and Discussion

3.1. Effect of Solvent

The effect of various solvents on the reaction may be seen from the following examples: oxidation of phenanthrene (**10**) with periodic acid gave a poor yield (3–6%) of phenanthrenequinone (**11**) in *N,N*-dimethylformamide or in glacial acetic acid, but a good yield (45–55%) in *p*-dioxane. Anthracene (**5**) afforded a moderate yield (30%) of anthraquinone (**6**) in acetic acid, a good yield (50 to 60%) in acetone or methyl sulfoxide, and an excellent yield (90%) in *N,N*-dimethylformamide. Naphthalene (**7**) in *p*-dioxane was practically unaffected; but, in acetic acid, showed oxidation in good yield (70%) to 1,4-naphthoquinone (**9**). Naphthacene (**3**) gave a low yield (10–15%) of naphthacenequinone (**4**) when oxidized in *p*-dioxane or acetic acid, but an excellent yield (80%) in *N,N*-dimethylformamide. Pyrene (**1**) was not oxidized in *N,N*-dimethylformamide, *p*-dioxane, acetone, or ethanol, but was oxidized in acetic acid. Fluorene (**20**) was not affected in *N,N*-dimethylformamide, *p*-dioxane, or acetonitrile, but dimerized in acetic acid.

It may be concluded from these experiments that the solvent participates in the overall reaction process. As noted by Ritchie and co-workers [44], the effect of the solvent on reactions in solution is associated with a so-called solvent reorganization, and this factor may make an appreciable contribution to energies of activation in solution. Furthermore, the polarity of the solvent may partake in promotion of the rate of oxidation, by hydrogen bonding in the transition state.

3.2. General Reactivity of Polycyclic, Aromatic Compounds Toward Periodic Acid

Results obtained in this study on the action of periodic acid on a variety of polycyclic, aromatic hydrocarbons reveal that linear and angular polycyclic, aromatic hydrocarbons having the acene structure (anthracene, benz[*a*]anthracene, naphthacene, pentacene, and their analogs) [45] are the most reactive; next are the condensed-ring aromatic compounds having the phene structure (acenaphthene, benzo[*a*]pyrene, pyrene, etc.) [46]; and chrysene and picene are less reactive. Little or no reaction was observed with biphenyl, coronene, fluoranthene, perylene, *p*-terphenyl, and triphenylene.

The stability of perylene and triphenylene toward periodic acid may partially be explained by an asymmetric annelation effect [47, 48], by which a hydrocarbon attains the maximum number of aromatic sextets and, consequently, the maximum degree of stability. Other factors that may influence the reactivity of polycyclic, aromatic hydrocarbons toward periodic acid are: (1) basicity of the hydrocarbon [49, 50], (2) presence of a reactive bond or a free-valence center [51, 52, 53], or a position of highest unpaired electron-densities [54, 55] or high unpaired spin-densities [56], (3) ability of periodic acid (as an electrophile) to form an association complex with a hydrocarbon, and (4) the ionization potential of the hydrocarbon [57, 58]. Increasing reactivity toward periodic acid is usually paralleled by a decreasing ionization potential of the hydrocarbon, as follows: naphthacene (**3**) > pentacene (**17**) > pyrene (**1**) > anthracene (**5**) > phenanthrene (**10**) > naphthalene (**7**). This may explain why naphthacene (**3**), having an ionization potential of 6.92 eV. [57], is most reactive, and naphthalene (**7**), having an ionization potential of 8.60 eV. [57], is the least reactive in the series.

In general, periodic acid preferably attacks a reactive center instead of a reactive bond of the aromatic ring in the polycyclic hydrocarbons. For example, anthracene (**5**) is attacked by periodic acid at the most reactive (*para*) centers (9,10-positions), instead of at the most reactive bond (the 1,2-positions). Phenanthrene (**10**) is attacked at the 9,10-positions, which constitute the most reactive bond and are the most reactive centers of the hydrocarbon.

a. Oxidation of Pyrene With Periodic Acid (1:1 Mole Ratio)

Treatment of pyrene (**1**) with periodic acid (1:1 mole ratio) in aqueous acetic acid has been shown [59] to give 1,1′-bipyrene (**2**) in a yield of over 70 percent. The formation of the radical intermediate postulated [59] in the coupling reaction has now been verified by electron-spin resonance measurement, and the pyrene radical (**1a**) has been observed at room temperature. Thus, oxidative dimerization of **1** to **2** probably proceeds through intermediate **1a** as depicted. Abstraction of a π-electron by a molecule of periodic acid from an aromatic nucleus would produce the pyrene radical **1a**; dimerization to the stable 1,1′-bipyrene (**2**) would follow the loss of one proton [60–62]. The overall oxidation process of **1** to dimer **2** involves the loss of two protons. In its ability to abstract an electron from the aromatic ring, the acceptor (periodic acid) functions like organic peroxides, which generally abstract electrons from donor molecules [63].

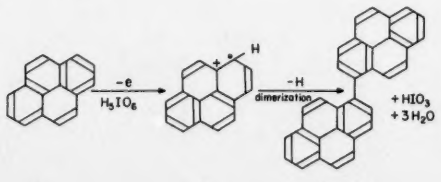

1 1a 2

The mechanism of π-electron abstraction and loss of a proton involved in the dimerization of **1** to **2** resembles the mechanism recently proposed by Cooper and Waters [64, 65]; this is an outer-sphere mechanism postulated to operate in the oxidation of aromatic hydrocarbons by cobaltic ions. Acetic acid may, by solvation, protect the radicals prior to dimerization. As may be seen by examination of a model of dimer **2**, dimerization of the radical cations (**1a**) probably proceeds by their approaching each other head-to-head to give a less sterically hindered product. The e.s.r. spectrum of pyrene radical **1a** is shown in figure 1 (spectrum A).

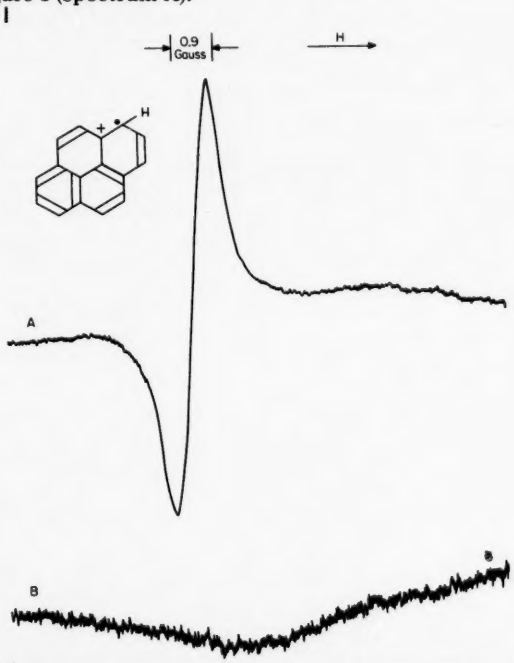

FIGURE 1. *(A) The electron-spin resonance spectrum of pyrene radical* **1a** *prepared by treatment of pyrene (in acetic acid) with periodic acid, H_5IO_6 (in water) at room temperature, g = 2.0041. (B) Anthracene (in N,N-dimethylformamide) on treatment with periodic acid in water. Sample B seen under comparable conditions. No radicals were observed, and the upper limit of radical concentration is at most $^1/_{1000}$th of that in sample A.*

The absence of the hyperfine structure for the pyrene radical cation (**1a**), as compared to the seven-line spectrum of the equivalent [54, 66] pyrene anion radical (splitting constant 1.09 gauss) [67] may be explained on the basis of a probable interaction of the π-electron radical (**1a**) originally formed with oxygen, to give a relatively stable pyrene peroxide (sigma) radical of type **24**; this reaction is probably in competition with the dimerization of **1a** to **2**. The oxygen was probably supplied by periodic acid, because dilution and deoxygenation (by bubbling nitrogen into the diluted solution) produced a similar one-line e.s.r. spectrum. It is known that dissolved oxygen can cause line-broadening in the e.s.r. spectrum by spin–spin inter-

action (dipole interaction); the spectrum can also be narrowed to one line by exchange interaction between the radical and the hydrocarbon.

b. Oxidation of Pyrene With Periodic Acid (1:4 Mole Ratio)

Treatment of pyrene (**1**) with periodic acid (1:4 molar ratio) at 95 °C initially affords green-yellow **2** which, on further stirring (30 min), changes to lustrous, brown crystals. The resulting crystalline compound is probably an addition complex between **2**, iodine, iodic acid, or periodic acid; but the structure of the compound is not yet known. The product cannot be recrystallized without loss of iodine. Analysis of the unknown indicated the presence of up to 59 percent iodine; titration of a solution of the unknown in *N,N*-dimethylformamide with sodium thiosulfate in acidic solution, and with arsenite in basic solution, confirmed the presence of iodine and iodate. The product loses iodine on being heated at 230 °C/0.05 mm, to yield crude **2** (identified by thin-layer chromatography) in addition to an unknown iodo compound. The same result was observed when the unknown was heated with a 30 percent aqueous solution of sodium hydrogen sulfite. Recrystallization of the unknown compound from boiling, glacial acetic acid gave a very small yield of the new compound as light-brown crystals; its infrared spectrum showed two bands, at 5.75 (nonconjugated C=O) and at 6.1 μm (conjugated C=O).

c. Oxidation of Polycyclic, Aromatic Hydrocarbons to Quinones; Possible Reaction Mechanisms

As reported by Bunton [68], periodic acid in aqueous solution exists as an equilibrium between the free acid and its various anions. When an aqueous solution

$$H_5IO_6 \leftrightarrows H_4IO_6^- \leftrightarrows H_3IO_6^{2-} \leftrightarrows H_2IO_6^{3-}$$

of periodic acid is mixed with an excess of acetic acid (or other water-miscible solvent used in the reaction), the equilibrium is shifted to the left (undissociated acid). Hence, under the reaction conditions described, periodic acid can function as the free acid and as the monoanion; these two forms will be used here in discussing possible reaction mechanisms for the oxidation of a variety of polycyclic, aromatic hydrocarbons to quinones.

It is assumed that, in the oxidation of polycyclic, aromatic hydrocarbons having a reactive center and a methine group, the properties of which can be compared to the nucleophilic character of the olefinic group [69], the attacking species is free periodic acid (an electrophile); whereas, in the oxidation of polycyclic, aromatic hydrocarbons having an active methylene group, which is more acidic than the methine group, the attacking species is probably the monoanion of periodic acid (a supplier of active hydroxyl groups); thus, the oxidizing species involved depends on the nature of the hydrocarbon employed.

To determine whether periodic acid would serve as a general reagent for effecting coupling reactions similar to that described for pyrene, a number of other polycyclic, aromatic hydrocarbons were treated with this reagent. Although it was found that many of these hydrocarbons are indeed affected by periodic acid, the reaction that occurs is oxidation to quinones instead of coupling.

d. Oxidation of Naphthacene (3)

A solution of naphthacene (**3**) in *N,N*-dimethylformamide was oxidized with aqueous periodic acid in a 1:4 mole ratio, to give 80 to 85 percent of naphthacenequinone (**4**). In a similar way, a series of other hydrocarbons have been converted into quinones, as described in the experimental part.

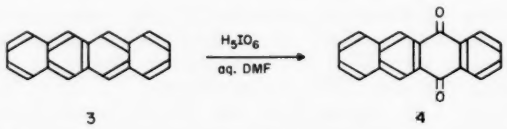

3 4

e. Oxidation of Anthracene (5)

In order to determine whether these reactions with periodic acid involve a free-radical mechanism, the oxidation of anthracene (**5**) was examined in the presence of inhibitors and radical-capture agents [70, 71].

Equimolar proportions (0.01 mole) of anthracene (**5**) and (a) acrylamide, (b) methyl methacrylate, (c) acrylonitrile, or (d) 2,5-di-*tert*-amylhydroquinone were stirred at 75 °C with periodic acid (0.04 mole) in 25:4 (v/v) acetonitrile–water (145 ml) for 45 min; in each case, a high yield of anthraquinone (**6**) was obtained, and practically no polymerization of reagents *a*, *b*, or *c* was observed. In the experiment with *d*, some yellow 2,5-di-*tert*-amylbenzoquinone crystallized out when the filtrate was cooled. Thus, these experiments gave no evidence of radical participation in the oxidation of **5** to **6**, a conclusion confirmed by e.s.r. monitoring of the oxidation path in the range from 0 to 100 °C in aqueous *N,N*-dimethylformamide or aqueous acetic acid. As may be seen from figure 1, the e.s.r. spectrum B for oxidation of **5** shows no radical; whereas, the dimerization of **1**, as discussed earlier, proceeds through a radical intermediate (spectrum A).

f. Oxidation of Naphthalene (7); Mechanism for Oxidation of an Active Center and a Methine Group

As suggested in the previous communication [59], the first step in the mechanism of the oxidation of naphthalene may involve association between periodic acid (an electrophile) and the free-valence center of the aromatic ring [51–53], or with a position having the highest unpaired electron densities [54]; these possibilities are in agreement with the basicity of the polycyclic, aromatic hydrocarbons [49, 50].

The reaction path for the oxidation of polycyclic, aromatic hydrocarbons to quinones by periodic acid may be contrasted with that of oxidation with chromic acid, for which an intermediate (resulting from electrophilic addition) as the initial step in oxidation of

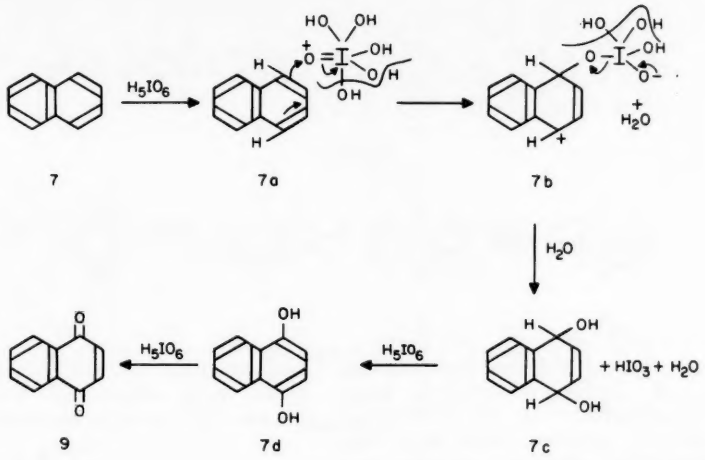

alkenes and polycyclic, aromatic hydrocarbons has been postulated [78, 79]. For example, the mechanism for the oxidation of naphthalene (**7**) to 1,4-naphthoquinone (**9**) apparently proceeds by a two-equivalent oxidation. This reaction involves electrophilic attack of periodic acid, as shown in **7a**, with the formation of intermediate **7b**. Collapse of **7b** by loss of iodic acid, and addition of water to the cationic center of **7b**, affords the 1,4-dihydro-1,4-diol (**7c**), which is then rapidly oxidized by periodic acid to dione **9** in 70 percent yield. The transformation of **7b** to **7c** is supported by the fact that only the mononegatively charged ion of periodic acid decomposes, and that the undissociated or dinegatively charged intermediate is inert to oxidative decomposition [80, 81, 82, 83]. The last step in this sequence of reactions is supported by the observation that 1,4-naphthalenediol (**7d**) is oxidized with periodic acid to dione **9** in a yield of 80 percent.

The suggested mechanism for the oxidation of **7** to **9** is another possible way in which periodic acid can transfer its oxygen atom to an aromatic moiety. Hence, the behavior of periodic acid toward polycyclic, aromatic hydrocarbons has a unique, two-fold character; it can (1) produce coupling products through a radical intermediate, or (2) convert them into quinones, apparently by a two-equivalent oxidation mechanism that does not involve a radical intermediate.

g. Oxidation of Anthrone (8); Mechanisms for the Oxidation of an Active Methylene Group

The oxidation of anthrone (**8**) with periodic acid was also investigated. This compound has a benzilic type of methylene group, similar to the methylene group of tetralin (**19**), for which a chain-radical intermediate, analogous to **8a** and supposedly initiated by treatment of **19** with chromic acid or periodic acid, has been postulated [72]. However, e.s.r. monitoring of the reaction mixture obtained on treatment of anthrone (**8**) with periodic acid showed no radicals, thus excluding scheme B, which would proceed through a radical intermediate (**8a**). Similar autoxidation of tetralin (**19**) to the hydroperoxide, which may involve a chain-radical intermediate, has been reported [72, 73].

It is believed that oxidation of anthrone (**8**) to anthraquinone (**6**) proceeds by a push-pull mechanism, as depicted in scheme A; a monoanion of periodic acid functions here as an active hydroxylating species; the dihydro intermediate **8d** is probably then oxidized further to anthraquinone (**6**). The attack by a monoanion of periodic acid on a methylene group of **8** is a type of insertion of a ligand oxygen atom into a C—H bond; this may possibly be the way in which the active oxygen of periodic acid is transferred; an alternative way, postulating the insertion of an unbound oxygen atom, was suggested by Bunton [74]. The insertion mechanism in the ozone oxidation of fluorene or anthrone has recently been proposed [14].

3.3. Oxidation of Malonic Acid (14)

Oxidation of malonic acid (**14**) with periodic acid or sodium periodate has been thoroughly studied [35, 75], and the products **14b** and **14c**, which may arise from intermediate **14a**, have been isolated and

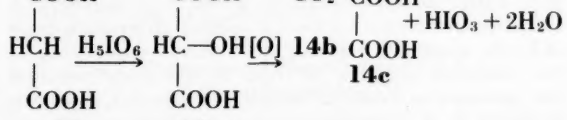

identified [35, 75]. Assuming that products **14b** and **14c** arise from **14**, as reported [35, 75], this oxidative cleavage reaction has been checked for possible participation of free radicals. By means of e.s.r. measurements, hydroxylation of malonic acid (**14**) with periodic acid and sodium periodate was examined in water; monitoring of the reaction path (at 0 to 60 °C) did not reveal free radicals, in agreement with an earlier ob-

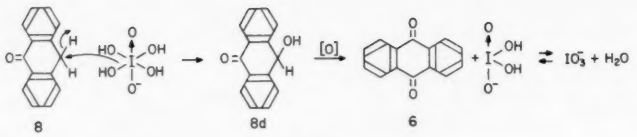

SCHEME A

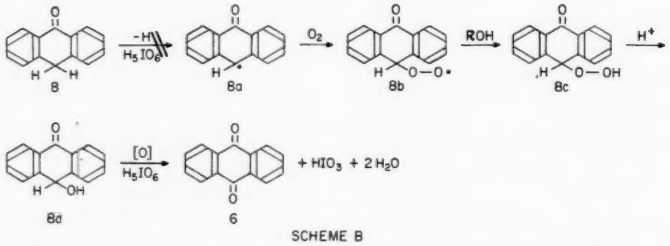

SCHEME B

servation [36] obtained by chemical evidence (no polymerization of acrylonitrile).

It is also believed that the reported [35, 75] hydroxylation of an active methylene group in malonic acid (**14**) and its derivatives by periodic acid or sodium periodate in aqueous solution also proceeds by a ligand push-pull mechanism, similar to that described for anthrone (**8**) (see sec. 3.8), although direct transfer of an oxygen atom by periodate to the active methylene group of malonic acid (electrophilic oxidation) has also been proposed [74]. However, x-ray irradiation of crystals of malonic acid (**14**) produces radicals having an unpaired electron centered on a methylene carbon atom [76, 77].

Finally, hydroxylation of an active methylene group of an acyclic compound (such as malonic acid and its derivatives) can be effected by periodic acid and sodium periodate, whereas the hydroxylation (and oxidation) of an active methylene group in polycyclic, aromatic hydrocarbons can be effected only by periodic acid, and no oxidation has been observed with sodium periodate.

3.4. Oxidative Coupling of Fluorene (20); Mechanism of Oxidation of an Extremely Active Methylene Group

Fluorene (**20**) has an unusually active methylene group [84], and consequently, it is an extremely reactive hydrocarbon. Treatment with periodic acid (1:2 mole ratio) in warm aqueous acetic acid produced a coupling product, 1,2-bis(2,2'-biphenylylene)ethylene (**23**), in about 10 percent yield. E.s.r. monitoring of the oxidation reaction at room temperature revealed the presence of a radical (moderate intensity), as shown in figure 2. A plausible reaction mechanism that can explain the formation of the coupling product (**23**) is shown here; periodic acid anion abstracts a hydrogen atom from a methylene group in **20** with formation of a radical (**21**); dimerization of **21** gives hydrocarbon **22**; elimination of two protons produces the orange-red **23**. Only traces of fluoren-9-one (**26**) could be identified in the reaction mixture (thin-layer chromatography); this mixture was not analyzed for its fluorene hydroperoxide (**25**) content. The low yield

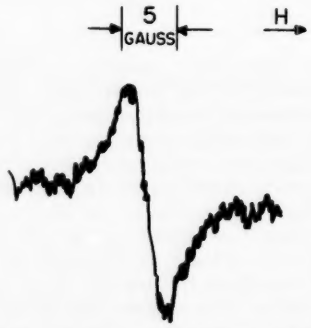

FIGURE 2. *The e.s.r. spectrum of fluorene radical, prepared by treatment of fluorene (in acetic acid) with periodic acid, H_5IO_6 (in water) at room temperature,* $g = 2.0036 \pm 0.0002$.

of hydrocarbon **23** can be explained on the basis of the relative reactivity of radical **21**, which apparently quickly absorbs oxygen (either from the air, or from the oxidant) to give the stable fluorene radical (**24**).

This is then easily converted into the stable fluorene hydroperoxide (**25**). Thus, the radical **21** may alternatively interact with oxygen prior to dimerization; fluorene (**20**), as known, reacts with molecular oxygen to give a stable hydroperoxide (**25**). Moreover, a possible interaction of radicals **21** and **24** can also contribute to lowering of the yield of the product. The above reaction is, therefore, a second example we have found of oxidative dimerization which proceeds through a radical intermediate.

Radical **21** has probably lost its hyperfine structure on contact with oxygen, and the hydroperoxide radical **24** is probably responsible for the broad, one-line e.s.r. spectrum that is actually observed (see fig. 2).

4. Experimental Procedures

4.1. Spectral Measurements

Infrared absorption spectra of compounds were recorded with Perkin-Elmer Model 137 and Model 257 spectrophotometers.[2] E.s.r. spectra were recorded

[2] Certain commercial instruments are identified in this paper in order to specify adequately the experimental procedure. In no case does such identification imply recommendation or endorsement by the National Bureau of Standards, nor does it imply that the equipment identified is necessarily the best available for the purpose.

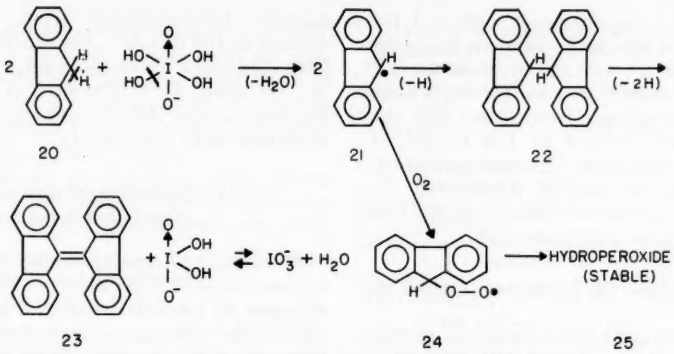

20 21 22 23 24 25

with a Varian Model 4500 EPR Spectrometer with 100-kHz field modulation; the samples were placed in a Varian Model V-4548 aqueous-solution sample-cell.

4.2. Purification of Quinones

Final purification of crude quinones was performed by column chromatography (silica gel, 100–200 mesh, acetic acid or benzene–acetic acid as eluant), by a technique described elsewhere [85].

4.3. Treatment of Pyrene (1) With Periodic Acid (1:1 Mole Ratio)

Treatment of pyrene (**1**) (0.1 mole in acetic acid) with periodic acid (0.1 mole in water) yielded a coupling product, 1,1′-bipyrene (**2**) in over 70 percent yield; the product was isolated according to the published procedure [59].

4.4. Treatment of Pyrene (1) With Periodic Acid (1:4 Mole Ratio)

A solution of pyrene (**1**), (2.02 g, 0.01 mole) in glacial acetic acid (50 ml) was stirred with an aqueous solution of periodic acid (9.2 g, 5 ml, 0.04 mole) at 50 °C for 2 min and then at 95 °C for 30 min; the grayish green **2** that originally crystallized out gradually changed to a brown-red solid. The product was filtered off, washed with glacial acetic acid (2×10 ml), and dried in a vacuum desiccator; yield 8.2–8.5 g, mp 245 to 250 °C (with evolution of iodine).

A sample washed with water, and dried to constant weight at room temperature, was analyzed. Found: C, 28.3; H, 1.23; I, 50.9.

A sample washed with glacial acetic acid, and dried at 25 °C/0.1 mm for 4 hr, was analyzed. Found: C, 18.6; H, 0.8; I, 59.0.

4.5. Oxidation of Naphthacene (3) to Naphthacenequinone (4)

A solution of naphthacene (**3**) (1.15 g, 0.005 mole) in *N*,*N*-dimethylformamide (100 ml) was stirred with an aqueous solution of periodic acid (4.6 g, 5 ml, 0.02 mole) at 120 °C for 8 min and then (to lessen the vigorous reaction) at 80 °C for 30 min. The reaction mixture was treated with water (50 ml), and cooled, to yield naphthacenequinone (**4**), 1.0–1.1g (80–85%), mp 278 to 281 °C. Sublimation at 200 °C/0.05 mm gave light-yellow needles, mp 288 to 290 °C, identical with an authentic sample [86, 87] by mixture mp, infrared spectrum, and thin-layer chromatography on silica gel G (250-μm layer, 5×20 cm glass plate) with 8:1:1 (v/v) benzene–*N*,*N*-dimethylformamide–acetic acid (solvent A), 60 min, R_f 0.70±0.02. On spraying with *ca.* 1.5*M* sulfuric acid in methanol (spray A) and heating (120 °C for 2 min), the yellow spot (thin-layer chromatogram), having a strong green fluorescence, changed to olive-brown.

4.6. Oxidation of Anthracene (5) to Anthraquinone (6)

A solution of anthracene (**5**) (3.56 g, 0.02 mole) in *N*,*N*-dimethylformamide (50 ml) was stirred with an aqueous solution of periodic acid (18.5 g, 40 ml, 0.08 mole) at 95 °C for 8 min, and then at 80 °C for 30 min. The rather dark reaction mixture was then cooled to about 5 °C; light-yellow needles of anthraquinone (**6**) crystallized out and were filtered off. The product was washed with methanol, and dried; yield 3.6–3.7 g (86–89%), mp 280 to 282 °C; dilution of the filtrate with water yielded an additional crop (0.2–0.3 g), bringing the total yield to 91–95 percent.

A sample purified by sublimation at 220 °C/0.05 mm, and recrystallized from glacial acetic acid, melted at 285 to 286 °C, lit [9] mp 281 to 282 °C: thin-layer chromatography on silica gel G (solvent A), 60 min, R_f 0.67±0.02. On a thin-layer chromatogram, quinone **6** gave a scarcely visible spot; spraying (spray A) and heating (120 °C) produced a strong yellow spot having a pink fluorescence.

4.7. Oxidation of Naphthalene (7) to 1,4-Naphthoquinone (9)

A solution of naphthalene (**7**) (2.56 g, 0.02 mole) in glacial acetic acid (75 ml) was stirred with an aqueous solution of periodic acid (18.5 g, 15 ml, 0.08 mole) at 110 °C for 8 min and then at 80 °C for 30 min. The reaction mixture was cooled, poured into about 250 ml of ice-cold water, and kept at room temperature for several hours. The yellow, powdery 1,4-naphthoquinone (**9**) was filtered off, washed with water, and dried; yield 2.0–2.3 g (67–72%). The product was purified by

column chromatography on silica gel with 2:1 (v/v) acetic acid–benzene as eluant to remove impurities (solvent A), R_f 0.90±0.01, R_f 0.83±0.01, R_f 0.54±0.02, and R_f 0.48±0.02 (probably due to 1,2-naphthoquinone). A sample recrystallized from ether and then from glacial acetic acid melted at 124 to 125 °C, lit [88] mp 125 °C; thin-layer chromatography on silica gel G (solvent A), 60 min, R_f 0.66±0.02. The yellow spot of **9** on a thin-layer chromatogram turns pink-brown on exposure to ultraviolet light.

4.8. Oxidation of Anthrone (8) to Anthraquinone (6)

A solution of anthrone [89] (**8**) (1.95 g, 0.02 mole) in glacial acetic acid (50 ml) was stirred with an aqueous solution of periodic acid (9.2 g, 5 ml, 0.04 mole) at 90 °C by the procedure described in section 4.6. The yield of anthraquinone (**6**) was 1.97 g (94%).

4.9. Oxidation of Phenanthrene (10) to Phenanthrenequinone (11)

A solution of phenanthrene (**10**) (3.56 g, 0.02 mole) in redistilled *p*-dioxane (50 ml) was stirred with an aqueous solution of periodic acid (18.6 g, 20 ml, 0.08 mole) at 95 °C for 5 to 7 min (or to the point where the clear, yellow solution just turned brown-red), and then at room temperature for 30 min. The reaction mixture was treated with water (20 ml), and stirred for 30 min in an ice-bath. The orange, crystalline product was filtered off, washed with 10 ml of 1:1 (v/v) cold, aqueous ethanol, and dried in the air. The thoroughly dry, orange product was stirred with cold benzene (20 ml), the suspension was filtered, and the solid was dried; yield of crude phenanthrenequinone (**11**) 1.6–1.8 g; concentration and cooling of the filtrate yielded an additional crop (0.3 g); total yield, 1.9–2.3 g (45–55%), mp 201 to 203 °C.

A sample recrystallized from benzene, and then from glacial acetic acid, melted at 205 to 207 °C, lit mp 205 °C [90], 198 °C [91]; thin-layer chromatography on silica gel G, (solvent A), 60 min, R_f 0.60±0.01. On spraying (spray A) and heating, the orange-yellow spot changed to olive-brown.

4.10. Oxidation of Benz[*a*]anthracene (12) to Benz[*a*]anthracene-7,12-dione (13)

A solution of benz[*a*]anthracene (**12**) (2.3 g, 0.01 mole) in *N*,*N*-dimethylformamide (40 ml) was stirred with an aqueous solution of periodic acid (9.2 g, 5 ml, 0.04 mole) at 100 °C for 10 min, and then at 85 °C for 30 min. The reaction mixture was then diluted with water (50 ml), and cooled in an ice-bath; yellow, powdery **13** was filtered off, washed with water, and dried; yield 1.9–2.9 g (70–78%). A good yield of the product was also obtained when acetic acid (50 ml, 110 °C) was used as the solvent.

The crude product was purified by column chromatography on silica gel with 1:1 (v/v) acetic acid–benzene to remove impurities (solvent A); R_f 0.53±0.02 and R_f 0.44±0.02 (strong green fluorescence). A sample recrystallized from methanol (charcoal), melted at 168 to 170 °C; lit mp 166 °C [92], 169 to 170 °C [93]; thin-layer chromatography on silica gel G (solvent A), 60 min, R_f 0.83±0.02. The yellow spot (pink fluorescence) of **13**, on spraying (spray A) and heating, darkened only very slowly.

4.11. Oxidation of Acenaphthene (15) to Acenaphthenequinone (16)

A solution of acenaphthene (**15**) (1.54 g, 0.01 mole) in glacial acetic acid (40 ml) was stirred with an aqueous solution of periodic acid (9.2 g, 6 ml, 0.04 mole) at 110 °C by the procedure described in section 4.6. Dilution with ice-water yielded a yellow, crystalline powder of **16**, 1.2–1.3 g (66–72%). The crude product was purified by column chromatography on silica gel with 3:1 (v/v) benzene–acetic acid. A sample recrystallized from glacial acetic acid gave yellow needles, mp 260 to 261 °C, lit mp 261 °C [94]; thin-layer chromatography on silica gel G, solvent A, 60 min, R_f 0.44±0.02.

4.12. Oxidation of Pentacene (17) to 6,13-Pentacenequinone (18)

A solution of pentacene (**17**) (0.28 g, 0.001 mole) in *N*,*N*-dimethylformamide (75 ml) was stirred with an aqueous solution of periodic acid (0.92 g, 2 ml, 0.004 mole) at 135 °C for 5 min, and then at 60 °C for 30 min. The reaction mixture was treated with water (35 ml), and cooled, to yield **18**, 0.250–0.267 g (81–87%), mp 382 to 384 °C. Sublimation at 250 °C/0.05 mm, followed by recrystallization from 1:1 (v/v) *N*,*N*-dimethylformamide–ethanol, gave light-yellow needles, mp 393 to 395 °C, lit mp 370 to 371 °C [95]; 394 °C [96]; thin-layer chromatography on silica gel G (solvent A), 60 min, R_f 0.78±0.01. The yellow spot (pink fluorescence), on spraying (spray A) and heating, turned cherry-red.

4.13. Oxidative Dimerization of Fluorene (20) to 1,2-Bis(2,2′-biphenylylene)ethylene (23)

A solution of fluorene (**20**) (1.66 g, 0.01 mole) in glacial acetic acid (50 ml) was stirred with an aqueous solution of periodic acid (5.7 g, 0.025 mole, 5 ml) at 110 °C for 15 min; the solution slowly turned orange-red, and a precipitate (iodic acid) appeared. The reaction mixture was treated with water (5 ml), stirred for an additional 15 min at 105 to 110 °C and then at room temperature (20 min), cooled (visible crystallization of the orange solid), and treated with an excess of cold water with stirring. The orange solid (sometimes mixed with a syrup) was separated by filtration (or decantation), dissolved in warm glacial acetic acid (50 ml), and passed through a column of silica gel (glacial acetic acid as eluant). Rechromatography of the orange band, and repeated recrystallization from warm glacial acetic acid, gave orange-red crystals of **23**, 0.16–0.18 g (9.6–10.8%) mp 185 to 187 °C, lit mp 182 to 183 °C [97]; 187 to 188 °C [98, 99]; thin-layer

chromatography on silica gel G with 4:3:3 (v/v) heptane–ethyl acetate–glacial acetic acid, 60 min, R_f 0.91 ± 0.01. When the reaction was conducted at 55 to 60 °C for 5 hr, the reaction mixture contained, in addition to compound **23**, a trace amount of fluoren-9-one; solvent A, 60 min, R_f 0.82 ± 0.01.

Hydrocarbon **23** belongs to the class of fulvalenes [100]; and alternative methods (and mechanisms) for preparation of **23** have recently been reviewed [100].

a. Attempted Oxidation of Biphenyl, Coronene, Fluoranthene, Perylene, *p*-Terphenyl, and Triphenylene

A solution of the hydrocarbon (0.001 to 0.01 mole) in acetic acid or 1:1 (v/v) acetic acid–*N*,*N*-dimethylformamide was stirred with aqueous periodic acid (0.004 to 0.04 mole) at 100 to 140° for 5 min, and then at 60 to 80° for 30 min. Treatment of the reaction mixture with water regenerated the starting compound, sometimes contaminated with iodine (thin-layer chromatography).

4.14 Oxidation of Pyrene (1), Anthracene (5), and Malonic Acid (14) in E.S.R. Cell

a. Pyrene (1)

An aliquot (0.4 ml) of pyrene (0.02 *M*, in glacial acetic acid) was pipeted into a cell and mixed with one drop of cold, aqueous periodic acid (0.5 *M*) at room temperature. The e.s.r. spectrum was immediately recorded, and showed the presence of free radicals.

b. Anthracene (5)

An aliquot (0.4 ml) of anthracene (0.2 *M*, in *N*,*N*-dimethylformamide) was cooled to about 0 °C, introduced into the cell, and mixed with two drops of cold, aqueous periodic acid (0.5 *M*); the e.s.r. spectrum was scanned from 0 to 60°, and showed no radicals. Another sample of anthracene (0.01 *M*, in acetic acid) was scanned from 20 to 60 °C, and showed no radicals; heating of the cell (boiling-water bath) and scanning of the spectrum did not reveal free radicals.

c. Malonic Acid (14)

An aliquot (0.4 ml) of malonic acid (0.3 *M*, in water) was mixed in the cell with two drops of aqueous periodic acid (0.5 *M*) at room temperature; the e.s.r. spectrum did not reveal any radicals; warming (hot-water bath) or cooling (ice-bath) of the cell and scanning of the spectrum did not reveal any radicals.

The oxidation was also repeated with aqueous sodium periodate solution; the result was negative.

The author thanks G. F. Kokoszka and N. Adams for the e.s.r. measurements.

5. References

[1] Fatiadi, A. J., Environ. Sci. Tech. **7,** 580 (1967).
[2] Cook, J. W., and Schoental, R., J. Chem. Soc. **1948,** 170.
[3] Wallace, J. G., Hydrogen Peroxide in Organic Chemistry, (Dupont Monograph), p. 67.
[4] Roitt, I. M., and Waters, W. A., J. Chem. Soc. **1952,** 2695.
[5] Davies, D. I., Hey, D. H., and Williams, G. H., J. Chem. Soc. **1958,** 1878.
[6] Beckwith, A. L. J., and Waters, W. A., J. Chem. Soc. **1957,** 1001.
[7] Norman, R. O. C., and Waters, W. A., J. Chem. Soc. **1958,** 167.
[8] Norman, R. O. C., Thompson, G. A., and Waters, W. A., J. Chem. Soc. **1958,** 175.
[9] Fieser, L. F., and Putman, S. T., J. Am. Chem. Soc. **69,** 1038 (1947).
[10] Criegee, R., in Oxidation in Organic Chemistry, K. B. Wiberg (Ed.) (Academic Press, New York, N.Y., 1965) p. 277.
[11] Bailey, P. S., Chem. Rev. **5,** 925 (1958).
[12] Copeland, P. G., Dean, R. E., and McNeil, D., J. Chem. Soc. **1961,** 1232.
[13] Moriconi, E. J., and Taranko, L. B., J. Org. Chem. **28,** 1831 (1963).
[14] Battersbee, J. E., and Bailey, P. S., J. Org. Chem. **32,** 3899 (1967).
[15] Van Duuren, B. L., Bekersky, J., and Lefar, M., J. Org. Chem. **29,** 686 (1964).
[16] Arnold, R. T., and Larson, R., J. Org. Chem. **5,** 250 (1940).
[17] Ogata, Y., Kotake, M., and Aoki, K., Chem. Ind. (London) **1965,** 1903.
[18] Ogata, Y., Kotake, M., and Aoki, K., Chem. Ind. (London) **1965,** 1904.
[19] Chambers, R. D., Goggin, P., and Musgrave, W. K. R., J. Chem. Soc. **1959,** 1804.
[20] Waring, A. J., and Hart, H., J. Am. Chem. Soc. **86,** 1454 (1964).
[21] Buehler, C. A., and Hart, H., J. Am. Chem. Soc. **85,** 2177 (1963).
[22] Treibs, W., and Thormer, J., Chem. Ber. **94,** 1925 (1961).
[23] Boyland, E., and Solomon, J. B., Biochem. J. **59,** 518 (1955).
[24] Clark, C. T., Downing, R. D., and Martin, J. B., J. Org. Chem. **27,** 4701 (1962).
[25] Bowen, E. J., Advan. Photochem. **1,** 23 (1963).
[26] Fried, J., and Schumm, D. E., J. Am. Chem. Soc. **89,** 5508 (1967).
[27] Tipson, R. S., Oxidation of polycyclic, aromatic hydrocarbons, NBS Mono. 87, Washington, D.C., 1965.
[28] Bobbitt, J. M., Advan. Carbohydrate Chem. 11, 1 (1956).
[29] Jackson, E. L., Org. Reactions **2,** 341 (1941).
[30] Dyer, J. R., Methods Biochem. Anal. **3,** 11 (1956).
[31] Guthrie, R. D., Advan. Carbohydrate Chem. **16,** 105 (1961).
[32] Bunton, C. A., in ref. 10, p. 367.
[33] Sklarz, B., Quart. Rev. (London) **21,** 3 (1967).
[34] Wolfrom, M. L., and Bobbitt, J. M., J. Am. Chem. Soc. **78,** 2840 (1956).
[35] Bose, J. L., Foster, A. N., and Stephens, R. W., J. Chem. Soc. **1959,** 3314.
[36] Symons, M. C. R., J. Chem. Soc. **1955,** 2794.
[37] Hesse, G., and Mix, K., Chem. Ber. **92,** 2427 (1959).
[38] Schwarz, J. C. P., Chem. Ind. (London) **1955,** 1588.
[39] Chatterjee, A., and Marjumdar, S. C., Anal. Chem. **28,** 878 (1956).
[40] Graber, R. P., Snoddy, C. S., Jr., Arnold, H. B., and Wendler, N. L., J. Org. Chem. **21,** 1517 (1956).
[41] Hudson, B. G., and Barker, R., J. Org. Chem. **32,** 2101 (1967).
[42] Oberender, F. G., and Dixon, J. A., J. Org. Chem. **24,** 1226 (1959).
[43] Fatiadi, A. J., Carbohyd. Res. **1,** 489 (1966).
[44] Ritchie, C. D., Skinner, G. A., and Badding, V. G., J. Am. Chem. Soc. **89,** 2063 (1967).
[45] Clar, E., Polycyclic Hydrocarbons, Vol. **1,** p. 50 (Academic Press, New York, N.Y., 1964).
[46] Ref. 45, p. 56.
[47] Ref. 45, p. 77.
[48] Ref. 45, p. 84.
[49] Mackor, E. L., and van der Waals, J. H., Trans. Faraday Soc. **66** (1958).
[50] Streitwieser, A., Jr., and Hammons, J. H., Progr. Phys. Org. Chem. **3,** 4 (1965).
[51] Brown, R. D., J. Chem. Soc. **1950,** 691, 3249.
[52] Dewar, M. J. S., J. Am. Chem. Soc. **74,** 3357 (1952).
[53] Pullman, B., and Pullman, A., Progr. Org. Chem. **4,** 31 (1958).
[54] Carrington, A., Quart. Rev. (London) **17,** 67 (1963).

[55] Streitwieser, A., Jr., Molecular Orbital Theory for Organic Chemists, p. 324 (John Wiley & Sons, Inc., New York, N.Y., 1961).
[56] Bolton, J. R., Carrington, J., and McLachlan, A. D., Mol. Phys. **5,** 31 (1962).
[57] Kiser, R. W., Tables of Ionization Potentials (United States Atomic Energy Commission, 1960) pp. 53, 54.
[58] Streitwieser, A., Jr., Progr. Phys. Org. Chem. **1,** 1 (1963).
[59] Fatiadi, A. J., J. Org. Chem. **32,** 2903 (1967).
[60] Lewis, I. C., and Singer, L. S., J. Chem. Phys. **43,** 2712 (1965).
[61] Wilk, M., Bez, W., and Rochlitz, J., Tetrahedron **22,** 2599 (1966).
[62] Reynolds, W. L., and Lumry, R. W., Mechanisms of Electron Transfer, p. 68 (The Ronald Press Co., New York, N.Y., 1966).
[63] Ref. 3, p. 99.
[64] Cooper, T. A., and Waters, W. A., J. Chem. Soc. (B) **1967,** 687.
[65] Cooper, T. A., and Waters, W. A., J. Chem. Soc. (B) **1967,** 455.
[66] Ingram, D. J. E., Spectroscopy at Radio and Microwave Frequencies, p. 370, 2d ed. (Plenum Press, New York, N.Y., 1967).
[67] Hoijtink, G. J., Townsend, J., and Weissman, S. I., J. Chem. Phys. **34,** 507 (1961).
[68] Bunton, C. A., in ref. 10, p. 370.
[69] Edwards, J. O., in Peroxide Reaction Mechanisms, p. 77, J. O. Edwards (Ed.) (Interscience Publishers, New York, N.Y., 1962).
[70] Walling, C., Free Radicals in Solution, pp. 162, 430 (John Wiley & Sons, Inc., New York, N.Y., 1957).
[71] Bevington, J. C., Radical Polymerization, chap. 7 (Academic Press, New York, N.Y., 1951).
[72] Stewart, R., Oxidation Mechanisms, p. 61 (W. A. Benjamin, Inc., New York, N.Y., 1964).
[73] Pryor, W. A., Free Radicals, p. 288 (McGraw-Hill Book Co., New York, N.Y., 1966).
[74] Bunton, C. A., in ref. 10, p. 391.
[75] Nuebner, C. F., Ames, S. R., and Bubl, E. C., J. Am. Chem. Soc. **68,** 1621 (1946).
[76] McConnell, H. M., Heller, C., Cole, T., and Fessenden, R. W., J. Am. Chem. Soc. **82,** 766 (1960).
[77] Cole, T., and Heller, C., J. Chem. Phys. **34,** 1085 (1961).
[78] Wiberg, K. B., in ref. 10, pp. 138, 142.
[79] Waters, W. A., Mechanisms of Oxidation of Organic Compounds, p. 110 (John Wiley & Sons, Inc., New York, N.Y., 1964).
[80] Buist, G. J., Bunton, C. A., and Miles, J. H., J. Chem. Soc. **1957,** 4567.
[81] Buist, G. J., and Bunton, C. A., J. Chem. Soc. **1954,** 1406.
[82] Bunton, C. A., in ref. 10, p. 381.
[83] Bunton, C. A., and Hellyer, J., J. Am. Chem. Soc. **89,** 6252 (1967).
[84] Clar, E., Polycyclic Hydrocarbons, Vol. **2** (Academic Press, New York, N.Y., 1960).
[85] Fatiadi, A. J., J. Chromatog. **20,** 319 (1965).
[86] Moriconi, E. J., O'Connor, W. F., and Taranko, L. B., Arch. Biochem. Biophys. **38,** 283 (1959).
[87] Fieser, L. F., J. Am. Chem. Soc. **53,** 2336 (1931).
[88] Groves, C. E., Ann. **167,** 357 (1873).
[89] Meyer, K. H., Ann. **379,** 38 (1911).
[90] Graebe, C., Ann. **167,** 131 (1873).
[91] Fittig, R., and Ostermayer, E., Ann. **167,** 361 (1873).
[92] Graebe, C., Ann. **340,** 259 (1905).
[93] Moriconi, E. J., O'Connor, W. F., and Wallenberger, F. T., J. Am. Chem. Soc. **81,** 6466 (1959).
[94] Weast, R. C., and Selby, S. M., Handbook of Chemistry and Physics, p. C75 (Chemical Rubber Pub. Co., Cleveland, Ohio, 1961).
[95] Clar, C., and John, F., Ber. **62,** 3021 (1929).
[96] Ried, W., and Anthofer, F., Angew. Chem. **65,** 601 (1953).
[97] de la Harpe, C., and van Dorp, W. A., Ber. **8,** 1048 (1875).
[98] Graebe, C., Ber. **25,** 3146 (1892).
[99] Graebe, C., and von Mantz, B., Ann. **290,** 238 (1896).
[100] Bergmann, E. D., Chem. Rev. **68,** 41 (1968).

(Paper 72A4–505)

JOURNAL OF RESEARCH of the National Bureau of Standards—A. Physics and Chemistry
Vol. 72A, No. 4, July–August 1968

A Galvanic Cell With a Low Emf-Temperature Coefficient

Gerald N. Roberts* and Walter J. Hamer

Institute for Basic Standards, National Bureau of Standards, Washington, D.C. 20234

(January 24, 1968)

This paper presents data on a modified cadmium sulfate saturated standard cell of the Vosburgh type in which a tertiary amalgam containing 11.2 percent bismuth and 8.4 percent cadmium is used as anode and the double salt, $CdSO_4 \cdot Na_2SO_4 \cdot 2H_2O$ is added to the usual $CdSO_4$ electrolyte in an amount more than sufficient to saturate the solution with the double salt. Crystals of $CdSO_4 \cdot Na_2SO_4 \cdot 2H_2O$ are placed over the surface of both electrodes. The emf of the cell, as a function of temperature, is given by

$$E \text{ (in volts)} = 1.018243 + 3.0956 \times 10^{-5}\, t - 8.559 \times 10^{-7} t^2 + 1.3534 \times 10^{-8} t^3.$$

At 25 °C the cell has an emf-temperature coefficient of +13.5 μV/°C while the conventional saturated cadmium sulfate cell has a dE/dT of −49.4 μV/°C. Data on the emf-temperature hysteresis of the cell on cooling and on heating are also given in graphical form. Data on the changes in Gibbs energy, enthalpy, entropy, and heat capacity for the cell reaction are given for the temperature range of 5 to 40 °C.

Key Words: Double salt; cell with low temperature coefficient; galvanic cells; standard cells.

1. Introduction

Conventional cadmium sulfate standard cells are of two general types: saturated and unsaturated where these terms refer to the state of the electrolytic solution used in the cell. These cells differ in two regards: the saturated type has the greater emf stability, and therefore the longer life; it also has the higher emf-temperature coefficient, −49.4 μV/°C at 25 °C. The unsaturated cell decreases in emf, on the average, at the rate of 20 μV per year and has an emf-temperature coefficient of the order of only a few microvolts per degree Celsius at room temperature [1].[1]

It would be highly desirable if a cell could be constructed which had the better feature of each of these two types, i.e., emf stability and low variation in emf with temperature. Vosburgh and co-workers [2, 3, 4, 5] have investigated this problem. Their general approach was to modify the conventional cadmium sulfate cell,[2] either by addition of a third metal to the cadmium amalgam or the addition of another component to the electrolyte, or both. Thus, Vosburgh, Guagenty, and Clayton [3] added bismuth to the amalgam (11.1% Bi, 8.9% Cd, 80% Hg) and the double salt, $CdSO_4 \cdot Na_2SO_4 \cdot 2H_2O$ to the saturated solution of $CdSO_4$ in sufficient quantity to make the solution also saturated in the double salt. They also added crystals of the double salt at both electrodes to assure saturation of the solution. In making the solution they used either 0.015 molar sulfuric acid or 0.1 molar acetic acid as solvent.

The present paper describes a further study of this type of cell. The cell was slightly modified by adding a higher concentration of sulfuric acid so that the acidity of the saturated electrolyte solution was 0.038 normal. Also the composition of the tertiary amalgam was slightly different and contained 11.16 percent Bi, 8.41 percent Cd, and 80.43 percent Hg. Various thermodynamic data for the cell reaction are also presented.

The cell may be represented by:

(−)Cd, Bi, Hg(3p)	$CdSO_4 \cdot 8/3\ H_2O$(c), $CdSO_4 \cdot Na_2SO \cdot 2H_2O$(c)	sat aq sol of the two salts in 0.038N H_2SO_4	$CdSO_4 \cdot 8/3\ H_2O$(c), $CdSO_4 \cdot Na_2SO_4 \cdot 2H_2O$(c)	Hg_2SO_4(s)	Hg(l)(+)

where the vertical lines indicate the interface of two distinct phases (the amalgam consists of 3 phases but vertical lines are not used in designating it).

*Presently, Research Associate in Chemistry, The American University, Washington, D.C. 20016.

[1] Figures in brackets indicate the literature references at the end of this paper.

[2] Also referred to as the Weston cell after Edward Weston who invented the cell in 1892.

2. Materials and Procedures

The materials employed in making the cells and descriptions of how they were purified or prepared for use follow:

Mercury: Triply distilled mercury was used at the cathode and in making the amalgam for the anode.

Cadmium: Redistilled spectrograde cadmium was used.

Bismuth: Cerro De Pasco high grade bismuth having a stated purity of 99.9992 percent was used in making the bismuth amalgam.

Sulfuric acid: Reagent grade sulfuric acid was distilled twice in an all Pyrex still. Only the middle fractions of the distillate were used.

Water: Doubly distilled conductivity water having a conductivity less than $1 \times 10^{-6}\ \Omega^{-1}\ cm^{-1}$ was used in making the solutions of cadmium sulfate and the double salt, $CdSO_4 \cdot Na_2SO_4 \cdot 2H_2O$.

Cadmium sulfate: Reagent grade cadmium sulfate was recrystallized two times from an aqueous solution. Spectrographic analysis showed that the recrystallized salt was of high purity.

Sodium sulfate: Reagent grade sodium sulfate was recrystallized two times from an aqueous solution. Spectrographic analysis showed that the recrystallized salt was of high purity.

Double salt: The double salt, $CdSO_4 \cdot Na_2SO_4 \cdot 2H_2O$ was prepared by mixing aqueous solutions of the two component salts. Solubility data [6] indicated that it is possible to produce both the double salt and an excess of $CdSO_4 \cdot 8/3\ H_2O$ by mixing at 20 °C 40.26 g of $CdSO_4$ dissolved in 50 ml of water with 5.16 g of Na_2SO_4 in a like volume of water. This procedure was followed and the resulting saturated solution was allowed to concentrate by evaporation. The salt thus produced was analyzed and found to have the two component salts in the correct stoichiometric ratio.

Amalgam: The amalgam was prepared by heating the required amounts of the three metals together in a porcelain casserole and was added, while homogeneous, to the cells using an electrically heated funnel.

Mercurous sulfate: The mercurous sulfate was prepared by dc electrolysis using the method of Wolff and Waters [7] or Hulett [8]. It was thoroughly washed with several portions of the same cadmium sulfate solution which was used in the cell.

Cell blanks and platinum cell-leads: These were identical to those described in reference [1].

The cell blanks were washed, filled, and sealed in the manner described in reference [1] for conventional $CdSO_4$ cells and the assembled cells were then placed in a constant temperature oil bath which could be operated at any temperature from 0 to 100 °C. The cells were supported in the bath on wooden racks with copper-mercury terminals as described in reference [1]. The temperature of the bath was controlled to within 0.001 °C above 15 °C and to within about 0.005 °C below 15 °C. The emfs of the cells were measured to 1 μV using potentiometers of high sensitivity.

In all, seventeen cells were made. Of these eleven showed good behavior whereas six were erratic in their performance for no apparent reason; data on the latter are not included in this paper.

3. Results

The average results obtained on the eleven cells which showed good performance are given in table 1 for temperatures from 5 to 40 °C, in the sequence in which the emfs were measured. Two sets of results are given for 25 °C and the averages of the two sets agree within 6 μV. Variations of the individual emfs about the average is indicated by the standard deviation, s, and the standard deviation of the mean emf is given by s_m listed at the bottom of table 1. These deviations increased as the temperature of the cells was lowered; thus, emf reproducibility is less marked at the lower temperatures. At 40 °C the emfs fall into two groups, one averaging 1.018976 V and the other 1.018837 V. This difference may be explained either on a phase transition or the appearance of a new salt phase; further work is required to decide this. Those cells with the higher emf, in either case, would correspond to cells with the salts in a metastable state. The higher emf was selected for preparations of figures 1 and 2.

TABLE 1. *Average emfs of Bi-Cd amalgam cell from 5 to 40 °C*

Cell No.	Temperature, °C								
	25	20	15	10	5	25	30	35	40
	Volts	*Volts*	*Volts*	*Volts*	*Volts*	*Volts*	*Volts*	*Volts*	*Volts*
1	1.018695	1.018633	1.018559	1.018498	1.018324	1.018668	1.018762	1.018859	1.018785
3	1.018695	1.018631	1.018571	1.018498	1.018399	1.018707	1.018787	1.018869	(1.018978)
4	1.018694	1.018633	1.018570	1.018494	1.018391	1.018693	1.018770	1.018862	(1.018973)
6	1.018693	1.018629	1.018567	1.018481	1.018385	1.018691	1.018768	1.018862	1.018762
7	1.018699	1.018635	1.018569	1.018495	1.018400	1.018694	1.018775	1.018867	1.018891
9	1.018685	1.018610	1.018517	1.018433	1.018307	1.018680	1.018762	1.018859	1.018866
10	1.018679	1.018617	1.018561	1.018490	1.018374	1.018680	1.018763	1.018864	(1.018976)
11	1.018691	1.018632	1.018576	1.018507	1.018415	1.018704	1.018778	1.018868	(1.018976)
12	1.018694	1.018634	1.018572	1.018497	1.018396	1.018694	1.018768	1.018860	1.018822
15	1.018680	1.018614	1.018529	1.018449	1.018360	1.018662	1.018757	1.018858	1.018641
17	1.018687	1.018633	1.018568	1.018495	1.018385	1.018653	1.018762	1.018859	1.018898
Mean	1.018690	1.018627	1.018560	1.018485	1.018376	1.018684	1.018768	1.018862	[a] 1.018976
s, μV	6.8	9.1	19.0	23.0	36.5	17.3	8.8	4.0	[a] 2.1
s_m, μV	2.1	2.7	5.7	6.9	11.0	5.2	2.7	1.2	[a] 0.6

[a] Mean of the values in parentheses.

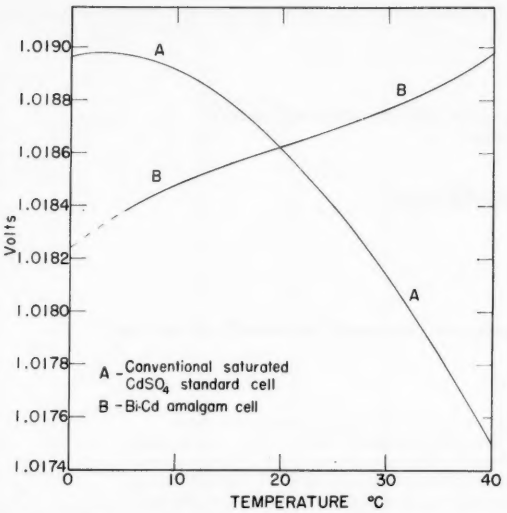

FIGURE 1. *The variation of the emf of the* Bi-Cd *amalgam cell and the conventional saturated* $CdSO_4$ *standard cell with temperature.*

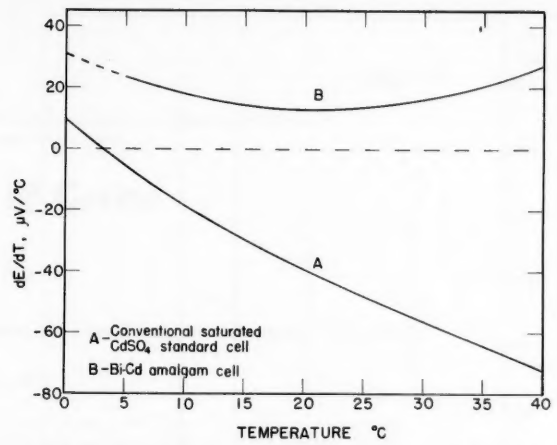

FIGURE 2. *The emf-temperature coefficient in microvolts per degree Celsius for the* Bi-Cd *amalgam cell and the conventional saturated* $CdSO_4$ *standard cell at various temperatures.*

The emfs are shown as a function of temperature in figure 1 and compared with those for the conventional saturated cadmium sulfate cell. The value at 0 °C (dotted extension) was obtained from eq (1), below. It is evident that the two types of cells show opposite behavior with changes in temperature. The conventional type shows a decrease in emf while the Bi-Cd type described herein shows an increase in emf as the temperature of the cell is raised. The emf-temperature coefficients of the two types of cells are shown in figure 2. The value at 0 °C (dotted extension) was obtained from equation 1, below. It is evident that the new type of cell, above 5 °C, has a lower emf-temperature coefficient and of opposite sign than the conventional type. For example, at 25 °C, the new type has a dE/dT of $+13.5\ \mu V/°C$ whereas the conventional type has a dE/dT of $-49.4\ \mu V/°C$. This value for dE/dT at 25 °C agrees closely with that observed by Vosburgh et al. [3].

The mean emfs of table 1 were fitted by the method of least squares using linear, quadratic, and cubic relations with temperature. As would be expected from the form of curve shown in figure 1, a cubic equation gave the best fit; the relation obtained is:

$$E\ (\text{in volts}) = 1.018243 + 3.0956 \times 10^{-5} t - 8.559 \times 10^{-7} t^2 + 1.3534 \times 10^{-8} t^3. \quad (1)$$

The overall chemical reaction for the cell is given by: $[x\text{Cd}, y\text{Bi}, z\text{Hg}]\,(3p) + Hg_2SO_4(s) + \frac{8/3}{m-8/3}(CdSO_4 \cdot mH_2O)$ (sat with $CdSO_4 \cdot 8/3\ H_2O$ and $CdSO_4 \cdot Na_2SO_4 \cdot 2H_2O$) $= \frac{m}{m-8/3}(CdSO_4 \cdot 8/3\ H_2O)$(c) (sat with $CdSO_4 \cdot 8/3H_2O$ and $CdSO_4 \cdot NaSO_4 \cdot 2H_2O$) + 2Hg(l) + $[(x-1)\text{Cd}, y\text{Bi}, z\text{Hg}](3p)$ where x moles of Cd are associated with y moles of Bi and z moles Hg and m is the number of moles of water associated with 1 mole of $CdSO_4$ in the saturated solution. The changes in Gibbs energy (free energy), enthalpy, entropy, and heat capacity for the cell reaction are given, respectively, by: $\Delta G = -nFE$; $\Delta H = -nFE + nFT(dE/dT)$: $\Delta S = nF(dE/dT)$; and $\Delta C_p = [d(\Delta H)/dT] = nFT(d^2E/dT^2)$ where F is the Faraday and n is the number of equivalents involved in the cell reaction; in the present case $n = 2$. The value of F is 96487 C/g equivalent on the ^{12}C scale of atomic weights [10, 11]; thus if E is expressed in volts, ΔG is given in volt coulombs per gram equivalent or in joules per gram equivalent. Values of ΔG, ΔH, ΔS, and ΔC_p are given in table 2.

The emf-temperature hysteresis of the cell was also determined on cooling and on heating; these effects are shown in figures 3 and 4 where α (the ordinate) is the difference in μV from 1.018 V. On cooling the emf first changes markedly in the opposite direction to the final value, i.e., the emf first increases and then decreases to the equilibrium value (a slight over

TABLE 2. *Thermodynamic data for the reaction in the galvanic cell described herein*

Temperature	Changes[a] in Gibbs energy	Enthalpy	Entropy	Heat capacity
°C	ΔG	ΔH	ΔS	ΔC_p
	J mol^{-1}	J mol^{-1}	J mol^{-1} deg^{-1}	J mol^{-1} deg^{-1}
[b](0)	(−196,494)	(−194,863)	(5.97)	(−90.2)
5	−196,520	−195,263	4.52	−70.1
10	−196,540	−195,563	3.45	−49.2
15	−196,556	−195,755	2.78	−27.5
20	−196,569	−195,836	2.50	−5.0
25	−196,581	−195,803	2.61	+18.3
30	−196,596	−195,650	3.12	+42.4
35	−196,613	−195,377	4.01	+67.2
40	−196,636	−194,976	5.30	+92.8

[a] These may be converted to the thermochemical calorie (defined) by the relation 1 thermochemical calorie (defined) = 4.1840 V [9].
[b] Values at 0 °C obtained from E and dE/dT given by eq (1).

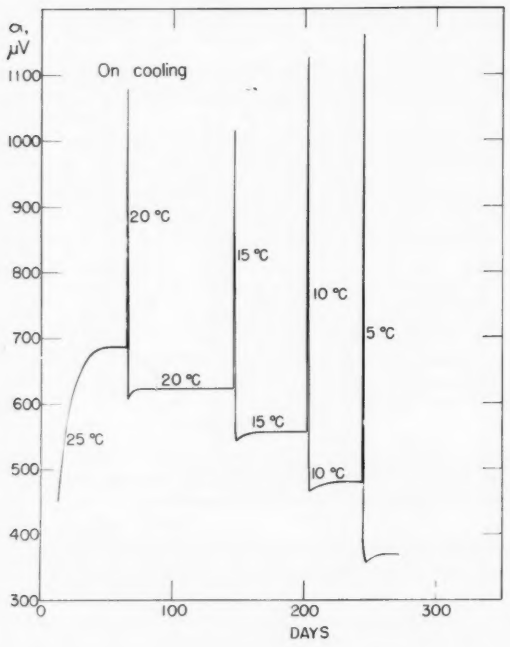

FIGURE 3. *Emf-temperature hysteresis of the* Bi-Cd *amalgam cell on cooling, α defined in text.*

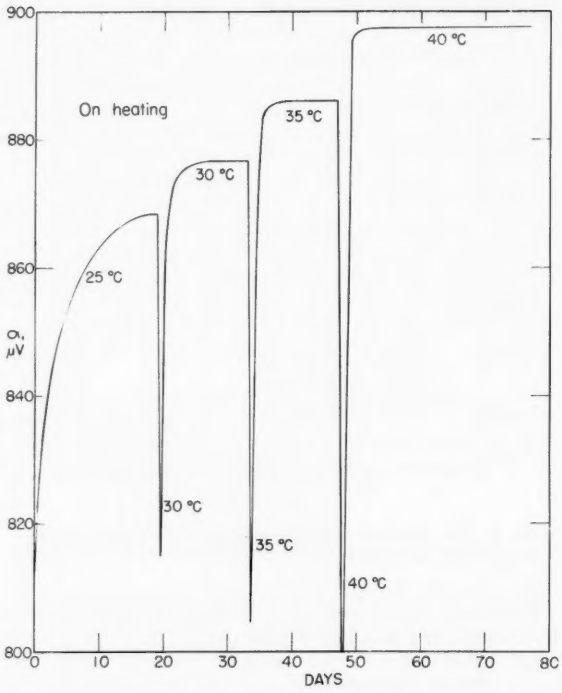

FIGURE 4. *Emf-temperature hysteresis of the* Bi-Cd *amalgam cell on heating, α defined in text.*

decrease is also noted at all temperatures). On heating the opposite effect is noted: the emf first decreases and then increases to the equilibrium value. The initial changes in emf in the direction opposite to that expected are called emf-temperature hysteresis. Although these hysteresis effects persist for less than a day, they are more marked than those observed for the conventional saturated cadmium sulfate cell [12], and more work would be required to ascertain if means could be found to reduce the magnitude and extent of the hysteresis.

4. Conclusions

The Bi-Cd amalgam cell described in this paper has a much lower emf-temperature coefficient, but of opposite sign, than the conventional saturated cadmium sulfate standard cell currently used as a standard of electromotive force. Also, the cell's short-term stability exceeds that shown by unsaturated $CdSO_4$ standard cells. The average emf of the first and second measurements at 25 °C, which were 300 days apart, agreed to 6 μV; the unsaturated $CdSO_4$ cell, on the other hand, decreases in emf at an average rate of 20 μV per year. Cells of this type appear also to have the long-term emf stability to within 10 μV [13].

The authors are indebted to Harold J. DeWane for writing the computer program, to Virginia C. Stewart for spectrographic analysis, to T. C. Rains for analysis of the double salt, and to Anne M. O'Toole for help in making some of the emf measurements.

5. References

[1] Hamer, W. J., Standard Cells, Their Construction, Maintenance, and Characteristics, NBS Mono. 84, 1965.
[2] Vosburgh, W. C., J. Am. Chem. Soc. **47,** 2531 (1925).
[3] Vosburgh, W. C., Guagenty, M., and Clayton, W. J., J. Am. Chem. Soc. **59,** 1256 (1937).
[4] Vosburgh, W. C., and Parks, H. C., J. Am. Chem. Soc. **61,** 652 (1939).
[5] Vosburgh, W. C., Derr, P. F., Cooper, G. R., and Pettengill, B., J. Am. Chem. Soc. **61,** 2687 (1939).
[6] Koppel, J., and Gumperz, A., Z. physik. chem. **52,** 413 (1905).
[7] Wolff, F. A., and Waters, C. E., BS Bull. **4,** 1 (1907).
[8] Hulett, G. A., Phys. Rev. **32,** 257 (1911).
[9] New Values for the Physical Constants—Recommended by NAS-NRC, NBS Tech. News Bull. 47, No. 10, 175 (1963); Consistent Set of Physical Constants Proposed, Chem. and Eng. News **41,** No. 46, 43 (Nov. 18, 1963).
[10] Craig, D. N., Hoffman, J. I., Law, C. A., and Hamer, W. J., J. Res. NBS (Phys. and Chem.) **64A,** 381 (1960).
[11] Hamer, W. J., and Craig, D. N., J. Electrochem. Soc. **111,** 1434 (1964).
[12] Eppley, M., and Vincent, G. D., Electrochemical Constants, NBS Circ. **524,** ch. 10, 1953.
[13] Vosburgh, W. C., and Bates, R. G., J. Electrochem. Soc. **111,** 997 (1964).

(Paper 72A-4-506)

JOURNAL OF RESEARCH of the National Bureau of Standards—A. Physics and Chemistry
Vol. 72A, No. 4, July–August 1968

Synthesis of Cerite

Jun Ito

Institute for Materials Research, National Bureau of Standards, Washington, D.C. 20234

(April 29, 1968)

Some compounds isostructural with cerite have been synthesized hydrothermally at temperatures from 500 to 720 °C. The compositional range for cerite, and its phase relation to the silicate apatites are established in terms of ionic radii of rare-earth and divalent ions. The proposed formula for cerite on the basis of isomorphism with whitlockite, $Ca_9(PO_4)_2$, is discussed. A solid-solution series between $Ca_9P_6O_{24}-Ca_7Mg_2P_6O_{24}$ (whitlockite–Mg-whitlockite) has been established.

Key Words: Ca, Mg phosphate, hydrothermal synthesis, inorganic synthesis, mineral chemistry, rare-earth silicate, x-ray powder analysis.

1. Introduction

During a study of silicate apatites, a very wide compositional range for the cerite phase was found under hydrothermal conditions [1].[1] This range adjoins that for the rare-earth silicate apatites. Despite its early description, the rare-mineral cerite [2–7], from which the element cerium was discovered, has not yet been fully characterized, because of the complexity of its composition. In this paper, therefore, I report the conditions for its formation and its compositional range. Recently Keppler [8] reported an isostructural relation between cerite and whitlockite. I suspect that the maximum number of Mg ions in Mg-whitlockite may equal the number of divalent ions in cerite, consequently, the whitlockite–Mg-whitlockite solid-solution series was also investigated and the results are given here.

2. Results and Discussion

Cerite was synthesized from hydrosilicates which were precipitated in the ratio $M^{2+}:M^{3+}$ (i.e., rare earth): M^{4+} (i.e., Si) = 2:7:6. The precipitates were centrifuged, washed, dried, and in some experiments admixed with carbonates. The synthesis was completed by hydrothermal heating at 2 kbar and 550 to 680 °C. Whitlockite was synthesized from stoichiometric mixtures, prepared by the slow evaporation of alkaline solution containing calcium, magnesium nitrate and ammonium dihydrogen phosphate and heated in air at 1050 to 1120 °C. Experimental results are given in table 1 with the unit-cell dimensions calculated according to the space group R3c [6]. X-ray powder diffraction data of Mg-La, Mg-Ho, and Co-La cerites and Mg-whitlockite, $Mg_2Ca_7P_6O_{24}$, were indexed and are given in tables 2 and 3.

TABLE 1. *Results of the synthesis of cerite, whitlockite and Mg-whitlockite and the unit cell dimensions*

Formula (tentative)	Temp °C	Pressure	Hour	*a*	*c*
$Mg_2La_7Si_6O_{23}(OH)_3$	550	2	20	10.77	38.40
$Mg_2Nd_7Si_6O_{23}(OH)_3$	700	2	20	10.64	37.63
$Mg_2Sm_7Si_6O_{23}(OH)_3$	550	2	20	10.62	36.8
$Mg_2Gd_7Si_6O_{23}(OH)_3$	550	2	20	10.49	36.64
$Mg_2Dy_7Si_6O_{23}(OH)_3$	700	2	20	10.47	36.32
$Mg_2Ho_7Si_6O_{23}(OH)_3$	680	2	48	10.44	35.92
$Ni_2Ce_7Si_6O_{23}(OH)_3$	650	2	20	cerite [a]	
$Ni_2Sm_7Si_6O_{23}(OH)_3$	550	2	20	10.58	36.74
$Ni_2Ho_7Si_6O_{23}(OH)_3$	680	2	20	10.47	36.34
$Co_2La_7Si_6O_{23}(OH)_3$	550	2	48	10.78	38.40
$Co_2Ce_7Si_6O_{23}(OH)_3$	680	2	20	cerite [a]	
$Co_2Sm_7Si_6O_{23}(OH)_3$	550	2	20	10.6	36.8
$Co_2Dy_7Si_6O_{23}(OH)_3$	590	2	20	cerite & apatite	
$Fe_2La_7Si_6O_{23}(OH)_3$	700	2	20	10.82	38.45
$Fe_2Nd_7Si_6O_{23}(OH)_3$	550	2	20	cerite [a]	
$Fe_2Sm_7Si_6O_{23}(OH)_3$	550	2	20	cerite [a]	
$Fe_2Gd_7Si_6O_{23}(OH)_3$	680	2	48	cerite & other phase	
$Mn_2La_7Si_6O_{23}(OH)_3$	680	2	20	10.88	38.5
$Mn_2Ce_7Si_6O_{23}(OH)_3$	650	2	10	cerite [a]	
$Mn_2Nd_7Si_6fl_{23}(OH)_3$	550	2	20	cerite & apatite	
$Mn_2Sm_7Si_6fl_{23}(OH)_3$	550	2	20	cerite & apatite	
$Mn_2Gd_7Si_6$ [b]	550	2	20	apatite	
$Mn_2Dy_7Si_6$ [b]	550	2	20	apatite	
$Mn_2Ho_7Si_6$ [b]	550	2	20	apatite	
$Mn_{1.5}Ca_{5.5}La_7Si_6O_{23}(OH)_3$	550	2	20	cerite & apatite	
$MnCaLa_7Si_6$ [b]	550	2	20	apatite	
$MnCaSm_7Si_6$ [b]	550	2	20	apatite	
$Mg_2Ca_7P_6O_{24}$	1120	in air	20	10.31	37.25
$MgCa_9P_6O_{24}$	1120	in air	20	10.36	37.24
$Ca_9P_6O_{24}$	1120	in air	20	10.45	37.32
$Co_2Ca_7P_6O_{24}$	1050	in air	20	10.32	37.2
$CoCa_9P_6O_{24}$	1050	in air	20	10.34	37.2

[a] Cell dimensions not measured.
[b] Cation ratio in starting gel.

[1] Figures in brackets indicate the literature references at the end of this paper.

TABLE 2. *X-ray powder diffraction data for synthetic cerites and magnesium whitlockite* (Cu Kα, Ni *filter*)

Space group R3c, Hexagonal

Formula	$Mg_2La_7Si_6O_{23}(OH)_3$		$Mg_3Ho_7Si_6O_{23}(OH)_3$		$Co_2La_7Si_6O_{23}(OH)_3$	
Conditions	550 °C 2 kbar $a=10.77$Å	$c=38.40$Å	550 °C 2 kbar $a=10.44$Å	$c=35.92$Å	550 °C 2 kbar $a=10.78$Å	$c=38.40$Å
hkl	*d* obs.	I/I_o	*d* obs.	I/I_o	*d* obs.	I/I_o
012	8.378	3	8.110	10	8.445	3
104	6.651	3	6.393	5		
006	6.421	5				
110	5.376	20	5.217	20	5.440	15
202	4.532	25	4.379	30	4.535	30
018	4.273	30	4.026	60	4.275	20
116	4.137	5				
024						
10.10	3.545	25	3.351	90	3.561	15
122	3.456	60			3.479	40
208	3.348	10	3.193	60	3.353	10
214	3.304	30			3.316	40
00.12	3.222	5	3.129	5		
300	3.112	25	3.019	50	3.116	40
02.10	2.954	100	2.813	100	2.968	100
128	2.859	20	2.728	30	2.848	20
300	2.801	25	2.693	50	2.801	20
220	2.691	50	2.608	60	2.698	70
21.10	2.600	20	2.478	30	2.606	15
312	2.547	3				
134	2.497	5	2.417	5		
20.14	2.357	3	2.224	5	2.366	5
042	2.327	5				
318	2.258	3	2.18	25	2.327	5
30.12	2.231	20	2.126	30	2.223	20
13.10	2.138	10	2.058	20	2.144	8
02.16		5			2.140	10
048	2.095	10	2.021	15	2.099	15
324		10				
410	2.053	10				
232	2.018	3				
40.10						
21.16	1.989	15	1.914	10	1.995	10
238	1.953	40	1.888	15	1.958	40
416	1.943	15	1.870	15	1.944	10
01.20.3114	1.884	10	1.797	20	1.871	3
	1.865	10				
502	1.857	10			1.860	10
054	1.831	10	1.771	10	1.836	10
	1.812	3				
330	1.794	5	1.737	10	1.799	5
20.20	1.776	20	1.668	20	1.779	20
30.18.13.16	1.761	15	1.657			
508	1.737	3				

Cerite was not found in previous studies of rare-earth oxides-silica systems. Divalent ions play an essential role in the formation of cerite. The compositional range of cerites and a part of that of apatites in terms of ionic radii of the divalent ions and the rare-earth ions has been determined and is given in figure 1. It appears likely that the divalent and rare-earth ion sites are ordered, and that no appreciable partial replacement of rare-earth sites by divalent ions takes place. Unit-cell dimensions of the cerite change only when the size of either the divalent or the rare-earth ion is changed, but not when the ratio of the amounts of two given cations in the source material is changed. A calcium end member of cerite phase does not exist under the present conditions, although the chemical analyses of natural cerite usually show several percent of calcium. The Mn analogs are converted to Mn-apatite at temperatures above 650 °C under 2 kbar H_2O pressure. The tentative boundary for cerite apatite conversion at 550 °C under 2 kbar is drawn in figure 1. The reverse reaction has not been observed, possibly because the reaction is too slow; but it may be that the equilibrium phase field for apatite is larger than indicated.

All the analogs of cerite were converted into apatite or apatite plus other phases after dehydration in air at temperatures above 900 °C. It was quite unexpected that the smaller rare-earth ions such as Dy or Ho also form cerite, because cerites found in nature contain exclusively large size rare-earth ions such as: La, Ce, Pr, Nd, and Sm.

Magnesium replacement in whitlockite was limited at the composition, $Ca_7Mg_2P_6O_{24}$. Starting material containing more Mg than corresponds to this end member gave an inferior whitlockite x-ray powder pattern without change in the unit-cell dimensions. With further increase of Mg in the charge, a second phase $Ca_3Mg_3(PO_4)_4$ appears. The whitlockite solid-solution series is demonstrated in figure 2. Unit-cell dimensions vary as a function of Mg content.

Only a partial solid-solution series exists between cerite and whitlockite despite their close isomorphism

TABLE 3. *X-ray powder diffraction data for synthetic Mg-whitlockite* $Ca_7Mg_2P_6O_{24}$. (Cu Kα, Ni *filter; 1150 °C in air*)

Space group R3c, Hexagonal.

$a = 10.31$ Å		$c = 37.23$ Å	
hkl	*d* obs. Å	I/I_0	*d* calc. Å
012	8.05	20	8.04
104	6.43	33	6.44
110	5.15	50	5.15
202	4.333	20	4.337
018	4.130	20	4.126
024	4.019	20	4.023
10,10	3.437	45	3.437
211	3.358	15	3.357
122	3.316	20	3.304
208	3.227	20	3.219
214	3.160	75	3.159
300	2.972	30	2.973
02,10	2.857	100	2.859
128	2.730	30	2.731
306	2.685	20	2.683
11,12	2.660	15	2.659
220	2.577	70	2.575
01,14	2.525	15	2.551
223	2.525	15	2.521
21,10	2.503	25	2.500
226	2.384	10	2.378
12,11			2.384
315	2.347	15	2.349
10,16	2.250	10	2.252
11,15	2.239	10	2.240
404	2.169	20	2.169
30,12	2.148	20	2.147
21,14	2.093	10	2.089
321	2.039	10	2.043
232			2.034
324	2.013	15	1.999
048			2.012
22,12	2.003	10	1.982
11,18	1.916	30	1.920
40,10			1.913
238	1.879	20	1.873
416	1.839	20	1.857
01,20; 31,14	1.824	20	1.823
32,10	1.795	10	1.794
502	1.762	10	1.776
054	1.753	10	1.752
20,20	1.719	30	1.719
30,18	1.700	15	1.724

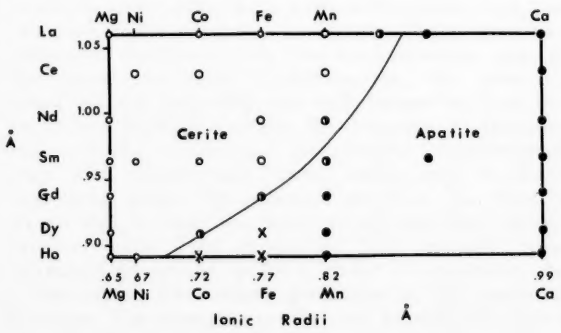

FIGURE 1. *Compositional stability range of cerites.*

Abscissa is the ionic radii for divalent cations given by Wells (1962) [9], ordinate is rare-earth radii given by Templeton and Dauben (1954) [10].

and close structural relationship. Large fields of stability for phospho-silico-apatites and monazites are present between the two compounds under the conditions used in the present experiments. Limited solid solution may extend from one toward the other. The

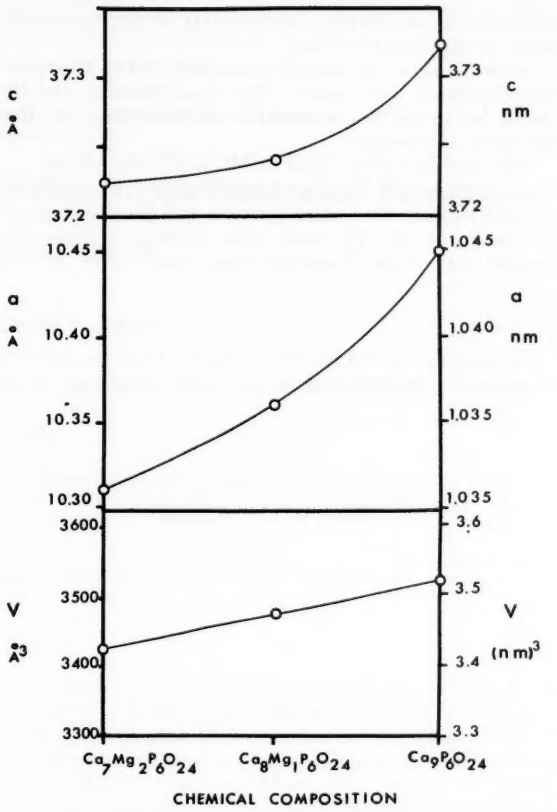

FIGURE 2. *Whitlockite and Mg-whitlockite solid-solution series.*

Open circles = cerite, closed circles = apatite, crosses = mixed unidentified phases.

probable limits of solid solution may be around $CaMg_2Ln_6Si_5PO_{23}(OH)_3$ for cerite, and $Ca_8LnP_5SiO_{24}$ for whitlockite, but there is evidence to indicate that the solid-solution limit is a function of the size of rare-earth ion.

Infrared absorption spectroscopic analysis by R. Wilkins at Harvard University, showed abundant hydroxyl ion (up to several percent) in the synthetic Mg-La cerite possibly in two crystallographic sites (3690 cm^{-1} strong infrared line and 3660 cm^{-1} medium line). Synthetic Ca and Ca-Mg whitlockite, however were shown to be anhydrous as originally expected.

Europium and terbium activation of Mg-Gd analogs of cerite show typical red and yellow visible emission under a mercury fluorescent lamp, but their luminescent intensities are much lower than those displayed by the silicate apatites [1].

From the results here presented, the formula $M_2^{2+}Ln_7Si_6O_{23}(OH)_3$ seems in best agreement with the chemical analysis, infrared analysis, and synthesis of cerites. This formula is essentially the same as that given by Gay [6] and is isomorphous with Mg whitlockite except for two additional hydroxyl ions. However, calcium and magnesium ions in cerite do

not seem to be distributed randomly within rare-earth sites as suggested by Gay.

In the absence to date of a complete x-ray structure determination on cerite, the experimental results could be given an alternative interpretation by the following formulas:

$$M_3^{2+}Ln_7Si_7O_{27}OH \cdot H_2O \text{ or } M_2^{2+}Ln_8Si_7O_{28} \cdot 3H_2O.$$

They correspond to that suggested by Keppler [8] for whitlockite. The latter formula was also that given by Glass et al. [7], from their extensive study on natural cerite from Mountain Pass, California.

Support by the Advanced Research Projects Agency is gratefully acknowledged.

3. References

[1] Ito, J., Am. Min. **53,** July–August, in press (1968).
[2] Hisinger, W. and Berzelius, J., Neues Allg. Jour. Chemie, **2,** 397–418 (1804).
[3] Hisinger, W., and Berzelius, J., Abhandl. Fysik, Kemioch Mineralogie, **1,** 58–84 (1806).
[4] Silberminz, V., Acad. Sci., USSR, C.R. **A, 55,** Abs. Neues Jahrb. Min., **1,** 123 (1930).
[5] Goddard, E. N., and Glass, J. J., Am. Min. **25,** 381–404 (1940).
[6] Gay, P., Min. Mag. **31,** 455–469 (1957).
[7] Glass, J. J., Evans, H. T., Jr., Carron, M. K., and Hildebrand, F. A., Am. Min. **43,** 460–475 (1958).
[8] Keppler, U., Naturwissenchaften, **54,** 139 (1967).
[9] Wells, A. F., Structural Inorganic Chemistry, 3rd ed., p. 483 (Clarendon Press, Oxford, 1962).
[10] Templeton, D., and Dauben, C. H., J. Am. Chem. Soc. **76,** 5237–5239 (1954).

(Paper 72A4–507)

JOURNAL OF RESEARCH of the National Bureau of Standards—A. Physics and Chemistry
Vol. 72A, No. 4, July–August 1968

Tables of Collision Integrals for the (m,6) Potential Function for 10 Values of m*

Max Klein and Francis J. Smith [1]

Institute for Basic Standards, National Bureau of Standards, Washington, D.C. 20234

(June 28, 1967)

Tables of collision integrals are presented for the (m, 6) potential function for 87 reduced temperatures for each of 10 values of m. The exponents m used were $m = 9, 12, 15, 18, 21, 24, 30, 40, 50$, and 75. Comparisons are made with five other calculations for the case $m = 12$. The accuracy of the calculation appears to be at least several parts in 10,000.

Key Words: Collision integrals; potential; viscosity; diffusion; thermal diffusion; thermal conductivity; transport properties.

1. Introduction

The kinetic theory of gases relates the macroscopic coefficients in the phenomenological flow equations, the so-called transport coefficients, to the microscopic intermolecular potential function between two of the constituent molecules. The connection is expressed, in the Chapman-Enskog solution of the Boltzmann equation [1, 2],[2] in terms of certain three-fold integrals, generally referred to as collision integrals and designated $\Omega^{(l,s)*}(T^*)$. Given the intermolecular potential function appropriate to a particular system, one can calculate these integrals, and hence the macroscopic transport coefficients of the corresponding gas in the ideal gas state. Unfortunately, the potential functions are generally not well known so that the procedure must, in practice, be inverted, the theoretical relations connecting macroscopic experimental data with microscopic theory being used to learn something about the potential function. The way in which this is done has been amply described in the literature [2]. This procedure has recently been examined by one of us [3] in order to determine the sensitivity of the various properties to the potential function. The transport coefficients were found to be a possibly good source for learning something about the potential function. This requires tables of collision integrals for different classes of potential functions. Such tables exist for the square-well [4], exp-6 [5, 6, 7], Morse [8], Kihara [9], inverse power [10], and one term exponential [11] families of functions. There are also tables for functions with a single term added to the (12, 6) function. These are the (12, 6, 3) [12], (12, 6, 4) [13], and (12, 6, 5) [14] functions. In addition, calculations exist for certain single functions, e.g., (9, 6), (28, 7), (16, 6) and (18, 6) potentials [15] and, of course, the (12, 6) function [2, 12, 16]. This work adds to these tables for the (m, 6) family for 10 values of m.

One hopes that the potential functions which turn out to be adequate for a description of macroscopic properties will be temperature independent and simple in form. Quantum mechanical perturbation theory indicates that the attraction for large separation should be described by a series of inverse powers of the internuclear distance starting with the inverse sixth power for neutral molecules. No theoretical justification exists for the repulsive part. Perhaps the simplest form which can be taken for this part is a single inverse power of the internuclear separation. It might be interesting to let the exponent of this repulsive term be a variable and to determine it, for any given system, from fits to experimental data. We have chosen to prepare the way for such an approach by calculating tables of collision integrals for such a potential.

The (m, 6) potential has the form

$$\phi^*(r^*) = \frac{\phi(r/\gamma)}{\epsilon} = \frac{1}{\left(\frac{6}{m}\right)^{\frac{6}{m-6}} - \left(\frac{6}{m}\right)^{\frac{m}{m-6}}} \left[\left(\frac{1}{r^*}\right)^m - \left(\frac{1}{r^*}\right)^6\right].$$

*Supported, in part, by the Air Force Systems Command, Arnold Engineering Development Center, Tullahoma, Tennessee. Delivery Order Number (40–600) 66–938 Program Element 61445014 AF Project 8951.

[1] Present address: School of Physics and Applied Mathematics, The Queen's University, Belfast, North Ireland.

[2] Figures in brackets indicate the literature references at the end of this paper.

This function should prove useful on several counts. First of all, it is simple in form. Second, the repulsive index, m, serves as a simple indicator of the hardness of the repulsive core. Furthermore, the potential has been used in a number of more complicated theories [17, 18]. In some instances [17], this form has proved useful because the theory involves derivatives of the potential which then leads to simple recursion formulas on the index m. Finally, the potential functions derived from two body scattering data have often been represented by simple inverse powers of the internuclear distance.

2. General Formulas

The collision integrals $\Omega^{(l,s)*}(T^*)$ are related to the potential functions through the relations

$$\Omega^{(l,s)*}(T^*)=\frac{2}{(s+1)!T^{*(s+2)}}\int_0^\infty \exp\left[\frac{-g^{*2}}{-T^*}\right] \times g^{*(2s+3)}Q^{(l)*}(g^*)dg^*$$

where $Q^{(l)*}(g^*)$ is a cross section given by

$$Q^{(l)*}(g^*)=\frac{2}{1-\frac{1}{2}\frac{1+(-1)^l}{1+l}}\int_0^\infty (1-\cos^l \mathrm{X})b^*db^*$$

with the intermolecular potential function being contained in the equation for the scattering angle

$$\mathrm{X}(g^*, b^*)=\pi-2b^*\int_{r_m}^\infty \frac{dr^*/r^*}{\sqrt{1-(b^*)^2/(r^*)^2-\phi^*(r^*)/g^{*2}}}.$$

r_m^* is the distance between a pair of molecules at the time of closest approach while b^* is the impact parameter.

Certain ratios of the collision integrals appear in the transport theory of multicomponent mixtures [2]. These ratios being slowly varying functions of T^* are also useful in interpolation. The relevant ratios are

$$A^*=\frac{\Omega^{(2,2)*}}{\Omega^{(1,1)*}}$$

$$B^*=\frac{5\Omega^{(1,2)*}-4\Omega^{(1,3)*}}{\Omega^{(1,1)*}}$$

$$C^*=\frac{\Omega^{(1,2)*}}{\Omega^{(1,1)*}}$$

$$E^*=\frac{\Omega^{(2,3)*}}{\Omega^{(2,2)*}}$$

$$F^*=\frac{\Omega^{(3,3)*}}{\Omega^{(1,1)*}}.$$

The thermal diffusion ratio, α_T, has long been considered a sensitive means for the determination of the intermolecular potential function. Of particular interest is the isotopic approximation to this quantity. In that approximation, the mixture consists of two isotopes of sufficiently large mass so that the difference in molecular weight between the isotopes can be neglected with respect to the molecular weights themselves. In addition, the differences between the intermolecular potential functions may also be neglected. The thermal diffusion ratio in this so-called isotopic approximation is called the isotopic thermal diffusion ratio.

We have calculated the isotopic thermal diffusion ratio for the first order solutions to the Boltzmann equation (at zero density) for both the Chapman-Cowling and Kihara methods [19, 20], as well as for the second order Kihara solution. The question of the convergence of the thermal diffusion ratio as higher order terms are taken has been examined by Mason [19] and others [20]. Our calculations are based on the following expressions:

The first order Chapman-Cowling approximation:

$$[\alpha_0]_{cc1}=\frac{15(6C^*-5)(2A^*+5)}{2A^*(16A^*-12B^*+55)}.$$

The first order Kihara expression:

$$[\alpha_0]_{k_1}=\frac{15(6C^*-5)}{16A^*}.$$

The second order Kihara expression:

$$[\alpha_0]_{k_2}=[\alpha_0]_{cc1}(1+\delta)$$

where

$$\delta=\frac{I^*}{9}\left[\frac{2A^*}{\frac{35}{4}+7A^*+4F^*}\left\{H^*+\frac{1}{2}\left(\frac{7(5-6C^*)+A^*I^*}{5+2A^*}\right)\left(\frac{\frac{35}{8}+28A^*-6F^*}{21A^*}\right)\right\}-\frac{5}{7}\left\{H^*-\frac{7}{5}\frac{5-6C^*}{5+2A^*}-\frac{3I^*}{10}\right\}\right]$$

where

$$I^*=7-8E^*$$

and

$$H^*=\frac{\frac{35}{4}-3B^*-6C^*}{5-6C^*}.$$

The factors f_η, f_λ, and $f_\mathscr{D}$ used to obtain Kihara's second approximation to the coefficients of viscosity,

diffusion and thermal conductivity are also presented. These are computed from the relations:

$$f_\eta = 1 + \frac{3}{196}(8E^* - 7)^2$$

$$f_\lambda = 1 + \frac{1}{42}(8E^* - 7)^2$$

$$f_{c'} = 1 + (6C^* - 5)^2/(16A^* + 40).$$

3. Numerical Results

The numerical methods employed have been described elsewhere [21]. These calculations differ from the earlier ones in that higher order Gaussian quadrature formulas have been used here.

Tables of collision integrals for the (12, 6) potential have been calculated by a number of other workers. For this reason, collision integrals for that function can be used to "calibrate" a new calculation. Our "calibration" is presented as table 1 in which are given differences, in parts per thousand, between our results for the (12, 6) function and those of other workers. Table 1 gives one an indication of the accuracy of our results. In particular, our results would appear to be good to at least one part per thousand over almost the entire range with strong indications that an accuracy of one part in ten thousand is likely for most values. As has been pointed out previously [8], the differences between our results and those of Monchick and Mason at high temperatures most likely result from errors in their calculations. The Hirshfelder, Curtiss, and Bird results [2] depart drastically from all calculations at the high and low temperature ends of the tables.

TABLE 1. *Deviations in parts per thousand between these results and other calculations*

	$\Omega^{(2,2)*}$						$\Omega^{(1,1)*}$				
T^*	I	II	III	IV	V	VI	I	II	III	V	VI
0.1	0.50				0.55		1.42			0.03	
.2	1.50				.25		1.25			.61	
.25		1.11						2.40			
.3	1.45	0.96			.15	21.19	1.06	1.86		.76	−3.67
.35		.23				19.03		1.61			−2.07
.4	1.05	.70			.10	16.72	1.26	1.86		1.08	−0.30
.45		−.12				14.03		1.16			−.53
.5	1.04	.78			.39	12.89	0.67	1.15		0.57	.72
.55		−.26				10.35		1.54			.78
.6	0.12	−.07	−0.45		−.36	9.23	.71	1.03	−2.11	.60	.55
.65		.21				8.74		0.65			.65
.7	.44	.33	−.08		.13	7.78	.46	.74	−1.68	.34	.63
.75						6.56					1.18
.8	−.17	−.28	−.62		−.39	5.56	1.08	1.33	−0.66	1.14	1.20
.85						4.79					1.06
.9	.01	−.05	−.40		−.17	4.37	0.29	0.49	−.70	0.29	0.62
.95						4.35					.36
1.0	.39	.32	.32	−0.18	.26	4.10	−.03	.11	−.86	−.03	.53
1.1			.0		−.20	2.64			.35	1.08	1.08
1.2	−.24	−.30	−.17	−1.40	−.30	1.90	.82	.29	.36	.74	1.12
1.3			−.47		−.12	1.67			−.70	.24	0.87
1.4	.14	.06	.21	−0.30	.06	1.69	.14	.06	−.18	.06	.63
1.5			.15		.78	0.91			.12	.22	.72
1.6	.11	.03		.11	−.05	.89	.24	.24		.24	1.01
1.7					−.07	.98				.36	1.15
1.8	−.07	−.15		.18	−.15	.67	.49	.49		.40	1.03
1.9			−.44		−.11	.39			−.59	.42	1.24
2.0	−.06	−.14		.45	−.14	.54	.43	.33		.43	0.71
2.2		−.09		.35	−.09	.08		.38		.38	.86
2.4		−.12		.33	−.03	−.03		.12		.02	1.31
2.6		−.07		.39	−.07	−.26		.01		−.09	1.22
2.8		−.03		.35	−.03	.25		−.03		−.08	0.96
3.0	−.01	−.01		.28	−.10	−.20	.01	.04		.04	1.09
3.2				.27		−.32					1.43
3.4				−1.77		−.48					1.43
3.6				0.20		−.21					1.39
3.8				.15		−.26					1.34
4.0	−.07	−.09		.22	−.09	−.19	.26	.18		.07	1.31
4.5		−.14			−.14	−.25		.10		.10	0.91
5.0	−.05	−.09		.23	−.09	−.20	.01	−.03		−.03	.69

TABLE 1. *Deviations in parts per thousand between these results and other calculations*—Continued

	$\Omega^{(2,2)*}$						$\Omega^{(1,1)*}$				
T^*	I	II	III	IV	V	VI	I	II	III	V	VI
5.5		−0.13	−1.55					−0.03	−0.88		
6.0	−0.04	−.08		0.14	−0.08	−0.20	−0.09	−.13		−0.13	0.48
7.0	−.06	−.15		.19	−.04	−.04	.01	−.04		−.04	.21
8.0	−.05	−.06		.17	−.06	−.06	.08	−.04		−.04	−.04
9.0	−.05	−.11		.13	−.11	.01	.09	.00		.00	.00
10.0	−.04	−.10		.14	−.10	.14	.06	.06		.06	−.21
11.0		−.12		.13				−.04			
12.0	−.04	−.12		.13	−.12		.00	.03		.03	
13.0				.08							
14.0	−.06			−.02	−.02		−.03			.03	
15.0				.04							
16.0	−.07	−.15		−.02	−.15		−.01	−.07		−.07	
18.0	−.09				−.12		−.01			−.01	
20.0	−.13	−.08			−.08	.46	−.02	−.10		−.10	.05
24.0		−.19						.04			
30.0	−.43				−.19	.24	−.09			−.09	.40
32.0		−.20		.23				−.10			
40.0	−1.08	−.16			−.16	−.31	−.25	−.09		−.09	.42
45.0					−.19					−.09	
50.0	−1.97	−.14			−.30	−1.07	−.55	−.10		−.10	.59
60.0						−2.00					.39
70.0						−2.69					.19
75.0	−4.31				−.94		−1.52			−.30	
80.0		−.05				−3.67		−.01			−.01
90.0						−4.48					−.39
100.0	−6.06	−.06			−2.16	−5.21	−2.45	−.08		−.66	−.47
200.0		−.05				−12.08		−.07			−3.09

I. L. Monchick and E. A. Mason, J. Chem. Phys. **35,** 1676 (1961).
II. E. C. Itean, A. R. Glueck, and R. A. Svehla, TND–481 National Aeronautics and Space Agency, Lewis Research Center, Cleveland, Ohio (1961).
III. J. A. Barker, W. Fock, and F. Smith, Phys. Fl. **7,** 897 (1964).
IV. F. A. Krieger, Report RM–646, The Rand Corporation, Santa Monica, California.
V. J. P. O'Connell and J. M. Prausnitz, Advances in Thermophysical Properties at Extreme Pressures, pp. 19–31, ASME, New York (1965).
VI. J. O. Hirshfelder, C. F. Curtiss, and R. B. Bird, Molecular Theory of Gases and Liquids (John Wiley & Sons, New York, N.Y., 1954).

TABLE 2. *Boyle parameters for the* (m, 6) *potentials*

m	T_B^*	$\frac{T_B^*}{(T_B^*)_{12,6}}$	V_B^*	$\frac{V_B^*}{(V_B^*)_{12,6}}$
9	4.5554	1.3328	0.7153	0.8817
12	3.4179	1.0000	.8112	1.0000
15	2.8766	0.8416	.8730	1.0761
18	2.5581	.7484	.9164	1.1296
21	2.3471	.6867	.9487	1.1296
24	2.1964	.6426	.9737	1.2002
30	1.9943	.5835	1.0099	1.2449
40	1.7997	.5266	1.0478	1.2916
50	1.6848	.4929	1.0714	1.3208
75	1.5314	.4481	1.1042	1.3612

We have also included a table of Boyle temperatures and Boyle volumes for these potentials. These quantities have proven useful in the correlation of gas properties. Also presented are the ratios of the Boyle temperatures and volumes for each function to those for the (12, 6) function. Such ratios can be used to obtain good first guesses at the parameters ϵ/k and b_0 appropriate to a given substance for any of these values of m, given the ϵ/k and b_0 values for the (12, 6) function for that substance. One need only to divide the ϵ/k and b_0 values for the (12, 6) function by the ratios for the other function.

The authors thank the computer staff of the Air Force Automatic Data Processing Systems at the Pentagon for making time available on their computers. The authors wish particularly to thank Ed. Hall of that organization for his cooperation.

TABLE 3a. *Collision integrals for the (9, 6) potential function*

T*	$\Omega^{(1,1)*}$	$\Omega^{(2,2)*}$	$\Omega^{(1,2)*}$	$\Omega^{(1,3)*}$	$\Omega^{(2,3)*}$	$\Omega^{(3,3)*}$
.10	4.7348	4.7232	4.1639	3.7719	4.3120	4.3589
.15	4.0703	4.1080	3.5435	3.1645	3.7606	3.7046
.20	3.6211	3.7308	3.1036	2.7174	3.4102	3.2510
.25	3.2752	3.4463	2.7585	2.3729	3.1232	2.9086
.30	2.9910	3.2046	2.4791	2.1062	2.8694	2.6410
.35	2.7606	2.9914	2.2577	1.9026	2.6468	2.4237
.40	2.5571	2.8090	2.0709	1.7402	2.4555	2.2436
.45	2.3935	2.6414	1.9232	1.6141	2.2883	2.0938
.50	2.2457	2.4901	1.7969	1.5114	2.1428	1.9676
.55	2.1174	2.3627	1.6906	1.4273	2.0202	1.8585
.60	2.0124	2.2456	1.6039	1.3589	1.9130	1.7648
.65	1.9177	2.1386	1.5287	1.3012	1.8193	1.6850
.70	1.8321	2.0449	1.4634	1.2521	1.7381	1.6142
.75	1.7558	1.9625	1.4064	1.2100	1.6675	1.5518
.80	1.6887	1.8895	1.3569	1.1735	1.6057	1.4969
.85	1.6310	1.8229	1.3141	1.1418	1.5510	1.4484
.90	1.5798	1.7612	1.2765	1.1141	1.5018	1.4050
.95	1.5324	1.7054	1.2426	1.0893	1.4580	1.3662
1.00	1.4886	1.6554	1.2120	1.0672	1.4189	1.3312
1.10	1.4118	1.5694	1.1594	1.0292	1.3522	1.2707
1.20	1.3475	1.4971	1.1160	.9979	1.2971	1.2202
1.30	1.2936	1.4360	1.0796	.9715	1.2512	1.1779
1.40	1.2489	1.3833	1.0490	.9490	1.2123	1.1418
1.50	1.2096	1.3375	1.0225	.9294	1.1789	1.1108
1.60	1.1747	1.2977	.9993	.9121	1.1499	1.0837
1.70	1.1437	1.2629	.9788	.8968	1.1246	1.0599
1.80	1.1160	1.2323	.9606	.8831	1.1023	1.0387
1.90	1.0912	1.2051	.9442	.8707	1.0825	1.0199
2.00	1.0689	1.1807	.9295	.8594	1.0647	1.0029
2.20	1.0304	1.1389	.9038	.8396	1.0341	.9737
2.40	.9987	1.1040	.8822	.8225	1.0086	.9493
2.60	.9722	1.0747	.8638	.8077	.9869	.9284
2.80	.9492	1.0495	.8477	.7945	.9682	.9104
3.00	.9289	1.0278	.8334	.7828	.9517	.8945
3.20	.9109	1.0088	.8206	.7721	.9371	.8804
3.40	.8948	.9919	.8090	.7624	.9241	.8678
3.60	.8804	.9768	.7985	.7534	.9122	.8563
3.80	.8674	.9631	.7889	.7452	.9014	.8459
4.00	.8555	.9508	.7801	.7375	.8915	.8363
4.50	.8298	.9241	.7606	.7204	.8699	.8154
5.00	.8086	.9020	.7441	.7057	.8516	.7977
5.50	.7907	.8834	.7297	.6928	.8359	.7826
6.00	.7752	.8673	.7171	.6813	.8221	.7693
6.50	.7616	.8531	.7058	.6710	.8099	.7576
7.00	.7495	.8406	.6956	.6617	.7990	.7471
7.50	.7385	.8293	.6864	.6531	.7891	.7375
8.00	.7286	.8190	.6778	.6452	.7799	.7288
8.50	.7195	.8097	.6700	.6379	.7716	.7208
9.00	.7111	.8011	.6627	.6312	.7638	.7134
9.50	.7033	.7931	.6560	.6248	.7566	.7065

TABLE 3a. *Collision integrals for the (9, 6) potential function*—Continued

T^*	$\Omega^{(1,1)*}$	$\Omega^{(2,2)*}$	$\Omega^{(1,2)*}$	$\Omega^{(1,3)*}$	$\Omega^{(2,3)*}$	$\Omega^{(3,3)*}$
10.00	.6961	.7857	.6496	.6189	.7498	.7000
11.00	.6830	.7722	.6380	.6079	.7375	.6882
12.00	.6714	.7603	.6277	.5982	.7264	.6777
13.00	.6610	.7496	.6183	.5893	.7164	.6682
14.00	.6516	.7398	.6097	.5812	.7072	.6595
15.00	.6430	.7309	.6019	.5737	.6988	.6515
16.00	.6351	.7227	.5947	.5668	.6910	.6441
17.00	.6278	.7150	.5879	.5603	.6837	.6372
18.00	.6210	.7079	.5817	.5543	.6769	.6307
19.00	.6147	.7012	.5758	.5487	.6705	.6246
20.00	.6087	.6950	.5703	.5434	.6645	.6189
22.00	.5978	.6834	.5601	.5336	.6533	.6084
24.00	.5881	.6730	.5509	.5248	.6433	.5989
26.00	.5792	.6636	.5426	.5169	.6342	.5903
28.00	.5711	.6549	.5351	.5096	.6258	.5824
30.00	.5637	.6469	.5281	.5028	.6180	.5751
32.00	.5568	.6395	.5216	.4966	.6108	.5683
34.00	.5505	.6325	.5156	.4908	.6041	.5620
36.00	.5445	.6261	.5099	.4854	.5978	.5561
38.00	.5389	.6200	.5046	.4803	.5919	.5505
40.00	.5337	.6142	.4997	.4755	.5864	.5453
45.00	.5218	.6012	.4884	.4647	.5737	.5334
50.00	.5113	.5897	.4785	.4552	.5626	.5229
55.00	.5020	.5794	.4697	.4467	.5526	.5136
60.00	.4936	.5701	.4617	.4391	.5436	.5052
65.00	.4860	.5617	.4545	.4321	.5354	.4975
70.00	.4791	.5539	.4479	.4258	.5279	.4905
75.00	.4727	.5468	.4419	.4200	.5210	.4840
80.00	.4667	.5402	.4362	.4146	.5146	.4780
85.00	.4612	.5340	.4310	.4096	.5087	.4724
90.00	.4561	.5282	.4262	.4049	.5031	.4672
95.00	.4512	.5228	.4216	.4005	.4979	.4623
100.00	.4467	.5177	.4173	.3964	.4930	.4577
125.00	.4273	.4960	.3990	.3789	.4720	.4381
150.00	.4121	.4787	.3846	.3651	.4553	.4226
175.00	.3995	.4645	.3727	.3537	.4416	.4098
200.00	.3889	.4524	.3627	.3441	.4300	.3989

TABLE 4a. *Collision integrals for the (12, 6) potential function*

T^*	$\Omega^{(1,1)*}$	$\Omega^{(2,2)*}$	$\Omega^{(1,2)*}$	$\Omega^{(1,3)*}$	$\Omega^{(2,3)*}$	$\Omega^{(3,3)*}$
.10	4.0127	4.1039	3.5538	3.2422	3.7626	3.7519
.15	3.4833	3.5879	3.0684	2.7772	3.2938	3.2320
.20	3.1328	3.2686	2.7334	2.4413	3.0018	2.8788
.25	2.8677	3.0336	2.4723	2.1779	2.7741	2.6109
.30	2.6509	2.8456	2.2574	1.9669	2.5815	2.3979
.35	2.4695	2.6777	2.0809	1.8000	2.4074	2.2248
.40	2.3171	2.5327	1.9353	1.6668	2.2566	2.0790
.45	2.1823	2.4003	1.8114	1.5583	2.1220	1.9569
.50	2.0662	2.2867	1.7074	1.4701	2.0072	1.8511
.55	1.9681	2.1774	1.6212	1.3981	1.9031	1.7615
.60	1.8779	2.0828	1.5455	1.3373	1.8137	1.6831
.65	1.7979	1.9994	1.4800	1.2857	1.7358	1.6137
.70	1.7298	1.9230	1.4247	1.2424	1.6671	1.5535
.75	1.6699	1.8521	1.3768	1.2052	1.6059	1.5008
.80	1.6139	1.7885	1.3336	1.1724	1.5515	1.4535
.85	1.5633	1.7327	1.2955	1.1439	1.5040	1.4113
.90	1.5175	1.6821	1.2616	1.1187	1.4615	1.3733
.95	1.4763	1.6360	1.2313	1.0963	1.4235	1.3392
1.00	1.4394	1.5933	1.2042	1.0762	1.3890	1.3084
1.10	1.3767	1.5175	1.1583	1.0421	1.3296	1.2553
1.20	1.3218	1.4542	1.1197	1.0137	1.2805	1.2109
1.30	1.2744	1.4010	1.0871	.9898	1.2395	1.1732
1.40	1.2335	1.3550	1.0591	.9692	1.2046	1.1409
1.50	1.1983	1.3151	1.0351	.9515	1.1747	1.1131
1.60	1.1678	1.2801	1.0143	.9359	1.1487	1.0888
1.70	1.1414	1.2491	.9960	.9221	1.1259	1.0675
1.80	1.1175	1.2215	.9796	.9096	1.1058	1.0486
1.90	1.0956	1.1971	.9648	.8984	1.0879	1.0317
2.00	1.0760	1.1753	.9515	.8882	1.0718	1.0165
2.20	1.0418	1.1379	.9284	.8703	1.0443	.9901
2.40	1.0131	1.1069	.9089	.8550	1.0213	.9681
2.60	.9888	1.0807	.8922	.8416	1.0019	.9495
2.80	.9679	1.0581	.8776	.8298	.9851	.9333
3.00	.9499	1.0386	.8647	.8193	.9704	.9191
3.20	.9342	1.0215	.8533	.8098	.9574	.9066
3.40	.9200	1.0064	.8430	.8011	.9458	.8954
3.60	.9071	.9929	.8336	.7931	.9353	.8852
3.80	.8954	.9807	.8250	.7858	.9258	.8760
4.00	.8847	.9697	.8170	.7789	.9171	.8676
4.50	.8617	.9461	.7996	.7638	.8981	.8492
5.00	.8427	.9266	.7849	.7507	.8822	.8337
5.50	.8266	.9102	.7721	.7393	.8685	.8204
6.00	.8127	.8961	.7609	.7291	.8564	.8088
6.50	.8005	.8837	.7508	.7199	.8457	.7984
7.00	.7897	.8726	.7418	.7116	.8361	.7891
7.50	.7800	.8627	.7335	.7039	.8273	.7807
8.00	.7711	.8537	.7260	.6969	.8193	.7729
8.50	.7631	.8454	.7190	.6904	.8118	.7657
9.00	.7556	.8378	.7125	.6843	.8049	.7591
9.50	.7487	.8308	.7064	.6786	.7985	.7529

TABLE 4a. *Collision integrals for the (12, 6) potential function*—Continued

T^*	$\Omega^{(1,1)*}$	$\Omega^{(2,2)*}$	$\Omega^{(1,2)*}$	$\Omega^{(1,3)*}$	$\Omega^{(2,3)*}$	$\Omega^{(3,3)*}$
10.00	.7422	.8242	.7007	.6732	.7925	.7471
11.00	.7306	.8123	.6904	.6634	.7814	.7365
12.00	.7202	.8017	.6811	.6546	.7715	.7269
13.00	.7109	.7921	.6727	.6466	.7625	.7183
14.00	.7025	.7834	.6650	.6392	.7543	.7105
15.00	.6948	.7754	.6579	.6325	.7468	.7032
16.00	.6877	.7681	.6514	.6262	.7398	.6966
17.00	.6811	.7613	.6453	.6204	.7333	.6903
18.00	.6750	.7549	.6397	.6150	.7272	.6845
19.00	.6693	.7489	.6343	.6099	.7215	.6791
20.00	.6640	.7433	.6293	.6051	.7161	.6740
22.00	.6542	.7330	.6202	.5962	.7062	.6645
24.00	.6453	.7238	.6119	.5883	.6973	.6560
26.00	.6374	.7153	.6044	.5810	.6892	.6483
28.00	.6301	.7076	.5975	.5744	.6817	.6412
30.00	.6234	.7005	.5912	.5683	.6748	.6347
32.00	.6172	.6939	.5853	.5626	.6685	.6286
34.00	.6114	.6878	.5798	.5573	.6625	.6229
36.00	.6060	.6820	.5747	.5524	.6569	.6176
38.00	.6010	.6766	.5699	.5478	.6516	.6126
40.00	.5962	.6715	.5654	.5434	.6467	.6079
45.00	.5854	.6599	.5551	.5335	.6354	.5972
50.00	.5759	.6496	.5461	.5247	.6255	.5878
55.00	.5674	.6405	.5380	.5169	.6165	.5793
60.00	.5598	.6322	.5307	.5099	.6085	.5717
65.00	.5528	.6246	.5241	.5035	.6011	.5647
70.00	.5465	.6177	.5180	.4976	.5944	.5584
75.00	.5406	.6113	.5124	.4922	.5882	.5525
80.00	.5352	.6053	.5072	.4872	.5824	.5470
85.00	.5301	.5998	.5024	.4825	.5770	.5419
90.00	.5254	.5946	.4979	.4782	.5719	.5371
95.00	.5209	.5897	.4936	.4741	.5672	.5327
100.00	.5167	.5851	.4896	.4702	.5627	.5284
125.00	.4989	.5654	.4726	.4537	.5436	.5104
150.00	.4847	.5497	.4590	.4406	.5283	.4960
175.00	.4729	.5366	.4478	.4299	.5157	.4841
200.00	.4630	.5256	.4383	.4207	.5050	.4740

TABLE 5a. *Collision integrals for the (15, 6) potential function*

T^*	$\Omega^{(1,1)*}$	$\Omega^{(2,2)*}$	$\Omega^{(1,2)*}$	$\Omega^{(1,3)*}$	$\Omega^{(2,3)*}$	$\Omega^{(3,3)*}$
.10	3.6513	3.7783	3.2394	2.9622	3.4684	3.4346
.15	3.1790	3.3103	2.8119	2.5591	3.0427	2.9780
.20	2.8718	3.0168	2.5250	2.2774	2.7745	2.6720
.25	2.6422	2.8068	2.3034	2.0556	2.5756	2.4406
.30	2.4585	2.6382	2.1238	1.8781	2.4083	2.2572
.35	2.3050	2.4971	1.9741	1.7341	2.2637	2.1053
.40	2.1721	2.3716	1.8471	1.6165	2.1340	1.9791
.45	2.0601	2.2585	1.7420	1.5217	2.0191	1.8716
.50	1.9599	2.1566	1.6511	1.4429	1.9172	1.7802
.55	1.8724	2.0682	1.5734	1.3773	1.8292	1.6991
.60	1.7975	1.9839	1.5082	1.3229	1.7498	1.6305
.65	1.7289	1.9085	1.4505	1.2763	1.6796	1.5696
.70	1.6668	1.8429	1.3998	1.2363	1.6190	1.5153
.75	1.6124	1.7833	1.3558	1.2019	1.5652	1.4675
.80	1.5647	1.7270	1.3176	1.1721	1.5164	1.4249
.85	1.5217	1.6756	1.2837	1.1460	1.4729	1.3873
.90	1.4814	1.6299	1.2530	1.1228	1.4342	1.3533
.95	1.4445	1.5889	1.2255	1.1021	1.3998	1.3224
1.00	1.4106	1.5509	1.2005	1.0836	1.3684	1.2940
1.10	1.3526	1.4845	1.1579	1.0518	1.3146	1.2456
1.20	1.3047	1.4271	1.1229	1.0257	1.2696	1.2052
1.30	1.2628	1.3777	1.0931	1.0036	1.2316	1.1707
1.40	1.2260	1.3360	1.0675	.9846	1.1996	1.1412
1.50	1.1937	1.3000	1.0453	.9682	1.1721	1.1157
1.60	1.1655	1.2682	1.0260	.9538	1.1481	1.0934
1.70	1.1407	1.2400	1.0089	.9409	1.1271	1.0737
1.80	1.1189	1.2148	.9938	.9295	1.1084	1.0563
1.90	1.0995	1.1923	.9804	.9192	1.0919	1.0407
2.00	1.0820	1.1722	.9682	.9098	1.0771	1.0267
2.20	1.0509	1.1376	.9469	.8933	1.0516	1.0025
2.40	1.0246	1.1091	.9289	.8793	1.0304	.9823
2.60	1.0023	1.0850	.9135	.8670	1.0125	.9651
2.80	.9830	1.0643	.9001	.8563	.9970	.9502
3.00	.9663	1.0464	.8883	.8466	.9835	.9372
3.20	.9516	1.0306	.8778	.8379	.9716	.9257
3.40	.9387	1.0167	.8683	.8301	.9610	.9155
3.60	.9271	1.0043	.8598	.8228	.9514	.9062
3.80	.9165	.9931	.8519	.8161	.9427	.8978
4.00	.9068	.9830	.8447	.8099	.9348	.8901
4.50	.8857	.9613	.8288	.7962	.9175	.8733
5.00	.8683	.9436	.8154	.7844	.9030	.8592
5.50	.8536	.9286	.8038	.7740	.8906	.8472
6.00	.8409	.9157	.7936	.7648	.8797	.8366
6.50	.8298	.9045	.7846	.7566	.8700	.8272
7.00	.8199	.8944	.7764	.7490	.8613	.8188
7.50	.8110	.8855	.7689	.7422	.8534	.8112
8.00	.8030	.8773	.7621	.7358	.8462	.8042
8.50	.7957	.8698	.7558	.7299	.8395	.7977
9.00	.7889	.8630	.7499	.7244	.8333	.7917
9.50	.7827	.8566	.7444	.7193	.8275	.7861

TABLE 5a. *Collision integrals for the (15, 6) potential function*—Continued

T^*	$\Omega^{(1,1)*}$	$\Omega^{(2,2)*}$	$\Omega^{(1,2)*}$	$\Omega^{(1,3)*}$	$\Omega^{(2,3)*}$	$\Omega^{(3,3)*}$
10.00	.7769	.8507	.7393	.7145	.8221	.7809
11.00	.7663	.8400	.7300	.7057	.8123	.7714
12.00	.7570	.8305	.7216	.6977	.8035	.7629
13.00	.7486	.8219	.7140	.6905	.7955	.7552
14.00	.7409	.8142	.7071	.6839	.7882	.7482
15.00	.7340	.8071	.7008	.6779	.7815	.7418
16.00	.7276	.8005	.6949	.6723	.7753	.7359
17.00	.7217	.7945	.6894	.6670	.7696	.7303
18.00	.7162	.7888	.6843	.6621	.7642	.7252
19.00	.7111	.7835	.6796	.6576	.7592	.7203
20.00	.7062	.7785	.6751	.6532	.7544	.7158
22.00	.6974	.7694	.6668	.6453	.7456	.7074
24.00	.6895	.7612	.6594	.6381	.7377	.6998
26.00	.6823	.7537	.6526	.6316	.7305	.6929
28.00	.6757	.7469	.6464	.6256	.7239	.6865
30.00	.6697	.7406	.6407	.6200	.7178	.6807
32.00	.6641	.7347	.6354	.6149	.7121	.6752
34.00	.6589	.7292	.6304	.6101	.7068	.6702
36.00	.6540	.7241	.6258	.6056	.7018	.6654
38.00	.6495	.7193	.6215	.6014	.6971	.6609
40.00	.6452	.7148	.6174	.5975	.6927	.6567
45.00	.6354	.7044	.6081	.5884	.6826	.6471
50.00	.6268	.6953	.5998	.5805	.6737	.6386
55.00	.6192	.6871	.5925	.5733	.6657	.6310
60.00	.6122	.6797	.5859	.5669	.6585	.6241
65.00	.6059	.6729	.5798	.5610	.6519	.6178
70.00	.6002	.6667	.5743	.5557	.6458	.6120
75.00	.5948	.6610	.5692	.5507	.6402	.6067
80.00	.5899	.6556	.5644	.5461	.6350	.6017
85.00	.5853	.6507	.5600	.5418	.6302	.5971
90.00	.5809	.6460	.5558	.5378	.6256	.5927
95.00	.5769	.6416	.5519	.5340	.6213	.5887
100.00	.5731	.6374	.5483	.5304	.6173	.5848
125.00	.5567	.6197	.5326	.5152	.5999	.5683
150.00	.5436	.6054	.5200	.5030	.5861	.5552
175.00	.5328	.5936	.5096	.4930	.5746	.5442
200.00	.5236	.5835	.5008	.4844	.5648	.5349

TABLE 6a. *Collision integrals for the (18, 6) potential function*

T^*	$\Omega^{(1,1)*}$	$\Omega^{(2,2)*}$	$\Omega^{(1,2)*}$	$\Omega^{(1,3)*}$	$\Omega^{(2,3)*}$	$\Omega^{(3,3)*}$
.10	3.4376	3.5794	3.0510	2.7923	3.2867	3.2385
.15	2.9961	3.1375	2.6548	2.4226	2.8848	2.8166
.20	2.7121	2.8620	2.3936	2.1703	2.6342	2.5371
.25	2.5030	2.6645	2.1957	1.9746	2.4495	2.3280
.30	2.3366	2.5101	2.0351	1.8163	2.2988	2.1614
.35	2.1977	2.3797	1.9010	1.6871	2.1674	2.0255
.40	2.0809	2.2634	1.7895	1.5824	2.0498	1.9126
.45	1.9778	2.1652	1.6929	1.4948	1.9489	1.8136
.50	1.8903	2.0714	1.6124	1.4235	1.8561	1.7308
.55	1.8107	1.9903	1.5415	1.3630	1.7759	1.6582
.60	1.7414	1.9179	1.4809	1.3122	1.7054	1.5937
.65	1.6812	1.8489	1.4291	1.2694	1.6414	1.5385
.70	1.6261	1.7873	1.3832	1.2325	1.5850	1.4896
.75	1.5756	1.7330	1.3422	1.2002	1.5354	1.4451
.80	1.5307	1.6836	1.3062	1.1721	1.4912	1.4057
.85	1.4914	1.6379	1.2749	1.1477	1.4515	1.3707
.90	1.4560	1.5950	1.2470	1.1262	1.4154	1.3394
.95	1.4228	1.5561	1.2216	1.1069	1.3829	1.3110
1.00	1.3919	1.5212	1.1984	1.0894	1.3538	1.2850
1.10	1.3377	1.4604	1.1586	1.0597	1.3038	1.2397
1.20	1.2926	1.4082	1.1256	1.0350	1.2620	1.2018
1.30	1.2545	1.3623	1.0979	1.0143	1.2264	1.1698
1.40	1.2212	1.3230	1.0742	.9966	1.1963	1.1423
1.50	1.1915	1.2892	1.0535	.9812	1.1703	1.1184
1.60	1.1651	1.2598	1.0353	.9676	1.1479	1.0975
1.70	1.1419	1.2337	1.0193	.9556	1.1282	1.0791
1.80	1.1212	1.2102	1.0051	.9449	1.1107	1.0626
1.90	1.1029	1.1892	.9924	.9353	1.0951	1.0480
2.00	1.0866	1.1704	.9810	.9265	1.0812	1.0349
2.20	1.0582	1.1378	.9612	.9112	1.0572	1.0123
2.40	1.0338	1.1110	.9445	.8981	1.0373	.9933
2.60	1.0130	1.0884	.9301	.8867	1.0204	.9772
2.80	.9950	1.0691	.9176	.8768	1.0060	.9633
3.00	.9793	1.0523	.9066	.8678	.9934	.9512
3.20	.9656	1.0376	.8968	.8598	.9823	.9405
3.40	.9533	1.0245	.8880	.8525	.9724	.9309
3.60	.9425	1.0129	.8801	.8459	.9635	.9223
3.80	.9328	1.0025	.8728	.8397	.9554	.9145
4.00	.9238	.9930	.8662	.8341	.9480	.9074
4.50	.9044	.9728	.8515	.8215	.9321	.8919
5.00	.8882	.9564	.8392	.8106	.9187	.8790
5.50	.8746	.9425	.8285	.8012	.9074	.8679
6.00	.8628	.9306	.8192	.7928	.8974	.8583
6.50	.8526	.9203	.8109	.7853	.8886	.8497
7.00	.8435	.9111	.8034	.7785	.8807	.8421
7.50	.8353	.9029	.7966	.7722	.8736	.8351
8.00	.8279	.8954	.7904	.7665	.8670	.8288
8.50	.8212	.8886	.7846	.7611	.8610	.8229
9.00	.8150	.8824	.7793	.7562	.8554	.8175
9.50	.8093	.8766	.7743	.7515	.8502	.8125

TABLE 6a. *Collision integrals for the (18, 6) potential function*—Continued

T^*	$\Omega^{(1,1)*}$	$\Omega^{(2,2)*}$	$\Omega^{(1,2)*}$	$\Omega^{(1,3)*}$	$\Omega^{(2,3)*}$	$\Omega^{(3,3)*}$
10.00	.8040	.8712	.7697	.7471	.8453	.8078
11.00	.7944	.8615	.7612	.7391	.8364	.7992
12.00	.7858	.8529	.7536	.7319	.8284	.7915
13.00	.7782	.8452	.7467	.7254	.8212	.7845
14.00	.7713	.8381	.7404	.7194	.8147	.7781
15.00	.7649	.8317	.7347	.7139	.8086	.7723
16.00	.7591	.8258	.7293	.7088	.8030	.7669
17.00	.7537	.8203	.7244	.7041	.7978	.7619
18.00	.7487	.8152	.7198	.6996	.7929	.7572
19.00	.7441	.8104	.7154	.6954	.7884	.7528
20.00	.7397	.8059	.7113	.6915	.7841	.7487
22.00	.7317	.7977	.7038	.6843	.7762	.7410
24.00	.7245	.7902	.6971	.6778	.7690	.7342
26.00	.7179	.7835	.6909	.6718	.7625	.7279
28.00	.7120	.7773	.6853	.6664	.7566	.7222
30.00	.7065	.7716	.6801	.6613	.7510	.7169
32.00	.7014	.7663	.6753	.6567	.7459	.7120
34.00	.6967	.7614	.6708	.6523	.7411	.7074
36.00	.6922	.7568	.6666	.6482	.7366	.7031
38.00	.6881	.7524	.6626	.6444	.7324	.6990
40.00	.6842	.7483	.6589	.6408	.7284	.6952
45.00	.6753	.7390	.6504	.6325	.7194	.6865
50.00	.6675	.7308	.6429	.6252	.7113	.6788
55.00	.6605	.7234	.6362	.6187	.7041	.6719
60.00	.6542	.7167	.6302	.6128	.6976	.6656
65.00	.6485	.7106	.6246	.6075	.6917	.6599
70.00	.6432	.7050	.6196	.6025	.6862	.6547
75.00	.6383	.6999	.6149	.5980	.6811	.6498
80.00	.6338	.6950	.6106	.5938	.6764	.6453
85.00	.6296	.6905	.6065	.5898	.6720	.6411
90.00	.6256	.6863	.6027	.5861	.6679	.6371
95.00	.6219	.6823	.5991	.5826	.6640	.6334
100.00	.6184	.6786	.5958	.5794	.6603	.6299
125.00	.6034	.6625	.5813	.5653	.6446	.6149
150.00	.5914	.6496	.5697	.5540	.6320	.6028
175.00	.5815	.6388	.5601	.5447	.6215	.5928
200.00	.5730	.6296	.5520	.5367	.6125	.5842

TABLE 7a. *Collision integrals for the (21, 6) potential function*

T^*	$\Omega^{(1,1)*}$	$\Omega^{(2,2)*}$	$\Omega^{(1,2)*}$	$\Omega^{(1,3)*}$	$\Omega^{(2,3)*}$	$\Omega^{(3,3)*}$
.10	3.2971	3.4469	2.9268	2.6796	3.1650	3.1075
.15	2.8750	3.0208	2.5495	2.3298	2.7767	2.7057
.20	2.6050	2.7542	2.3038	2.0954	2.5345	2.4439
.25	2.4083	2.5659	2.1202	1.9161	2.3606	2.2484
.30	2.2527	2.4186	1.9722	1.7712	2.2191	2.0945
.35	2.1244	2.2947	1.8497	1.6532	2.0965	1.9692
.40	2.0159	2.1906	1.7466	1.5561	1.9915	1.8621
.45	1.9210	2.0954	1.6580	1.4753	1.8958	1.7728
.50	1.8395	2.0127	1.5830	1.4083	1.8127	1.6939
.55	1.7676	1.9345	1.5185	1.3525	1.7368	1.6278
.60	1.7021	1.8672	1.4612	1.3043	1.6710	1.5675
.65	1.6460	1.8060	1.4127	1.2639	1.6127	1.5151
.70	1.5958	1.7476	1.3702	1.2292	1.5594	1.4693
.75	1.5497	1.6959	1.3323	1.1989	1.5124	1.4283
.80	1.5075	1.6501	1.2984	1.1723	1.4710	1.3912
.85	1.4696	1.6081	1.2683	1.1489	1.4339	1.3580
.90	1.4364	1.5686	1.2419	1.1283	1.3999	1.3280
.95	1.4062	1.5322	1.2183	1.1102	1.3693	1.3013
1.00	1.3781	1.4987	1.1968	1.0938	1.3416	1.2771
1.10	1.3273	1.4412	1.1591	1.0654	1.2941	1.2343
1.20	1.2842	1.3921	1.1276	1.0420	1.2545	1.1983
1.30	1.2482	1.3496	1.1014	1.0223	1.2210	1.1680
1.40	1.2172	1.3124	1.0790	1.0055	1.1924	1.1421
1.50	1.1896	1.2799	1.0594	.9910	1.1677	1.1195
1.60	1.1649	1.2520	1.0423	.9782	1.1465	1.0997
1.70	1.1429	1.2274	1.0272	.9669	1.1278	1.0824
1.80	1.1233	1.2054	1.0137	.9568	1.1114	1.0670
1.90	1.1059	1.1857	1.0017	.9477	1.0967	1.0532
2.00	1.0902	1.1679	.9909	.9395	1.0835	1.0408
2.20	1.0635	1.1371	.9722	.9252	1.0609	1.0195
2.40	1.0408	1.1116	.9565	.9129	1.0421	1.0017
2.60	1.0212	1.0904	.9430	.9023	1.0263	.9866
2.80	1.0043	1.0721	.9313	.8930	1.0127	.9735
3.00	.9895	1.0563	.9210	.8847	1.0008	.9621
3.20	.9765	1.0425	.9118	.8772	.9904	.9521
3.40	.9650	1.0302	.9036	.8704	.9811	.9431
3.60	.9547	1.0193	.8961	.8642	.9728	.9350
3.80	.9455	1.0094	.8894	.8585	.9652	.9277
4.00	.9371	1.0006	.8832	.8533	.9583	.9210
4.50	.9191	.9816	.8696	.8416	.9434	.9066
5.00	.9039	.9662	.8581	.8316	.9310	.8946
5.50	.8912	.9532	.8482	.8229	.9204	.8843
6.00	.8802	.9422	.8396	.8152	.9112	.8754
6.50	.8707	.9325	.8319	.8083	.9031	.8675
7.00	.8622	.9240	.8250	.8020	.8958	.8604
7.50	.8547	.9163	.8187	.7963	.8892	.8540
8.00	.8478	.9094	.8130	.7910	.8832	.8482
8.50	.8416	.9032	.8077	.7861	.8776	.8428
9.00	.8358	.8974	.8028	.7815	.8725	.8378
9.50	.8306	.8921	.7982	.7773	.8677	.8332

TABLE 7a. *Collision integrals for the (21, 6) potential function*—Continued

T^*	$\Omega^{(1,1)*}$	$\Omega^{(2,2)*}$	$\Omega^{(1,2)*}$	$\Omega^{(1,3)*}$	$\Omega^{(2,3)*}$	$\Omega^{(3,3)*}$
10.00	.8257	.8871	.7940	.7733	.8633	.8289
11.00	.8168	.8782	.7862	.7660	.8552	.8210
12.00	.8089	.8703	.7792	.7594	.8479	.8140
13.00	.8019	.8632	.7729	.7534	.8414	.8077
14.00	.7955	.8568	.7672	.7480	.8354	.8019
15.00	.7897	.8510	.7619	.7429	.8299	.7966
16.00	.7844	.8456	.7570	.7383	.8248	.7916
17.00	.7794	.8406	.7525	.7339	.8201	.7871
18.00	.7748	.8359	.7483	.7299	.8156	.7828
19.00	.7706	.8315	.7443	.7261	.8115	.7788
20.00	.7665	.8275	.7406	.7225	.8076	.7750
22.00	.7592	.8199	.7337	.7158	.8004	.7681
24.00	.7526	.8132	.7275	.7099	.7939	.7618
26.00	.7466	.8070	.7219	.7044	.7880	.7561
28.00	.7412	.8014	.7168	.6994	.7825	.7508
30.00	.7361	.7962	.7120	.6948	.7775	.7460
32.00	.7315	.7914	.7076	.6906	.7728	.7415
34.00	.7272	.7869	.7035	.6866	.7685	.7373
36.00	.7231	.7827	.6996	.6828	.7644	.7334
38.00	.7193	.7788	.6960	.6793	.7606	.7297
40.00	.7158	.7751	.6926	.6760	.7569	.7262
45.00	.7076	.7666	.6848	.6684	.7487	.7182
50.00	.7005	.7591	.6780	.6617	.7414	.7112
55.00	.6941	.7524	.6718	.6558	.7348	.7049
60.00	.6883	.7463	.6663	.6503	.7289	.6992
65.00	.6830	.7407	.6612	.6454	.7235	.6940
70.00	.6782	.7357	.6565	.6409	.7185	.6892
75.00	.6737	.7309	.6522	.6367	.7139	.6847
80.00	.6696	.7266	.6482	.6328	.7096	.6806
85.00	.6657	.7225	.6445	.6291	.7056	.6768
90.00	.6621	.7186	.6410	.6257	.7018	.6731
95.00	.6587	.7150	.6377	.6225	.6983	.6697
100.00	.6555	.7116	.6346	.6195	.6950	.6665
125.00	.6417	.6969	.6213	.6065	.6806	.6527
150.00	.6306	.6851	.6106	.5961	.6690	.6416
175.00	.6214	.6753	.6017	.5874	.6594	.6324
200.00	.6136	.6669	.5941	.5800	.6512	.6245

TABLE 8a. *Collision integrals for the (24, 6) potential function*

T^*	$\Omega^{(1,1)*}$	$\Omega^{(2,2)*}$	$\Omega^{(1,2)*}$	$\Omega^{(1,3)*}$	$\Omega^{(2,3)*}$	$\Omega^{(3,3)*}$
.10	3.1968	3.3499	2.8378	2.5987	3.0761	3.0123
.15	2.7882	2.9360	2.4739	2.2628	2.6988	2.6249
.20	2.5283	2.6773	2.2392	2.0412	2.4641	2.3744
.25	2.3397	2.4933	2.0649	1.8725	2.2945	2.1903
.30	2.1919	2.3510	1.9260	1.7374	2.1595	2.0449
.35	2.0709	2.2344	1.8115	1.6272	2.0455	1.9255
.40	1.9677	2.1348	1.7140	1.5356	1.9460	1.8250
.45	1.8796	2.0440	1.6321	1.4603	1.8558	1.7415
.50	1.8014	1.9664	1.5604	1.3965	1.7780	1.6666
.55	1.7346	1.8944	1.5003	1.3438	1.7077	1.6036
.60	1.6738	1.8288	1.4469	1.2985	1.6445	1.5476
.65	1.6192	1.7717	1.4000	1.2596	1.5898	1.4977
.70	1.5723	1.7181	1.3600	1.2266	1.5399	1.4536
.75	1.5297	1.6683	1.3245	1.1979	1.4951	1.4153
.80	1.4902	1.6245	1.2925	1.1727	1.4556	1.3803
.85	1.4541	1.5847	1.2638	1.1503	1.4202	1.3485
.90	1.4217	1.5480	1.2383	1.1305	1.3882	1.3200
.95	1.3933	1.5140	1.2159	1.1131	1.3593	1.2945
1.00	1.3671	1.4824	1.1956	1.0975	1.3330	1.2714
1.10	1.3195	1.4266	1.1598	1.0704	1.2871	1.2307
1.20	1.2786	1.3803	1.1298	1.0480	1.2494	1.1964
1.30	1.2437	1.3401	1.1045	1.0292	1.2175	1.1674
1.40	1.2143	1.3049	1.0832	1.0132	1.1902	1.1427
1.50	1.1883	1.2736	1.0646	.9993	1.1665	1.1211
1.60	1.1651	1.2468	1.0484	.9871	1.1461	1.1023
1.70	1.1442	1.2232	1.0339	.9764	1.1282	1.0857
1.80	1.1255	1.2023	1.0211	.9668	1.1125	1.0709
1.90	1.1088	1.1835	1.0096	.9581	1.0984	1.0578
2.00	1.0937	1.1664	.9992	.9503	1.0858	1.0459
2.20	1.0681	1.1372	.9814	.9366	1.0642	1.0256
2.40	1.0468	1.1127	.9665	.9251	1.0462	1.0086
2.60	1.0282	1.0923	.9537	.9150	1.0311	.9942
2.80	1.0121	1.0749	.9426	.9062	1.0182	.9819
3.00	.9980	1.0598	.9328	.8984	1.0069	.9710
3.20	.9857	1.0466	.9241	.8914	.9969	.9615
3.40	.9747	1.0350	.9164	.8850	.9882	.9530
3.60	.9649	1.0246	.9094	.8792	.9802	.9454
3.80	.9561	1.0152	.9029	.8739	.9731	.9384
4.00	.9481	1.0067	.8971	.8690	.9665	.9321
4.50	.9311	.9888	.8843	.8581	.9525	.9186
5.00	.9169	.9741	.8736	.8488	.9408	.9072
5.50	.9049	.9619	.8643	.8407	.9309	.8976
6.00	.8945	.9514	.8563	.8335	.9223	.8892
6.50	.8855	.9423	.8491	.8271	.9147	.8819
7.00	.8776	.9343	.8427	.8213	.9079	.8753
7.50	.8705	.9272	.8368	.8159	.9017	.8693
8.00	.8641	.9207	.8315	.8111	.8961	.8639
8.50	.8582	.9149	.8266	.8065	.8910	.8589
9.00	.8529	.9095	.8220	.8023	.8863	.8543
9.50	.8479	.9045	.8178	.7984	.8819	.8500

TABLE 8a. *Collision integrals for the (24, 6) potential function*—Continued

T^*	$\Omega^{(1,1)*}$	$\Omega^{(2,2)*}$	$\Omega^{(1,2)*}$	$\Omega^{(1,3)*}$	$\Omega^{(2,3)*}$	$\Omega^{(3,3)*}$
10.00	.8434	.8999	.8139	.7947	.8777	.8460
11.00	.8351	.8916	.8067	.7879	.8702	.8388
12.00	.8278	.8843	.8002	.7819	.8635	.8323
13.00	.8213	.8777	.7944	.7764	.8575	.8264
14.00	.8154	.8718	.7891	.7713	.8520	.8211
15.00	.8100	.8664	.7842	.7667	.8469	.8162
16.00	.8050	.8614	.7797	.7624	.8423	.8117
17.00	.8005	.8568	.7756	.7584	.8379	.8075
18.00	.7962	.8525	.7717	.7547	.8339	.8035
19.00	.7923	.8485	.7680	.7512	.8301	.7999
20.00	.7886	.8447	.7646	.7479	.8265	.7964
22.00	.7818	.8378	.7583	.7418	.8199	.7900
24.00	.7757	.8316	.7526	.7363	.8139	.7842
26.00	.7702	.8260	.7474	.7313	.8085	.7790
28.00	.7651	.8209	.7426	.7267	.8035	.7742
30.00	.7605	.8161	.7383	.7224	.7989	.7698
32.00	.7562	.8117	.7342	.7185	.7947	.7656
34.00	.7522	.8076	.7304	.7148	.7907	.7618
36.00	.7485	.8037	.7269	.7114	.7869	.7582
38.00	.7450	.8001	.7235	.7081	.7834	.7548
40.00	.7417	.7967	.7204	.7051	.7801	.7516
45.00	.7342	.7889	.7132	.6981	.7725	.7442
50.00	.7276	.7821	.7069	.6919	.7658	.7378
55.00	.7217	.7759	.7012	.6864	.7598	.7320
60.00	.7164	.7703	.6961	.6814	.7544	.7267
65.00	.7115	.7653	.6914	.6768	.7494	.7219
70.00	.7071	.7606	.6871	.6727	.7449	.7175
75.00	.7030	.7563	.6831	.6688	.7406	.7135
80.00	.6991	.7523	.6794	.6652	.7367	.7097
85.00	.6956	.7485	.6760	.6618	.7330	.7061
90.00	.6922	.7450	.6728	.6586	.7296	.7028
95.00	.6891	.7417	.6697	.6557	.7263	.6997
100.00	.6861	.7385	.6668	.6529	.7233	.6967
125.00	.6734	.7250	.6545	.6408	.7101	.6840
150.00	.6631	.7142	.6446	.6311	.6994	.6737
175.00	.6546	.7052	.6363	.6230	.6906	.6652
200.00	.6473	.6974	.6293	.6161	.6830	.6579

TABLE 9a. *Collision integrals for the (30, 6) potential function*

T^*	$\Omega^{(1,1)*}$	$\Omega^{(2,2)*}$	$\Omega^{(1,2)*}$	$\Omega^{(1,3)*}$	$\Omega^{(2,3)*}$	$\Omega^{(3,3)*}$
.10	3.0631	3.2201	2.7198	2.4914	2.9574	2.8871
.15	2.6728	2.8226	2.3733	2.1732	2.5946	2.5180
.20	2.4258	2.5735	2.1520	1.9666	2.3682	2.2819
.25	2.2482	2.3977	1.9904	1.8127	2.2075	2.1097
.30	2.1101	2.2624	1.8627	1.6901	2.0808	1.9750
.35	1.9973	2.1518	1.7574	1.5895	1.9744	1.8650
.40	1.9023	2.0567	1.6690	1.5066	1.8813	1.7740
.45	1.8215	1.9756	1.5943	1.4379	1.8012	1.6956
.50	1.7502	1.9010	1.5295	1.3799	1.7280	1.6286
.55	1.6879	1.8368	1.4736	1.3310	1.6650	1.5695
.60	1.6335	1.7763	1.4256	1.2897	1.6072	1.5185
.65	1.5839	1.7226	1.3829	1.2540	1.5562	1.4731
.70	1.5391	1.6742	1.3450	1.2228	1.5108	1.4318
.75	1.5006	1.6299	1.3128	1.1964	1.4703	1.3962
.80	1.4653	1.5885	1.2838	1.1731	1.4333	1.3643
.85	1.4325	1.5511	1.2575	1.1524	1.4002	1.3351
.90	1.4024	1.5175	1.2337	1.1340	1.3706	1.3084
.95	1.3752	1.4867	1.2125	1.1176	1.3439	1.2845
1.00	1.3510	1.4579	1.1936	1.1029	1.3195	1.2630
1.10	1.3082	1.4060	1.1609	1.0779	1.2767	1.2253
1.20	1.2707	1.3624	1.1331	1.0570	1.2412	1.1933
1.30	1.2383	1.3253	1.1096	1.0394	1.2113	1.1662
1.40	1.2103	1.2928	1.0895	1.0245	1.1858	1.1429
1.50	1.1864	1.2638	1.0722	1.0116	1.1636	1.1227
1.60	1.1653	1.2385	1.0572	1.0003	1.1444	1.1052
1.70	1.1462	1.2163	1.0439	.9904	1.1276	1.0897
1.80	1.1290	1.1968	1.0320	.9815	1.1129	1.0760
1.90	1.1135	1.1793	1.0213	.9736	1.0998	1.0638
2.00	1.0994	1.1634	1.0117	.9664	1.0881	1.0528
2.20	1.0753	1.1361	.9952	.9539	1.0680	1.0340
2.40	1.0555	1.1135	.9814	.9433	1.0515	1.0184
2.60	1.0386	1.0943	.9697	.9342	1.0375	1.0051
2.80	1.0238	1.0781	.9595	.9263	1.0256	.9938
3.00	1.0108	1.0642	.9506	.9193	1.0153	.9839
3.20	.9994	1.0520	.9427	.9130	1.0062	.9752
3.40	.9893	1.0413	.9357	.9073	.9982	.9675
3.60	.9803	1.0317	.9293	.9021	.9910	.9606
3.80	.9722	1.0232	.9235	.8973	.9845	.9544
4.00	.9648	1.0154	.9182	.8929	.9786	.9487
4.50	.9493	.9990	.9068	.8832	.9659	.9365
5.00	.9365	.9857	.8972	.8750	.9555	.9264
5.50	.9256	.9746	.8889	.8679	.9466	.9177
6.00	.9163	.9651	.8818	.8616	.9389	.9103
6.50	.9082	.9570	.8754	.8559	.9321	.9038
7.00	.9010	.9498	.8697	.8508	.9261	.8979
7.50	.8947	.9434	.8646	.8462	.9207	.8927
8.00	.8889	.9376	.8599	.8419	.9157	.8879
8.50	.8837	.9324	.8556	.8380	.9112	.8835
9.00	.8790	.9277	.8516	.8343	.9071	.8795
9.50	.8746	.9233	.8479	.8309	.9032	.8757

TABLE 9a. *Collision integrals for the (30, 6) potential function*—Continued

T^*	$\Omega^{(1,1)*}$	$\Omega^{(2,2)*}$	$\Omega^{(1,2)*}$	$\Omega^{(1,3)*}$	$\Omega^{(2,3)*}$	$\Omega^{(3,3)*}$
10.00	.8705	.9192	.8444	.8277	.8996	.8722
11.00	.8632	.9119	.8381	.8218	.8930	.8659
12.00	.8568	.9054	.8325	.8165	.8872	.8602
13.00	.8511	.8997	.8274	.8117	.8820	.8551
14.00	.8459	.8945	.8228	.8074	.8772	.8505
15.00	.8411	.8898	.8186	.8034	.8728	.8462
16.00	.8368	.8854	.8147	.7997	.8688	.8423
17.00	.8328	.8814	.8111	.7962	.8650	.8387
18.00	.8291	.8777	.8077	.7930	.8615	.8353
19.00	.8257	.8742	.8045	.7900	.8582	.8321
20.00	.8224	.8710	.8016	.7871	.8551	.8291
22.00	.8165	.8650	.7961	.7818	.8495	.8236
24.00	.8112	.8596	.7912	.7771	.8444	.8186
26.00	.8065	.8548	.7867	.7728	.8397	.8141
28.00	.8021	.8503	.7826	.7688	.8354	.8100
30.00	.7981	.8462	.7788	.7651	.8315	.8062
32.00	.7944	.8425	.7753	.7617	.8278	.8026
34.00	.7909	.8389	.7720	.7586	.8244	.7993
36.00	.7877	.8356	.7690	.7556	.8212	.7962
38.00	.7847	.8325	.7661	.7528	.8182	.7933
40.00	.7818	.8296	.7634	.7501	.8153	.7905
45.00	.7753	.8229	.7572	.7441	.8089	.7842
50.00	.7696	.8170	.7517	.7388	.8031	.7787
55.00	.7645	.8118	.7468	.7340	.7980	.7737
60.00	.7599	.8070	.7424	.7297	.7934	.7692
65.00	.7557	.8027	.7383	.7257	.7891	.7651
70.00	.7519	.7987	.7346	.7221	.7852	.7613
75.00	.7483	.7950	.7312	.7187	.7816	.7578
80.00	.7450	.7915	.7280	.7156	.7782	.7545
85.00	.7419	.7883	.7250	.7127	.7751	.7515
90.00	.7390	.7853	.7222	.7099	.7721	.7486
95.00	.7363	.7825	.7195	.7073	.7693	.7459
100.00	.7337	.7798	.7170	.7049	.7667	.7433
125.00	.7227	.7682	.7063	.6944	.7554	.7323
150.00	.7138	.7589	.6977	.6859	.7462	.7235
175.00	.7064	.7512	.6905	.6789	.7386	.7161
200.00	.7001	.7445	.6843	.6728	.7321	.7097

TABLE 10a. *Collision integrals for the (40, 6) potential function*

T^*	$\Omega^{(1,1)*}$	$\Omega^{(2,2)*}$	$\Omega^{(1,2)*}$	$\Omega^{(1,3)*}$	$\Omega^{(2,3)*}$	$\Omega^{(3,3)*}$
.10	2.9341	3.0924	2.6065	2.3889	2.8412	2.7668
.15	2.5621	2.7121	2.2769	2.0873	2.4937	2.4158
.20	2.3275	2.4734	2.0682	1.8944	2.2765	2.1931
.25	2.1596	2.3042	1.9172	1.7526	2.1218	2.0321
.30	2.0302	2.1749	1.7994	1.6412	2.0019	1.9071
.35	1.9257	2.0699	1.7038	1.5511	1.9026	1.8062
.40	1.8386	1.9821	1.6240	1.4767	1.8182	1.7220
.45	1.7633	1.9054	1.5553	1.4139	1.7438	1.6501
.50	1.6992	1.8376	1.4976	1.3620	1.6781	1.5888
.55	1.6420	1.7771	1.4468	1.3176	1.6197	1.5354
.60	1.5918	1.7231	1.4027	1.2797	1.5681	1.4878
.65	1.5478	1.6736	1.3648	1.2476	1.5216	1.4471
.70	1.5073	1.6286	1.3306	1.2193	1.4798	1.4098
.75	1.4708	1.5887	1.3003	1.1947	1.4431	1.3766
.80	1.4389	1.5518	1.2740	1.1735	1.4099	1.3474
.85	1.4099	1.5174	1.2505	1.1547	1.3796	1.3211
.90	1.3829	1.4857	1.2291	1.1379	1.3521	1.2970
.95	1.3580	1.4578	1.2097	1.1229	1.3278	1.2752
1.00	1.3353	1.4319	1.1922	1.1095	1.3056	1.2553
1.10	1.2959	1.3850	1.1620	1.0864	1.2665	1.2206
1.20	1.2626	1.3447	1.1371	1.0675	1.2338	1.1916
1.30	1.2332	1.3104	1.1156	1.0514	1.2062	1.1667
1.40	1.2075	1.2808	1.0972	1.0377	1.1827	1.1452
1.50	1.1851	1.2544	1.0812	1.0259	1.1622	1.1266
1.60	1.1658	1.2313	1.0675	1.0156	1.1445	1.1104
1.70	1.1487	1.2107	1.0554	1.0066	1.1289	1.0962
1.80	1.1333	1.1925	1.0446	.9986	1.1152	1.0836
1.90	1.1192	1.1763	1.0350	.9914	1.1031	1.0723
2.00	1.1063	1.1617	1.0262	.9849	1.0922	1.0621
2.20	1.0842	1.1366	1.0111	.9736	1.0737	1.0448
2.40	1.0658	1.1157	.9986	.9642	1.0584	1.0305
2.60	1.0505	1.0981	.9880	.9561	1.0456	1.0184
2.80	1.0373	1.0831	.9789	.9490	1.0347	1.0081
3.00	1.0255	1.0702	.9709	.9428	1.0253	.9991
3.20	1.0152	1.0590	.9638	.9373	1.0171	.9913
3.40	1.0061	1.0492	.9576	.9323	1.0098	.9843
3.60	.9980	1.0405	.9519	.9278	1.0033	.9782
3.80	.9906	1.0327	.9468	.9236	.9975	.9726
4.00	.9840	1.0256	.9421	.9198	.9922	.9675
4.50	.9699	1.0108	.9320	.9115	.9809	.9567
5.00	.9585	.9987	.9237	.9044	.9717	.9477
5.50	.9490	.9889	.9166	.8983	.9639	.9402
6.00	.9408	.9805	.9104	.8930	.9572	.9338
6.50	.9336	.9732	.9049	.8882	.9513	.9281
7.00	.9274	.9669	.9001	.8839	.9462	.9231
7.50	.9219	.9614	.8957	.8800	.9415	.9187
8.00	.9169	.9563	.8917	.8765	.9373	.9146
8.50	.9124	.9518	.8881	.8732	.9335	.9108
9.00	.9083	.9477	.8847	.8701	.9299	.9074
9.50	.9045	.9439	.8816	.8673	.9267	.9043

299-547 O-68—7

TABLE 10a. *Collision integrals for the (40, 6) potential function*—Continued

T^*	$\Omega^{(1,1)*}$	$\Omega^{(2,2)*}$	$\Omega^{(1,2)*}$	$\Omega^{(1,3)*}$	$\Omega^{(2,3)*}$	$\Omega^{(3,3)*}$
10.00	.9010	.9404	.8787	.8646	.9236	.9013
11.00	.8948	.9342	.8734	.8597	.9181	.8960
12.00	.8893	.9287	.8687	.8554	.9132	.8913
13.00	.8845	.9238	.8645	.8515	.9089	.8870
14.00	.8801	.9195	.8607	.8479	.9049	.8832
15.00	.8761	.9155	.8572	.8446	.9013	.8797
16.00	.8725	.9119	.8539	.8415	.8980	.8764
17.00	.8692	.9086	.8510	.8387	.8949	.8735
18.00	.8661	.9055	.8482	.8361	.8920	.8707
19.00	.8632	.9026	.8456	.8336	.8893	.8681
20.00	.8605	.8999	.8431	.8312	.8868	.8656
22.00	.8556	.8950	.8386	.8269	.8822	.8611
24.00	.8512	.8905	.8346	.8231	.8780	.8570
26.00	.8472	.8866	.8309	.8195	.8742	.8533
28.00	.8437	.8829	.8276	.8163	.8707	.8500
30.00	.8403	.8796	.8245	.8133	.8675	.8468
32.00	.8373	.8765	.8216	.8105	.8645	.8439
34.00	.8345	.8736	.8189	.8079	.8617	.8412
36.00	.8318	.8709	.8164	.8055	.8591	.8387
38.00	.8293	.8684	.8141	.8032	.8567	.8363
40.00	.8270	.8660	.8119	.8011	.8544	.8341
45.00	.8217	.8606	.8068	.7961	.8492	.8290
50.00	.8170	.8558	.8023	.7918	.8445	.8245
55.00	.8129	.8515	.7983	.7879	.8404	.8205
60.00	.8091	.8477	.7947	.7844	.8367	.8168
65.00	.8057	.8442	.7914	.7811	.8332	.8135
70.00	.8025	.8409	.7884	.7782	.8301	.8104
75.00	.7996	.8380	.7856	.7754	.8271	.8075
80.00	.7969	.8352	.7830	.7729	.8244	.8049
85.00	.7944	.8326	.7805	.7705	.8219	.8024
90.00	.7920	.8301	.7782	.7682	.8195	.8001
95.00	.7898	.8278	.7761	.7661	.8172	.7979
100.00	.7877	.8257	.7740	.7641	.8151	.7958
125.00	.7786	.8163	.7653	.7555	.8059	.7868
150.00	.7714	.8088	.7582	.7485	.7986	.7797
175.00	.7653	.8025	.7523	.7427	.7924	.7736
200.00	.7601	.7971	.7472	.7377	.7871	.7685

TABLE 11a. *Collision integrals for the (50, 6) potential function*

T^*	$\Omega^{(1,1)*}$	$\Omega^{(2,2)*}$	$\Omega^{(1,2)*}$	$\Omega^{(1,3)*}$	$\Omega^{(2,3)*}$	$\Omega^{(3,3)*}$
.10	2.8571	3.0144	2.5391	2.3282	2.7703	2.6945
.15	2.4963	2.6452	2.2201	2.0367	2.4332	2.3553
.20	2.2693	2.4133	2.0188	1.8516	2.2219	2.1408
.25	2.1075	2.2490	1.8743	1.7173	2.0719	1.9864
.30	1.9834	2.1234	1.7624	1.6124	1.9558	1.8671
.35	1.8834	2.0221	1.6718	1.5277	1.8606	1.7707
.40	1.8000	1.9372	1.5961	1.4576	1.7799	1.6904
.45	1.7293	1.8633	1.5323	1.3995	1.7089	1.6231
.50	1.6680	1.7991	1.4774	1.3503	1.6471	1.5641
.55	1.6146	1.7414	1.4304	1.3091	1.5920	1.5143
.60	1.5667	1.6901	1.3886	1.2733	1.5432	1.4691
.65	1.5252	1.6437	1.3530	1.2432	1.4999	1.4304
.70	1.4877	1.6009	1.3214	1.2169	1.4605	1.3959
.75	1.4535	1.5628	1.2930	1.1939	1.4257	1.3648
.80	1.4226	1.5285	1.2679	1.1737	1.3947	1.3370
.85	1.3955	1.4964	1.2459	1.1561	1.3665	1.3122
.90	1.3705	1.4665	1.2259	1.1404	1.3406	1.2897
.95	1.3474	1.4396	1.2079	1.1264	1.3176	1.2694
1.00	1.3261	1.4153	1.1915	1.1139	1.2968	1.2508
1.10	1.2885	1.3718	1.1630	1.0922	1.2604	1.2183
1.20	1.2573	1.3340	1.1396	1.0745	1.2297	1.1911
1.30	1.2301	1.3014	1.1197	1.0596	1.2037	1.1679
1.40	1.2060	1.2736	1.1024	1.0468	1.1817	1.1479
1.50	1.1849	1.2490	1.0875	1.0357	1.1624	1.1303
1.60	1.1665	1.2274	1.0746	1.0262	1.1458	1.1151
1.70	1.1505	1.2080	1.0632	1.0177	1.1310	1.1017
1.80	1.1362	1.1909	1.0532	1.0103	1.1181	1.0899
1.90	1.1231	1.1755	1.0443	1.0036	1.1066	1.0793
2.00	1.1112	1.1617	1.0361	.9976	1.0962	1.0696
2.20	1.0904	1.1380	1.0220	.9871	1.0786	1.0532
2.40	1.0732	1.1184	1.0104	.9783	1.0642	1.0397
2.60	1.0587	1.1016	1.0005	.9708	1.0519	1.0281
2.80	1.0464	1.0874	.9920	.9643	1.0415	1.0183
3.00	1.0356	1.0753	.9847	.9586	1.0327	1.0100
3.20	1.0260	1.0646	.9781	.9536	1.0249	1.0025
3.40	1.0174	1.0552	.9723	.9490	1.0179	.9959
3.60	1.0099	1.0470	.9671	.9449	1.0119	.9901
3.80	1.0031	1.0398	.9624	.9412	1.0065	.9850
4.00	.9970	1.0331	.9582	.9377	1.0016	.9803
4.50	.9839	1.0190	.9489	.9302	.9910	.9701
5.00	.9734	1.0079	.9413	.9239	.9825	.9620
5.50	.9646	.9984	.9349	.9185	.9753	.9551
6.00	.9572	.9908	.9294	.9138	.9693	.9493
6.50	.9506	.9841	.9245	.9096	.9640	.9442
7.00	.9449	.9782	.9201	.9058	.9592	.9397
7.50	.9399	.9732	.9163	.9024	.9552	.9357
8.00	.9354	.9687	.9128	.8993	.9514	.9321
8.50	.9314	.9645	.9095	.8964	.9480	.9288
9.00	.9277	.9608	.9066	.8938	.9448	.9258
9.50	.9243	.9574	.9038	.8913	.9420	.9230

TABLE 11a. *Collision integrals for the (50, 6) potential function*—Continued

T^*	$\Omega^{(1,1)*}$	$\Omega^{(2,2)*}$	$\Omega^{(1,2)*}$	$\Omega^{(1,3)*}$	$\Omega^{(2,3)*}$	$\Omega^{(3,3)*}$
10.00	.9212	.9544	.9013	.8890	.9393	.9204
11.00	.9156	.9487	.8967	.8848	.9344	.9157
12.00	.9108	.9439	.8926	.8811	.9302	.9116
13.00	.9065	.9396	.8890	.8777	.9264	.9079
14.00	.9027	.9357	.8857	.8746	.9230	.9046
15.00	.8992	.9323	.8827	.8718	.9198	.9016
16.00	.8961	.9291	.8799	.8692	.9170	.8988
17.00	.8932	.9262	.8773	.8668	.9143	.8963
18.00	.8905	.9235	.8749	.8645	.9119	.8939
19.00	.8880	.9210	.8727	.8624	.9096	.8917
20.00	.8856	.9187	.8706	.8604	.9074	.8896
22.00	.8814	.9145	.8668	.8568	.9035	.8857
24.00	.8776	.9107	.8633	.8535	.9000	.8823
26.00	.8742	.9073	.8602	.8505	.8967	.8791
28.00	.8711	.9042	.8574	.8478	.8938	.8763
30.00	.8683	.9013	.8547	.8452	.8911	.8736
32.00	.8657	.8987	.8523	.8429	.8885	.8712
34.00	.8633	.8963	.8500	.8407	.8862	.8689
36.00	.8610	.8940	.8479	.8386	.8840	.8668
38.00	.8589	.8918	.8459	.8367	.8819	.8648
40.00	.8569	.8898	.8440	.8349	.8800	.8629
45.00	.8524	.8852	.8397	.8307	.8756	.8586
50.00	.8484	.8812	.8360	.8270	.8717	.8548
55.00	.8449	.8776	.8326	.8237	.8682	.8514
60.00	.8417	.8744	.8295	.8208	.8651	.8483
65.00	.8388	.8714	.8267	.8180	.8622	.8455
70.00	.8361	.8687	.8242	.8155	.8595	.8429
75.00	.8337	.8662	.8218	.8132	.8570	.8404
80.00	.8314	.8638	.8196	.8110	.8547	.8382
85.00	.8292	.8616	.8175	.8090	.8526	.8361
90.00	.8272	.8596	.8156	.8071	.8506	.8341
95.00	.8253	.8576	.8137	.8053	.8486	.8322
100.00	.8236	.8558	.8120	.8036	.8468	.8305
125.00	.8159	.8479	.8046	.7963	.8391	.8228
150.00	.8097	.8415	.7985	.7904	.8328	.8167
175.00	.8046	.8362	.7935	.7854	.8277	.8117
200.00	.8002	.8317	.7892	.7812	.8233	.8074

TABLE 12a. *Collision integrals for the (75, 6) potential function*

T*	$\Omega^{(1,1)*}$	$\Omega^{(2,2)*}$	$\Omega^{(1,2)*}$	$\Omega^{(1,3)*}$	$\Omega^{(2,3)*}$	$\Omega^{(3,3)*}$
.10	2.7535	2.9095	2.4490	2.2473	2.6750	2.5985
.15	2.4083	2.5547	2.1443	1.9695	2.3511	2.2740
.20	2.1916	2.3320	1.9529	1.7946	2.1482	2.0700
.25	2.0378	2.1743	1.8166	1.6691	2.0042	1.9242
.30	1.9204	2.0538	1.7120	1.5725	1.8934	1.8121
.35	1.8263	1.9572	1.6279	1.4948	1.8035	1.7221
.40	1.7485	1.8762	1.5585	1.4314	1.7272	1.6477
.45	1.6828	1.8068	1.5001	1.3786	1.6615	1.5847
.50	1.6259	1.7463	1.4499	1.3340	1.6040	1.5308
.55	1.5766	1.6928	1.4069	1.2965	1.5537	1.4843
.60	1.5331	1.6444	1.3694	1.2644	1.5083	1.4434
.65	1.4942	1.6021	1.3364	1.2367	1.4689	1.4074
.70	1.4600	1.5626	1.3077	1.2128	1.4327	1.3753
.75	1.4292	1.5270	1.2824	1.1921	1.4008	1.3473
.80	1.4011	1.4952	1.2596	1.1739	1.3723	1.3220
.85	1.3755	1.4659	1.2390	1.1576	1.3464	1.2988
.90	1.3526	1.4391	1.2209	1.1434	1.3233	1.2784
.95	1.3320	1.4142	1.2048	1.1309	1.3021	1.2600
1.00	1.3129	1.3915	1.1901	1.1196	1.2830	1.2433
1.10	1.2786	1.3515	1.1642	1.1000	1.2498	1.2135
1.20	1.2496	1.3175	1.1427	1.0840	1.2221	1.1889
1.30	1.2251	1.2878	1.1249	1.0706	1.1986	1.1680
1.40	1.2035	1.2618	1.1094	1.0592	1.1782	1.1498
1.50	1.1845	1.2397	1.0960	1.0494	1.1610	1.1342
1.60	1.1677	1.2202	1.0844	1.0409	1.1459	1.1204
1.70	1.1529	1.2027	1.0741	1.0334	1.1326	1.1083
1.80	1.1397	1.1868	1.0650	1.0267	1.1206	1.0973
1.90	1.1282	1.1728	1.0571	1.0208	1.1100	1.0877
2.00	1.1176	1.1603	1.0499	1.0154	1.1006	1.0791
2.20	1.0990	1.1386	1.0374	1.0062	1.0844	1.0639
2.40	1.0834	1.1206	1.0269	.9984	1.0709	1.0513
2.60	1.0704	1.1055	1.0182	.9918	1.0597	1.0409
2.80	1.0591	1.0923	1.0106	.9861	1.0500	1.0317
3.00	1.0496	1.0809	1.0041	.9811	1.0417	1.0239
3.20	1.0412	1.0714	.9984	.9768	1.0347	1.0174
3.40	1.0336	1.0627	.9933	.9728	1.0284	1.0114
3.60	1.0267	1.0549	.9887	.9693	1.0227	1.0060
3.80	1.0207	1.0482	.9846	.9661	1.0178	1.0014
4.00	1.0153	1.0423	.9810	.9633	1.0136	.9974
4.50	1.0037	1.0295	.9730	.9571	1.0043	.9886
5.00	.9945	1.0195	.9666	.9519	.9971	.9817
5.50	.9869	1.0114	.9612	.9476	.9911	.9760
6.00	.9805	1.0046	.9566	.9438	.9860	.9711
6.50	.9750	.9989	.9527	.9405	.9817	.9670
7.00	.9701	.9940	.9491	.9375	.9778	.9634
7.50	.9659	.9896	.9460	.9349	.9744	.9601
8.00	.9621	.9858	.9432	.9324	.9714	.9572
8.50	.9587	.9824	.9406	.9302	.9686	.9546
9.00	.9557	.9793	.9383	.9282	.9661	.9521
9.50	.9529	.9765	.9361	.9263	.9637	.9499

TABLE 12a. *Collision integrals for the (75, 6) potential function*—Continued

T^*	$\Omega^{(1,1)*}$	$\Omega^{(2,2)*}$	$\Omega^{(1,2)*}$	$\Omega^{(1,3)*}$	$\Omega^{(2,3)*}$	$\Omega^{(3,3)*}$
10.00	.9504	.9739	.9341	.9245	.9616	.9478
11.00	.9459	.9694	.9305	.9213	.9578	.9442
12.00	.9420	.9654	.9274	.9184	.9545	.9410
13.00	.9385	.9621	.9246	.9159	.9516	.9382
14.00	.9355	.9590	.9220	.9136	.9490	.9357
15.00	.9327	.9562	.9197	.9115	.9466	.9334
16.00	.9303	.9538	.9176	.9096	.9444	.9313
17.00	.9280	.9516	.9157	.9078	.9425	.9294
18.00	.9259	.9495	.9139	.9061	.9406	.9276
19.00	.9240	.9476	.9122	.9045	.9388	.9259
20.00	.9222	.9459	.9107	.9031	.9372	.9244
22.00	.9190	.9426	.9078	.9004	.9343	.9215
24.00	.9161	.9397	.9052	.8979	.9315	.9188
26.00	.9135	.9371	.9029	.8957	.9291	.9165
28.00	.9112	.9348	.9008	.8937	.9269	.9143
30.00	.9091	.9327	.8989	.8918	.9249	.9124
32.00	.9071	.9307	.8970	.8901	.9230	.9105
34.00	.9053	.9288	.8954	.8885	.9213	.9088
36.00	.9036	.9271	.8938	.8870	.9197	.9073
38.00	.9020	.9256	.8924	.8856	.9183	.9059
40.00	.9005	.9241	.8910	.8843	.9169	.9045
45.00	.8972	.9207	.8879	.8813	.9137	.9015
50.00	.8943	.9178	.8851	.8787	.9111	.8989
55.00	.8917	.9153	.8827	.8763	.9086	.8965
60.00	.8894	.9130	.8805	.8742	.9065	.8944
65.00	.8872	.9109	.8785	.8722	.9045	.8925
70.00	.8853	.9090	.8766	.8705	.9027	.8907
75.00	.8835	.9073	.8749	.8688	.9010	.8891
80.00	.8819	.9057	.8734	.8673	.8994	.8876
85.00	.8803	.9042	.8719	.8658	.8980	.8861
90.00	.8789	.9028	.8705	.8645	.8966	.8848
95.00	.8775	.9014	.8692	.8631	.8952	.8834
100.00	.8762	.9001	.8680	.8619	.8939	.8822
125.00	.8707	.8945	.8626	.8566	.8882	.8766
150.00	.8663	.8900	.8582	.8523	.8837	.8721
175.00	.8626	.8862	.8546	.8487	.8799	.8684
200.00	.8594	.8827	.8514	.8455	.8765	.8650

TABLE 3b. *Ratios of collision integrals for the (9, 6) potential function*

T*	A*	B*	C*	E*	F*
.10	.9976	1.2106	.8794	.9129	.9206
.15	1.0093	1.2430	.8706	.9154	.9101
.20	1.0303	1.2836	.8571	.9141	.8978
.25	1.0523	1.3132	.8422	.9062	.8881
.30	1.0714	1.3276	.8289	.8954	.8830
.35	1.0836	1.3324	.8178	.8848	.8780
.40	1.0985	1.3272	.8098	.8741	.8774
.45	1.1036	1.3200	.8035	.8663	.8748
.50	1.1088	1.3086	.8001	.8605	.8762
.55	1.1158	1.2958	.7984	.8550	.8777
.60	1.1159	1.2838	.7970	.8519	.8770
.65	1.1152	1.2718	.7972	.8507	.8787
.70	1.1161	1.2600	.7987	.8499	.8810
.75	1.1177	1.2486	.8010	.8497	.8838
.80	1.1189	1.2380	.8035	.8498	.8864
.85	1.1176	1.2281	.8057	.8508	.8881
.90	1.1148	1.2191	.8080	.8527	.8893
.95	1.1129	1.2109	.8109	.8549	.8915
1.00	1.1120	1.2033	.8142	.8571	.8943
1.10	1.1117	1.1899	.8212	.8616	.9001
1.20	1.1110	1.1787	.8282	.8665	.9055
1.30	1.1100	1.1690	.8346	.8713	.9105
1.40	1.1076	1.1605	.8400	.8764	.9143
1.50	1.1057	1.1533	.8453	.8814	.9183
1.60	1.1047	1.1474	.8507	.8861	.9225
1.70	1.1043	1.1425	.8558	.8905	.9267
1.80	1.1042	1.1384	.8607	.8945	.9308
1.90	1.1044	1.1348	.8653	.8982	.9346
2.00	1.1047	1.1317	.8696	.9017	.9383
2.20	1.1052	1.1266	.8771	.9080	.9450
2.40	1.1055	1.1226	.8834	.9135	.9505
2.60	1.1054	1.1193	.8885	.9183	.9550
2.80	1.1057	1.1168	.8930	.9225	.9591
3.00	1.1065	1.1150	.8971	.9260	.9630
3.20	1.1074	1.1137	.9008	.9290	.9665
3.40	1.1085	1.1127	.9041	.9316	.9698
3.60	1.1095	1.1120	.9070	.9339	.9727
3.80	1.1104	1.1114	.9096	.9359	.9753
4.00	1.1114	1.1110	.9119	.9377	.9776
4.50	1.1135	1.1103	.9166	.9413	.9826
5.00	1.1155	1.1099	.9201	.9441	.9865
5.50	1.1173	1.1097	.9229	.9462	.9898
6.00	1.1189	1.1095	.9251	.9479	.9925
6.50	1.1203	1.1094	.9267	.9494	.9948
7.00	1.1216	1.1093	.9282	.9505	.9968
7.50	1.1229	1.1094	.9293	.9515	.9987
8.00	1.1242	1.1094	.9304	.9523	1.0003
8.50	1.1254	1.1095	.9313	.9529	1.0018
9.00	1.1266	1.1096	.9320	.9535	1.0033
9.50	1.1277	1.1098	.9327	.9540	1.0045

TABLE 3b. *Ratios of collision integrals for the (9, 6) potential function*—Continued

T*	A*	B*	C*	E*	F*
10.00	1.1287	1.1099	.9332	.9544	1.0057
11.00	1.1306	1.1102	.9341	.9550	1.0077
12.00	1.1324	1.1106	.9348	.9554	1.0094
13.00	1.1340	1.1110	.9354	.9557	1.0108
14.00	1.1354	1.1113	.9358	.9560	1.0121
15.00	1.1367	1.1117	.9361	.9561	1.0131
16.00	1.1379	1.1121	.9363	.9561	1.0141
17.00	1.1389	1.1124	.9365	.9562	1.0149
18.00	1.1399	1.1127	.9366	.9562	1.0156
19.00	1.1408	1.1130	.9367	.9562	1.0162
20.00	1.1417	1.1133	.9368	.9561	1.0168
22.00	1.1432	1.1139	.9369	.9560	1.0177
24.00	1.1445	1.1144	.9369	.9559	1.0185
26.00	1.1456	1.1149	.9369	.9557	1.0192
28.00	1.1466	1.1153	.9368	.9555	1.0197
30.00	1.1475	1.1157	.9367	.9554	1.0202
32.00	1.1484	1.1160	.9367	.9552	1.0206
34.00	1.1491	1.1164	.9366	.9550	1.0209
36.00	1.1498	1.1167	.9365	.9549	1.0212
38.00	1.1504	1.1169	.9364	.9547	1.0215
40.00	1.1510	1.1172	.9363	.9546	1.0218
45.00	1.1522	1.1178	.9360	.9543	1.0223
50.00	1.1533	1.1183	.9358	.9540	1.0227
55.00	1.1542	1.1187	.9356	.9537	1.0231
60.00	1.1550	1.1191	.9354	.9535	1.0234
65.00	1.1557	1.1194	.9352	.9533	1.0236
70.00	1.1563	1.1197	.9350	.9531	1.0238
75.00	1.1569	1.1200	.9349	.9529	1.0240
80.00	1.1574	1.1202	.9347	.9527	1.0242
85.00	1.1579	1.1205	.9346	.9526	1.0243
90.00	1.1583	1.1207	.9344	.9524	1.0244
95.00	1.1587	1.1209	.9343	.9523	1.0246
100.00	1.1591	1.1211	.9342	.9521	1.0247
125.00	1.1606	1.1219	.9337	.9516	1.0251
150.00	1.1617	1.1224	.9332	.9512	1.0254
175.00	1.1626	1.1229	.9329	.9509	1.0257
200.00	1.1633	1.1233	.9326	.9506	1.0258

TABLE 4b. *Ratios of collision integrals for the (12, 6) potential function*

T*	A*	B*	C*	E*	F*
.10	1.0227	1.1962	.8856	.9168	.9350
.15	1.0300	1.2153	.8809	.9180	.9279
.20	1.0433	1.2455	.8725	.9184	.9189
.25	1.0579	1.2727	.8621	.9144	.9105
.30	1.0735	1.2899	.8516	.9072	.9046
.35	1.0843	1.2976	.8426	.8990	.9009
.40	1.0930	1.2988	.8352	.8910	.8973
.45	1.0999	1.2938	.8300	.8841	.8967
.50	1.1067	1.2858	.8263	.8777	.8959
.55	1.1064	1.2773	.8238	.8740	.8950
.60	1.1091	1.2666	.8230	.8708	.8963
.65	1.1121	1.2555	.8232	.8681	.8975
.70	1.1117	1.2452	.8236	.8669	.8981
.75	1.1091	1.2355	.8245	.8671	.8987
.80	1.1081	1.2257	.8263	.8675	.9006
.85	1.1083	1.2166	.8287	.8680	.9027
.90	1.1085	1.2080	.8314	.8689	.9050
.95	1.1082	1.1999	.8341	.8701	.9071
1.00	1.1069	1.1923	.8366	.8718	.9090
1.10	1.1023	1.1792	.8414	.8762	.9118
1.20	1.1002	1.1680	.8471	.8805	.9161
1.30	1.0994	1.1585	.8530	.8848	.9206
1.40	1.0986	1.1502	.8587	.8890	.9250
1.50	1.0975	1.1432	.8639	.8932	.9289
1.60	1.0962	1.1370	.8685	.8973	.9324
1.70	1.0944	1.1316	.8726	.9014	.9353
1.80	1.0931	1.1269	.8766	.9052	.9384
1.90	1.0926	1.1230	.8806	.9088	.9416
2.00	1.0923	1.1197	.8843	.9120	.9447
2.20	1.0923	1.1143	.8912	.9177	.9504
2.40	1.0926	1.1101	.8972	.9227	.9556
2.60	1.0929	1.1067	.9023	.9271	.9602
2.80	1.0933	1.1040	.9067	.9310	.9643
3.00	1.0934	1.1017	.9103	.9343	.9676
3.20	1.0935	1.0999	.9134	.9373	.9705
3.40	1.0939	1.0984	.9163	.9398	.9733
3.60	1.0945	1.0973	.9189	.9421	.9759
3.80	1.0953	1.0964	.9213	.9440	.9784
4.00	1.0961	1.0957	.9235	.9458	.9806
4.50	1.0979	1.0944	.9280	.9493	.9855
5.00	1.0996	1.0936	.9314	.9520	.9893
5.50	1.1012	1.0930	.9341	.9541	.9925
6.00	1.1026	1.0927	.9362	.9558	.9952
6.50	1.1039	1.0925	.9379	.9571	.9974
7.00	1.1050	1.0923	.9393	.9581	.9993
7.50	1.1061	1.0922	.9405	.9590	1.0009
8.00	1.1071	1.0922	.9414	.9597	1.0023
8.50	1.1080	1.0922	.9422	.9602	1.0035
9.00	1.1088	1.0923	.9429	.9607	1.0046
9.50	1.1097	1.0923	.9436	.9611	1.0056

TABLE 4b. *Ratios of collision integrals for the (12, 6) potential function*—Continued

T*	A*	B*	C*	E*	F*
10.00	1.1105	1.0924	.9441	.9614	1.0065
11.00	1.1119	1.0926	.9450	.9620	1.0081
12.00	1.1131	1.0928	.9457	.9624	1.0094
13.00	1.1142	1.0930	.9462	.9626	1.0104
14.00	1.1152	1.0932	.9466	.9628	1.0114
15.00	1.1161	1.0934	.9469	.9630	1.0122
16.00	1.1169	1.0935	.9472	.9631	1.0129
17.00	1.1176	1.0937	.9474	.9632	1.0135
18.00	1.1183	1.0938	.9476	.9633	1.0141
19.00	1.1190	1.0939	.9477	.9633	1.0146
20.00	1.1195	1.0941	.9479	.9634	1.0151
22.00	1.1206	1.0943	.9480	.9634	1.0159
24.00	1.1215	1.0945	.9482	.9634	1.0166
26.00	1.1223	1.0947	.9482	.9634	1.0171
28.00	1.1231	1.0949	.9483	.9634	1.0176
30.00	1.1237	1.0951	.9483	.9633	1.0181
32.00	1.1244	1.0952	.9483	.9633	1.0185
34.00	1.1249	1.0954	.9483	.9632	1.0188
36.00	1.1254	1.0955	.9483	.9632	1.0191
38.00	1.1259	1.0957	.9483	.9631	1.0194
40.00	1.1263	1.0958	.9483	.9631	1.0197
45.00	1.1272	1.0961	.9483	.9629	1.0202
50.00	1.1281	1.0963	.9482	.9628	1.0206
55.00	1.1287	1.0966	.9481	.9626	1.0210
60.00	1.1293	1.0968	.9480	.9625	1.0213
65.00	1.1299	1.0970	.9480	.9624	1.0215
70.00	1.1303	1.0971	.9479	.9623	1.0217
75.00	1.1307	1.0973	.9478	.9622	1.0219
80.00	1.1311	1.0974	.9478	.9621	1.0221
85.00	1.1315	1.0975	.9477	.9620	1.0223
90.00	1.1318	1.0976	.9476	.9619	1.0224
95.00	1.1320	1.0977	.9476	.9618	1.0225
100.00	1.1323	1.0978	.9475	.9617	1.0226
125.00	1.1334	1.0982	.9473	.9614	1.0231
150.00	1.1341	1.0985	.9471	.9612	1.0234
175.00	1.1347	1.0988	.9469	.9610	1.0236
200.00	1.1352	1.0990	.9468	.9608	1.0238

TABLE 5b. *Ratios of collision integrals for the (15, 6) potential function*

T*	A*	B*	C*	E*	F*
.10	1.0348	1.1909	.8872	.9180	.9407
.15	1.0413	1.2026	.8845	.9191	.9368
.20	1.0505	1.2241	.8793	.9197	.9304
.25	1.0623	1.2468	.8718	.9176	.9237
.30	1.0731	1.2636	.8639	.9128	.9181
.35	1.0833	1.2730	.8565	.9065	.9133
.40	1.0918	1.2750	.8504	.8998	.9112
.45	1.0963	1.2734	.8456	.8940	.9085
.50	1.1003	1.2674	.8424	.8890	.9083
.55	1.1046	1.2595	.8403	.8844	.9074
.60	1.1037	1.2513	.8390	.8820	.9071
.65	1.1038	1.2420	.8390	.8801	.9078
.70	1.1057	1.2321	.8398	.8785	.9091
.75	1.1060	1.2227	.8408	.8777	.9101
.80	1.1038	1.2139	.8421	.8780	.9106
.85	1.1012	1.2056	.8436	.8790	.9117
.90	1.1003	1.1975	.8459	.8800	.9135
.95	1.1000	1.1899	.8484	.8810	.9155
1.00	1.0994	1.1826	.8510	.8823	.9173
1.10	1.0976	1.1697	.8561	.8855	.9209
1.20	1.0938	1.1587	.8607	.8897	.9238
1.30	1.0909	1.1493	.8656	.8940	.9271
1.40	1.0898	1.1412	.8707	.8979	.9309
1.50	1.0890	1.1343	.8757	.9016	.9346
1.60	1.0881	1.1282	.8803	.9053	.9381
1.70	1.0871	1.1229	.8845	.9089	.9413
1.80	1.0858	1.1182	.8882	.9124	.9440
1.90	1.0844	1.1141	.8916	.9158	.9465
2.00	1.0833	1.1106	.8948	.9189	.9489
2.20	1.0826	1.1048	.9010	.9244	.9540
2.40	1.0824	1.1004	.9066	.9291	.9586
2.60	1.0825	1.0970	.9115	.9332	.9629
2.80	1.0827	1.0941	.9157	.9368	.9666
3.00	1.0829	1.0918	.9193	.9399	.9699
3.20	1.0831	1.0899	.9224	.9427	.9728
3.40	1.0831	1.0882	.9251	.9452	.9753
3.60	1.0833	1.0868	.9274	.9474	.9775
3.80	1.0836	1.0857	.9295	.9493	.9796
4.00	1.0840	1.0848	.9315	.9509	.9816
4.50	1.0854	1.0832	.9358	.9544	.9860
5.00	1.0867	1.0821	.9391	.9570	.9896
5.50	1.0879	1.0814	.9417	.9590	.9925
6.00	1.0890	1.0808	.9438	.9606	.9949
6.50	1.0900	1.0805	.9455	.9619	.9969
7.00	1.0909	1.0802	.9469	.9629	.9987
7.50	1.0917	1.0800	.9480	.9638	1.0002
8.00	1.0925	1.0798	.9490	.9645	1.0014
8.50	1.0932	1.0796	.9498	.9651	1.0025
9.00	1.0938	1.0795	.9505	.9656	1.0035
9.50	1.0944	1.0795	.9511	.9660	1.0044

TABLE 5b. *Ratios of collision integrals for the (15, 6) potential function*—Continued

T*	A*	B*	C*	E*	F*
10.00	1.0950	1.0794	.9516	.9664	1.0052
11.00	1.0961	1.0794	.9525	.9670	1.0067
12.00	1.0971	1.0793	.9533	.9675	1.0079
13.00	1.0980	1.0793	.9539	.9678	1.0089
14.00	1.0988	1.0793	.9543	.9681	1.0098
15.00	1.0995	1.0794	.9547	.9684	1.0106
16.00	1.1002	1.0794	.9550	.9685	1.0113
17.00	1.1008	1.0794	.9553	.9687	1.0120
18.00	1.1014	1.0794	.9555	.9688	1.0125
19.00	1.1019	1.0795	.9557	.9689	1.0130
20.00	1.1024	1.0795	.9559	.9690	1.0135
22.00	1.1033	1.0796	.9561	.9691	1.0143
24.00	1.1040	1.0797	.9563	.9692	1.0149
26.00	1.1047	1.0798	.9565	.9692	1.0155
28.00	1.1053	1.0799	.9566	.9692	1.0160
30.00	1.1058	1.0799	.9567	.9692	1.0164
32.00	1.1063	1.0800	.9567	.9692	1.0168
34.00	1.1068	1.0801	.9568	.9692	1.0171
36.00	1.1072	1.0802	.9568	.9692	1.0174
38.00	1.1075	1.0803	.9569	.9691	1.0176
40.00	1.1079	1.0803	.9569	.9691	1.0178
45.00	1.1086	1.0805	.9569	.9690	1.0183
50.00	1.1092	1.0806	.9569	.9689	1.0187
55.00	1.1097	1.0807	.9569	.9689	1.0190
60.00	1.1102	1.0808	.9569	.9688	1.0193
65.00	1.1106	1.0809	.9569	.9687	1.0195
70.00	1.1109	1.0810	.9569	.9687	1.0197
75.00	1.1112	1.0811	.9569	.9686	1.0199
80.00	1.1115	1.0811	.9568	.9685	1.0201
85.00	1.1117	1.0812	.9568	.9685	1.0202
90.00	1.1120	1.0813	.9568	.9685	1.0203
95.00	1.1122	1.0813	.9568	.9684	1.0204
100.00	1.1124	1.0814	.9567	.9684	1.0205
125.00	1.1131	1.0815	.9567	.9682	1.0209
150.00	1.1137	1.0817	.9566	.9681	1.0212
175.00	1.1141	1.0818	.9565	.9679	1.0214
200.00	1.1144	1.0819	.9565	.9679	1.0216

TABLE 6b. *Ratios of collision integrals for the (18, 6) potential function*

T*	A*	B*	C*	E*	F*
.10	1.0412	1.1886	.8875	.9182	.9421
.15	1.0472	1.1960	.8861	.9194	.9401
.20	1.0553	1.2119	.8826	.9204	.9355
.25	1.0645	1.2305	.8772	.9193	.9301
.30	1.0743	1.2455	.8710	.9158	.9250
.35	1.0828	1.2544	.8650	.9108	.9216
.40	1.0877	1.2580	.8600	.9056	.9192
.45	1.0947	1.2564	.8559	.9001	.9170
.50	1.0958	1.2527	.8530	.8961	.9156
.55	1.0992	1.2457	.8513	.8923	.9158
.60	1.1014	1.2378	.8504	.8892	.9152
.65	1.0997	1.2300	.8500	.8878	.9151
.70	1.0992	1.2214	.8506	.8868	.9160
.75	1.0999	1.2123	.8519	.8860	.9172
.80	1.0999	1.2037	.8533	.8857	.9183
.85	1.0982	1.1958	.8548	.8862	.9191
.90	1.0955	1.1884	.8565	.8874	.9200
.95	1.0937	1.1812	.8586	.8887	.9214
1.00	1.0929	1.1743	.8610	.8900	.9232
1.10	1.0917	1.1618	.8661	.8928	.9267
1.20	1.0894	1.1511	.8708	.8962	.9298
1.30	1.0860	1.1417	.8752	.9003	.9325
1.40	1.0833	1.1339	.8796	.9042	.9354
1.50	1.0821	1.1270	.8842	.9078	.9386
1.60	1.0812	1.1210	.8886	.9112	.9419
1.70	1.0804	1.1158	.8927	.9145	.9450
1.80	1.0794	1.1112	.8965	.9178	.9478
1.90	1.0783	1.1071	.8998	.9208	.9503
2.00	1.0771	1.1035	.9029	.9238	.9525
2.20	1.0753	1.0975	.9084	.9291	.9566
2.40	1.0746	1.0930	.9136	.9337	.9608
2.60	1.0744	1.0894	.9182	.9376	.9647
2.80	1.0744	1.0865	.9222	.9410	.9681
3.00	1.0745	1.0841	.9257	.9440	.9713
3.20	1.0746	1.0821	.9288	.9467	.9740
3.40	1.0747	1.0804	.9315	.9491	.9765
3.60	1.0747	1.0789	.9337	.9512	.9786
3.80	1.0747	1.0776	.9358	.9530	.9804
4.00	1.0749	1.0766	.9376	.9547	.9822
4.50	1.0757	1.0746	.9416	.9581	.9862
5.00	1.0767	1.0733	.9448	.9607	.9896
5.50	1.0777	1.0724	.9474	.9627	.9924
6.00	1.0786	1.0717	.9494	.9643	.9947
6.50	1.0794	1.0712	.9511	.9656	.9967
7.00	1.0801	1.0707	.9525	.9667	.9983
7.50	1.0808	1.0704	.9536	.9675	.9998
8.00	1.0815	1.0702	.9546	.9683	1.0010
8.50	1.0821	1.0699	.9555	.9689	1.0021
9.00	1.0826	1.0697	.9562	.9694	1.0031
9.50	1.0831	1.0696	.9568	.9699	1.0039

TABLE 6b. *Ratios of collision integrals for the (18, 6) potential function*—Continued

T*	A*	B*	C*	E*	F*
10.00	1.0836	1.0695	.9573	.9702	1.0047
11.00	1.0845	1.0693	.9582	.9709	1.0060
12.00	1.0853	1.0692	.9590	.9713	1.0072
13.00	1.0861	1.0691	.9596	.9717	1.0081
14.00	1.0867	1.0691	.9600	.9720	1.0089
15.00	1.0873	1.0690	.9604	.9722	1.0096
16.00	1.0878	1.0690	.9608	.9724	1.0103
17.00	1.0883	1.0690	.9611	.9726	1.0108
18.00	1.0888	1.0690	.9613	.9727	1.0113
19.00	1.0892	1.0690	.9615	.9728	1.0118
20.00	1.0896	1.0689	.9617	.9729	1.0121
22.00	1.0902	1.0689	.9620	.9731	1.0128
24.00	1.0908	1.0689	.9622	.9732	1.0134
26.00	1.0913	1.0689	.9624	.9732	1.0139
28.00	1.0918	1.0689	.9625	.9733	1.0144
30.00	1.0922	1.0689	.9627	.9733	1.0147
32.00	1.0926	1.0689	.9628	.9734	1.0151
34.00	1.0929	1.0690	.9628	.9734	1.0154
36.00	1.0932	1.0690	.9629	.9734	1.0156
38.00	1.0935	1.0690	.9630	.9734	1.0159
40.00	1.0938	1.0690	.9630	.9734	1.0161
45.00	1.0944	1.0691	.9631	.9734	1.0165
50.00	1.0948	1.0691	.9632	.9734	1.0169
55.00	1.0952	1.0691	.9632	.9733	1.0172
60.00	1.0956	1.0692	.9633	.9733	1.0174
65.00	1.0959	1.0692	.9633	.9733	1.0177
70.00	1.0962	1.0692	.9633	.9733	1.0178
75.00	1.0964	1.0693	.9633	.9732	1.0180
80.00	1.0966	1.0693	.9633	.9732	1.0181
85.00	1.0968	1.0693	.9633	.9732	1.0183
90.00	1.0970	1.0693	.9633	.9732	1.0184
95.00	1.0971	1.0694	.9633	.9731	1.0185
100.00	1.0973	1.0694	.9633	.9731	1.0186
125.00	1.0979	1.0695	.9633	.9730	1.0190
150.00	1.0983	1.0695	.9633	.9729	1.0192
175.00	1.0986	1.0696	.9633	.9729	1.0194
200.00	1.0988	1.0696	.9633	.9728	1.0195

TABLE 7b. *Ratios of collision integrals for the (21, 6) potential function*

T*	A*	B*	C*	E*	F*
.10	1.0454	1.1876	.8877	.9182	.9425
.15	1.0507	1.1925	.8868	.9192	.9411
.20	1.0573	1.2043	.8844	.9202	.9381
.25	1.0654	1.2194	.8804	.9200	.9336
.30	1.0737	1.2324	.8755	.9175	.9298
.35	1.0802	1.2407	.8707	.9136	.9269
.40	1.0866	1.2445	.8664	.9091	.9237
.45	1.0908	1.2436	.8631	.9047	.9229
.50	1.0942	1.2403	.8606	.9006	.9209
.55	1.0944	1.2348	.8591	.8978	.9209
.60	1.0970	1.2273	.8585	.8949	.9209
.65	1.0972	1.2198	.8583	.8930	.9205
.70	1.0951	1.2122	.8586	.8923	.9207
.75	1.0944	1.2041	.8597	.8918	.9217
.80	1.0946	1.1959	.8613	.8915	.9228
.85	1.0942	1.1880	.8630	.8917	.9240
.90	1.0920	1.1808	.8646	.8924	.9245
.95	1.0896	1.1741	.8664	.8937	.9254
1.00	1.0875	1.1677	.8685	.8952	.9267
1.10	1.0858	1.1555	.8732	.8979	.9299
1.20	1.0840	1.1449	.8781	.9011	.9331
1.30	1.0813	1.1357	.8824	.9047	.9358
1.40	1.0782	1.1278	.8864	.9086	.9383
1.50	1.0759	1.1209	.8906	.9124	.9411
1.60	1.0748	1.1149	.8948	.9157	.9441
1.70	1.0739	1.1097	.8988	.9189	.9470
1.80	1.0731	1.1050	.9024	.9220	.9498
1.90	1.0722	1.1010	.9058	.9249	.9524
2.00	1.0713	1.0974	.9089	.9278	.9547
2.20	1.0693	1.0913	.9142	.9330	.9586
2.40	1.0680	1.0866	.9190	.9375	.9624
2.60	1.0677	1.0829	.9234	.9413	.9661
2.80	1.0675	1.0800	.9273	.9446	.9693
3.00	1.0675	1.0776	.9308	.9475	.9723
3.20	1.0675	1.0756	.9338	.9501	.9749
3.40	1.0676	1.0739	.9364	.9523	.9773
3.60	1.0677	1.0724	.9387	.9544	.9794
3.80	1.0677	1.0711	.9407	.9562	.9812
4.00	1.0677	1.0700	.9424	.9578	.9828
4.50	1.0681	1.0679	.9462	.9611	.9865
5.00	1.0688	1.0665	.9493	.9636	.9896
5.50	1.0696	1.0655	.9518	.9656	.9923
6.00	1.0703	1.0647	.9538	.9671	.9945
6.50	1.0710	1.0640	.9555	.9684	.9963
7.00	1.0716	1.0635	.9568	.9695	.9979
7.50	1.0722	1.0631	.9580	.9704	.9992
8.00	1.0727	1.0628	.9589	.9711	1.0004
8.50	1.0732	1.0625	.9598	.9717	1.0015
9.00	1.0737	1.0623	.9605	.9723	1.0024
9.50	1.0741	1.0621	.9611	.9727	1.0032

TABLE 7b. *Ratios of collision integrals for the (21, 6) potential function*—Continued

T*	A*	B*	C*	E*	F*
10.00	1.0745	1.0619	.9616	.9731	1.0039
11.00	1.0752	1.0616	.9625	.9738	1.0052
12.00	1.0759	1.0614	.9633	.9743	1.0063
13.00	1.0765	1.0612	.9639	.9747	1.0072
14.00	1.0771	1.0611	.9644	.9750	1.0080
15.00	1.0776	1.0610	.9648	.9752	1.0087
16.00	1.0780	1.0609	.9652	.9754	1.0093
17.00	1.0784	1.0609	.9655	.9756	1.0098
18.00	1.0788	1.0608	.9657	.9758	1.0103
19.00	1.0791	1.0608	.9659	.9759	1.0107
20.00	1.0795	1.0608	.9661	.9760	1.0110
22.00	1.0800	1.0607	.9665	.9761	1.0117
24.00	1.0805	1.0606	.9667	.9763	1.0122
26.00	1.0809	1.0606	.9669	.9764	1.0127
28.00	1.0813	1.0606	.9671	.9764	1.0130
30.00	1.0816	1.0606	.9672	.9765	1.0134
32.00	1.0819	1.0605	.9673	.9765	1.0137
34.00	1.0822	1.0605	.9674	.9766	1.0139
36.00	1.0824	1.0605	.9675	.9766	1.0142
38.00	1.0827	1.0605	.9676	.9766	1.0144
40.00	1.0829	1.0605	.9676	.9766	1.0146
45.00	1.0833	1.0604	.9678	.9767	1.0150
50.00	1.0837	1.0604	.9679	.9767	1.0153
55.00	1.0840	1.0604	.9679	.9767	1.0156
60.00	1.0843	1.0604	.9680	.9767	1.0158
65.00	1.0845	1.0604	.9680	.9767	1.0160
70.00	1.0847	1.0604	.9681	.9767	1.0162
75.00	1.0849	1.0604	.9681	.9767	1.0163
80.00	1.0851	1.0604	.9681	.9767	1.0165
85.00	1.0852	1.0604	.9681	.9767	1.0166
90.00	1.0854	1.0604	.9682	.9767	1.0167
95.00	1.0855	1.0604	.9682	.9766	1.0168
100.00	1.0856	1.0604	.9682	.9766	1.0169
125.00	1.0861	1.0604	.9682	.9766	1.0172
150.00	1.0864	1.0604	.9683	.9766	1.0175
175.00	1.0866	1.0604	.9683	.9765	1.0176
200.00	1.0868	1.0604	.9683	.9765	1.0178

TABLE 8b. *Ratios of collision integrals for the (24, 6) potential function*

T*	A*	B*	C*	E*	F*
.10	1.0479	1.1869	.8877	.9183	.9423
.15	1.0530	1.1901	.8873	.9192	.9414
.20	1.0589	1.1990	.8857	.9204	.9391
.25	1.0656	1.2115	.8826	.9203	.9362
.30	1.0726	1.2228	.8787	.9185	.9329
.35	1.0790	1.2306	.8747	.9154	.9298
.40	1.0849	1.2339	.8711	.9116	.9275
.45	1.0875	1.2337	.8683	.9079	.9265
.50	1.0916	1.2302	.8662	.9042	.9252
.55	1.0921	1.2256	.8649	.9014	.9245
.60	1.0926	1.2189	.8644	.8992	.9246
.65	1.0942	1.2112	.8646	.8973	.9249
.70	1.0927	1.2042	.8649	.8963	.9245
.75	1.0906	1.1968	.8659	.8962	.9253
.80	1.0901	1.1891	.8674	.8961	.9263
.85	1.0898	1.1814	.8691	.8962	.9273
.90	1.0888	1.1742	.8710	.8968	.9284
.95	1.0867	1.1677	.8727	.8978	.9291
1.00	1.0843	1.1615	.8746	.8992	.9300
1.10	1.0812	1.1499	.8790	.9023	.9327
1.20	1.0795	1.1395	.8836	.9052	.9358
1.30	1.0775	1.1305	.8881	.9085	.9387
1.40	1.0746	1.1227	.8920	.9121	.9410
1.50	1.0718	1.1158	.8959	.9159	.9434
1.60	1.0701	1.1100	.8998	.9192	.9461
1.70	1.0690	1.1048	.9036	.9223	.9488
1.80	1.0682	1.1002	.9072	.9253	.9515
1.90	1.0674	1.0962	.9105	.9281	.9540
2.00	1.0665	1.0926	.9136	.9309	.9563
2.20	1.0646	1.0866	.9188	.9358	.9602
2.40	1.0630	1.0818	.9233	.9402	.9636
2.60	1.0623	1.0780	.9275	.9440	.9670
2.80	1.0621	1.0750	.9313	.9472	.9701
3.00	1.0619	1.0725	.9347	.9501	.9729
3.20	1.0618	1.0705	.9376	.9526	.9754
3.40	1.0618	1.0688	.9402	.9548	.9777
3.60	1.0618	1.0673	.9424	.9567	.9797
3.80	1.0618	1.0659	.9444	.9585	.9816
4.00	1.0618	1.0648	.9462	.9601	.9831
4.50	1.0619	1.0626	.9498	.9633	.9865
5.00	1.0624	1.0610	.9528	.9658	.9895
5.50	1.0630	1.0599	.9552	.9678	.9920
6.00	1.0636	1.0591	.9572	.9693	.9941
6.50	1.0641	1.0584	.9588	.9706	.9958
7.00	1.0646	1.0578	.9602	.9717	.9973
7.50	1.0651	1.0573	.9613	.9726	.9986
8.00	1.0655	1.0570	.9623	.9733	.9998
8.50	1.0660	1.0566	.9631	.9739	1.0008
9.00	1.0664	1.0563	.9639	.9745	1.0017
9.50	1.0667	1.0561	.9645	.9749	1.0025

299-547 O-68—8

TABLE 8b. *Ratios of collision integrals for the (24, 6) potential function*—Continued

T*	A*	B*	C*	E*	F*
10.00	1.0671	1.0559	.9650	.9753	1.0032
11.00	1.0677	1.0555	.9659	.9760	1.0044
12.00	1.0682	1.0553	.9667	.9765	1.0054
13.00	1.0687	1.0551	.9673	.9769	1.0063
14.00	1.0692	1.0549	.9678	.9773	1.0070
15.00	1.0696	1.0548	.9682	.9775	1.0077
16.00	1.0700	1.0546	.9686	.9778	1.0082
17.00	1.0704	1.0545	.9689	.9780	1.0087
18.00	1.0707	1.0545	.9692	.9781	1.0092
19.00	1.0710	1.0544	.9694	.9782	1.0096
20.00	1.0713	1.0543	.9696	.9784	1.0099
22.00	1.0717	1.0542	.9699	.9786	1.0105
24.00	1.0722	1.0541	.9702	.9787	1.0111
26.00	1.0725	1.0541	.9704	.9788	1.0115
28.00	1.0728	1.0540	.9706	.9789	1.0118
30.00	1.0731	1.0539	.9708	.9790	1.0122
32.00	1.0734	1.0539	.9709	.9790	1.0124
34.00	1.0736	1.0539	.9710	.9791	1.0127
36.00	1.0738	1.0538	.9711	.9791	1.0129
38.00	1.0740	1.0538	.9712	.9791	1.0131
40.00	1.0741	1.0538	.9712	.9792	1.0133
45.00	1.0745	1.0537	.9714	.9792	1.0136
50.00	1.0748	1.0537	.9715	.9793	1.0140
55.00	1.0751	1.0536	.9716	.9793	1.0142
60.00	1.0753	1.0536	.9716	.9793	1.0144
65.00	1.0755	1.0536	.9717	.9793	1.0146
70.00	1.0757	1.0535	.9717	.9793	1.0148
75.00	1.0758	1.0535	.9718	.9793	1.0149
80.00	1.0760	1.0535	.9718	.9793	1.0150
85.00	1.0761	1.0535	.9719	.9793	1.0151
90.00	1.0762	1.0535	.9719	.9793	1.0153
95.00	1.0763	1.0535	.9719	.9793	1.0153
100.00	1.0764	1.0535	.9719	.9793	1.0154
125.00	1.0768	1.0534	.9720	.9793	1.0157
150.00	1.0770	1.0534	.9720	.9793	1.0160
175.00	1.0772	1.0534	.9721	.9793	1.0161
200.00	1.0774	1.0534	.9721	.9793	1.0163

TABLE 9b. *Ratios of collision integrals for the (30, 6) potential function*

T*	A*	B*	C*	E*	F*
.10	1.0513	1.1861	.8879	.9184	.9426
.15	1.0560	1.1874	.8879	.9192	.9421
.20	1.0609	1.1929	.8871	.9202	.9407
.25	1.0665	1.2014	.8853	.9207	.9384
.30	1.0721	1.2101	.8827	.9197	.9360
.35	1.0774	1.2162	.8799	.9175	.9337
.40	1.0811	1.2188	.8773	.9147	.9325
.45	1.0846	1.2188	.8753	.9117	.9309
.50	1.0861	1.2158	.8739	.9090	.9305
.55	1.0882	1.2111	.8730	.9065	.9298
.60	1.0874	1.2057	.8727	.9048	.9296
.65	1.0876	1.1989	.8731	.9034	.9300
.70	1.0878	1.1915	.8739	.9024	.9303
.75	1.0861	1.1849	.8748	.9021	.9304
.80	1.0841	1.1782	.8761	.9023	.9311
.85	1.0828	1.1712	.8778	.9027	.9320
.90	1.0821	1.1643	.8797	.9032	.9330
.95	1.0811	1.1578	.8817	.9040	.9341
1.00	1.0792	1.1519	.8835	.9051	.9349
1.10	1.0748	1.1411	.8874	.9080	.9366
1.20	1.0722	1.1313	.8917	.9110	.9391
1.30	1.0703	1.1226	.8961	.9140	.9418
1.40	1.0681	1.1150	.9002	.9172	.9443
1.50	1.0653	1.1082	.9038	.9207	.9464
1.60	1.0629	1.1024	.9072	.9240	.9485
1.70	1.0611	1.0973	.9107	.9271	.9507
1.80	1.0600	1.0928	.9141	.9299	.9531
1.90	1.0591	1.0888	.9173	.9326	.9554
2.00	1.0582	1.0851	.9203	.9353	.9577
2.20	1.0566	1.0791	.9255	.9401	.9616
2.40	1.0549	1.0742	.9298	.9443	.9648
2.60	1.0537	1.0703	.9337	.9481	.9678
2.80	1.0531	1.0671	.9372	.9513	.9707
3.00	1.0528	1.0646	.9405	.9541	.9734
3.20	1.0526	1.0625	.9433	.9565	.9758
3.40	1.0525	1.0607	.9458	.9586	.9780
3.60	1.0525	1.0592	.9480	.9605	.9799
3.80	1.0524	1.0578	.9500	.9622	.9817
4.00	1.0524	1.0567	.9517	.9638	.9833
4.50	1.0524	1.0543	.9552	.9669	.9865
5.00	1.0525	1.0527	.9580	.9694	.9892
5.50	1.0529	1.0515	.9604	.9713	.9915
6.00	1.0533	1.0505	.9623	.9728	.9935
6.50	1.0538	1.0498	.9639	.9740	.9952
7.00	1.0541	1.0492	.9653	.9750	.9966
7.50	1.0545	1.0487	.9664	.9759	.9978
8.00	1.0548	1.0483	.9673	.9766	.9988
8.50	1.0551	1.0479	.9681	.9773	.9997
9.00	1.0554	1.0476	.9688	.9778	1.0006
9.50	1.0557	1.0473	.9695	.9783	1.0013

TABLE 9b. *Ratios of collision integrals for the (30, 6) potential function*—Continued

T*	A*	B*	C*	E*	F*
10.00	1.0559	1.0470	.9700	.9787	1.0019
11.00	1.0563	1.0466	.9709	.9793	1.0030
12.00	1.0568	1.0463	.9716	.9799	1.0040
13.00	1.0571	1.0460	.9722	.9803	1.0048
14.00	1.0575	1.0458	.9728	.9806	1.0055
15.00	1.0578	1.0456	.9732	.9809	1.0060
16.00	1.0581	1.0454	.9736	.9812	1.0066
17.00	1.0583	1.0453	.9739	.9814	1.0070
18.00	1.0586	1.0451	.9742	.9816	1.0074
19.00	1.0588	1.0450	.9744	.9817	1.0078
20.00	1.0590	1.0449	.9746	.9818	1.0081
22.00	1.0594	1.0448	.9750	.9821	1.0087
24.00	1.0597	1.0446	.9753	.9822	1.0091
26.00	1.0599	1.0445	.9755	.9824	1.0095
28.00	1.0602	1.0444	.9757	.9825	1.0098
30.00	1.0604	1.0443	.9759	.9826	1.0101
32.00	1.0605	1.0443	.9760	.9826	1.0104
34.00	1.0607	1.0442	.9761	.9827	1.0106
36.00	1.0608	1.0441	.9762	.9827	1.0108
38.00	1.0610	1.0441	.9763	.9828	1.0110
40.00	1.0611	1.0440	.9764	.9828	1.0111
45.00	1.0614	1.0439	.9766	.9829	1.0115
50.00	1.0616	1.0438	.9767	.9830	1.0117
55.00	1.0618	1.0438	.9768	.9830	1.0120
60.00	1.0619	1.0437	.9769	.9831	1.0122
65.00	1.0621	1.0437	.9770	.9831	1.0123
70.00	1.0622	1.0436	.9770	.9832	1.0125
75.00	1.0623	1.0436	.9771	.9832	1.0126
80.00	1.0624	1.0435	.9771	.9832	1.0128
85.00	1.0625	1.0435	.9772	.9832	1.0129
90.00	1.0626	1.0435	.9772	.9832	1.0130
95.00	1.0627	1.0435	.9772	.9832	1.0130
100.00	1.0628	1.0434	.9773	.9832	1.0131
125.00	1.0630	1.0434	.9774	.9833	1.0134
150.00	1.0632	1.0433	.9774	.9833	1.0136
175.00	1.0634	1.0433	.9775	.9833	1.0137
200.00	1.0635	1.0433	.9775	.9833	1.0138

TABLE 10b. *Ratios of collision integrals for the (40, 6) potential function*

T*	A*	B*	C*	E*	F*
.10	1.0540	1.1850	.8883	.9188	.9430
.15	1.0586	1.1849	.8887	.9195	.9429
.20	1.0627	1.1874	.8886	.9204	.9423
.25	1.0669	1.1926	.8877	.9209	.9410
.30	1.0712	1.1980	.8863	.9205	.9393
.35	1.0749	1.2020	.8848	.9192	.9380
.40	1.0780	1.2037	.8833	.9173	.9366
.45	1.0806	1.2027	.8820	.9152	.9358
.50	1.0814	1.2004	.8813	.9132	.9350
.55	1.0823	1.1958	.8811	.9115	.9351
.60	1.0825	1.1905	.8812	.9100	.9346
.65	1.0813	1.1847	.8818	.9092	.9349
.70	1.0804	1.1781	.8828	.9087	.9353
.75	1.0802	1.1712	.8841	.9084	.9360
.80	1.0784	1.1649	.8854	.9086	.9364
.85	1.0763	1.1587	.8870	.9092	.9370
.90	1.0744	1.1524	.8888	.9100	.9379
.95	1.0734	1.1463	.8908	.9108	.9390
1.00	1.0723	1.1405	.8928	.9118	.9401
1.10	1.0688	1.1301	.8967	.9144	.9419
1.20	1.0650	1.1210	.9006	.9175	.9437
1.30	1.0626	1.1128	.9046	.9205	.9460
1.40	1.0607	1.1055	.9086	.9234	.9484
1.50	1.0585	1.0991	.9124	.9265	.9506
1.60	1.0562	1.0935	.9157	.9295	.9525
1.70	1.0540	1.0886	.9187	.9324	.9543
1.80	1.0522	1.0842	.9218	.9352	.9562
1.90	1.0510	1.0804	.9247	.9378	.9581
2.00	1.0500	1.0769	.9276	.9402	.9601
2.20	1.0483	1.0709	.9326	.9447	.9637
2.40	1.0468	1.0662	.9369	.9487	.9668
2.60	1.0453	1.0622	.9405	.9522	.9694
2.80	1.0442	1.0590	.9437	.9553	.9718
3.00	1.0435	1.0563	.9467	.9580	.9742
3.20	1.0431	1.0541	.9494	.9604	.9764
3.40	1.0428	1.0523	.9518	.9624	.9784
3.60	1.0426	1.0507	.9539	.9643	.9802
3.80	1.0425	1.0494	.9558	.9659	.9818
4.00	1.0423	1.0481	.9575	.9674	.9832
4.50	1.0421	1.0458	.9609	.9705	.9863
5.00	1.0419	1.0439	.9636	.9729	.9887
5.50	1.0420	1.0426	.9658	.9748	.9908
6.00	1.0422	1.0416	.9677	.9763	.9926
6.50	1.0424	1.0407	.9692	.9775	.9941
7.00	1.0426	1.0401	.9705	.9785	.9954
7.50	1.0429	1.0395	.9716	.9794	.9965
8.00	1.0431	1.0390	.9725	.9801	.9975
8.50	1.0432	1.0386	.9733	.9807	.9983
9.00	1.0434	1.0382	.9741	.9813	.9991
9.50	1.0436	1.0379	.9747	.9817	.9997

TABLE 10b. *Ratios of collision integrals for the (40, 6) potential function*—Continued

T*	A*	B*	C*	E*	F*
10.00	1.0437	1.0376	.9752	.9821	1.0003
11.00	1.0440	1.0371	.9761	.9828	1.0014
12.00	1.0443	1.0367	.9768	.9834	1.0022
13.00	1.0445	1.0364	.9774	.9838	1.0029
14.00	1.0447	1.0361	.9779	.9842	1.0035
15.00	1.0449	1.0359	.9784	.9845	1.0041
16.00	1.0451	1.0357	.9787	.9847	1.0045
17.00	1.0453	1.0355	.9791	.9850	1.0050
18.00	1.0455	1.0353	.9794	.9852	1.0053
19.00	1.0456	1.0352	.9796	.9853	1.0057
20.00	1.0458	1.0351	.9798	.9855	1.0059
22.00	1.0460	1.0349	.9802	.9857	1.0065
24.00	1.0462	1.0347	.9805	.9859	1.0069
26.00	1.0464	1.0346	.9807	.9860	1.0072
28.00	1.0466	1.0345	.9809	.9862	1.0075
30.00	1.0467	1.0343	.9811	.9863	1.0077
32.00	1.0468	1.0342	.9813	.9864	1.0079
34.00	1.0469	1.0342	.9814	.9864	1.0081
36.00	1.0470	1.0341	.9815	.9865	1.0083
38.00	1.0471	1.0340	.9816	.9866	1.0084
40.00	1.0472	1.0339	.9817	.9866	1.0086
45.00	1.0473	1.0338	.9819	.9867	1.0089
50.00	1.0475	1.0337	.9820	.9868	1.0091
55.00	1.0476	1.0336	.9822	.9869	1.0094
60.00	1.0477	1.0335	.9823	.9870	1.0095
65.00	1.0478	1.0334	.9823	.9870	1.0097
70.00	1.0479	1.0334	.9824	.9871	1.0098
75.00	1.0480	1.0333	.9825	.9871	1.0099
80.00	1.0480	1.0333	.9825	.9871	1.0100
85.00	1.0481	1.0332	.9826	.9871	1.0101
90.00	1.0482	1.0332	.9826	.9872	1.0102
95.00	1.0482	1.0332	.9827	.9872	1.0102
100.00	1.0482	1.0332	.9827	.9872	1.0103
125.00	1.0484	1.0331	.9828	.9873	1.0105
150.00	1.0485	1.0330	.9829	.9873	1.0107
175.00	1.0486	1.0329	.9830	.9874	1.0109
200.00	1.0487	1.0328	.9830	.9874	1.0110

TABLE 11b. *Ratios of collision integrals for the (50, 6) potential function*

T*	A*	B*	C*	E*	F*
.10	1.0551	1.1840	.8887	.9190	.9431
.15	1.0597	1.1831	.8893	.9199	.9435
.20	1.0635	1.1842	.8896	.9207	.9434
.25	1.0672	1.1874	.8893	.9212	.9426
.30	1.0706	1.1910	.8886	.9211	.9414
.35	1.0736	1.1937	.8876	.9202	.9401
.40	1.0762	1.1945	.8867	.9188	.9391
.45	1.0775	1.1933	.8861	.9171	.9386
.50	1.0786	1.1904	.8857	.9155	.9377
.55	1.0785	1.1862	.8859	.9142	.9378
.60	1.0787	1.1807	.8863	.9131	.9377
.65	1.0777	1.1752	.8871	.9125	.9379
.70	1.0761	1.1690	.8882	.9123	.9383
.75	1.0752	1.1625	.8896	.9123	.9390
.80	1.0744	1.1559	.8912	.9125	.9398
.85	1.0723	1.1500	.8928	.9132	.9404
.90	1.0701	1.1441	.8945	.9142	.9411
.95	1.0684	1.1383	.8965	.9152	.9421
1.00	1.0673	1.1327	.8985	.9163	.9432
1.10	1.0647	1.1223	.9026	.9188	.9455
1.20	1.0610	1.1135	.9064	.9219	.9474
1.30	1.0580	1.1057	.9102	.9249	.9494
1.40	1.0561	1.0987	.9141	.9278	.9518
1.50	1.0541	1.0924	.9178	.9307	.9539
1.60	1.0522	1.0870	.9212	.9335	.9560
1.70	1.0500	1.0823	.9242	.9363	.9576
1.80	1.0481	1.0782	.9270	.9389	.9592
1.90	1.0466	1.0745	.9298	.9414	.9609
2.00	1.0455	1.0712	.9324	.9437	.9626
2.20	1.0437	1.0655	.9373	.9478	.9658
2.40	1.0421	1.0609	.9415	.9515	.9687
2.60	1.0406	1.0571	.9450	.9549	.9711
2.80	1.0392	1.0540	.9480	.9578	.9731
3.00	1.0383	1.0514	.9508	.9604	.9752
3.20	1.0376	1.0491	.9533	.9627	.9771
3.40	1.0371	1.0472	.9556	.9647	.9788
3.60	1.0368	1.0457	.9576	.9664	.9804
3.80	1.0365	1.0443	.9594	.9680	.9819
4.00	1.0362	1.0431	.9611	.9695	.9833
4.50	1.0357	1.0405	.9644	.9725	.9860
5.00	1.0354	1.0387	.9671	.9748	.9883
5.50	1.0351	1.0371	.9692	.9768	.9901
6.00	1.0352	1.0361	.9710	.9783	.9918
6.50	1.0352	1.0351	.9725	.9795	.9932
7.00	1.0353	1.0344	.9738	.9806	.9944
7.50	1.0354	1.0338	.9748	.9814	.9955
8.00	1.0356	1.0332	.9758	.9822	.9965
8.50	1.0356	1.0328	.9765	.9828	.9972
9.00	1.0357	1.0324	.9772	.9834	.9979
9.50	1.0358	1.0320	.9779	.9838	.9986

TABLE 11b. *Ratios of collision integrals for the (50, 6) potential function*—Continued

T*	A*	B*	C*	E*	F*
10.00	1.0360	1.0318	.9784	.9842	.9991
11.00	1.0361	1.0312	.9793	.9850	1.0001
12.00	1.0363	1.0308	.9800	.9855	1.0009
13.00	1.0365	1.0304	.9806	.9860	1.0016
14.00	1.0366	1.0301	.9811	.9863	1.0021
15.00	1.0367	1.0298	.9816	.9867	1.0026
16.00	1.0369	1.0296	.9819	.9870	1.0031
17.00	1.0370	1.0294	.9823	.9872	1.0035
18.00	1.0371	1.0292	.9826	.9874	1.0038
19.00	1.0372	1.0291	.9828	.9876	1.0042
20.00	1.0373	1.0289	.9830	.9877	1.0044
22.00	1.0376	1.0287	.9834	.9880	1.0049
24.00	1.0377	1.0285	.9837	.9882	1.0054
26.00	1.0378	1.0284	.9840	.9884	1.0057
28.00	1.0380	1.0282	.9842	.9885	1.0059
30.00	1.0380	1.0281	.9844	.9886	1.0061
32.00	1.0381	1.0280	.9845	.9887	1.0063
34.00	1.0382	1.0279	.9846	.9888	1.0065
36.00	1.0383	1.0278	.9848	.9888	1.0067
38.00	1.0383	1.0278	.9849	.9889	1.0068
40.00	1.0384	1.0277	.9850	.9890	1.0070
45.00	1.0385	1.0275	.9852	.9891	1.0073
50.00	1.0387	1.0274	.9853	.9892	1.0075
55.00	1.0387	1.0273	.9854	.9893	1.0077
60.00	1.0388	1.0272	.9855	.9894	1.0078
65.00	1.0389	1.0271	.9856	.9894	1.0080
70.00	1.0389	1.0271	.9857	.9894	1.0081
75.00	1.0390	1.0270	.9858	.9895	1.0081
80.00	1.0390	1.0270	.9858	.9895	1.0082
85.00	1.0391	1.0270	.9859	.9895	1.0083
90.00	1.0391	1.0270	.9859	.9895	1.0083
95.00	1.0391	1.0269	.9859	.9895	1.0083
100.00	1.0391	1.0269	.9860	.9895	1.0084
125.00	1.0392	1.0268	.9861	.9896	1.0085
150.00	1.0392	1.0267	.9862	.9897	1.0087
175.00	1.0393	1.0265	.9862	.9898	1.0088
200.00	1.0394	1.0265	.9863	.9899	1.0090

TABLE 12b. *Ratios of collision integrals for the (75, 6) potential function*

T*	A*	B*	C*	E*	F*
.10	1.0567	1.1825	.8894	.9194	.9437
.15	1.0608	1.1807	.8904	.9203	.9442
.20	1.0641	1.1801	.8911	.9212	.9445
.25	1.0670	1.1809	.8914	.9218	.9443
.30	1.0695	1.1821	.8915	.9219	.9436
.35	1.0717	1.1827	.8914	.9215	.9430
.40	1.0730	1.1820	.8913	.9206	.9423
.45	1.0737	1.1801	.8914	.9196	.9417
.50	1.0740	1.1767	.8917	.9185	.9415
.55	1.0737	1.1723	.8924	.9178	.9414
.60	1.0726	1.1673	.8932	.9172	.9415
.65	1.0722	1.1614	.8944	.9169	.9419
.70	1.0703	1.1557	.8957	.9169	.9420
.75	1.0684	1.1497	.8972	.9173	.9427
.80	1.0672	1.1436	.8990	.9178	.9435
.85	1.0657	1.1375	.9008	.9185	.9442
.90	1.0639	1.1318	.9026	.9195	.9451
.95	1.0617	1.1265	.9045	.9208	.9459
1.00	1.0599	1.1213	.9065	.9220	.9470
1.10	1.0571	1.1113	.9106	.9247	.9491
1.20	1.0544	1.1026	.9145	.9276	.9514
1.30	1.0511	1.0952	.9182	.9307	.9534
1.40	1.0484	1.0885	.9218	.9338	.9554
1.50	1.0466	1.0826	.9253	.9365	.9575
1.60	1.0449	1.0775	.9286	.9391	.9595
1.70	1.0432	1.0730	.9317	.9417	.9613
1.80	1.0414	1.0690	.9345	.9442	.9628
1.90	1.0396	1.0656	.9370	.9465	.9641
2.00	1.0382	1.0626	.9394	.9486	.9655
2.20	1.0360	1.0574	.9439	.9523	.9680
2.40	1.0343	1.0532	.9478	.9556	.9704
2.60	1.0328	1.0497	.9512	.9586	.9725
2.80	1.0313	1.0467	.9542	.9613	.9741
3.00	1.0299	1.0442	.9567	.9637	.9756
3.20	1.0290	1.0421	.9589	.9658	.9771
3.40	1.0281	1.0401	.9610	.9677	.9785
3.60	1.0274	1.0384	.9629	.9695	.9798
3.80	1.0269	1.0370	.9646	.9710	.9811
4.00	1.0266	1.0357	.9661	.9724	.9823
4.50	1.0257	1.0329	.9694	.9755	.9849
5.00	1.0252	1.0308	.9719	.9780	.9871
5.50	1.0248	1.0292	.9740	.9799	.9889
6.00	1.0246	1.0279	.9757	.9815	.9905
6.50	1.0246	1.0269	.9771	.9827	.9919
7.00	1.0246	1.0262	.9784	.9838	.9930
7.50	1.0246	1.0255	.9794	.9846	.9940
8.00	1.0246	1.0250	.9803	.9853	.9949
8.50	1.0247	1.0245	.9811	.9859	.9956
9.00	1.0247	1.0241	.9818	.9865	.9963
9.50	1.0247	1.0238	.9824	.9869	.9968

TABLE 12b. *Ratios of collision integrals for the (75, 6) potential function*—Continued

T*	A*	B*	C*	E*	F*
10.00	1.0248	1.0235	.9829	.9873	.9973
11.00	1.0249	1.0229	.9838	.9880	.9982
12.00	1.0249	1.0224	.9845	.9886	.9990
13.00	1.0251	1.0220	.9851	.9891	.9997
14.00	1.0251	1.0217	.9856	.9895	1.0002
15.00	1.0252	1.0214	.9860	.9899	1.0007
16.00	1.0253	1.0211	.9864	.9901	1.0011
17.00	1.0254	1.0209	.9867	.9904	1.0015
18.00	1.0255	1.0207	.9870	.9906	1.0018
19.00	1.0255	1.0206	.9873	.9908	1.0020
20.00	1.0256	1.0205	.9875	.9909	1.0023
22.00	1.0258	1.0203	.9879	.9911	1.0027
24.00	1.0258	1.0201	.9882	.9913	1.0030
26.00	1.0259	1.0200	.9884	.9914	1.0033
28.00	1.0259	1.0199	.9886	.9916	1.0034
30.00	1.0260	1.0197	.9888	.9917	1.0036
32.00	1.0260	1.0196	.9889	.9918	1.0038
34.00	1.0260	1.0195	.9890	.9919	1.0039
36.00	1.0260	1.0193	.9892	.9920	1.0041
38.00	1.0261	1.0192	.9893	.9921	1.0043
40.00	1.0261	1.0191	.9894	.9922	1.0044
45.00	1.0262	1.0189	.9896	.9924	1.0048
50.00	1.0264	1.0187	.9898	.9926	1.0051
55.00	1.0265	1.0185	.9899	.9927	1.0054
60.00	1.0266	1.0184	.9900	.9929	1.0057
65.00	1.0267	1.0183	.9901	.9930	1.0059
70.00	1.0268	1.0182	.9902	.9930	1.0061
75.00	1.0269	1.0181	.9903	.9931	1.0063
80.00	1.0270	1.0181	.9904	.9931	1.0064
85.00	1.0271	1.0181	.9904	.9931	1.0065
90.00	1.0272	1.0181	.9905	.9931	1.0067
95.00	1.0272	1.0181	.9905	.9931	1.0067
100.00	1.0273	1.0181	.9905	.9931	1.0067
125.00	1.0273	1.0182	.9906	.9930	1.0067
150.00	1.0273	1.0182	.9907	.9929	1.0066
175.00	1.0274	1.0182	.9907	.9929	1.0067
200.00	1.0272	1.0181	.9907	.9930	1.0066

TABLE 3c. *Tables of additional functions of the collision integrals (9, 6) potential function*

Higher order corrections				Isotopic thermal diffusion ratios		
T*	f_η	f_λ	$f_\mathscr{D}$	c.c.$_1$	Kihara$_1$	Kihara$_2$
.10	1.0014	1.0022	1.0014	.258	.260	.263
.15	1.0016	1.0025	1.0009	.207	.208	.214
.20	1.0015	1.0023	1.0004	.131	.130	.138
.25	1.0010	1.0015	1.0001	.048	.048	.054
.30	1.0004	1.0006	1.0000	−.024	−.023	−.021
.35	1.0001	1.0001	1.0002	−.082	−.080	−.081
.40	1.0000	1.0000	1.0003	−.122	−.120	−.122
.45	1.0001	1.0001	1.0006	−.154	−.152	−.155
.50	1.0002	1.0003	1.0007	−.170	−.168	−.170
.55	1.0004	1.0006	1.0008	−.178	−.176	−.177
.60	1.0005	1.0008	1.0008	−.185	−.183	−.183
.65	1.0006	1.0009	1.0008	−.183	−.183	−.181
.70	1.0006	1.0010	1.0007	−.175	−.174	−.172
.75	1.0006	1.0010	1.0006	−.163	−.163	−.160
.80	1.0006	1.0010	1.0006	−.149	−.150	−.146
.85	1.0006	1.0009	1.0005	−.139	−.139	−.135
.90	1.0005	1.0008	1.0004	−.127	−.128	−.124
.95	1.0004	1.0006	1.0003	−.113	−.114	−.110
1.00	1.0003	1.0005	1.0002	−.096	−.097	−.093
1.10	1.0002	1.0003	1.0001	−.061	−.061	−.058
1.20	1.0001	1.0001	1.0000	−.026	−.026	−.024
1.30	1.0000	1.0000	1.0000	.006	.006	.007
1.40	1.0000	1.0000	1.0000	.033	.034	.033
1.50	1.0000	1.0001	1.0001	.060	.061	.059
1.60	1.0001	1.0002	1.0002	.086	.088	.085
1.70	1.0002	1.0004	1.0003	.112	.115	.110
1.80	1.0004	1.0006	1.0005	.136	.140	.135
1.90	1.0005	1.0008	1.0006	.159	.163	.157
2.00	1.0007	1.0011	1.0008	.180	.185	.178
2.20	1.0011	1.0017	1.0012	.217	.223	.216
2.40	1.0015	1.0023	1.0016	.248	.255	.247
2.60	1.0018	1.0029	1.0019	.273	.281	.273
2.80	1.0022	1.0034	1.0022	.295	.304	.296
3.00	1.0025	1.0040	1.0025	.315	.324	.317
3.20	1.0029	1.0044	1.0028	.333	.343	.336
3.40	1.0031	1.0049	1.0031	.349	.359	.353
3.60	1.0034	1.0053	1.0034	.363	.374	.368
3.80	1.0036	1.0057	1.0036	.375	.386	.381
4.00	1.0039	1.0060	1.0038	.386	.398	.393
4.50	1.0043	1.0067	1.0043	.409	.420	.417
5.00	1.0047	1.0073	1.0047	.425	.438	.436
5.50	1.0050	1.0077	1.0050	.438	.451	.450
6.00	1.0052	1.0081	1.0052	.448	.461	.461
6.50	1.0054	1.0084	1.0054	.456	.469	.470
7.00	1.0056	1.0087	1.0056	.462	.476	.477

TABLE 3c. *Tables of additional functions of the collision integrals (9, 6) potential function* – Continued

Higher order corrections				Isotopic thermal diffusion ratios		
T^*	f_η	f_λ	$f_\mathscr{D}$	c.c.$_1$	Kihara$_1$	Kihara$_2$
7.50	1.0057	1.0089	1.0057	.467	.481	.483
8.00	1.0058	1.0091	1.0058	.472	.486	.488
8.50	1.0060	1.0093	1.0060	.476	.489	.492
9.00	1.0060	1.0094	1.0060	.479	.493	.496
9.50	1.0061	1.0095	1.0061	.482	.496	.499
10.00	1.0062	1.0096	1.0062	.484	.498	.502
11.00	1.0063	1.0098	1.0063	.487	.502	.506
12.00	1.0063	1.0099	1.0064	.490	.504	.509
13.00	1.0064	1.0099	1.0064	.492	.506	.511
14.00	1.0064	1.0100	1.0065	.493	.507	.513
15.00	1.0064	1.0100	1.0065	.494	.508	.514
16.00	1.0064	1.0100	1.0066	.495	.509	.515
17.00	1.0065	1.0100	1.0066	.495	.509	.516
18.00	1.0065	1.0100	1.0066	.496	.510	.516
19.00	1.0065	1.0100	1.0066	.496	.510	.516
20.00	1.0064	1.0100	1.0066	.496	.510	.516
22.00	1.0064	1.0100	1.0066	.496	.509	.516
24.00	1.0064	1.0100	1.0066	.495	.509	.516
26.00	1.0064	1.0099	1.0066	.495	.508	.515
28.00	1.0064	1.0099	1.0066	.494	.508	.514
30.00	1.0063	1.0098	1.0066	.493	.507	.514
32.00	1.0063	1.0098	1.0066	.493	.506	.513
34.00	1.0063	1.0098	1.0066	.492	.505	.512
36.00	1.0063	1.0097	1.0066	.491	.505	.511
38.00	1.0062	1.0097	1.0065	.490	.504	.511
40.00	1.0062	1.0097	1.0065	.490	.503	.510
45.00	1.0062	1.0096	1.0065	.488	.501	.508
50.00	1.0061	1.0095	1.0065	.487	.500	.507
55.00	1.0061	1.0094	1.0064	.485	.498	.505
60.00	1.0060	1.0094	1.0064	.484	.497	.504
65.00	1.0060	1.0093	1.0064	.483	.496	.502
70.00	1.0060	1.0093	1.0064	.482	.495	.501
75.00	1.0059	1.0092	1.0063	.481	.494	.500
80.00	1.0059	1.0092	1.0063	.480	.493	.499
85.00	1.0059	1.0092	1.0063	.479	.492	.498
90.00	1.0059	1.0091	1.0063	.478	.491	.497
95.00	1.0058	1.0091	1.0063	.477	.490	.496
100.00	1.0058	1.0091	1.0063	.477	.489	.496
125.00	1.0057	1.0089	1.0062	.474	.486	.492
150.00	1.0057	1.0088	1.0061	.471	.484	.490
175.00	1.0056	1.0088	1.0061	.469	.482	.488
200.00	1.0056	1.0087	1.0061	.468	.480	.486

TABLE 4c. *Tables of additional functions of the collision integrals (12, 6) potential function*

	Higher order corrections			Isotopic thermal diffusion ratios		
T*	f_η	f_λ	f_ϑ	c.c.$_1$	Kihara$_1$	Kihara$_2$
.10	1.0017	1.0027	1.0017	.284	.288	.290
.15	1.0018	1.0028	1.0014	.258	.260	.264
.20	1.0018	1.0029	1.0010	.211	.211	.219
.25	1.0015	1.0024	1.0005	.154	.153	.161
.30	1.0010	1.0016	1.0002	.096	.096	.102
.35	1.0006	1.0009	1.0001	.049	.048	.052
.40	1.0003	1.0004	1.0000	.010	.010	.012
.45	1.0001	1.0001	1.0000	−.017	−.017	−.016
.50	1.0000	1.0000	1.0000	−.036	−.036	−.036
.55	1.0000	1.0000	1.0001	−.049	−.049	−.049
.60	1.0000	1.0000	1.0001	−.052	−.052	−.052
.65	1.0000	1.0001	1.0001	−.052	−.051	−.051
.70	1.0001	1.0001	1.0001	−.049	−.049	−.049
.75	1.0001	1.0001	1.0000	−.045	−.045	−.044
.80	1.0001	1.0001	1.0000	−.036	−.036	−.035
.85	1.0000	1.0001	1.0000	−.023	−.023	−.023
.90	1.0000	1.0001	1.0000	−.010	−.010	−.009
.95	1.0000	1.0000	1.0000	.004	.004	.004
1.00	1.0000	1.0000	1.0000	.016	.017	.017
1.10	1.0000	1.0000	1.0000	.041	.041	.040
1.20	1.0000	1.0000	1.0001	.069	.071	.069
1.30	1.0001	1.0001	1.0002	.099	.101	.098
1.40	1.0002	1.0003	1.0004	.127	.130	.126
1.50	1.0003	1.0005	1.0006	.153	.157	.152
1.60	1.0005	1.0008	1.0008	.176	.181	.175
1.70	1.0007	1.0011	1.0010	.197	.202	.195
1.80	1.0009	1.0014	1.0012	.217	.223	.216
1.90	1.0011	1.0017	1.0014	.237	.243	.236
2.00	1.0013	1.0021	1.0016	.256	.263	.255
2.20	1.0018	1.0028	1.0021	.290	.298	.290
2.40	1.0022	1.0035	1.0026	.319	.329	.320
2.60	1.0027	1.0041	1.0030	.345	.355	.347
2.80	1.0031	1.0048	1.0034	.366	.377	.370
3.00	1.0034	1.0054	1.0037	.384	.396	.389
3.20	1.0038	1.0059	1.0040	.399	.412	.405
3.40	1.0041	1.0064	1.0043	.413	.427	.421
3.60	1.0044	1.0069	1.0046	.426	.440	.435
3.80	1.0047	1.0073	1.0048	.438	.452	.447
4.00	1.0049	1.0076	1.0051	.448	.463	.459
4.50	1.0054	1.0084	1.0056	.470	.485	.482
5.00	1.0058	1.0090	1.0060	.486	.502	.500
5.50	1.0061	1.0095	1.0063	.498	.515	.514
6.00	1.0064	1.0099	1.0066	.508	.525	.526
6.50	1.0066	1.0103	1.0068	.516	.533	.535
7.00	1.0068	1.0105	1.0070	.522	.540	.542

TABLE 4c. *Tables of additional functions of the collision integrals (12, 6) potential function*—Continued

Higher order corrections				Isotopic thermal diffusion ratios		
T^*	f_η	f_λ	$f_\mathcal{D}$	c.c.$_1$	Kihara$_1$	Kihara$_2$
7.50	1.0069	1.0107	1.0072	.528	.545	.548
8.00	1.0070	1.0109	1.0073	.532	.549	.553
8.50	1.0071	1.0111	1.0074	.535	.553	.557
9.00	1.0072	1.0112	1.0075	.538	.556	.560
9.50	1.0073	1.0113	1.0076	.541	.559	.563
10.00	1.0073	1.0114	1.0076	.543	.561	.566
11.00	1.0074	1.0115	1.0078	.547	.565	.570
12.00	1.0075	1.0116	1.0079	.550	.568	.574
13.00	1.0075	1.0117	1.0079	.552	.570	.576
14.00	1.0076	1.0118	1.0080	.553	.571	.578
15.00	1.0076	1.0118	1.0080	.555	.573	.579
16.00	1.0076	1.0118	1.0081	.555	.574	.580
17.00	1.0076	1.0119	1.0081	.556	.574	.581
18.00	1.0076	1.0119	1.0081	.557	.575	.582
19.00	1.0076	1.0119	1.0081	.557	.575	.582
20.00	1.0077	1.0119	1.0082	.557	.575	.583
22.00	1.0077	1.0119	1.0082	.558	.576	.583
24.00	1.0077	1.0119	1.0082	.558	.576	.583
26.00	1.0077	1.0119	1.0082	.558	.576	.584
28.00	1.0077	1.0119	1.0082	.558	.576	.583
30.00	1.0076	1.0119	1.0082	.558	.576	.583
32.00	1.0076	1.0119	1.0082	.557	.575	.583
34.00	1.0076	1.0119	1.0082	.557	.575	.583
36.00	1.0076	1.0118	1.0082	.557	.575	.583
38.00	1.0076	1.0118	1.0082	.557	.575	.582
40.00	1.0076	1.0118	1.0082	.556	.574	.582
45.00	1.0076	1.0118	1.0082	.556	.573	.581
50.00	1.0075	1.0117	1.0082	.555	.573	.581
55.00	1.0075	1.0117	1.0082	.554	.572	.580
60.00	1.0075	1.0117	1.0082	.554	.571	.579
65.00	1.0075	1.0116	1.0081	.553	.571	.578
70.00	1.0075	1.0116	1.0081	.553	.570	.578
75.00	1.0074	1.0116	1.0081	.552	.570	.577
80.00	1.0074	1.0116	1.0081	.552	.569	.577
85.00	1.0074	1.0115	1.0081	.551	.569	.576
90.00	1.0074	1.0115	1.0081	.551	.568	.576
95.00	1.0074	1.0115	1.0081	.550	.568	.575
100.00	1.0074	1.0115	1.0081	.550	.567	.575
125.00	1.0073	1.0114	1.0080	.548	.565	.573
150.00	1.0073	1.0113	1.0080	.547	.564	.572
175.00	1.0072	1.0113	1.0080	.546	.563	.570
200.00	1.0072	1.0112	1.0080	.545	.562	.570

TABLE 5c. *Tables of additional functions of the collision integrals (15, 6) potential function*

Higher order corrections				Isotopic thermal diffusion ratios		
T*	f_η	f_λ	$f_\mathscr{D}$	c.c.$_1$	Kihara$_1$	Kihara$_2$
.10	1.0018	1.0028	1.0018	.289	.293	.295
.15	1.0019	1.0030	1.0017	.274	.277	.280
.20	1.0020	1.0030	1.0013	.245	.246	.252
.25	1.0018	1.0028	1.0009	.203	.203	.211
.30	1.0014	1.0022	1.0006	.160	.160	.167
.35	1.0010	1.0015	1.0003	.121	.120	.125
.40	1.0006	1.0009	1.0002	.088	.088	.091
.45	1.0004	1.0005	1.0001	.063	.063	.065
.50	1.0002	1.0003	1.0001	.047	.047	.048
.55	1.0001	1.0001	1.0000	.036	.036	.036
.60	1.0000	1.0001	1.0000	.029	.029	.029
.65	1.0000	1.0000	1.0000	.029	.029	.029
.70	1.0000	1.0000	1.0000	.033	.033	.033
.75	1.0000	1.0000	1.0000	.038	.038	.038
.80	1.0000	1.0000	1.0000	.044	.044	.044
.85	1.0000	1.0000	1.0001	.052	.053	.052
.90	1.0000	1.0000	1.0001	.063	.064	.063
.95	1.0000	1.0001	1.0001	.076	.077	.076
1.00	1.0001	1.0001	1.0002	.089	.091	.089
1.10	1.0001	1.0002	1.0003	.115	.117	.114
1.20	1.0002	1.0003	1.0005	.138	.141	.137
1.30	1.0004	1.0006	1.0007	.163	.166	.162
1.40	1.0005	1.0008	1.0009	.189	.193	.188
1.50	1.0007	1.0011	1.0011	.214	.219	.213
1.60	1.0009	1.0014	1.0014	.237	.243	.236
1.70	1.0011	1.0018	1.0016	.258	.265	.257
1.80	1.0014	1.0021	1.0019	.277	.284	.277
1.90	1.0016	1.0025	1.0021	.294	.302	.294
2.00	1.0019	1.0029	1.0024	.310	.319	.311
2.20	1.0024	1.0037	1.0029	.341	.352	.343
2.40	1.0029	1.0045	1.0034	.369	.381	.372
2.60	1.0033	1.0052	1.0038	.393	.406	.398
2.80	1.0037	1.0058	1.0043	.414	.428	.420
3.00	1.0041	1.0064	1.0046	.432	.447	.440
3.20	1.0045	1.0070	1.0050	.448	.463	.456
3.40	1.0048	1.0075	1.0053	.461	.476	.471
3.60	1.0051	1.0080	1.0056	.472	.488	.483
3.80	1.0054	1.0084	1.0058	.483	.499	.495
4.00	1.0057	1.0088	1.0061	.493	.510	.506
4.50	1.0062	1.0096	1.0066	.513	.531	.529
5.00	1.0066	1.0102	1.0070	.529	.548	.547
5.50	1.0069	1.0108	1.0074	.541	.560	.561
6.00	1.0072	1.0112	1.0076	.551	.571	.572
6.50	1.0074	1.0115	1.0079	.559	.579	.581
7.00	1.0076	1.0118	1.0081	.565	.585	.588

TABLE 5c. *Tables of additional functions of the collision integrals (15, 6) potential function* – Continued

Higher order corrections				Isotopic thermal diffusion ratios		
T*	f_η	f_A	$f_\mathscr{D}$	c.c.$_1$	Kihara$_1$	Kihara$_2$
7.50	1.0077	1.0120	1.0082	.571	.591	.595
8.00	1.0078	1.0122	1.0084	.575	.596	.600
8.50	1.0080	1.0124	1.0085	.579	.599	.604
9.00	1.0080	1.0125	1.0086	.582	.603	.607
9.50	1.0081	1.0126	1.0087	.585	.605	.611
10.00	1.0082	1.0127	1.0088	.587	.608	.613
11.00	1.0083	1.0129	1.0089	.591	.612	.618
12.00	1.0084	1.0130	1.0090	.594	.615	.621
13.00	1.0084	1.0131	1.0091	.596	.617	.624
14.00	1.0085	1.0132	1.0092	.598	.619	.627
15.00	1.0085	1.0133	1.0092	.600	.621	.628
16.00	1.0086	1.0133	1.0093	.601	.622	.630
17.00	1.0086	1.0134	1.0093	.602	.623	.631
18.00	1.0086	1.0134	1.0093	.603	.624	.632
19.00	1.0086	1.0134	1.0094	.603	.625	.633
20.00	1.0087	1.0135	1.0094	.604	.625	.633
22.00	1.0087	1.0135	1.0094	.605	.626	.634
24.00	1.0087	1.0135	1.0094	.605	.627	.635
26.00	1.0087	1.0135	1.0095	.606	.627	.635
28.00	1.0087	1.0135	1.0095	.606	.627	.636
30.00	1.0087	1.0135	1.0095	.606	.627	.636
32.00	1.0087	1.0135	1.0095	.606	.627	.636
34.00	1.0087	1.0135	1.0095	.606	.627	.636
36.00	1.0087	1.0135	1.0095	.606	.627	.636
38.00	1.0087	1.0135	1.0095	.606	.627	.636
40.00	1.0087	1.0135	1.0095	.606	.627	.636
45.00	1.0087	1.0135	1.0095	.606	.627	.636
50.00	1.0086	1.0134	1.0095	.605	.627	.636
55.00	1.0086	1.0134	1.0095	.605	.626	.635
60.00	1.0086	1.0134	1.0095	.605	.626	.635
65.00	1.0086	1.0134	1.0095	.605	.626	.635
70.00	1.0086	1.0134	1.0095	.604	.626	.634
75.00	1.0086	1.0134	1.0095	.604	.625	.634
80.00	1.0086	1.0133	1.0095	.604	.625	.634
85.00	1.0086	1.0133	1.0095	.604	.625	.633
90.00	1.0086	1.0133	1.0095	.603	.625	.633
95.00	1.0085	1.0133	1.0095	.603	.624	.633
100.00	1.0085	1.0133	1.0095	.603	.624	.633
125.00	1.0085	1.0132	1.0095	.602	.623	.632
150.00	1.0085	1.0132	1.0095	.601	.622	.631
175.00	1.0085	1.0132	1.0094	.601	.622	.630
200.00	1.0084	1.0131	1.0094	.600	.621	.630

TABLE 6c. *Tables of additional functions of the collision integrals (18, 6) potential function*

Higher order corrections				Isotopic thermal diffusion ratios		
T*	f_η	f_A	$f_\mathscr{D}$	c.c.$_1$	Kihara$_1$	Kihara$_2$
.10	1.0018	1.0028	1.0019	.289	.293	.295
.15	1.0019	1.0030	1.0018	.280	.283	.286
.20	1.0020	1.0031	1.0015	.260	.262	.267
.25	1.0019	1.0030	1.0012	.231	.232	.238
.30	1.0016	1.0025	1.0009	.197	.197	.203
.35	1.0013	1.0019	1.0006	.165	.164	.170
.40	1.0009	1.0014	1.0004	.138	.138	.142
.45	1.0006	1.0010	1.0003	.116	.116	.119
.50	1.0004	1.0007	1.0002	.101	.101	.103
.55	1.0003	1.0005	1.0002	.092	.092	.093
.60	1.0002	1.0003	1.0002	.087	.087	.088
.65	1.0002	1.0002	1.0002	.085	.085	.085
.70	1.0001	1.0002	1.0002	.088	.088	.088
.75	1.0001	1.0002	1.0002	.094	.095	.094
.80	1.0001	1.0002	1.0002	.101	.102	.101
.85	1.0001	1.0002	1.0003	.109	.110	.109
.90	1.0002	1.0002	1.0003	.117	.119	.117
.95	1.0002	1.0003	1.0004	.128	.130	.128
1.00	1.0002	1.0003	1.0005	.140	.142	.140
1.10	1.0003	1.0005	1.0007	.166	.169	.165
1.20	1.0004	1.0007	1.0009	.190	.193	.189
1.30	1.0006	1.0010	1.0011	.212	.217	.211
1.40	1.0008	1.0013	1.0013	.235	.240	.234
1.50	1.0011	1.0016	1.0016	.258	.264	.257
1.60	1.0013	1.0020	1.0019	.280	.287	.280
1.70	1.0015	1.0024	1.0022	.301	.309	.301
1.80	1.0018	1.0028	1.0025	.320	.329	.321
1.90	1.0021	1.0032	1.0028	.337	.347	.338
2.00	1.0023	1.0036	1.0030	.352	.363	.354
2.20	1.0029	1.0045	1.0035	.380	.393	.384
2.40	1.0034	1.0052	1.0041	.407	.420	.411
2.60	1.0038	1.0060	1.0045	.430	.444	.436
2.80	1.0043	1.0066	1.0050	.450	.465	.458
3.00	1.0047	1.0073	1.0054	.467	.484	.477
3.20	1.0050	1.0078	1.0057	.483	.500	.494
3.40	1.0054	1.0084	1.0061	.496	.514	.508
3.60	1.0057	1.0088	1.0063	.507	.526	.521
3.80	1.0060	1.0093	1.0066	.517	.536	.532
4.00	1.0062	1.0097	1.0068	.526	.545	.542
4.50	1.0068	1.0105	1.0074	.546	.566	.564
5.00	1.0072	1.0112	1.0078	.562	.582	.582
5.50	1.0075	1.0117	1.0082	.574	.595	.596
6.00	1.0078	1.0122	1.0085	.584	.605	.607
6.50	1.0080	1.0125	1.0087	.592	.614	.616
7.00	1.0082	1.0128	1.0089	.598	.620	.624

299-547 O-68—9

TABLE 6c. *Tables of additional functions of the collision integrals (18, 6) potential function*—Continued

Higher order corrections				Isotopic thermal diffusion ratios		
T*	f_η	f_λ	$f_\mathscr{D}$	c.c.$_1$	Kihara$_1$	Kihara$_2$
7.50	1.0084	1.0131	1.0091	.603	.626	.630
8.00	1.0085	1.0133	1.0092	.608	.631	.635
8.50	1.0086	1.0134	1.0094	.612	.635	.640
9.00	1.0087	1.0136	1.0095	.615	.638	.644
9.50	1.0088	1.0137	1.0096	.618	.641	.647
10.00	1.0089	1.0138	1.0097	.620	.644	.650
11.00	1.0090	1.0140	1.0098	.624	.648	.654
12.00	1.0091	1.0141	1.0099	.627	.651	.658
13.00	1.0092	1.0142	1.0100	.630	.654	.661
14.00	1.0092	1.0143	1.0101	.632	.656	.664
15.00	1.0093	1.0144	1.0101	.634	.658	.666
16.00	1.0093	1.0145	1.0102	.635	.659	.667
17.00	1.0093	1.0145	1.0102	.636	.660	.669
18.00	1.0094	1.0145	1.0103	.637	.661	.670
19.00	1.0094	1.0146	1.0103	.638	.662	.671
20.00	1.0094	1.0146	1.0103	.639	.663	.671
22.00	1.0094	1.0147	1.0104	.640	.664	.673
24.00	1.0094	1.0147	1.0104	.640	.665	.674
26.00	1.0095	1.0147	1.0104	.641	.665	.674
28.00	1.0095	1.0147	1.0105	.641	.666	.675
30.00	1.0095	1.0147	1.0105	.642	.666	.675
32.00	1.0095	1.0147	1.0105	.642	.666	.676
34.00	1.0095	1.0147	1.0105	.642	.667	.676
36.00	1.0095	1.0148	1.0105	.642	.667	.676
38.00	1.0095	1.0148	1.0105	.643	.667	.676
40.00	1.0095	1.0148	1.0105	.643	.667	.676
45.00	1.0095	1.0148	1.0105	.643	.667	.677
50.00	1.0095	1.0147	1.0106	.643	.667	.677
55.00	1.0095	1.0147	1.0106	.643	.667	.677
60.00	1.0095	1.0147	1.0106	.643	.667	.677
65.00	1.0095	1.0147	1.0106	.643	.667	.677
70.00	1.0095	1.0147	1.0106	.643	.667	.676
75.00	1.0095	1.0147	1.0106	.643	.667	.676
80.00	1.0094	1.0147	1.0106	.643	.667	.676
85.00	1.0094	1.0147	1.0106	.642	.667	.676
90.00	1.0094	1.0147	1.0106	.642	.667	.676
95.00	1.0094	1.0147	1.0106	.642	.666	.676
100.00	1.0094	1.0147	1.0106	.642	.666	.676
125.00	1.0094	1.0146	1.0106	.642	.666	.676
150.00	1.0094	1.0146	1.0106	.642	.666	.675
175.00	1.0094	1.0146	1.0106	.641	.665	.675
200.00	1.0094	1.0146	1.0106	.641	.665	.675

TABLE 7c. *Tables of additional functions of the collision integrals (21, 6) potential function*

Higher order corrections				Isotopic thermal diffusion ratios		
T*	f_η	f_λ	$f_\mathscr{D}$	c.c.$_1$	Kihara$_1$	Kihara$_2$
.10	1.0018	1.0028	1.0019	.289	.292	.294
.15	1.0019	1.0030	1.0018	.283	.286	.289
.20	1.0020	1.0031	1.0016	.269	.272	.276
.25	1.0020	1.0031	1.0014	.247	.248	.254
.30	1.0018	1.0028	1.0011	.220	.221	.227
.35	1.0015	1.0023	1.0009	.194	.195	.200
.40	1.0011	1.0018	1.0007	.171	.171	.176
.45	1.0009	1.0013	1.0006	.153	.153	.157
.50	1.0006	1.0010	1.0005	.140	.140	.142
.55	1.0005	1.0008	1.0004	.132	.132	.134
.60	1.0004	1.0006	1.0004	.128	.129	.130
.65	1.0003	1.0005	1.0004	.127	.128	.128
.70	1.0003	1.0005	1.0004	.129	.130	.130
.75	1.0003	1.0004	1.0004	.134	.136	.135
.80	1.0003	1.0004	1.0005	.142	.144	.142
.85	1.0003	1.0004	1.0006	.151	.153	.151
.90	1.0003	1.0005	1.0006	.159	.161	.159
.95	1.0003	1.0005	1.0007	.168	.171	.168
1.00	1.0004	1.0006	1.0008	.179	.182	.179
1.10	1.0005	1.0008	1.0010	.203	.207	.202
1.20	1.0007	1.0010	1.0013	.227	.232	.227
1.30	1.0009	1.0013	1.0015	.249	.255	.249
1.40	1.0011	1.0017	1.0018	.270	.277	.270
1.50	1.0014	1.0021	1.0021	.292	.299	.292
1.60	1.0016	1.0025	1.0024	.313	.322	.314
1.70	1.0019	1.0029	1.0027	.333	.343	.334
1.80	1.0022	1.0034	1.0030	.352	.362	.354
1.90	1.0024	1.0038	1.0033	.369	.380	.371
2.00	1.0027	1.0042	1.0036	.385	.397	.388
2.20	1.0033	1.0051	1.0041	.412	.425	.416
2.40	1.0038	1.0059	1.0046	.436	.451	.443
2.60	1.0043	1.0067	1.0051	.458	.475	.467
2.80	1.0047	1.0074	1.0056	.478	.495	.488
3.00	1.0051	1.0080	1.0060	.495	.513	.507
3.20	1.0055	1.0086	1.0064	.510	.529	.523
3.40	1.0059	1.0091	1.0067	.524	.543	.538
3.60	1.0062	1.0096	1.0070	.535	.555	.551
3.80	1.0065	1.0100	1.0073	.545	.565	.562
4.00	1.0067	1.0104	1.0075	.554	.575	.572
4.50	1.0073	1.0113	1.0080	.572	.594	.593
5.00	1.0077	1.0120	1.0085	.588	.610	.610
5.50	1.0080	1.0125	1.0088	.600	.623	.624
6.00	1.0083	1.0129	1.0091	.609	.633	.635
6.50	1.0085	1.0133	1.0094	.617	.641	.644
7.00	1.0087	1.0136	1.0096	.624	.648	.652

TABLE 7c. *Tables of additional functions of the collision integrals (21, 6) potential function* – Continued

Higher order corrections				Isotopic thermal diffusion ratios		
T*	f_η	f_λ	$f_\mathscr{D}$	c.c.$_1$	Kihara$_1$	Kihara$_2$
7.50	1.0089	1.0139	1.0098	.629	.654	.658
8.00	1.0090	1.0141	1.0099	.634	.659	.664
8.50	1.0092	1.0143	1.0101	.638	.663	.668
9.00	1.0093	1.0144	1.0102	.641	.666	.672
9.50	1.0094	1.0146	1.0103	.644	.669	.675
10.00	1.0094	1.0147	1.0104	.646	.672	.678
11.00	1.0096	1.0149	1.0105	.650	.676	.683
12.00	1.0097	1.0150	1.0106	.654	.679	.687
13.00	1.0097	1.0151	1.0107	.656	.682	.690
14.00	1.0098	1.0152	1.0108	.658	.684	.693
15.00	1.0098	1.0153	1.0109	.660	.686	.695
16.00	1.0099	1.0154	1.0109	.662	.688	.697
17.00	1.0099	1.0154	1.0110	.663	.689	.698
18.00	1.0099	1.0155	1.0110	.664	.690	.699
19.00	1.0100	1.0155	1.0111	.665	.691	.700
20.00	1.0100	1.0155	1.0111	.666	.692	.701
22.00	1.0100	1.0156	1.0111	.667	.693	.703
24.00	1.0100	1.0156	1.0112	.668	.694	.704
26.00	1.0101	1.0157	1.0112	.669	.695	.705
28.00	1.0101	1.0157	1.0112	.669	.696	.706
30.00	1.0101	1.0157	1.0113	.670	.696	.706
32.00	1.0101	1.0157	1.0113	.670	.697	.707
34.00	1.0101	1.0157	1.0113	.670	.697	.707
36.00	1.0101	1.0157	1.0113	.671	.697	.707
38.00	1.0101	1.0157	1.0113	.671	.697	.707
40.00	1.0101	1.0157	1.0113	.671	.698	.708
45.00	1.0101	1.0157	1.0113	.671	.698	.708
50.00	1.0101	1.0158	1.0114	.672	.698	.708
55.00	1.0101	1.0158	1.0114	.672	.698	.709
60.00	1.0101	1.0158	1.0114	.672	.699	.709
65.00	1.0101	1.0158	1.0114	.672	.699	.709
70.00	1.0101	1.0158	1.0114	.672	.699	.709
75.00	1.0101	1.0158	1.0114	.672	.699	.709
80.00	1.0101	1.0158	1.0114	.672	.699	.709
85.00	1.0101	1.0157	1.0114	.672	.699	.709
90.00	1.0101	1.0157	1.0114	.672	.699	.709
95.00	1.0101	1.0157	1.0114	.672	.699	.709
100.00	1.0101	1.0157	1.0114	.672	.699	.709
125.00	1.0101	1.0157	1.0114	.672	.699	.709
150.00	1.0101	1.0157	1.0114	.672	.699	.709
175.00	1.0101	1.0157	1.0114	.672	.698	.709
200.00	1.0101	1.0157	1.0114	.672	.698	.709

TABLE 8c. *Tables of additional functions of the collision integrals (24, 6) potential function*

Higher order corrections				Isotopic thermal diffusion ratios		
T*	f_η	f_λ	$f_\mathscr{D}$	c.c.$_1$	Kihara$_1$	Kihara$_2$
.10	1.0018	1.0029	1.0019	.288	.292	.294
.15	1.0019	1.0030	1.0018	.285	.288	.290
.20	1.0020	1.0031	1.0017	.275	.278	.281
.25	1.0020	1.0031	1.0015	.258	.260	.265
.30	1.0019	1.0029	1.0013	.237	.238	.243
.35	1.0016	1.0025	1.0011	.215	.216	.221
.40	1.0013	1.0020	1.0009	.195	.196	.200
.45	1.0011	1.0017	1.0008	.180	.181	.184
.50	1.0008	1.0013	1.0007	.169	.169	.172
.55	1.0007	1.0011	1.0006	.162	.163	.164
.60	1.0006	1.0009	1.0006	.159	.160	.161
.65	1.0005	1.0008	1.0006	.159	.161	.161
.70	1.0004	1.0007	1.0006	.161	.163	.162
.75	1.0004	1.0007	1.0007	.166	.168	.167
.80	1.0004	1.0007	1.0007	.173	.176	.174
.85	1.0004	1.0007	1.0008	.182	.185	.183
.90	1.0005	1.0007	1.0009	.191	.194	.192
.95	1.0005	1.0008	1.0010	.200	.204	.200
1.00	1.0006	1.0009	1.0011	.210	.214	.210
1.10	1.0007	1.0011	1.0013	.232	.237	.233
1.20	1.0009	1.0014	1.0016	.256	.262	.256
1.30	1.0011	1.0017	1.0019	.279	.286	.280
1.40	1.0014	1.0021	1.0022	.299	.307	.300
1.50	1.0016	1.0025	1.0025	.319	.328	.320
1.60	1.0019	1.0030	1.0028	.339	.349	.341
1.70	1.0022	1.0034	1.0031	.359	.370	.361
1.80	1.0025	1.0039	1.0034	.377	.389	.380
1.90	1.0028	1.0043	1.0038	.394	.407	.398
2.00	1.0031	1.0048	1.0041	.410	.423	.414
2.20	1.0036	1.0056	1.0046	.437	.452	.443
2.40	1.0042	1.0065	1.0051	.460	.476	.468
2.60	1.0047	1.0073	1.0056	.481	.499	.491
2.80	1.0051	1.0079	1.0061	.500	.519	.512
3.00	1.0055	1.0086	1.0065	.517	.537	.530
3.20	1.0059	1.0092	1.0069	.532	.552	.547
3.40	1.0062	1.0097	1.0072	.545	.566	.561
3.60	1.0065	1.0102	1.0075	.556	.578	.574
3.80	1.0068	1.0106	1.0078	.567	.589	.585
4.00	1.0071	1.0110	1.0080	.575	.598	.595
4.50	1.0076	1.0119	1.0086	.593	.617	.615
5.00	1.0081	1.0126	1.0090	.608	.632	.632
5.50	1.0084	1.0131	1.0094	.620	.645	.646
6.00	1.0087	1.0136	1.0097	.630	.655	.658
6.50	1.0090	1.0139	1.0099	.638	.663	.667
7.00	1.0092	1.0142	1.0102	.644	.670	.674

TABLE 8c. *Tables of additional functions of the collision integrals (24, 6) potential function*—Continued

Higher order corrections				Isotopic thermal diffusion ratios		
T*	f_η	f_λ	$f_\mathscr{D}$	c.c.$_1$	Kihara$_1$	Kihara$_2$
7.50	1.0093	1.0145	1.0103	.650	.676	.681
8.00	1.0095	1.0147	1.0105	.654	.681	.686
8.50	1.0096	1.0149	1.0106	.658	.685	.691
9.00	1.0097	1.0151	1.0107	.662	.688	.695
9.50	1.0098	1.0152	1.0108	.664	.692	.698
10.00	1.0099	1.0153	1.0109	.667	.694	.701
11.00	1.0100	1.0155	1.0111	.671	.699	.706
12.00	1.0101	1.0157	1.0112	.674	.702	.710
13.00	1.0102	1.0158	1.0113	.677	.705	.713
14.00	1.0102	1.0159	1.0114	.679	.707	.716
15.00	1.0103	1.0160	1.0115	.681	.709	.718
16.00	1.0103	1.0161	1.0115	.683	.711	.720
17.00	1.0104	1.0162	1.0116	.684	.712	.722
18.00	1.0104	1.0162	1.0116	.685	.714	.723
19.00	1.0104	1.0162	1.0117	.686	.715	.724
20.00	1.0105	1.0163	1.0117	.687	.715	.725
22.00	1.0105	1.0163	1.0118	.689	.717	.727
24.00	1.0105	1.0164	1.0118	.690	.718	.728
26.00	1.0106	1.0164	1.0118	.691	.719	.729
28.00	1.0106	1.0165	1.0119	.691	.720	.730
30.00	1.0106	1.0165	1.0119	.692	.720	.731
32.00	1.0106	1.0165	1.0119	.692	.721	.731
34.00	1.0106	1.0165	1.0119	.693	.721	.732
36.00	1.0106	1.0165	1.0119	.693	.722	.732
38.00	1.0106	1.0165	1.0120	.693	.722	.732
40.00	1.0106	1.0165	1.0120	.694	.722	.733
45.00	1.0106	1.0166	1.0120	.694	.723	.733
50.00	1.0106	1.0166	1.0120	.694	.723	.734
55.00	1.0107	1.0166	1.0120	.695	.723	.734
60.00	1.0107	1.0166	1.0120	.695	.724	.734
65.00	1.0107	1.0166	1.0120	.695	.724	.734
70.00	1.0107	1.0166	1.0121	.695	.724	.735
75.00	1.0107	1.0166	1.0121	.695	.724	.735
80.00	1.0107	1.0166	1.0121	.695	.724	.735
85.00	1.0107	1.0166	1.0121	.695	.724	.735
90.00	1.0107	1.0166	1.0121	.695	.724	.735
95.00	1.0107	1.0166	1.0121	.696	.724	.735
100.00	1.0107	1.0166	1.0121	.696	.724	.735
125.00	1.0107	1.0166	1.0121	.696	.724	.735
150.00	1.0107	1.0166	1.0121	.696	.724	.735
175.00	1.0107	1.0166	1.0121	.696	.724	.735
200.00	1.0107	1.0166	1.0121	.696	.724	.735

TABLE 9c. *Tables of additional functions of the collision integrals (30, 6) potential function*

Higher order corrections				Isotopic thermal diffusion ratios		
T*	f_η	f_λ	$f_\mathscr{D}$	c.c.$_1$	Kihara$_1$	Kihara$_2$
.10	1.0018	1.0029	1.0019	.288	.292	.294
.15	1.0019	1.0030	1.0019	.287	.291	.293
.20	1.0020	1.0031	1.0018	.282	.285	.288
.25	1.0020	1.0032	1.0017	.271	.274	.278
.30	1.0020	1.0030	1.0015	.257	.259	.264
.35	1.0018	1.0028	1.0014	.241	.243	.248
.40	1.0015	1.0024	1.0012	.228	.229	.233
.45	1.0013	1.0021	1.0011	.216	.218	.221
.50	1.0011	1.0018	1.0010	.208	.210	.212
.55	1.0010	1.0015	1.0010	.204	.205	.207
.60	1.0009	1.0013	1.0010	.202	.204	.205
.65	1.0008	1.0012	1.0010	.204	.206	.206
.70	1.0007	1.0011	1.0010	.207	.210	.209
.75	1.0007	1.0011	1.0011	.212	.215	.213
.80	1.0007	1.0011	1.0011	.219	.222	.220
.85	1.0008	1.0012	1.0012	.227	.231	.228
.90	1.0008	1.0012	1.0014	.237	.241	.238
.95	1.0008	1.0013	1.0015	.247	.252	.248
1.00	1.0009	1.0014	1.0016	.256	.262	.257
1.10	1.0011	1.0017	1.0018	.277	.283	.278
1.20	1.0013	1.0020	1.0021	.299	.306	.300
1.30	1.0015	1.0023	1.0025	.321	.330	.323
1.40	1.0017	1.0027	1.0028	.342	.352	.344
1.50	1.0020	1.0032	1.0031	.361	.372	.364
1.60	1.0024	1.0037	1.0034	.379	.391	.382
1.70	1.0027	1.0041	1.0038	.397	.410	.401
1.80	1.0030	1.0046	1.0041	.415	.428	.419
1.90	1.0033	1.0051	1.0045	.431	.446	.436
2.00	1.0036	1.0055	1.0048	.447	.462	.453
2.20	1.0041	1.0065	1.0054	.474	.491	.482
2.40	1.0047	1.0073	1.0059	.496	.515	.506
2.60	1.0052	1.0081	1.0064	.516	.536	.528
2.80	1.0057	1.0089	1.0068	.534	.555	.548
3.00	1.0061	1.0095	1.0073	.551	.572	.566
3.20	1.0065	1.0101	1.0077	.565	.588	.582
3.40	1.0069	1.0107	1.0080	.578	.601	.596
3.60	1.0072	1.0112	1.0083	.589	.613	.609
3.80	1.0075	1.0116	1.0086	.599	.623	.620
4.00	1.0077	1.0120	1.0089	.608	.633	.630
4.50	1.0083	1.0129	1.0094	.626	.652	.651
5.00	1.0087	1.0136	1.0099	.640	.666	.667
5.50	1.0091	1.0141	1.0102	.652	.679	.681
6.00	1.0094	1.0146	1.0105	.661	.689	.692
6.50	1.0096	1.0149	1.0108	.669	.697	.701
7.00	1.0098	1.0153	1.0110	.675	.704	.709

TABLE 9c. *Tables of additional functions of the collision integrals (30, 6) potential function* – Continued

Higher order corrections				Isotopic thermal diffusion ratios		
T*	f_η	f_λ	$f_\mathscr{D}$	c.c.$_1$	Kihara$_1$	Kihara$_2$
7.50	1.0100	1.0155	1.0112	.681	.710	.715
8.00	1.0101	1.0157	1.0114	.685	.714	.720
8.50	1.0102	1.0159	1.0115	.689	.719	.725
9.00	1.0104	1.0161	1.0116	.693	.722	.729
9.50	1.0104	1.0162	1.0117	.696	.725	.732
10.00	1.0105	1.0164	1.0118	.698	.728	.736
11.00	1.0107	1.0166	1.0120	.702	.733	.741
12.00	1.0108	1.0168	1.0121	.706	.736	.745
13.00	1.0109	1.0169	1.0122	.709	.739	.748
14.00	1.0109	1.0170	1.0123	.711	.742	.751
15.00	1.0110	1.0171	1.0124	.713	.744	.753
16.00	1.0110	1.0172	1.0124	.715	.745	.755
17.00	1.0111	1.0172	1.0125	.716	.747	.757
18.00	1.0111	1.0173	1.0125	.717	.748	.758
19.00	1.0112	1.0174	1.0126	.718	.749	.760
20.00	1.0112	1.0174	1.0126	.719	.750	.761
22.00	1.0112	1.0175	1.0127	.721	.752	.763
24.00	1.0113	1.0175	1.0127	.722	.753	.764
26.00	1.0113	1.0176	1.0128	.723	.754	.765
28.00	1.0113	1.0176	1.0128	.724	.755	.766
30.00	1.0113	1.0176	1.0128	.725	.756	.767
32.00	1.0113	1.0176	1.0129	.725	.757	.768
34.00	1.0114	1.0177	1.0129	.726	.757	.768
36.00	1.0114	1.0177	1.0129	.726	.758	.769
38.00	1.0114	1.0177	1.0129	.726	.758	.769
40.00	1.0114	1.0177	1.0129	.727	.758	.770
45.00	1.0114	1.0177	1.0130	.727	.759	.770
50.00	1.0114	1.0178	1.0130	.728	.760	.771
55.00	1.0114	1.0178	1.0130	.728	.760	.772
60.00	1.0114	1.0178	1.0130	.729	.760	.772
65.00	1.0115	1.0178	1.0130	.729	.761	.772
70.00	1.0115	1.0178	1.0130	.729	.761	.773
75.00	1.0115	1.0178	1.0131	.729	.761	.773
80.00	1.0115	1.0178	1.0131	.730	.761	.773
85.00	1.0115	1.0178	1.0131	.730	.761	.773
90.00	1.0115	1.0178	1.0131	.730	.762	.773
95.00	1.0115	1.0179	1.0131	.730	.762	.773
100.00	1.0115	1.0179	1.0131	.730	.762	.774
125.00	1.0115	1.0179	1.0131	.730	.762	.774
150.00	1.0115	1.0179	1.0131	.731	.762	.774
175.00	1.0115	1.0179	1.0131	.731	.763	.774
200.00	1.0115	1.0179	1.0131	.731	.763	.774

TABLE 10c. *Tables of additional functions of the collision integrals (40, 6) potential function*

Higher order corrections				Isotopic thermal diffusion ratios		
T^*	f_η	f_λ	$f_\mathscr{D}$	c.c.$_1$	Kihara$_1$	Kihara$_2$
.10	1.0019	1.0029	1.0019	.290	.294	.295
.15	1.0019	1.0030	1.0019	.290	.294	.296
.20	1.0020	1.0031	1.0019	.289	.293	.295
.25	1.0021	1.0032	1.0019	.283	.287	.290
.30	1.0020	1.0032	1.0018	.275	.278	.282
.35	1.0019	1.0030	1.0017	.266	.269	.273
.40	1.0018	1.0027	1.0016	.258	.261	.264
.45	1.0016	1.0025	1.0015	.251	.254	.256
.50	1.0014	1.0022	1.0014	.247	.250	.252
.55	1.0013	1.0020	1.0014	.245	.248	.249
.60	1.0012	1.0019	1.0014	.246	.249	.249
.65	1.0011	1.0018	1.0015	.249	.252	.252
.70	1.0011	1.0017	1.0015	.254	.257	.256
.75	1.0011	1.0017	1.0016	.260	.264	.262
.80	1.0011	1.0017	1.0017	.267	.272	.269
.85	1.0011	1.0018	1.0018	.275	.280	.277
.90	1.0012	1.0019	1.0019	.284	.290	.287
.95	1.0013	1.0020	1.0021	.295	.301	.297
1.00	1.0013	1.0021	1.0022	.305	.312	.307
1.10	1.0015	1.0024	1.0025	.325	.333	.327
1.20	1.0018	1.0028	1.0029	.346	.355	.348
1.30	1.0020	1.0031	1.0032	.367	.377	.370
1.40	1.0023	1.0036	1.0036	.387	.399	.391
1.50	1.0026	1.0040	1.0040	.407	.420	.411
1.60	1.0029	1.0045	1.0043	.425	.439	.430
1.70	1.0032	1.0050	1.0046	.441	.456	.447
1.80	1.0036	1.0055	1.0050	.457	.473	.464
1.90	1.0039	1.0060	1.0053	.472	.489	.480
2.00	1.0042	1.0065	1.0056	.487	.505	.496
2.20	1.0048	1.0074	1.0063	.513	.533	.524
2.40	1.0053	1.0083	1.0068	.536	.557	.549
2.60	1.0058	1.0091	1.0073	.555	.577	.569
2.80	1.0063	1.0098	1.0077	.572	.595	.588
3.00	1.0068	1.0105	1.0082	.587	.611	.605
3.20	1.0071	1.0111	1.0086	.601	.626	.621
3.40	1.0075	1.0117	1.0089	.613	.639	.635
3.60	1.0078	1.0121	1.0092	.624	.650	.647
3.80	1.0081	1.0126	1.0095	.634	.661	.658
4.00	1.0084	1.0130	1.0098	.642	.670	.668
4.50	1.0089	1.0139	1.0103	.660	.689	.689
5.00	1.0094	1.0146	1.0108	.674	.703	.704
5.50	1.0097	1.0152	1.0111	.685	.715	.718
6.00	1.0100	1.0156	1.0115	.694	.725	.728
6.50	1.0103	1.0160	1.0117	.702	.733	.738
7.00	1.0105	1.0163	1.0120	.709	.740	.745

TABLE 10c. *Tables of additional functions of the collision integrals (40, 6) potential function* – Continued

Higher order corrections				Isotopic thermal diffusion ratios		
T*	f_η	f_λ	$f_\mathscr{D}$	c.c.$_1$	Kihara$_1$	Kihara$_2$
7.50	1.0107	1.0166	1.0121	.714	.746	.752
8.00	1.0108	1.0168	1.0123	.719	.751	.757
8.50	1.0109	1.0170	1.0124	.723	.755	.762
9.00	1.0111	1.0172	1.0126	.726	.759	.766
9.50	1.0112	1.0174	1.0127	.729	.762	.769
10.00	1.0112	1.0175	1.0128	.732	.765	.773
11.00	1.0114	1.0177	1.0129	.736	.769	.778
12.00	1.0115	1.0179	1.0131	.740	.773	.782
13.00	1.0116	1.0180	1.0132	.742	.776	.786
14.00	1.0117	1.0182	1.0133	.745	.779	.788
15.00	1.0117	1.0183	1.0134	.747	.781	.791
16.00	1.0118	1.0184	1.0134	.749	.783	.793
17.00	1.0118	1.0184	1.0135	.750	.784	.795
18.00	1.0119	1.0185	1.0135	.752	.786	.796
19.00	1.0119	1.0186	1.0136	.753	.787	.798
20.00	1.0120	1.0186	1.0136	.754	.788	.799
22.00	1.0120	1.0187	1.0137	.755	.790	.801
24.00	1.0120	1.0187	1.0137	.757	.791	.803
26.00	1.0121	1.0188	1.0138	.758	.792	.804
28.00	1.0121	1.0188	1.0138	.759	.793	.805
30.00	1.0121	1.0189	1.0139	.760	.794	.806
32.00	1.0121	1.0189	1.0139	.760	.795	.807
34.00	1.0122	1.0189	1.0139	.761	.796	.808
36.00	1.0122	1.0189	1.0139	.761	.796	.808
38.00	1.0122	1.0190	1.0139	.762	.797	.809
40.00	1.0122	1.0190	1.0140	.762	.797	.809
45.00	1.0122	1.0190	1.0140	.763	.798	.810
50.00	1.0123	1.0191	1.0140	.764	.799	.811
55.00	1.0123	1.0191	1.0140	.764	.799	.812
60.00	1.0123	1.0191	1.0141	.765	.800	.812
65.00	1.0123	1.0191	1.0141	.765	.800	.812
70.00	1.0123	1.0191	1.0141	.765	.800	.813
75.00	1.0123	1.0191	1.0141	.765	.801	.813
80.00	1.0123	1.0192	1.0141	.766	.801	.813
85.00	1.0123	1.0192	1.0141	.766	.801	.814
90.00	1.0123	1.0192	1.0141	.766	.801	.814
95.00	1.0123	1.0192	1.0141	.766	.801	.814
100.00	1.0123	1.0192	1.0141	.766	.801	.814
125.00	1.0123	1.0192	1.0142	.767	.802	.815
150.00	1.0124	1.0192	1.0142	.767	.802	.815
175.00	1.0124	1.0192	1.0142	.767	.803	.815
200.00	1.0124	1.0192	1.0142	.768	.803	.816

TABLE 11c. *Tables of additional functions of the collision integrals (50, 6) potential function*

Higher order corrections				Isotopic thermal diffusion ratios		
T*	f_η	f_λ	$f_\mathscr{D}$	c.c.$_1$	Kihara$_1$	Kihara$_2$
.10	1.0019	1.0030	1.0019	.291	.295	.297
.15	1.0020	1.0031	1.0020	.293	.297	.299
.20	1.0020	1.0032	1.0020	.294	.298	.300
.25	1.0021	1.0033	1.0020	.291	.295	.298
.30	1.0021	1.0032	1.0019	.287	.290	.293
.35	1.0020	1.0031	1.0019	.281	.285	.288
.40	1.0019	1.0029	1.0018	.276	.279	.282
.45	1.0017	1.0027	1.0018	.272	.275	.278
.50	1.0016	1.0025	1.0017	.270	.273	.275
.55	1.0015	1.0023	1.0017	.270	.274	.275
.60	1.0014	1.0022	1.0018	.272	.276	.276
.65	1.0014	1.0021	1.0018	.276	.281	.280
.70	1.0014	1.0021	1.0019	.282	.287	.285
.75	1.0014	1.0021	1.0020	.289	.294	.292
.80	1.0014	1.0021	1.0021	.297	.303	.300
.85	1.0014	1.0022	1.0022	.305	.312	.308
.90	1.0015	1.0023	1.0024	.315	.322	.318
.95	1.0016	1.0025	1.0025	.325	.332	.328
1.00	1.0017	1.0026	1.0027	.335	.344	.338
1.10	1.0019	1.0029	1.0030	.356	.366	.360
1.20	1.0022	1.0033	1.0034	.376	.387	.380
1.30	1.0024	1.0038	1.0037	.397	.409	.401
1.40	1.0027	1.0042	1.0041	.417	.430	.422
1.50	1.0030	1.0047	1.0045	.436	.451	.442
1.60	1.0034	1.0052	1.0049	.454	.470	.461
1.70	1.0037	1.0057	1.0052	.470	.487	.478
1.80	1.0040	1.0062	1.0056	.485	.503	.494
1.90	1.0043	1.0067	1.0059	.500	.518	.509
2.00	1.0046	1.0072	1.0062	.514	.533	.524
2.20	1.0052	1.0081	1.0069	.539	.560	.552
2.40	1.0057	1.0089	1.0074	.561	.584	.576
2.60	1.0062	1.0097	1.0079	.580	.604	.597
2.80	1.0067	1.0104	1.0084	.596	.621	.615
3.00	1.0071	1.0111	1.0088	.611	.636	.631
3.20	1.0075	1.0117	1.0092	.624	.651	.646
3.40	1.0079	1.0123	1.0095	.636	.663	.659
3.60	1.0082	1.0127	1.0098	.646	.674	.671
3.80	1.0085	1.0132	1.0101	.656	.684	.682
4.00	1.0087	1.0136	1.0104	.664	.693	.692
4.50	1.0093	1.0145	1.0109	.682	.712	.712
5.00	1.0098	1.0152	1.0114	.695	.727	.728
5.50	1.0101	1.0158	1.0117	.706	.738	.741
6.00	1.0104	1.0162	1.0121	.715	.748	.752
6.50	1.0107	1.0166	1.0123	.723	.756	.761
7.00	1.0109	1.0170	1.0125	.730	.763	.768

TABLE 11c. *Tables of additional functions of the collision integrals (50, 6) potential function*—Continued

Higher order corrections				Isotopic thermal diffusion ratios		
T*	f_η	f_A	$f_\mathscr{D}$	c.c.$_1$	Kihara$_1$	Kihara$_2$
7.50	1.0111	1.0173	1.0127	.735	.769	.775
8.00	1.0113	1.0175	1.0129	.740	.774	.780
8.50	1.0114	1.0177	1.0131	.744	.778	.785
9.00	1.0115	1.0179	1.0132	.747	.782	.789
9.50	1.0116	1.0181	1.0133	.750	.785	.793
10.00	1.0117	1.0182	1.0134	.753	.788	.796
11.00	1.0118	1.0184	1.0136	.757	.792	.802
12.00	1.0120	1.0186	1.0137	.761	.796	.806
13.00	1.0121	1.0188	1.0138	.764	.799	.809
14.00	1.0121	1.0189	1.0139	.766	.802	.812
15.00	1.0122	1.0190	1.0140	.768	.804	.815
16.00	1.0123	1.0191	1.0140	.770	.806	.817
17.00	1.0123	1.0192	1.0141	.772	.808	.819
18.00	1.0124	1.0193	1.0142	.773	.809	.821
19.00	1.0124	1.0193	1.0142	.774	.811	.822
20.00	1.0125	1.0194	1.0143	.775	.812	.823
22.00	1.0125	1.0195	1.0143	.777	.814	.825
24.00	1.0126	1.0195	1.0144	.779	.815	.827
26.00	1.0126	1.0196	1.0144	.780	.817	.829
28.00	1.0126	1.0196	1.0145	.781	.818	.830
30.00	1.0126	1.0197	1.0145	.782	.818	.831
32.00	1.0127	1.0197	1.0145	.782	.819	.832
34.00	1.0127	1.0197	1.0146	.783	.820	.832
36.00	1.0127	1.0197	1.0146	.783	.820	.833
38.00	1.0127	1.0198	1.0146	.784	.821	.834
40.00	1.0127	1.0198	1.0146	.784	.821	.834
45.00	1.0128	1.0198	1.0147	.785	.822	.835
50.00	1.0128	1.0199	1.0147	.786	.823	.836
55.00	1.0128	1.0199	1.0147	.787	.824	.837
60.00	1.0128	1.0199	1.0147	.787	.824	.837
65.00	1.0128	1.0199	1.0147	.787	.825	.838
70.00	1.0128	1.0200	1.0148	.788	.825	.838
75.00	1.0128	1.0200	1.0148	.788	.825	.838
80.00	1.0128	1.0200	1.0148	.788	.826	.839
85.00	1.0128	1.0200	1.0148	.788	.826	.839
90.00	1.0128	1.0200	1.0148	.789	.826	.839
95.00	1.0129	1.0200	1.0148	.789	.826	.839
100.00	1.0129	1.0200	1.0148	.789	.826	.840
125.00	1.0129	1.0200	1.0148	.790	.827	.840
150.00	1.0129	1.0200	1.0149	.790	.827	.841
175.00	1.0129	1.0201	1.0149	.790	.828	.841
200.00	1.0129	1.0201	1.0149	.790	.828	.841

TABLE 12c. *Tables of additional functions of the collision integrals (75, 6) potential function*

Higher order corrections				Isotopic thermal diffusion ratios		
T*	f_η	f_λ	$f_\mathscr{D}$	c.c.$_1$	Kihara$_1$	Kihara$_2$
.10	1.0019	1.0030	1.0020	.294	.299	.300
.15	1.0020	1.0031	1.0021	.298	.302	.304
.20	1.0021	1.0032	1.0021	.301	.305	.307
.25	1.0021	1.0033	1.0021	.302	.306	.308
.30	1.0022	1.0033	1.0021	.302	.306	.308
.35	1.0021	1.0033	1.0021	.300	.305	.307
.40	1.0020	1.0032	1.0021	.300	.304	.306
.45	1.0019	1.0030	1.0021	.300	.304	.306
.50	1.0019	1.0029	1.0021	.301	.306	.307
.55	1.0018	1.0028	1.0022	.304	.309	.309
.60	1.0017	1.0027	1.0023	.309	.314	.314
.65	1.0017	1.0027	1.0023	.314	.320	.319
.70	1.0017	1.0027	1.0025	.321	.328	.326
.75	1.0018	1.0027	1.0026	.330	.336	.334
.80	1.0018	1.0028	1.0027	.338	.346	.343
.85	1.0019	1.0029	1.0029	.348	.356	.352
.90	1.0019	1.0030	1.0030	.358	.366	.362
.95	1.0021	1.0032	1.0032	.368	.377	.372
1.00	1.0022	1.0034	1.0034	.378	.388	.382
1.10	1.0024	1.0038	1.0038	.399	.411	.404
1.20	1.0027	1.0042	1.0042	.420	.433	.425
1.30	1.0030	1.0047	1.0046	.440	.454	.446
1.40	1.0034	1.0053	1.0050	.459	.475	.466
1.50	1.0037	1.0058	1.0054	.477	.494	.485
1.60	1.0040	1.0063	1.0058	.495	.513	.504
1.70	1.0044	1.0068	1.0061	.511	.530	.521
1.80	1.0047	1.0073	1.0065	.526	.546	.537
1.90	1.0050	1.0078	1.0068	.540	.561	.552
2.00	1.0053	1.0082	1.0072	.553	.575	.566
2.20	1.0059	1.0091	1.0078	.577	.600	.592
2.40	1.0064	1.0099	1.0083	.598	.623	.615
2.60	1.0068	1.0106	1.0089	.616	.642	.636
2.80	1.0073	1.0113	1.0093	.632	.659	.653
3.00	1.0077	1.0120	1.0097	.645	.674	.669
3.20	1.0081	1.0126	1.0101	.658	.687	.682
3.40	1.0084	1.0131	1.0104	.669	.699	.695
3.60	1.0087	1.0136	1.0107	.679	.710	.707
3.80	1.0090	1.0141	1.0110	.688	.719	.717
4.00	1.0093	1.0145	1.0113	.696	.728	.727
4.50	1.0099	1.0154	1.0118	.713	.746	.747
5.00	1.0104	1.0162	1.0123	.727	.760	.762
5.50	1.0108	1.0168	1.0126	.737	.772	.775
6.00	1.0111	1.0173	1.0129	.746	.781	.786
6.50	1.0114	1.0177	1.0132	.754	.789	.795
7.00	1.0116	1.0180	1.0134	.760	.796	.802

TABLE 12c. *Tables of additional functions of the collision integrals (75, 6) potential function*—Continued

Higher order corrections				Isotopic thermal diffusion ratios		
T*	f_η	f_λ	$f_\mathscr{D}$	c.c.$_1$	Kihara$_1$	Kihara$_2$
7.50	1.0118	1.0183	1.0136	.765	.802	.809
8.00	1.0119	1.0186	1.0138	.770	.807	.814
8.50	1.0121	1.0188	1.0139	.774	.811	.819
9.00	1.0122	1.0189	1.0141	.778	.815	.823
9.50	1.0123	1.0191	1.0142	.781	.818	.827
10.00	1.0124	1.0192	1.0143	.783	.821	.830
11.00	1.0125	1.0195	1.0144	.788	.826	.835
12.00	1.0126	1.0197	1.0146	.791	.830	.840
13.00	1.0128	1.0198	1.0147	.794	.833	.844
14.00	1.0128	1.0200	1.0148	.797	.836	.847
15.00	1.0129	1.0201	1.0149	.799	.838	.849
16.00	1.0130	1.0202	1.0150	.801	.840	.851
17.00	1.0130	1.0203	1.0150	.802	.841	.853
18.00	1.0131	1.0204	1.0151	.804	.843	.855
19.00	1.0131	1.0204	1.0151	.805	.844	.856
20.00	1.0132	1.0205	1.0152	.806	.845	.858
22.00	1.0132	1.0205	1.0152	.808	.847	.860
24.00	1.0133	1.0206	1.0153	.809	.849	.862
26.00	1.0133	1.0207	1.0153	.811	.850	.863
28.00	1.0133	1.0207	1.0154	.812	.851	.864
30.00	1.0133	1.0207	1.0154	.812	.852	.865
32.00	1.0134	1.0208	1.0154	.813	.853	.866
34.00	1.0134	1.0208	1.0155	.814	.854	.867
36.00	1.0134	1.0209	1.0155	.814	.854	.868
38.00	1.0134	1.0209	1.0155	.815	.855	.868
40.00	1.0135	1.0209	1.0155	.815	.855	.869
45.00	1.0135	1.0210	1.0156	.816	.856	.870
50.00	1.0135	1.0211	1.0156	.817	.857	.871
55.00	1.0136	1.0211	1.0156	.818	.858	.872
60.00	1.0136	1.0212	1.0157	.818	.859	.873
65.00	1.0136	1.0212	1.0157	.819	.859	.873
70.00	1.0136	1.0212	1.0157	.819	.859	.874
75.00	1.0137	1.0212	1.0157	.819	.860	.874
80.00	1.0137	1.0213	1.0157	.820	.860	.874
85.00	1.0137	1.0213	1.0157	.820	.860	.874
90.00	1.0137	1.0213	1.0158	.820	.860	.875
95.00	1.0137	1.0213	1.0158	.820	.861	.875
100.00	1.0137	1.0213	1.0158	.820	.861	.875
125.00	1.0136	1.0212	1.0158	.821	.861	.876
150.00	1.0136	1.0212	1.0158	.821	.862	.876
175.00	1.0136	1.0212	1.0158	.821	.862	.876
200.00	1.0136	1.0212	1.0158	.821	.862	.876

4. References

[1] Chapman, S., and Cowling, T. G., The Mathematical Theory of Non-Uniform Gases (Cambridge University Press, New York, 1952).

[2] Hirschfelder, J. O., Curtiss, C. F., and Bird, R. B., Molecular Theory of Gases and Liquids (John Wiley & Sons, Inc., New York, 1954).

[3] Klein, Max, J. Research, NBS **70A** (Phys. and Chem.) No. 3, 259 (1966).

[4] Holleran, E. M., and Hulbert, H. M., J. Chem. Phys. **19,** 232 (1951); Brush, S. G. and Lawrence, J. D., Report UCRL–7376, Lawrence Radiation Laboratory, Livermore, California (1963); Brush, S. G., J. Chem. Phys. **42,** 792 (1965).

[5] Mason, E. A., J. Chem. Phys. **22,** 169 (1954).

[6] Mason, E. A., J. Chem. Phys. **27,** 782 (1957).

[7] Saxena, S. C., and Mason, E. A., J. Chem. Phys. **28,** 623 (1958).

[8] Smith, F. J., and Munn, R. J., J. Chem. Phys. **41,** 3560 (1964); Lovell, S. E., and Hirschfelder, J. O., Report WI–AF–21, Theoretical Chemistry Laboratory, University of Wisconsin, Madison, Wisconsin (1962).

[9] Barker, J. A., Fock, W., and Smith, F., Phys. Fluids **7,** 897 (1964); O'Connell, J. P., and Prausnitz, J. M., Advances in Thermophysical Properties at Extreme Temperatures and Pressures, pp. 19–31, ASME, New York (1965).

[10] Eliason, M. A., Stogryn, D. E., and Hirschfelder, J. O., Report WIS–ONR–19, University of Wisconsin, Madison, Wisconsin (1956); Kihara, T., Taylor, M. H., and Hirschfelder, J. O., Report WIS–R–26, University of Wisconsin, Madison, Wisconsin (1960).

[11] Smith, F. J., Mason, E. A., and Munn, R. J., Phys. Fl. **8,** 1907 (1965); Monchick, L., Phys. Fl. **2,** 695 (1959); Munn, R. J., Mason, E. A., and Smith, F. J., Phys. Fl. **8,** 1103 (1963); Mason, E. A., Munn, R. J., and Smith, F. J., Phys. Fl. (1967) to be published.

[12] Krieger, F. J., Report RM–646, The Rand Corporation, Santa Monica, California; Itean, E. C., Glueck, A. R., and Svehla, R. A., TND–481 National Aeronautics and Space Agency Lewis Research Center, Cleveland, Ohio (1961); Monchick, L., and Mason, E. A., J. Chem. Phys. **35,** 1676 (1961).

[13] Mason, E. A., and Schamp, H. W., Jr., Am. Phys. (N.Y.) **4,** 233 (1958).

[14] Smith, F. J., Munn, R. J., and Mason, E. A., J. Chem. Phys. **46,** 317 (1967).

[15] Smith, F. J., Mason, E. A., and Munn, R. J., J. Chem. Phys. **42,** 1334 (1965); Dymond, J. H., Rigby, M., and Smith, E. B., Phys. Fl. **9,** 1222 (1966).

[16] Liley, P. E., TRPC Report 15, Thermophysical Properties Research Center, Purdue University, Lafayette, Indiana (1963).

[17] Mountain, R., and Zwanzig, R. W., J. Chem. Phys. **43,** 4464 (1965).

[18] Horton, G. K., and Leech, J. W., Proc. Phys. Soc. (London) **82,** 816 (1963).

[19] Mason, E. A., J. Chem. Phys. **27,** 782 (1957).

[20] Saxena, S. C., J. Phys. Soc. (Japan) **11,** 367 (1956).

[21] Smith, F. J., Physica **30,** 497 (1964); see also reference [8].

(Paper 72A4–508)

JOURNAL OF RESEARCH of the National Bureau of Standards—A. Physics and Chemistry
Vol. 72A, No. 4, July–August 1968

Spectrum of Relaxation Times in GeO_2 Glass

A. Napolitano and P. B. Macedo

Institute for Materials Research, National Bureau of Standards, Washington, D.C. 20234

(April 29, 1968)

Index-of-refraction versus time isotherms have been established for germania glass. Using the crossover technique with air-quenched samples and applying the two relaxation time model previously reported for borosilicate glass, it was found that the width of the spectrum of relaxation times for germania glass was temperature dependent. Upon analyzing this in terms of a distribution of activation energies, the results showed that, similarly to B_2O_3, activation energies smaller than the activation energy present in the Arrhenius region appear at low temperatures.

Extensive viscosity measurements by the fiber elongation method were made from 10^{11} to 6×10^{14} poises. From this data a lower and more precise value of the activation energy ($E_\eta = 72.3$ kcal/mol) was obtained in the annealing range.

Key Words: Activation energy; annealing; germania glass; index of refraction; relaxation times; thermal expansion; two relaxation model; viscosity.

1. Introduction

In a recent paper [1][1] a two relaxation model was proposed for obtaining distribution of relaxation times from annealing experiments on a borosilicate crown (BSC) glass [2]. Since this model was only applied to a BSC glass, and there was a remote possibility that this glass was immiscible, it was decided to apply this interpretation to similar annealing experiments performed on a one component glass—GeO_2.

Another reason for choosing GeO_2 is that the temperature dependence of its viscosity is almost Arrhenius i.e., $\eta = A \exp(E_\eta/RT)$ [3, 4]. A series of papers by Macedo, Litovitz and others [5, 6, 7, and 8] have connected the transition between Arrhenius and non-Arrhenius behavior with the appearance of a distribution of relaxation times. Thus this study of GeO_2 glass might provide further information into the nature of the distribution of relaxation times.

2. Experimental Procedure

2.1. Sample Preparation

The GeO_2 batch[2] used to make the glass was obtained from the Eagle-Pitcher Company, Semi-Conductor Branch, Miami, Oklahoma. It was specified as "electronic grade." Spectrographic analysis of the GeO_2 batch revealed faint traces (less than 0.0001%) of Ca, Fe, and Pb and traces (less than 0.001%) of Mg and Si. The detection of Al and Cu was questionable.

The GeO_2 batch was melted in a platinum crucible at 1600 °C and refined overnight at 1500 °C. This produced a seed-free glass. The crucible of molten glass was then quickly cooled to room temperature so that the glass could be removed in several large pieces. These pieces were "fine annealed" (cooled at a relatively slow constant rate through the transformation range). Small samples approximately 1 cm square and 1 mm thick were cut from these large pieces for the annealing experiments. Since GeO_2 glass is hygroscopic, kerosene was used not only in the preparation of these small samples but also for storage at room temperature.

2.2. Refractive Index Measurements

All the index measurements were made at room temperature on the Grauer refractometer [9] using the sodium D line. The GeO_2 glass was found to be still hygroscopic at elevated temperatures in the annealing range and under these conditions a white hydrated film formed on the sample and hampered index measurements. The rate of formation of this film was reduced somewhat by flooding the furnace with dry nitrogen gas during the annealing experiments. Even so, this film quite often slowly formed during the longer annealing experiments and prevented accurate index measurements. In order to

[1] Figures in brackets indicate the literature references at the end of this paper.

[2] Certain commercial materials are identified in this paper in order to adequately specify the experimental procedure. In no case does such identification imply recommendation or endorsement by the National Bureau of Standards, nor does it imply that the material identified is necessarily the best available for the purpose.

proceed with the heat treatments the edges of each sample had to be repeatedly ground during the tests. It is recalled [2] that the accuracy of the measured index of refraction depends on the angle between edges being 90° or very close to 90°. This continuous regrinding affected this angle and reduced both the accuracy and the precision of the measurements. As a result there is a larger scatter in the GeO_2 index measurements than those previously reported for BSC glass [2].

2.3. Heat Treatment

The annealing procedure used here is the same as that used for the BSC glass [2]. All samples were held at 600 °C for $\frac{1}{2}$ hr before quenching from the furnace to room temperature. This determined the starting and equilibrium value of index which was the same for all samples. The special rotating-type furnace was then set at some lower temperature in the transformation range, the samples were inserted into the furnace, held for a given time, one sample was dropped out, and its index measured. Then, the sample was reinserted into the furnace, another sample dropped out at a later time and the process was repeated until a complete time-index (approach) curve for each temperature had been established. The insertion into the furnace and release of samples (1 to 9) from the furnace at different time intervals was made without disturbing the temperature stability.

3. Results

3.1. Thermal Expansion

In order to find the transformation region (annealing range) the linear thermal expansion of the GeO_2 glass was measured by the interferometric method [10]. The furnace was heated at the rate of 2 °C per minute from room temperature through the deformation temperature of the germania sample under test. The resulting linear thermal expansion curve is shown in figure 1 and calculated to be 7.70×10^{-6}/°C between 30 and 400 °C. This is in good agreement with Mackenzie [11] and verifies the measurements reported by Dennis and Laubengayer [12]. The deformation point (600 °C) and critical point (505 °C) roughly denote the limits of the annealing range. The annealing range is where structural equilibrium can be reached within reasonable times and lies in the upper part of the transformation region. The low temperature thermal expansion data shown in figure 1, were reported by Spinner and Cleek [13].

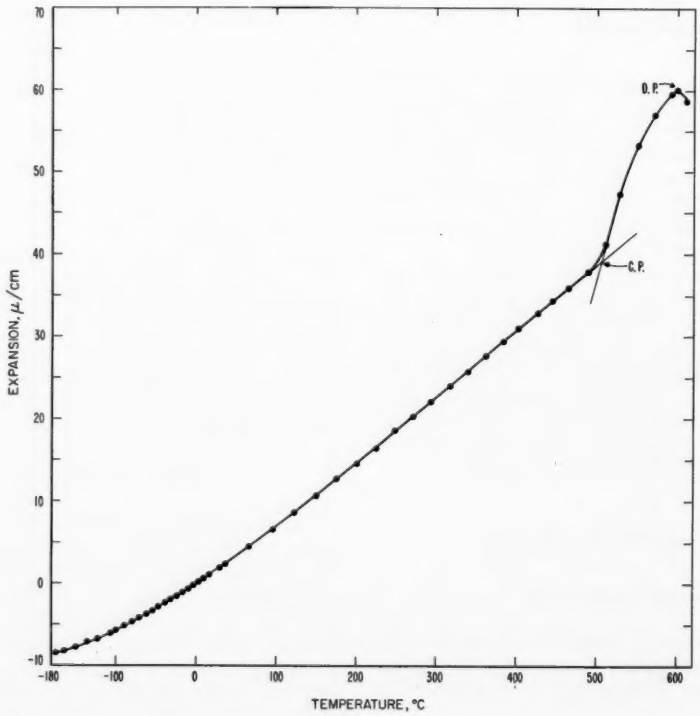

FIGURE 1. *Thermal expansion of vitreous* GeO_2 *showing the critical point and the deformation point.*
Data below 30 °C from ref. (13).

3.2. Approach Curves

The index versus time isotherms for several temperatures in the transformation region are shown in figure 2. All of these curves start at the equilibrium index (1.60500) for 600 °C (deformation point) at zero time. The change in index for each temperature was obtained from 600 to 421 °C within reasonable lengths of time. In addition, two approach curves were obtained for temperatures more than 150 °C below the critical point. One of these (351 °C) is shown plotted in figure 2, and it is noted that the change in index is still quite considerable. At a still lower temperature (250 °C) the change in index was still evident but its rate was too small for the time scale used [$(7\pm1)\times10^{-5}$ in 20 hr] to be plotted in figure 2. As a result, it can be seen from these approach curves that the transformation region of a glass is very difficult to define. For practical experiments, the limits of the deformation point and a temperature of about 75 °C below the critical point will provide enough information in reasonable times for annealing studies. In comparison, for the same change in index for GeO_2 the temperature range is about 1.5 times that of the BSC glass [2] but the changes in index for GeO_2 were observed in about 1/4 of the time scale.

3.3. Equilibrium Index

Equilibrium indices were reached for several temperatures between 600 and 465 °C. These are shown plotted in figure 3. Unlike curves for most optical glasses this curve is not a straight line. It has a definite curvature much larger than any experimental uncertainty. The slope, $\partial N/\partial T$ decreases with increasing temperature. It is reasonable to assume that the expansion coefficient,

$$\alpha = 1/V\frac{\partial V}{\partial T} = C\frac{\partial N}{\partial T}, \tag{1}$$

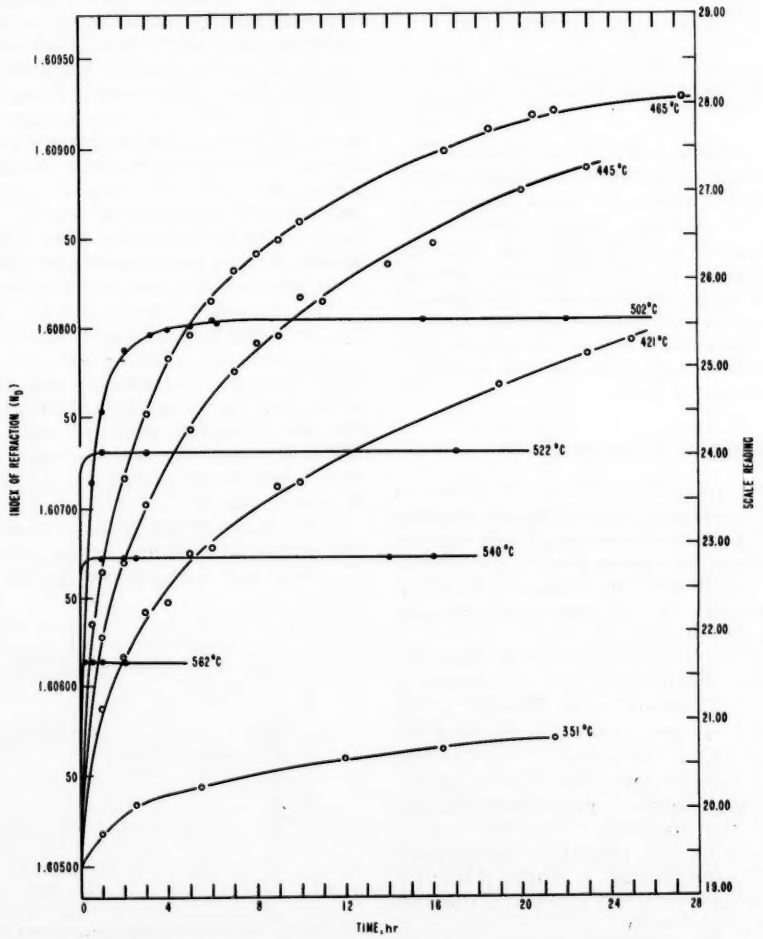

FIGURE 2. *Index of refraction versus time isotherms for vitreous* GeO_2.

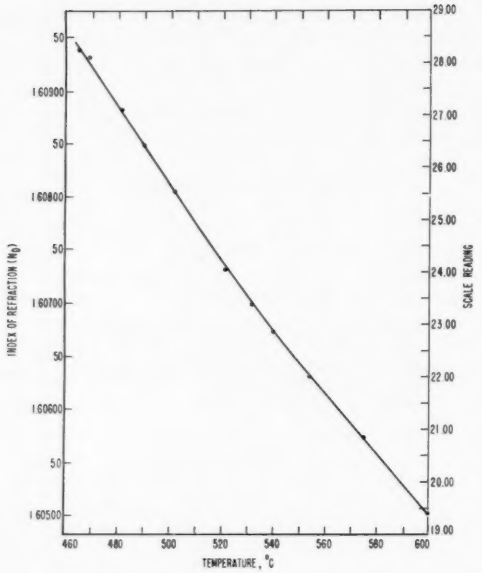

FIGURE 3. *Equilibrium index versus temperature for vitreous* GeO_2.

in which V is the volume, and C is a constant. This leads to α decreasing with increasing temperatures for GeO_2 a behavior contrary to most liquids, but similar to B_2O_3 [14]. Macedo, Capps, and Litovitz [15] attributed this behavior in B_2O_3, to the existence of two states separated by a step in energy, entropy, and volume. Unlike their work, because of the limited temperature range in GeO_2, it is not possible to specify the two states in this case. Even so, the pronounced curvature in figure 3 strongly indicates the existence of a two state structure for GeO_2.

3.4. Spectrum of Relaxation Times

In describing the relaxation curves [1] shown in figure 2 one has to consider both (a) the distribution of relaxation times as linear i.e., nonamplitude dependent and (b) a nonlinear relaxation process i.e., at any instant there is a distribution of relaxation times but at subsequent intervals each relaxation time changes with distance from equilibrium [16].

The existence of both a distribution of relaxation times and nonlinear effects make the calculation of the relaxation time spectrum very difficult if not impossible. In order to circumvent this problem the crossover technique [1, 2] will be used. The thermal history involved in the crossover can best be understood if one first understands the mathematical model used to represent the spectrum. The spectrum is assumed to be given by two relaxation mechanisms of equal strength, each having a single relaxation time. Thus the average index N is given as a function of time by the following relation

$$N = \tfrac{1}{2}\,[M_1(t) + M_2(t)] \qquad (2)$$

where $M_i(t) = N_\infty + N_i \exp(-t/\tau_i)$, in which N_∞ is the equilibrium value of index; N_i, the initial deviation of index from N_∞ associated with mechanism i having relaxation times τ_i. This formulation can be thought of as describing the relaxation (change of volume) to a final equilibrium value following a change in temperature (analogous to an isothermal recovery function) in terms of two separate mechanisms, the first of which relaxes appreciably faster than the second. N_1 and N_2 are measures of the total relaxation undergone by the two separate mechanisms in reaching equilibrium. If the starting point is one of equilibrium $[M_1(0) = M_2(0)]$, the two mechanisms will have to relax the same total amount $N_1 = N_2 = [N_\infty(T_1) - N_\infty(T_2)]$. However, when starting from a nonequilibrium approach curve, N_1 and N_2 will depend on the particular approach curve being followed. Figure 4 due to Macedo and Napolitano [1] shows schematically the time dependence of N, M_1 and M_2 at T_2 for a glass initially at equilibrium at T_1, where $T_1 > T_2$. As the structure rearranges itself to the new equilibrium, M_1 will rise faster since it is associated with the shorter relaxation time τ_1; while M_2 will change more slowly. Thus, around the bend of the approach curve, there will be the largest difference between M_1 and M_2 in the glass. As time progresses, M_1 will reach its equilibrium value for T_2 first and stay there. From then on the spread between M_1 and M_2 narrows because the relaxation process associated with M_2 continuously approaches the same equilibrium but at a slower rate. Finally, when the structure is completely at the new equilibrium, the spread becomes zero, and one has again an equilibrium glass $(M_1 = M_2)$.

The crossover experiment involves taking a glass having index, a, (see fig. 4) from the approach curve and introducing it into a furnace whose temperature is T_x. T_x is preselected such that the equilibrium index at T_x, $N_\infty(T_x)$, is equal to a. Thus at a crossover, a, the fast relaxation time (τ_1) corresponds to an index M_1 higher than the (average) measured value, N, and the slow relaxation time (τ_2) corresponds to an index M_2 lower than N.

If the index at the point of crossover, a, is equal to the equilibrium index at the crossover temperature T_x, then $N_2 = -N_1$. A prerequisite for a minimum in

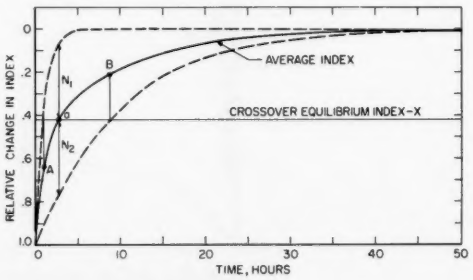

FIGURE 4. *Illustration of two relaxation times (ref.* [1]*) represented by upper and lower dashed curves.*

The average or measured index is given by solid line. The crossover equilibrium index (x) and the transfer point (a) are also shown.

the crossover experiment is that N_1 and N_2 have opposite signs. This is fulfilled when N has a value between A and B in figure 4. Figure 5, from Macedo and Napolitano [1] shows M_1 (the upper curve), M_2 (the lower curve) and N the solid line (calculated index). The agreement of the calculated curve with the actual experimental points for a borosilicate crown glass is seen to be good.

In the first crossover for GeO_2, the glass was held to equilibrium at 600 °C before quenching (see 2.3). The samples were then inserted into the furnace set at 421 °C until their index approximately equaled N_∞ (519 °C). At spaced time intervals, three samples were dropped from the furnace, one having an index equal to N_∞ (519 °C), one with a higher index and one with a lower index. Finally, the temperature of the furnace is reset to 519 °C, the three samples reinserted into the furnace, and successive index readings are then taken after short intervals in the furnace on each of the three samples. The results are plotted in figure 6. As a check for linearity all three curves were fitted with the same relaxation times $\tau_1 = 4.7$ min and $\tau_2 = 18.0$ min, but with different initial values (N_1 and N_2). The dip varied between 0.33 and 0.55 scale divisions as can be seen in figure 6. The fit was equally good for all three curves.

A more drastic check of linearity is to use relaxation times obtained from the crossover to calculate the approach curve. Figure 7 shows an approach curve from 538 to 523 °C. The larger scatter in data is due to the fact that three different samples were used and as previously mentioned hydration was a problem. Since

$$N_1 = N_2 = N_\infty(523\ °C) - N_\infty(538\ °C) \qquad (3)$$

and τ_1 and τ_2 were obtained from the crossover (519 °C) there are no adjustable parameters in this curve.

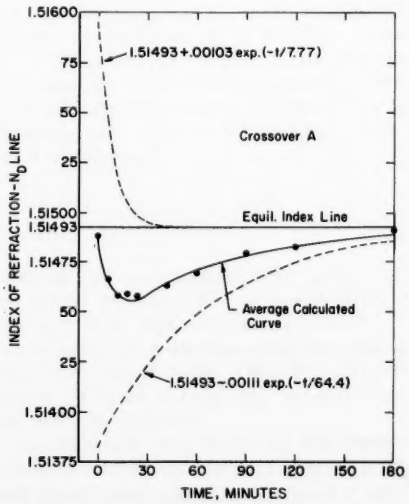

FIGURE 5. *Crossover A for BSC glass (ref. [1], [2]) showing the average of the fast and the slow relaxation processes.*

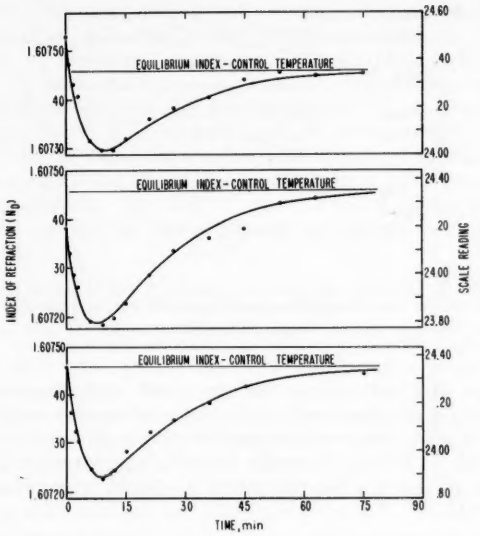

FIGURE 6. *Index versus time for crossover having 421 °C approach samples heat treated at 519 °C.*

Curves represent model with $\tau_1 = 4.7$ min and $\tau_2 = 18.0$ min are compared against experimental data.

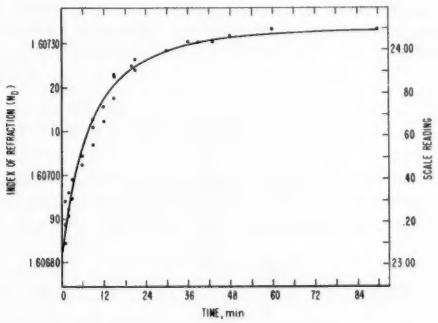

FIGURE 7. *Approach curve for glass in equilibrium at 538 °C to new equilibrium at 523 °C.*

Curve having same relaxation times as crossover in figure 6 is compared with experimental points obtained from three samples of glass.

This shows that the relaxation times were not changing with structural arrangements during the crossover, and that the spectrum obtained from the crossover does represent the full spectrum and not just the short and long times.

In addition two crossovers were measured at 489 °C. One of these with an equilibrium value of index [$1.60500_{600\ °C}$] at zero time, 465 °C approach temperature is shown at the top of figure 8 (curve B). The ratio of the relaxation time was much larger than that of 519 °C where the ratio was 3.8. Since the dip was so shallow it was decided to repeat this experiment selecting two temperatures which would give a deeper dip. Using an equilibrium value of index ($1.60745_{518\ °C}$) at zero time, 428 °C approach temperature and the same 489 °C crossover temperature, the dip was 44

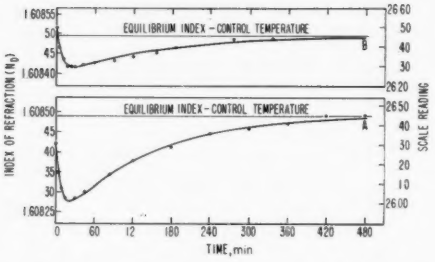

FIGURE 8. *Index versus time for crossover* A *and* B *having equilibrium temperature 489 °C.*

Both curves have the same relaxation times ($\tau_1 = 9.3$ min and $\tau_2 = 130$ min). Sample A came from a 428 °C approach, while samples B came from a 465 °C approach.

scale divisions (curve A) compared with the earlier 15 scale divisions (curve B). Both crossovers could be fitted with the same relaxation times of $\tau_1 = 9.3$ min and $\tau_2 = 130$ min. Thus the ratio of the relaxation times τ_2/τ_1 at 489 °C, 14, was about 3.7 times larger than at 519 °C.

3.5. Viscosity

Low temperature viscosities on the GeO_2 glass were measured by the fiber elongation method [17]. Measurements were made with two types of fiber, flame-drawn and fibers drawn directly from the melt. Since no differences were found in the viscosity values using each type of fiber, all subsequent measurements were made with the flame-drawn fibers because of the ease of fabrication. The measured values are given in table 1 as well as the stabilization or annealing times and melt numbers. Since there was no trend between different melts, they were not distinguished in subsequent treatments.

Figure 9 shows both the data from this work and those of Fontana and Plummer [3] below 600 °C plotted versus reciprocal absolute temperature. In general the data from both laboratories agree with each other. The scatter in the data is about the same for each set of data. Even so, the least squares fit of each set of data gave considerably different activation energies shown in table 2. The solid curve represents the combined fit, which is practically identical to the NBS curve, and has a lower slope than the short dashed line (Fontana and Plummer data below 600 °C fitted to the Arrhenius curve). This probably occurs because Fontana and Plummer have only two data points below 535 °C while NBS has 10 points, one of which was stabilized for 138 hr (481.3 °C).

Fontana and Plummer report that all the data above ~ 650 °C (below 5×10^{10} P) is fitted by an Arrhenius curve with an activation energy of 64.2 kcal/mol (1 cal = 4.184J). This curve is also plotted in figure 9 as the long dashed line. Even though the viscosity has unquestionably departed from the Arrhenius curve it is in the "near" Arrhenius region.

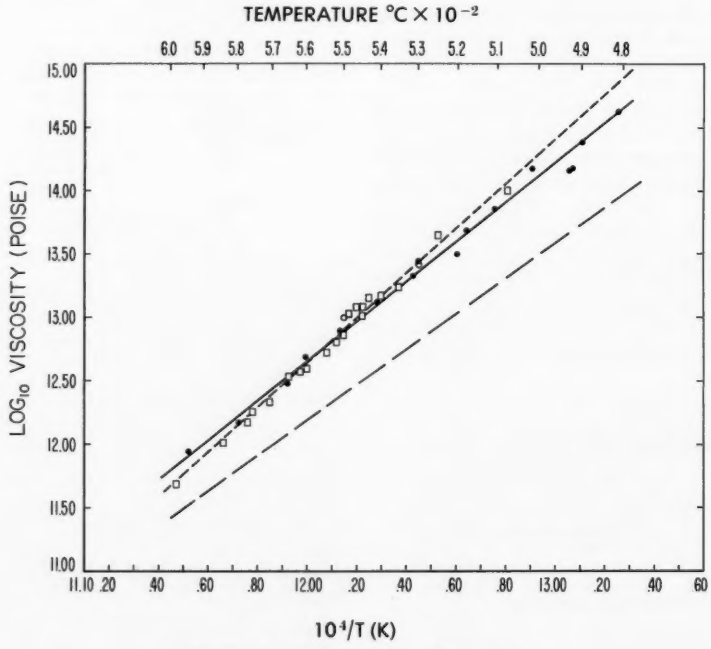

FIGURE 9. *Arrehenius plot of viscosity.*

□, F & P ref. [3].
●, Flame drawn fibers.
○, Fiber drawn from crucible } from present work.
– – –, least squares fit to F & P data.
——, least squares fit of combined data – NBS and F & P.
—— —— ——, least squares fit-extrapolation of high temperature Arrhenius fit of F & P data.

TABLE 1. *Viscosity data for germania glass by the fiber elongation method*

Melt No.	Temp. °C	η	Time held
3	481.3	14.615	138 hr
2	489.7	14.382	8 hr
3	492.0	14.169	23 hr
2	492.9	14.152	71 hr
3	501.9	14.167	17 hr
3	511.1	13.854	17 hr
3	518.3	13.681	2 hr
2	520.1	13.490	3 hr
1	[a] 530	13.408	16 hr
1	530	13.437	21 hr
2	531.3	13.323	18 hr
3	540.9	13.113	16 hr
1	[a] 550.2	12.995	7 hr
3	551.1	12.887	1 hr
3	560.7	12.685	1 hr
2	566.1	12.475	1 hr
1	579.3	12.167	1 hr
3	594.8	11.939	1 hr
1	633.4	10.996	45 min

[a] Fibers drawn from crucible.

TABLE 2. *Coefficients of data from table 1 and reference 3, plotted in figure 9, from the equation* $\ln \eta = A + E_\eta/RT$

	A	E_η kcal/mol	ΔE_η [a] kcal/mol
Fontana and Plummer	−8.646	81.7	1.7
NBS	−5.739	70.6	1.8
Combined	−6.178	72.3	1.5

[a] Standard error of E_η.

4. Discussion

4.1. Comparison of Volume and Shear Relaxation Times

The shear viscosity, η, is given by [18]

$$\eta = G_\infty \int_0^\infty \tau_s g(\tau_s) d\tau_s = G_\infty \bar{\tau}_s \tag{4}$$

where G_∞ is the modulus of shear rigidity. Thus, the temperature dependence of η is either equal to that of $\bar{\tau}_s$ or a little larger depending on the behavior of G_∞. First, one can compare the temperature dependence of the average volume relaxation times $\bar{\tau}_{PT}$ as measured by annealing, with the shear viscosity. The $\bar{\tau}_{PT}$ was calculated according to

$$\bar{\tau}_{PT} = \frac{1}{2}(\tau_1 + \tau_2), \tag{5}$$

remembering our assumption that both mechanisms were weighted equally. The average time ($\bar{\tau}_{PT}$) was 11.4 min at 419 °C and 69.6 min at 489 °C. The ratio is 6.1 as compared with the ratio for the shear viscosity 6.2 for these same two temperatures. This discrepancy is well within the experimental uncertainty of both experiments.

Next the absolute magnitude of the shear and volume relaxation time should be compared. Since the annealing experiments were carried out at atmospheric pressure and constant temperature the volume relaxation time reported above is isobaric isothermal. Because most of the data of this type are obtained by acoustical techniques [19], the proper thermal condition to compare is isochoric, adiabatic ($\bar{\tau}_{vs}$). Unfortunately we do not have the necessary data to perform the transformation (see ref [1]), but we should expect that the ratio of $\bar{\tau}_{PT}/\bar{\tau}_s$ to be larger than $\bar{\tau}_{vs}/\bar{\tau}_s$ because $\bar{\tau}_{PT}/\bar{\tau}_{vs} > 1$ [1]. The average shear relaxation time was calculated by eq (4), using the G_∞ of Strakna et al. [20], and our viscosity data. For 519 °C, $\bar{\tau}_s = 3.7$ min and the ratio, $\bar{\tau}_{PT}/\bar{\tau}_s$ was 3.1, a value in good agreement with other liquids [19].

4.2. Temperature Dependence of Spectrum of Relaxation Times

Unlike BSC glass, the GeO_2 spectrum is temperature dependent. Between 489 and 519 °C the ratio of τ_2/τ_1 changes from 14 to 3.8. The equal weight given to the two relaxation times which was originally assumed is required to fit the data in figures 6, 7, and 8. Thus, the symmetry of the spectrum is characteristic of the data and not a mathematical artifact. Symmetric spectrums can also be represented in terms of Gaussian distributions. Figure 10 shows the equivalent Gaussian distribution of relaxation times

$$g_\tau(\tau) = \frac{b}{\sqrt{\pi}} \exp\,(b \ln \tau/\tau')^2 \tag{6}$$

where the most probable relaxation time, τ', has been set to

$$\tau' = \sqrt{\tau_1 \cdot \tau_2}. \tag{7}$$

The width, b, has been chosen such that the frequency dependence of the real part of the compressibility most closely matches the function obtained from

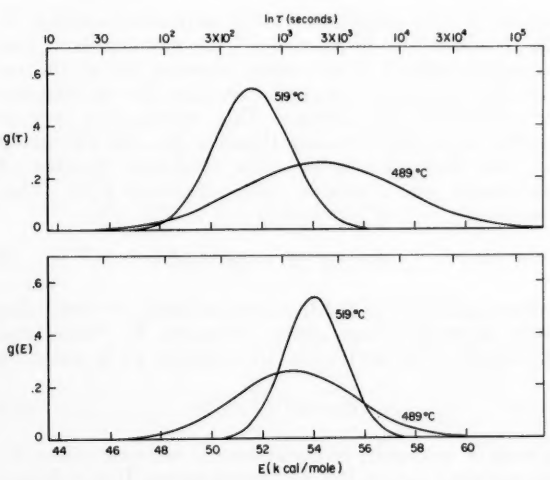

FIGURE 10. *Plot of the relaxation time spectrum and the activation energy distribution.*

Note that since A in eq 10 is unknown the position of the peaks in the activation energy distribution is arbitrary.

$\tau_1 - \tau_2$ calculation [5]. The broadening of the spectrum resembles that observed for B_2O_3 [7]. In B_2O_3 the spectrum is single where the temperature dependence of the viscosity is Arrhenius and it broadens as the viscosity departs from the Arrhenius curve. Thus, a probable explanation for a temperature dependent spectrum is that the measurements were made in the transition zone between Arrhenius and non-Arrhenius region. In fact at 489 °C the viscosity is only a factor of 3.5 above the Arrhenius curve.

The two relaxation time model provides us with four different activation energies. A comparison of the activation energy E_a, associated with the average relaxation time with that for shear viscosity in this temperature range was made and found to be in good agreement. These activation energies are respectively $E_a = 73$ kcal/mol and $E_\eta = 72.3$ kcal/mol. The activation energy E_2 associated with τ_2, the long relaxation time, is 79 kcal/mol which is larger than E_η as would be expected. On the other hand the activation energy E_1, associated with τ_1 the short relaxation time, is 28 kcal/mol. The *surprising fact* here is that E_1 is so much smaller than E_a. In fact it is much smaller than the Arrhenius activation energy for shear viscosity. This confirms the surprising conclusion obtained for B_2O_3 [7] that the cause of the non-Arrhenius region is not a higher average activation but rather the appearance of a distribution of energies some of which are larger than $\bar{E}$. It should be emphasized at this point that not only have higher activation energies appeared but also lower ones.

For better comparison with the B_2O_3 work, Gaussian distributions of activation energies $g_E(E)$ were calculated in the following manner: By using Eyring's rate equation [21]

$$\tau = A \exp(E/RT) \tag{8}$$

where A is a constant; E, the activation energy; T, the temperature in K; and R, the gas constant, and assuming that A is the same constant for all the relaxation spectrum one can calculate the distribution of activation free energy. This assumption is consistent with the viscosity theories [22, 23, 24] which will be discussed below. The fractional number of molecules which relaxes with relaxation time τ_i between $\ln \tau_i - \frac{1}{2}\, d \ln \tau$ and $\ln \tau_i + \frac{1}{2}\, d \ln \tau$ is

$$g_\tau(\tau_i)\, d \ln \tau = g_E(E_i) dE \tag{9}$$

where $g_E(E_i)\, dE$ is the fractional number of molecules with activation free energy between $E_i - \frac{1}{2} dE$ and $E_i + \frac{1}{2} dE$. The activation free energy E_i is given by

$$E_i = RT \ln (\tau_i / A) \tag{10}$$

where A (seconds) is an unknown constant since we do not have data in the Arrhenius region. It was chosen such that the curves superimposed for better comparison. Figure 10 also shows $g_E(E)$ for both temperatures. Note that $g_E(E)$ is a Gaussian in E not in $\ln E$. Thus, the average and most probable values coincide. The distributions shown in figure 10 for GeO_2 agree with the B_2O_3 work.

We have found in GeO_2 supporting evidence that the departure from the Arrhenius curve for viscosity is caused by the appearance of a distribution of relaxation times, and, further, that the associated distribution of activation energies has not only higher activation energies but also lower. The present theories which predict non-Arrhenius behavior are typified by the work of Ree, Ree, and Eyring [22], Adam and Gibbs [23], and Davies and Matheson [24]. These theories picture the molecules as being relatively free at high temperatures in the Arrhenius region, and connect the appearance of non-Arrhenius behavior with some increase in cooperation between molecules, or a loss in certain degrees of freedom as the temperature is lowered. This leads to an increase in apparent activation energies but it is *not* clear how any of these theories can lead to the presence of *smaller* activation energies.

5. Summary

The glass transition region of GeO_2 has been studied by, first, measuring thermal expansion (7.7×10^{-6}/°C) in a slowly heated sample (deformation point 600 °C, critical point 505 °C); second, measuring shear viscosity by fiber elongation (from 10^{11} to 6×10^{14} P); and third, measuring the effect of annealing from index of refraction-time isotherms and the crossover technique. The viscosity values were found to be in good agreement with those of Fontana and Plummer. In view of the more extensive low temperature data in this report a lower and more precise value of the activation energy in the annealing region ($E_\eta = 72.3$ kcal/mol) was obtained. The equilibrium index was not linear with temperature. The negative departure of the slope indicates that the structure of GeO_2 can probably be fitted by a two state model similar to B_2O_3.

The previously reported [1] two relaxation time model was used to analyze the annealing experiment data for GeO_2, and proved to be equally good as in BSC glass. This ruled out the original contention that the two-relaxation model might be due to a two-liquid immiscibility in the BSC glass. Since these experiments were designed with "a priori" knowledge of the mathematical model, very clear evidence of its applicability was demonstrated by comparing a crossover with an approach curve.

Unlike most materials GeO_2 has a spectrum of relaxation times which *is* temperature dependent in the annealing range. This occurs because the viscosity values are only just departing from Arrhenius behavior, and the origin of this departure is the appearance of a distribution of relaxation times. The temperature dependence of the spectrum was analyzed in terms of a distribution of activation energies. A conclusion of this study is that, similar to B_2O_3, activation energies smaller than the activation energy present in the Arrhenius region appear at low temperatures.

We thank J. M. Nivert for preparing the samples; E. G. Hawkins for making the fiber viscosity measurements and E. H. Hamilton (retired) for making the expansion run above room temperature.

6. References

[1] Macedo, P. B., and Napolitano, A., Effects of a distribution of volume relaxation times in the annealing of BSC glass, J. Res. NBS **71A** (Phys. and Chem.) No. 3, 231–238 (1967).

[2] Spinner, S., and Napolitano, A., Further studies in the annealing of a borosilicate glass, J. Res. NBS **70A** (Phys. and Chem.) No. 2, 147–152 (1965).

[3] Fontana, E. H., and Plummer, W. A., A Study of viscosity-temperature relationships in the GeO_2 and SiO_2 systems, Phys. Chem. Glasses **7,** No. 4, 139–146 (1966).

[4] Kurkjan, C. R., and Douglas, R. W., Viscosity of glasses in the system Na_2O-GeO_2, Phys. Chem. Glasses **1,** No. 1, 19–25 (1960).

[5] Macedo, P. B., and Litovitz, T. A., Ultrasonic viscous relaxation in molten boron trioxide, Phys. Chem. Glasses **6,** No. 3, 69–80 (1965).

[6] Litovitz, T. A., and McDuffie, G., Comparison of Dielectric and mechanical relaxation in associated liquids, J. Chem. Phys. **39,** 729 (1963).

[7] Tauke, J., Litovitz, T. A., and Macedo, P. B., Viscous relaxation and non-Arrhenius behavior in B_2O_3, J. Am. Ceram. Soc. **51,** 158–163 (1968).

[8] Litovitz, T. A., and Macedo, P. B., Ultrasonic Relaxation, Viscosity and Free Volume in Molten Glasses, "Phys. of Non-Crystalline Solids", Delft Conference 1964 (North Holland Publishing Co., Amsterdam, pp. 220–228 (1965)).

[9] Grauer, O. W., An improved refractometer, NBS Tech. News Bull. **37** (9) 135 (1953); **38** (4) 63 (1954).

[10] Saunders, J. B., Improved interferometric procedure with application to expansion measurements, J. Res. NBS **23,** 179–195 (1939) RP1227.

[11] Mackenzie, J. D., Density and expansivity of vitreous germania, J. Am. Ceram. Soc. **42,** 310 (1959).

[12] Dennis, L. M., and Laubengayer, A. W., Germanium XVII. Fused germanium dioxide and some germanium glasses, J. Phys. Chem. **30,** No. 11, 1510–1526 (1926).

[13] Spinner, S., and Cleek, G. W., Temperature dependence of Young's modulus of vitreous germania and silica, J. Appl. Phys. **31,** No. 8, 1407–1410 (1960).

[14] Napolitano, A., Macedo, P. B., and Hawkins, E. G., Viscosity and density of boron trioxide, J. Amer. Ceram. Soc. **48,** [12] 613–616 (1965).

[15] Macedo, P. B., Capps, W., and Litovitz, T. A., Two-State Model for the Free Volume of Vitreous B_2O_3, J. Chem. Phys. **44,** 3357–64 (1966).

[16] Condon, E. U., "Comments on—The annealing of flat glass", The Glass Industry **33,** 307, 322–3 (1952).

[17] Napolitano, A., and Hawkins, E. G., Viscosity of a standard soda-lime-silicia glass, J. Res. NBS **68A** (Phys. and Chem.), No. 5, 439–448 (1964).

[18] Herzfeld, K., and Litovitz, T. A., Absorption and Dispersion of Ultrasonic Waves (Academic Press, New York and London 1959).

[19] Litovitz, T. A., and Davis, C. M., *Physical Acoustics,* Vol. **II,** Ch. 5 (Academic Press, New York and London, 1965).

[20] Strakna, R. E., and Savage, H. T., Ultrasonic relaxation loss in SiO_2, GeO_2, B_2O_3, and As_2O_3 glass, J. Appl. Phys. **35,** [5] 1445–50 (1964).

[21] Glasstone, S. N., Laidler, K., and Eyring, A., The Theory of Rate Processes (McGraw-Hill Book Company, Inc., New York, 1941).

[22] Ree, T. S., Ree, T., and Eyring, A., Significant liquid structure theory IX. Properties of dense gases and liquids, Proc. N.A.S., **48,** 501 (1962).

[23] Adam, G., and Gibbs, J. H., On the temperature dependence of cooperative relaxation properties in glass-forming liquids, J. Chem. Phys. **43,** 139 (1965).

[24] Davies, D. B., and Matheson, A. J., Influence of molecular rotation of the viscosity of liquids, J. Chem. Phys. **45,** 1000 (1966).

(Paper 72A4–509)

JOURNAL OF RESEARCH of the National Bureau of Standards—A. Physics and Chemistry
Vol. 72A, No. 4, July–August 1968

Resumé of Values of the Faraday

Walter J. Hamer

Institute for Basic Standards, National Bureau of Standards, Washington, D.C. 20234

(April 30, 1968)

A resumé is given of the determinations of the value of the Faraday. Values obtained by silver deposition, iodide oxidation, oxalate oxidation, the omegatron, and silver dissolution are reviewed. All values are converted to the unified ^{12}C international scale of atomic weights using the international atomic weights of 1967. Values of the Faraday are given in terms of both the NBS (legal) and absolute units of electrical measure. In the latter the new value for the acceleration due to gravity is used in computing the absolute value of electric current. On this basis and using the atomic weight of silver determined by Shields, Craig, and Dibeler, and converting to the ^{12}C scale, the value of the Faraday is 96,486.9 ± 1.6 absolute coulombs per gram-equivalent which differs by only 1 part per million from the value recommended by the National Academy of Sciences—National Research Council. If the atomic weight of silver recommended in 1967 by the International Atomic Weight Commission is used, the Faraday on the new gravity value is 96,486.5 ± 1.6 absolute coulombs per gram-equivalent which differs by 5 parts per million from that recommended by the National Academy of Sciences—National Research Council. No change in the value of the Faraday adopted by the NAS—NRC Committee is recommended.

Key Words: Coulometers; Faraday; inclusions in silver coulometers; values of Faraday.

In 1962, Remy [1][1] in a review article converted all published values of the Faraday to the 1961 unified ^{12}C scale of atomic weights. In so doing, he used the international atomic weights of 1961 and several inappropriate conversion factors. It is the purpose of this resumé to clarify this matter and to bring the values of the Faraday as determined by various experimenters, up to date. International atomic weights of 1967 are used.

1. Silver Deposition Method

The classical method for the determination of the Faraday involves the electrolytic deposition of silver on platinum from an aqueous solution of silver nitrate. This method has been extensively studied and under closely specified conditions was used for many years in defining the international ampere. The international ampere was defined as that steady or unvarying current which when passed through a solution of silver nitrate in water deposits 1.11800 mg of silver per second [2]. This definition became the definition of the international ampere in the United States by Public Law 105 passed by the 53rd U.S. Congress [3]. The value of the Faraday on this basis, using the 1967 international atomic weight of silver [4],[2] is then:

$$F = \frac{107.868 \pm 0.001}{0.00111800} = 96{,}483.0 \pm 0.9 \text{ int C g-equiv}^{-1},$$

where the ±0.001 represents the "experimental uncertainty" in the atomic weight of silver.

At the time the above definition was formulated it was realized that additional and more accurate measurements were needed to place the electrical units more closely on the theoretical MKSA electromagnetic units. By 1948, after interruptions caused by the two World Wars and after improvements in techniques, an accurate determination of the electrical quantities in centimeter-gram-second electromagnetic units was achieved and on January 1, 1948, changes from international to absolute units were officially made internationally. These conversion factors for the volt, ohm, ampere, and coulomb were as follows:

1 mean international volt
= 1.00034 absolute volts

1 mean international ohm
= 1.00049 absolute ohms

1 mean international ampere
= 0.99985 absolute ampere

[1] Figures in brackets indicate the literature references at the end of this paper.

[2] This value is based on the mass spectrometer measurements of Shields, Craig, and Dibeler [5]. On the ^{16}O physical scale of atomic weights they obtained 107.9028 ± 0.0013 which on the ^{16}C scale becomes 107.8685 ± 0.0013 using 1.000317917 ± 17 × 10^{-9} to convert from the physical to the ^{12}C unified scale of atomic weights. The International Atomic Weight Commission rounded this value to 107.868 in 1965 and proposed the same value in 1967 [4]. See also footnote i of table 2.

1 mean international coulomb
$= 0.99985$ absolute coulomb

These factors were based on the conversion factors found by the various national laboratories and would be applied only by an international laboratory such as the Bureau International des Poids et Mesures (BIPM), Sèvres, France. The factors for the various countries differed from the means given above and for the United States were [6]:

1 international volt (USA)
$= 1.00033$ absolute volts

1 international ohm (USA)
$= 1.000495$ absolute ohms

1 international ampere (USA)
$= 0.999835$ absolute ampere

1 international coulomb (USA)
$= 0.999835$ absolute coulomb

Accordingly, the Faraday as given by silver deposition, in absolute units in the USA is:

$$F = \frac{(107.868 \pm 0.001)(0.999835)}{0.00111800}$$

$$= 96467.1 \pm 0.9 \text{ abs C g-equiv}^{-1}.$$

Since the measurements were made in the USA the USA conversion factor given above must be used.

During the decades that the international ampere was defined as above, it became generally recognized that the value 1.11800 mg for the *electrochemical equivalent of silver* was too high owing to inclusions present in the silver deposited in the silver coulometer. Extensive work was carried out to ascertain the exact magnitude of these inclusions using various types of silver coulometers. Three methods were employed: (1) determination of the loss in weight of the deposit on heating to redness, (2) direct analysis of volatile material of the deposit on heating, and (3) direct analysis of the deposited silver for its silver content.

In method No. (2) Duschak and Hulett [7] detached the silver crystals from the platinum crucible and placed them in a glass tube provided with a manometer and a small side tube, after which the tube was evacuated and sealed. The crystals were heated and the pressure measured before and after the water vapor present was condensed in the side tube. Hulett later pointed out that the results of this method were uncertain because of the possibility that some of the gases expelled may have come from the glass container. Laird and Hulett [8] at a later time attempted to avoid this difficulty by dissolving the crystals in molten tin at 400 to 500 °C. As before, by working in an evacuated system, the volatile inclusions which were insoluble in the molten tin were measured by fractional condensation. In method No. (3) the crystals were dissolved in nitric acid and the silver precipitated as chloride or bromide.

A summary of the results obtained by these three methods is given in table 1. Scott [21] from a review

TABLE 1. *Amounts of inclusions in silver deposits in silver coulometers*

Year	Experimenters	Method	Number of experiments	Results	
				Mean	Range
				Percent	*Percent*
1884	Rayleigh and Sidgwick [9]	[a] (1)	[b] 20	0.0108	0.028
1886	Gray [10]	[a] (1)		[c]	
1902	Richards and Heimrod [11]	[a] (1)	12	0.018	0.027
1906	Van Dijk [12]	[a] (1)	7	.000	.015
1908	Ayrton, Mather, and Smith [13]	[a] (1)	[d] 11	.000	
1912	Boltzmann [14]	[a] (1)	19	.024	.0113
1915	Jaeger and von Steinwehr [15]	[a] (1)	18	.0008	.007
1915	Richards and Anderegg [16]	[a] (1)	27	.0139	.0313
1916	Vinal and Bovard [17]*	[a] (1)	25	.0040	.0081
1905	Duschak and Hulett [7]	[a] (2)	[f] 8	0.0079	0.0052
1912	Laird and Hulett [8]	[a] (2)	[g] 15	.0051	.0055
1917	Bovard and Hulett [18]	[a] (2)	19	.0113	.0304
1899	Richards, Collins, and Heimrod [19]	[a] (3)	7	[h] 0.006	0.026
1915	Richards and Anderegg [16]	[e] (3)	7	[i] .0141	.0070
	mean (weighted by number of experiments)[c, d, f] = 0.0102 ± 0.0014				

[a] Number refers to number of method given in text.
[b] Two additional experiments gave abnormally high results; the silver nitrate solution had been filtered through silver acetate. For two more experiments the deposit was not heated to redness.
[c] Gray gave no quantitative data and merely stated that "a plate will . . . be found to lose slightly in weight if heated to redness"; omitted from mean.
[d] Heated 8 deposits to 240 °C only and 3 only to 400 °C; omitted from mean.
[e] Rosa, Vinal, and McDaniel [20] previously made some experiments on inclusions, but considered their results inconclusive.
[f] As Hulett later pointed out this method gave uncertain results because of the possibility that some of the expelled gases may have come from the glass container; omitted from mean.
[g] Laird and Hulett made 20 measurements but determined only water in first five deposits.
[h] Richards, Collins, and Heimrod originally reported 0.007 percent but van Dijk [12] uncovered an error in their computations which when corrected gave 0.006 percent for the inclusions; see also, Laird and Hulett [8].
[i] This becomes 0.0119 on the presently (1967) accepted values for the atomic weights of silver and chlorine.

of these results concluded that the amount of inclusions varies from 0.006 to 0.016 percent and like Richards and Anderegg [16] stated that there is "little prospect at this time of finding a universally applicable correction for inclusions in silver deposits." Although most of Richard's results are higher than those of others, they have been included in the mean value, given in table 1. An unequivocal value for the uncertainty of the mean is difficult to arrive at but an uncertainty based on the standard deviation of the mean of all the 176 experimental data is considered as good as any other choice.

The mean of data in table 1 is 0.0102 ± 0.0014 percent. Accordingly, the denominator of the above equation must be multiplied by $1 - 0.000102$ (± 0.000014) or 0.999898 ± 0.000014, hence:

$$F = \frac{(107.868 \pm 0.001)(0.999835)}{(0.00111800)(0.999898 \pm 0.000014)}$$

$$= 96476.9 \pm 2.3 \text{ abs C g-equiv}^{-1} \qquad (1)$$

Remy [1] used Richards and Anderegg's value of 0.0155 percent for the inclusions obtained with coulometers using roughened porous crucibles. Richards and Anderegg used the heating method to

determine the amount of inclusions. Although this higher value for inclusions leads to better agreement with subsequent determinations of the Faraday by other methods its selection over the others cannot be justified, a posteriori. If a single group of determinations were to be selected that of Vinal and Bovard [17], namely, 0.0040 percent, should be chosen since it was arrived at by the same procedures and in the same laboratory where the Faraday was determined by silver deposition.

2. Iodide Oxidation Method

In 1916 Vinal and Bates [22, 23] made a direct comparison of the silver and iodine coulometers in the laboratories of NBS. The silver coulometer was used to establish the charge in international units and in 6 of 10 experiments the international coulombs were determined directly from the duration of the run and values of standard cells and standard resistors known in international units. A weighted mean of the 10 experiments gave 0.850176 ± 0.000009 for the ratio of the weight of silver deposited to the weight of iodine liberated. A weighted mean of the 6 experiments in which the coulombs were determined directly in terms of the duration of the run, the standard cells, and standard resistors gave 1.315008 ± 0.000014 for the electrochemical equivalent of iodine. In each case the uncertainty is based on a 95 percent confidence limit in terms of the standard deviation of the mean value. Using the 1967 international atomic weight of iodine, 126.9044, the Faraday in absolute units is, in each case:

$$F = \frac{(0.850176 \pm 0.000009)\,(126.9044)\,(0.999835)}{.00111800} = 96487.7 \pm 1.0 \text{ abs C g-equiv}^{-1}, \quad (2)$$

$$F = \frac{(126.9044)\,(0.999835)}{1.315008 \pm 0.000014} = 96488.7 \pm 1.0 \text{ abs C g-equiv}^{-1}. \quad (3)$$

3. Oxalate Oxidation Method

In 1953, Craig and Hoffman [24] determined the Faraday in absolute units by the electrolytic oxidation of oxalate ions in aqueous solutions of sulfuric acid using gold electrodes. They obtained 96492 ± 3 for the Faraday using 67.007 for the equivalent weight of sodium oxalate based on the international chemical atomic weights of 1950 [25] where the uncertainty is presumed to be a probable error. Using the 1967 atomic weights their value of the Faraday becomes:

$$F = (96492 \pm 3)\left(\frac{66.99975}{67.007}\right) = 96{,}481.6 \pm 3.0 \text{ abs C g-equiv}^{-1} \quad (4)$$

where the second parenthesis encloses the ratio of the ^{12}C unified equivalent weight of $Na_2C_2O_4$ to that used by Craig and Hoffman. Remy [1] used an incorrect correction factor in converting Craig and Hoffman's equivalent weight of $Na_2C_2O_4$ based on the 1950 international atomic weights [25] to the ^{12}C unified scale. Furthermore, he converted the value from the NBS (legal)[3] scale to the absolute value using the relation 1 NBS ampere $= 1.000010 \pm 0.000005$ absolute amperes [26]; more on this point is given later.

4. Omegatron Method

Also in 1953 Sommer and Hipple reported a value for the Faraday from measurements made with the omegatron, a special type of cyclotron [27], in which protons are accelerated to a maximum orbital radius of about one centimeter. In this method a knowledge of the values of the proton rest mass 1.00727663(8)u, the ratio of the proton magnetic moment and the nuclear magneton 2.79276(2), and the gyromagnetic ratio of the proton $2.675192(7) \times 10^8$ rad s^{-1} T^{-1} are needed. The latter two values include corrections for diamagnetic effects present in the original measurements [28]. The values listed above are the most recent ones [29], and the numbers in parentheses represent the uncertainty in the last decimal. Using these values the Faraday is:

$$F = \frac{1.00727663(8) \times 2.675192(7) \cdot 10^8}{2.79276(2) \cdot 10^3} = 96487.3 \pm 0.9 \text{ abs C g-equiv}^{-1}. \quad (5)^4$$

5. Silver Dissolution Method

Finally, in 1960, Craig, Hoffman, Law, and Hamer [30] reported a value for the Faraday based on the electrolytic dissolution of metallic silver in aqueous solutions of perchloric acid. Their value corrected to the ^{12}C unified scale of international atomic weights (107.868 for Ag, see footnote 2) is:

$$F = 96485.4 \pm 2.4 \text{ abs C g-equiv}^{-1} \quad (6)$$

where the uncertainties are overall limits of error. (See footnote 6 given later.)

A summary of these six values for the Faraday are given in column 2 of table 2.

During the late 1950's Driscoll and Cutkosky [26] as a result of measurements with a current balance and a Pellat electrodynamometer reported that:

$$1 \text{ NBS ampere} = 1.000010 \pm 0.000005 \text{ absolute amperes}. \quad (7)^5$$

[3] The NBS (legal) ampere in the United States is maintained by the ratio of the values of standard cells and standard resistors as maintained by the National Bureau of Standards.

[4] Sommer and Hipple [27] in their original paper gave an uncertainty of 3.0 C g-equiv^{-1} which was "estimated to be several times the probable error"; the uncertainties given here are those cited by Cohen and DuMond [29]. Also see footnote [6] of table 2.

[5] The NBS ampere is also known in the United States as the legal ampere and the above relation is a final adjustment needed to bring the legal ampere to the theoretical or absolute MKSA units.

TABLE 2. *Summary of values for the Faraday*

Method	Values		
	U.S. legal basis	Absolute basis 1 [a]	Absolute basis 2 [b]
	(coulombs per gram-equivalent)		
Silver deposition	96476.9 ± 2.3 (eq 1)	96478.1 ± 2.3	96478.0 ± 2.3
Iodide oxidation [c]	96487.7 ± 1.0 (eq 2)	96488.9 ± 1.0	96488.8 ± 1.0
Iodide oxidation [d]	96488.7 ± 1.0 (eq 3)	96489.9 ± 1.0	96489.8 ± 1.0
Oxalate oxidation	96481.6 ± 3.0 (eq 4)	96482.8 ± 3.0	96482.7 ± 3.0
Omegatron	[g] 96487.3 ± 0.9 (eq 5)	96486.1 ± 0.9	96486.2 ± 0.9
Silver dissolution	96485.4 ± 2.4 (eq 6)	96486.6 ± 2.4	96486.5 ± 2.4
Silver dissolution [e]	96485.4 ± 1.6	96486.6 ± 1.6	96486.5 ± 1.6
Silver dissolution [e, f]	96485.8 ± 1.6	[h] 96487.0 ± 1.6 [i]	96486.9 ± 1.6

[a] Based on the relation 1 NBS ampere = 1.000012 absolute ampere.
[b] Based on the relation 1 NBS ampere = 1.000011 absolute ampere.
[c] Based on the silver/iodine weight ratio.
[d] Based on coulombs used to liberate iodine.
[e] Based only on the vacuum values of Craig, Hoffman, Law, and Hamer [30].
[f] Using 107.8685 (see footnote 2) for the atomic weight of silver.
[g] The original value corrected for ^{12}C, ω_s/ω_c in water and for a new value for the gyromagnetic ratio of the proton is 1.1 greater than the value given here.
[h] Value recommended by the National Academy of Sciences – National Research Council [31].
[i] Cohen and DuMond [28] by using an atomic weight of 107.86827 ± 0.00030 obtained 96486.82 ± 0.66. They based their atomic weight on the nuclidic mass values for the two isotopes of silver given by Everling, König, Mattauch, and Wapstra [34], a weighted mean of the abundance ratios determined by Shields, Craig, and Dibeler [5], and Shields, Garner, and Dibeler [35], and a value of 1.1179722 ± 0.0000070 mg C^{-1} for the electrochemical equivalent of silver based on the NBS results.

The uncertainty, here given, is a "50 percent error" as cited by the authors. In these measurements they used a value for gravity 17 ppm lower than that derived from Potsdam. Later studies showed that −13 ppm was a better correction to the value derived from Potsdam. Using this correction:

1 NBS ampere = 1.000012

$$\pm 0.000005 \text{ absolute amperes.} \quad (8)$$

This was the correction accepted and used by the Committee of the National Academy of Sciences – National Research Council which in 1963 issued a consistent set of physical constants [31]. Using this factor, accepting the value of the Faraday as given by the silver-dissolution method (equation 6 above) and accepting the *unrounded* value of the atomic weight of silver as determined by Shields, Craig, and Dibeler [5], namely 107.8685 ± 0.0013 on ^{12}C scale, the NAS–NRC committee recommended:

$$F = 96487.0 \pm 1.6 \text{ abs C mol}^{-1} \quad (9)$$

for the Faraday.[6]

If the internationally recommended value for the atomic weight of silver, namely, 107.868 ± 0.001 is used, the value in equation 9 becomes 96486.6 abs C mol^{-1}.

In column 3 of table 2 are listed the values all converted to the absolute base using the relation of equation 8. The conversion factor from NBS (legal) to absolute units is assumed to apply throughout. This assumption is consistent with the known stability of standard resistors [32, 3] and standard cells [33] used to define the NBS (legal) ampere. A value given by Cohen and DuMond is discussed in footnote i of table 2.

[6] The NAS–NRC committee actually accepted only the vacuum values of Craig, Hoffman, et al. [30], i.e., results obtained with silver melted in *vacuo*. The mean of these, however, agreed with the total mean of these authors but the vacuum values showed less spread, thus the lower uncertainty given in equation 9. The NAS–NRC committee also defined the Faraday in terms of a mole of electrons or singly charged ions.

In 1966–68, Tate [36, 37] reported on a new determination of acceleration due to gravity at the National Bureau of Standards. He gave 980.1018 cm/s² for absolute gravity from which a value of 980.0834 cm/s² is derived for the pier site at the old location of NBS in Washington, D.C., where the absolute current measurements are performed. This value leads to

1 NBS ampere = 1.000011

$$\pm 0.000005 \text{ absolute amperes.} \quad (10)$$

The values in the last column of table 2 were obtained from this relation. This conversion factor is the same as the one given by Terrien [32] of the International Bureau on Weights and Measures.[7]

Since the apparent correction for the acceleration due to gravity and the uncertainty in the correction for the relation between the NBS and absolute ampere are of the order of 1 ppm, the value of the Faraday presently recommended by the National Academy of Sciences – National Research Council (underscored value in column 3 of table 2) should be retained.

The author wishes to acknowledge that Footnote 7 contained in this paper was submitted by Dr. Forest K. Harris. His contribution is gratefully appreciated.

[7] A new ampere determination, using a Pellat dynamometer, has just been completed at NBS by Driscoll and Olsen, but has not yet been published. Prior to this determination, a number of modifications were made on the dynamometer to improve its performance, and the resulting value is in better agreement with the value published in 1958 by Driscoll and Cutkosky, using the NBS Current Balance. Accepting the value of gravity used for the ampere determinations reported in 1958, and taking the mean of the 1958 NBS current balance determination and the 1968 Pellat dynamometer determination, one may say that

1 NBS ampere = 1.000009 ± 0.000005 absolute amperes.

If one uses Tate's value of gravity [36, 37] rather than the Dryden reduction (17 ppm below Potsdam), one would say that

1 NBS ampere = 1.000010 ± 0.000005 absolute amperes.

It seems likely that this latter value must be considered together with that reported by Vigoureux in 1965 [38], before the Advisory Committee for Electricity of the International Committee of Weights and Measures makes a final recommendation on the value to be adopted.

6. References

[1] Remy, H., Chemiker-Ztg. **86,** 167 (1962).
[2] Report of the Chicago International Electrical Congress, 1893, Reports of the Electrical Standards Committee of the British Association, p. 469, Cambridge University Press, 1913.
[3] Hamer, W. J., Standard Cells, Their Construction, Maintenance, and Characteristics, NBS Mono. **84,** Appendix 1, 1965.
[4] Compt. rendu, XXIV Conference International Union of Pure and Applied Chemistry, Prague, 4–10 Sept. 1967.
[5] Shields, W. R., Craig, D. N., and Dibeler, V. H., J. Am. Chem. Soc., **82,** 5033 (1960).
[6] Announcement of Changes in Electrical and Photometric Units, NBS Circ. C459 (1947).
[7] Duschak, L. H., and Hulett, G. A., Trans. Am. Electrochem. Soc., **12,** 257 (1907).
[8] Laird, J. S., and Hulett, G. A., Trans. Am. Electrochem. Soc., **22,** 345 (1912).
[9] Rayleigh, Lord, and Sidgwick, Mrs. H., Phil. Trans. Roy. Soc. London Ser. **A, 175,** 438 (1884).
[10] Gray, T., Phil. Mag. **22,** 399 (1886).
[11] Richards, T. W., and Heimrod, J. W., Z. Physik. Chem., **41,** 323 (1902).
[12] Van Dijk, G., Ann. Physik. **19,** No. 4, 266 (1906).
[13] Ayrton, W. E., Mather, T., and Smith, F. E., Phil. Trans. Roy. Soc. London Ser. **A, 207,** 570 (1908).
[14] Boltzmann, A., Sitzber. Akad. Wiss., Wien., **121,** 1062 (1912).
[15] Jaeger, W., and von Steinwehr, H., Z. Instrumentenk. **35,** 226 (1915).
[16] Richards, T. W., and Anderegg, F. O., J. Am. Chem. Soc., **37,** 7 (1915).
[17] Vinal, G. W., and Bovard, W. M., Bull. BS **13,** 147, S271 (1916).
[18] Bovard, W. M., and Hulett, G. A., J. Am. Chem. Soc., **39,** 1077 (1917).
[19] Richards, T. W., Collins, E., and Heimrod, J. W., Proc. Am. Acad. Art. Sci., **35,** 123 (1899).
[20] Rosa, E. B., Vinal, G. W., and McDaniel, A. S., Bull. BS **10,** 475, S220 (1914).
[21] Scott, A. F., Electrochemical Constants, NBS Circ. 524, ch. 1 (1953).
[22] Vinal, G. W., and Bates, S. J., Bull. BS **10,** 425, S218 (1914).
[23] Bates, S. J., and Vinal, G. W., J. Am Chem. Soc., **36,** 916 (1914).
[24] Craig, D. N., and Hoffman, J. I., Electrochemical Constants, NBS Circ. 524 ch. 2 (1953).
[25] Wichers, E., J. Am. Chem. Soc., **72,** 1432 (1950).
[26] Driscoll, R. L., and Cutkosky, R. D., J. Res. NBS **60,** 297 (1958) RP2846.
[27] Sommer, H., and Hipple, J. A., Electrochemical Constants, NBS Circ. 524, ch. 3 (1953).
[28] Cohen, E. R., and DuMond, J. W. M., Rev. Mod. Phys. **37,** 537 (1965).
[29] Cohen, E. R., and DuMond, J. W. M., Handbook of Physics, 2d ed., Editors, E. W. Condon and H. Odishaw, Part 7, ch. 10 (McGraw-Hill Book Co., New York, 1967).
[30] Craig, D. N., Hoffman, J. I., Law, C. A., and Hamer, W. J., J. Res. NBS **64A** (Phys. and Chem.) No. 5, 381 (1960).
[31] New Values for the Physical Constants-Recommended by NAS–NRC, NBS Tech. News Bull. **47,** No. 10 (1963); Consistent Set of Physical Constants Proposed, Chem. & Eng. News **41,** No. 46, 43, (Nov. 18, 1963).
[32] Terrien, J., IEEE Trans. Inst. & Meas. IM–**15,** No. 4, Dec. 1966.
[33] Hamer, W. J., Instr. Soc. Am., M2–1–Mestind–67, Sept. 11–14, 1967, Chicago, Ill.
[34] Everling, F., König, L. A., Mattauch, J. H. E., and Wapstra, A. H., Nucl. Phys. **15,** 342 (1960); **18,** 529 (1960).
[35] Shields, W. R., Garner, E. L., and Dibeler, V. H., J. Res. NBS **66A** (Phys. and Chem.) No. 1, 1 (1962).
[36] Tate, D. R., J. Res. NBS **70C** (Engr. and Instr.), No. 2, 149, (1966).
[37] Tate, D. R., J. Res. NBS **70C** (Engr. and Instr.), No. 1, 1 (1968).
[38] Vigoureux, P., Metrologia **1,** 1, 3 (1965).

(Paper 72A4–510)

JOURNAL OF RESEARCH of the National Bureau of Standards—A. Physics and Chemistry
Vol. 72A, No. 4, July–August 1968

Publications of the National Bureau of Standards*

Selected Abstracts

Ausloos, P., **Chemical changes induced by high energy radiation. The present state of our knowledge,** *Scientia CII, 1–14 (Sept.–Oct. 1967).*
The chemical changes in matter brought about by absorption of low energy radiation such as visible and ultraviolet light have been intensively investigated for several decades. On the other hand, the chemical transformations induced by high energy radiation (X, gamma, β, α-rays) were long considered to be of such complexity that the task of unravelling them was considered insurmountably difficult. However, during the last decade, impressive advances have been made towards achieving an understanding of the fundamental chemical processes induced by high energy radiation. Many experimental techniques, some of which are new and some of which have been used in other areas of physics or physical chemistry, have now been brought to bear on the problem. Through these various approaches definitive information has been obtained concerning the existence and reactions of the various highly reactive intermediate species (radicals, ions, excited molecules produced by high energy radiation. The understanding of such systems has now reached a degree of sophistication such that high energy radiation can be used to obtain accurate information about various well defined chemical and physical processes which are of general scientific interest.

Key Words: Chemical changes; free radical reactions; high-energy radiation; ion-molecule reactions.

Balling, L. C., **g_I/g_J ratios of Rb^{85} and Rb^{87},** *Phys. Rev.* **163,** *No. 1, 114–118 (Nov. 5, 1967).*
An optical pumping experiment has been performed to measure $g_I/g_J(Rb^{85})$ and $g_I/g_J(Rb^{87})$. The measurements were made in a magnetic field of 40 G. The field was produced by a precision wound solenoid surrounded by three concentric magnetic shields. The magnetic field varied by 3 parts in 10^6 over the volume of the optical pumping cells. The optical pumping cells were filled with various pressures of helium and neon buffer gases. The measured ratios did not depend upon the nature or pressure of the buffer gas. The results of the measurements were:

$$g_I/g_J(Rb^{85}) = -1.46648(8) \times 10^{-4};$$
$$g_I/g_J(Rb^{87}) = -4.96997(9) \times 10^{-4}.$$

Key Words: g-factor; nuclear moment; optical pumping; rubidium.

Bender, P. L., **Radio reflection by free radicals in earth's atmosphere,** *Science* **158,** *No. 3807, 1487–1488 (Dec. 15, 1967).*
The suggestion by Barry, Coleman, Libby, and Libby that some of the signals observed by the Alouette II satellite were due to stimulated emission of magnetic dipole radiation from free radicals is shown to be incorrect.

Key Words: Alouette II satellite; earth's atmosphere; free radicals; magnetic dipole radiation.

Berman, H. A., West, E. D., and Rozner, A. G., **Anomalous heat capacity of TiNi,** *J. Appl. Phys.* **38,** *No. 11, 4473–4476 (Oct. 1967).*
Calorimetric measurements on a sample of TiNi (50 atomic percent Ti) show that the heat-capacity maximum at approximately 87 °C represents a higher-order transition. The transition was shifted to lower temperatures each time the material was heated through the transition from slightly above room temperature to about 150–200 °C. The transition enthalpy decreased in three such cycles from 4150 to 3375 J/mole TiNi.

Key Words: Titanium-nickel heat capacity; titanium-nickel phase transition.

Brady, E. L., and Wallenstein, M. B., **The national standard reference data system,** *Science* **156,** *No. 3776, 754–762 (May 12, 1967).*
The National Standard Reference Data System is a government-wide effort to give to the technical community of the United States optimum access to the quantitative data of physical science, critically evaluated and compiled for convenience. This program was established in 1963 through action of the President's Office of Science and Technology and the Federal Council for Science and Technology, acting upon the recommendation of FCST's Committee on Scientific and Technical Information. The National Bureau of Standards has been assigned responsibility for administering the effort. The general objective of the System is to coordinate and integrate existing data evaluation and compilation activities into a systematic, comprehensive program, supplementing and expanding technical coverage when necessary, establishing and maintaining standards for the output of the participating groups, and providing mechanisms for the dissemination of the output as required.

Key Words: Critical evaluation; information centers; information services; NSRDS; physical properties; standard reference data.

Brauer, G. M., **New developments in zinc oxide-eugenol cement,** *Ann. Dentistry* **26,** *No. 2, 44–50 (1967).*
During the last few years considerable interest has been generated in improving zinc oxide-eugenol materials. A better understanding of the setting mechanism of these cements has become available which has lead to the development of modified ZOE cements usually containing *o*-ethoxy-benzoic acid (EBA). These materials show reactions to the tissues including the dental pulp similar to ZOE cements. Physical properties of the EBA containing cements approach those of the biologically less desirable zinc phosphate cements.

Key Words: Dental cements; dental materials; EBA cements; new developments in dental materials; zinc oxide eugenol cements.

Brehm, B., Gusinow, M. A., and Hall, J. L., **Electron affinity of helium via laser photodetachment of its negative ion,** *Phys. Rev. Letters* **19,** *No. 13, 737–741 (Sept. 5, 1967).*
We have measured the electron affinity of helium (2^3S) using the technique of energy analysis of electrons photodetached from a beam of negative ions by monochromatic (laser) light. Uncertainties in the contact potentials are eliminated by comparison with an ion of known affinity (H^-). The $4P_{5/2}$ state of He^- is found to be bound with respect to the 2^3S state of neutral helium by 80.0 millivolts, with a probable error of 2 millivolts.

Key Words: Electron affinity; electrons; energy analysis; helium; laser photodetachment; monochromatic (laser) light; negative ions.

Brennan, J. A., Edmonds, D. K., and Smith, R. V., **Two-phase (liquid-vapor), mass-limiting flow with hydrogen and nitrogen,** *Tech. Note 359 (Jan. 30, 1968), 25 cents.*
Experimental data on critical (choked) mass flow in a constant area test section are presented. The data are compared to some simple analytical models which have been recommended for design pur-

299-547 O-68—11

poses. The data show the same general behavior as that reported for other noncryogenic fluids.

Key Words: Choking; hydrogen; nitrogen; shocks; two-phase flow.

Burley, G., **The "memory effect" in silver iodide,** *Act. Cryst.* **23,** *Part 1, 1–5 (July 1967).*
Radial distribution and least squares site occupation analyses were performed on powder diffraction patterns of the high temperature phase of silver iodide taken at 155 °C and 250 °C. A preferential occupation of certain sites by the silver atoms occurs near the transition temperature at 147 °C, involving those silver atom positions nearest to those in the low-temperature wurtzite- and sphalerite-type structures, respectively. The regeneration of a particular derivative low-temperature structure is thus facilitated, and a crystallographic explanation can be given for the observed "memory effect".

Key Words: Alpha-phase; crystallography; silver iodide; site-occupation; structure; structure memory.

Cassidy, E. C., and Abramowitz, S., **Time-resolved spectroscopic studies of exploding wires in controlled atmospheres,** *Appl. Spectry.* **21,** *No. 6, 360–364 (Nov.–Dec. 1967).*
Electrically exploded wires in various controlled atmospheres were employed for excitation of atomic and molecular species. The spectrographic time histories of the various constituents (stable and unstable) of the explosion mixture were studied with the use of a rotating drum camera, focused on the exit slit plane of a spectrograph. A rotating high-speed shutter was then utilized to study the spectrum of selected intermediate species. Results obtained with aluminum wires in various atmospheres are presented, in order to illustrate the experimental techniques involved. Several considerations found to be important in the design of the explosion chamber are discussed.

Key Words: Electrical discharges; exploding wires; high-speed measurement techniques; high-speed photography; time-resolved spectroscopy.

Chappell, S. E., and Sparrow, J. H., **The average energy required to produce an iron pair in argon, nitrogen, and air for 1- to 5-MeV alpha particles,** *Rad. Res.* **32,** *No. 3, 383–403 (Nov. 1967).*
The absolute value of W, the average energy required to produce an ion pair, has been measured in argon, nitrogen and air for alpha particles with initial energies between 1 and 5 MeV. Six alpha-particle sources having different energies were fabricated by placing various thicknesses of mylar film over a collimated polonium–210 (5.3 MeV) alpha-particle source. For each source the total ionization produced in each gas by a determined number of alpha particles was measured in a parallel plate ionization chamber. Then the mean energy of each source was evaluated by using a time-of-flight apparatus. From these combined results, W was calculated. It was found to be constant within experimental error for argon but exhibited an increase in value of approximately 1 percent for nitrogen and air over the specified energy range. These results for nitrogen and air disagree with the energy dependence for W found by other investigators.

Key Words: Air; alpha particles; argon; average energy; ion pair; measurement; nitrogen.

Christ, B. W., and Smith, G. V., **Strengthening of polycrystalline iron by nitrogen,** *Trans. ASM* **60,** *732–734 (1967).*
The strengthening of polycrystalline iron by an interstitial impurity has been measured in tensile tests on 0.050-inch diameter wire. Nitrogen was introduced into hydrogen-purified iron by equilibration with an ammonia-hydrogen mixture. The distribution of nitrogen was changed by varying the rate of cooling from the solution temperature. Nitrogen in solid solution is not as effective a strengthener as carbon in solid solution. Nitride precipitation occurring during air cooling results in strengthening comparable to that due to carbide precipitation during quench aging. The observed linear variation of flow strength with nitrogen concentration supports the Schoeck-Seeger or Mott-Nabarro models of solution strengthening.

Key Words: Carbide strengthening; hydrogen-purified iron; nitride strengthening; nitrogen ferrite; polycrystalline; solid solution strengthening; tensile tests.

Christ, B. W., and Smith, G. V., **Yield and flow stress increase in pure polycrystalline iron during 600 °C treatment after wet hydrogen purification,** *Scripta Met.* **1,** *No. 3, 123–130 (1967).*
The tensile properties of polycrystalline iron (0.060 mm grain size) have been measured at 298 and 163 °K. Wet hydrogen treatment of rolled and drawn zone-refined iron for 7 hours at 750 °C decreased the average yield stress and ultimate tensile stress at 298 °K from 16,500 and 30,600 psi to 7,600 and 27,600 psi, respectively. The wet-hydrogen purified iron displayed practically no Luder's extension at room temperature, but exhibited 6–7% Luder's extension at 163 °K. Annealing at 600 °C for 20 and 40 hours in both dry hydrogen and sealed vycor capsules (10^{-5} torr) caused an upward shift in the stress-elongation curve at 163 °K. These results are discussed in terms of the influence of possible structural modifications during 600 °C annealing on the athermal and thermal components of stress.

Key Words: Hydrogen-purified iron; Luder's strain; polycrystalline iron; tensile properties; ultimate tensile stress; yield stress.

Chueh, P. L., and Prausnitz, J. M., **Third virial coefficients of nonpolar gases and their mixtures,** *AIChE J.* **13,** *No. 5, 896–902 (Sept. 1967).*
While much attention has been given to second virial coefficients of nonpolar gases, experimental and theoretical studies on third virial coefficients are scarce. This work presents a correlation of third virial coefficients within the framework of the corresponding-states principle. The correlation is useful for estimating third virial coefficients of pure and mixed nonpolar gases, including the quantum gases helium, hydrogen and neon. The importance of third virial cross-coefficients in phase equilibrium predictions is illustrated with calculations for the solid-gas, methane-hydrogen system at 76 °K.
Brief attention is given to the pressure-series form of the virial equation. Because of fortuitous cancellations, it is shown that, for reduced temperatures above 1.4, the pressure-series, truncated after the second term, is applicable to a wider range of density than the density series truncated after the second term. However, when both series are truncated after the third term, the density series appears to be superior regardless of reduced temperature.

Key Words: Nonpolar gases; quantum gases; third virial coefficients; virial equation.

Colwell, J. H., **The heat capacity of a mixed titanate superconductor,** *Physics Letters* **25A,** *No. 8, 623–624 (Oct. 1967).*
The heat capacity of semiconducting $Sr_{0.925}Ba_{0.075}TiO_3$ has been measured in the temperature region 0.3 to 4 °K. This material becomes superconducting with a transition temperature, T_c, of about 0.53 °K. The heat capacity increases gradually with decreasing temperature below T_c and has a broad maximum at 0.45 °K. There is an unusual heat capacity anomaly just above T_c which is described as a gradual decrease in the electronic heat capacity coefficient, γ, between 0.8 and 2.0 °K. The change in γ is interpreted as a phase transition causing a change in the number of occupied valleys in the conduction band. In the phase existing at the superconducting transition the conduction band has the same number of valleys and a comparable density of states at the Fermi surface as that in semiconducting $SrTiO_3$.

Key Words: Electronic band structure; heat capacity; mixed titanate; phase transition; semiconductor; $SrTiO_3$; superconductor.

Corliss, C. H., **Revision of the NBS tables of spectral-line intensities below 2450 Å,** *Spectrochim. Acta* **23B,** *117–127 (1967).*
A calibration is applied to the intensity measurements of the 1400 lines below 2500 Å in the NBS Tables of Spectral-Line Intensities. Tables of the new values are presented with the lines arranged by element and by wavelength.

Key Words: Atomic spectra; intensities; spectral-line intensities; ultraviolet intensities.

Daney, D. E., and Mann, D. B., **Quality determination of liquid-solid hydrogen mixtures,** *Cryogenics* **7,** *No. 5, 280–285 (Oct. 1967).*
A theoretical and experimental investigation of the feasibility of predicting the quality of liquid-solid hydrogen mixtures from the mass fraction of vapor pumped off in the freeze-thaw process is presented. Three independent methods of experimental quality determination were used to check the correctness of the qualities predicted from the measured mass fraction pumped off in forming liquid-solid mixtures. In all cases only freshly made mixtures were used.
It is suggested that an independent means of determining the edge of the triple-point region, such as measurement of the vapor pressure, be used. With this modification, measurement of the mass fraction pumped off during the freeze-thaw process provides a simple, nondestructive and accurate method of bulk quality determination. The method is not appropriate for cases in which a partial transfer from the dewar is made and it requires accurate knowledge of the heat leak if long storage times are to be used. Low accuracy in large volume gas flowmeters also places a restriction on the method.

Key Words: Liquid-solid hydrogen mixtures, quality determination, rocket propellant, slush hydrogen.

DeVoe, J. R., Editor, **Activation analysis: Cockcroft-Walton Generator nuclear reaction, LINAC, July 1966 through June 1967,** *Tech. Note 428 (Nov. 1967), 55 cents.*
This is the first separate (not combined with that of Radiochemical Analysis) summary of progress for the Activation Analysis Section of the Analytical Chemistry Division of the National Bureau of Standards.
Pertinent information on the irradiation facilities of the nuclear reactor, Linac and Cockcroft-Walton generator are described. The initial installation of pneumatic transfer tubes is completed. Of great significance is the completion of a clean room that is used for pre-irradiation chemical separation for high sensitivity activation analysis.
A dual-sample biaxial rotating 14 MeV neutron-irradiation assembly has been tested. This assembly is part of a system that is controlled by a relay type of programmer to automate those irradiation steps that adversely affect precision of the analysis. This system was used to improve greatly the precision of analysis for oxygen and fluorine.
As a result of improved precision with the 14 MeV neutron irradiation, a study of systematic errors is now possible. Efforts to establish a reproducible correction factor for neutron and gamma-ray absorption between different matrices within the sample have shown considerable promise.
Standard Reference Material (SRM) steel chip Nos., 3b, 3c, and 30f have been analyzed for vanadium. Preliminary analyses of high purity platinum (a potential SRM) showed silver, copper, gold, palladium, and iridium at the ppm level. Future biological SRM's, (tree leaves, and beef liver) were tested for homogeneity and found satisfactory.
A variety of service analyses were performed. In particular, very pure aluminum was found to contain fractions of a ppm of chromium and scandium.
Additional efforts are being made to monitor reactor neutron fluxes. Additional nuclear instrumentation is being assembled to improve the versatility of the analysis technique.
Performance of the bremsstrahlung target, used with the linear electron accelerator, has been evaluated. Photon intensity distribution and stability was found to be within usable range. Analyses using the (γ,n) or (γ,p) reactions have been developed for magnesium in steels, and carbon in sodium metal.

Key Words: Activation analysis; biological; botanical samples; carbon in sodium; Cockcroft-Walton generator; digital computers; flux monitors; high precision 14 MeV neutron activation; homogeneity testing; instrumentation; NBS Linac; NBS reactor; photoneutron reactions; self absorption corrections; standard reference materials; vanadium in irons and steels.

Dickson, G., and Oglesby, P. L., **Elastic constants of dental amalgam,** *J. Dental Res.* **46,** *No. 6, Part 2, 1475 (Nov.–Dec. 1967).*
Elastic constants of dental amalgam were determined by an ultrasonic pulse-echo technic. Longitudinal and transverse wave velocities of a 5.5 MHz pulse were determined in cylindrical amalgam specimens 8mm in diameter by 6 to 15 mm in length. Values of 9.1×10^6 psi for Young's modulus, 3.4×10^6 psi for shear modulus, 9.1×10^6 psi for bulk modulus and 0.33 for Poisson's ratio were obtained for amalgams containing 49 percent mercury. Values for all of these constants increased as the mercury content of specimens was reduced to 35 percent.

Key Words: Bulk modulus; dental amalgam; elastic constants; Poisson's ratio; pulse-echo technic; shear modulus; Young's modulus.

DiMarzio, E. A., **Some contributions to the kinetics of growth of multicomponent chains with application to the problems of ciliation and fractionation in polymer crystallization,** *J. Chem. Phys.* **47,** *No. 9, 3451–3469 (Nov. 1, 1967).*
The problem of the growth rate and purity of crystals formed by the sequential deposition of molecules in a mixed system is solved. The solution is given in terms of the fundamental rates $\alpha_\nu^{ij}(\beta_{\nu+1}^{ij})$ for laying down (taking off) species j at the $(\nu+1)$th position ot the growing crystal given that species i occupies the (ν)th position. The fundamental rates are thus dependent on nearest-neighbor interaction but not on neighbors further removed. The method used complements a previously used method and additionally solves the problem for ν dependent α_ν^{ij} and β_ν^{ij}. The ν-dependence of the α's and β's allows for the stochastic-like distribution of the various species in the substrate upon which we are growing our linear chain of molecules. It is shown that there exists one unique flux-determined steady state solution for a wide variety of initial conditions. Several diagrams descriptive of various physical processes are displayed. The one describing ciliation (the growth process which results in the ends of polymer chains dangling out of the crystal lamella) is treated in some detail. It is found that there are two classes of α's and β's. One class gives large growth rates and very little ciliation. The second class gives growth rates which are orders of magnitudes smaller and results in much ciliation. It is concluded that when chain folded crystallization occurs the amount of material dangling out of the crystal is less than 50 percent of the total amount of material participating. The problem of fractionation in polymers is treated. Formulae are given for the purity of polymer crystals which are formed by high molecular weight material crystallizing concomitantly with polymeric material of lower molecular weight and/or of different kind. Fractionation can be substantial even when the molecular weights of the mixed system are all large. Simple formulae are derived. More complicated diagrams that allow for more than nearest neighbor interaction can be reduced to the nearest neighbor case but with a larger number of components.

Key Words: Crystal composition; crystal growth; multicomponent growth kinetics; polymer crystallization.

Eberhard, J. P., and Schofer, R. E., **The role of technology in developing future transportation systems,** *Proc. Analysis and Control of Traffic Flow Symp., Detroit, Michigan, Jan. 9–10, 1968, pp. 1–4 (Society of Automotive Engineers, Inc., New York, N.Y., 1968).*
As we approach the twenty-first century it is becoming increasingly apparent that, as megalopolitan areas increase in size and number throughout the country, we must search for new transportation technologies. In this paper, the authors set forth some of the areas where more and better coordinated research needs to be done.
There are three basic types of transportation technologies. The planning technology entails the obtaining of enough information in advance to develop sound transportation systems to meet future requirements. More research is needed to determine the impact on transportation requirements made by a changing city form. Secondly, research directed at improved operating strategies for existing systems will provide information needed for the development of future systems. Finally, more work is needed in the area of transportation hardware technology. No proposal should go without careful evaluation; latent technologies must be explored in the search for better systems.
Governments can encourage technological innovation by defining areas of needed research, sponsoring research, disseminating information on research activities, and by coordinating research efforts. To preserve the vitality of transportation in the United States, the

Federal Government must assume the overall responsibility for encouraging development of new transportation technologies.

Key Words: Future transportation; regional transportation; technology; transportation; transportation technology; urban transportation.

Eick, J. D., Caul, H. J., Smith, D. L., and Rasberry, S. D., **Analysis of gold and platinum group alloys by x-ray emission with corrections for interelement effects,** *Appl. Spectry.* **21,** *No. 5, 324–328 (Sept.–Oct. 1967).*
The x-ray emission analysis of noble metal alloys was investigated critically to determine optimum conditions for accurate analysis. The analytical curves for the elements Cu, Pd, Pt, and Zn were found to be linear with a deviation of less than ±0.2 percent. However, a nonlinear relationship existed for gold and for silver. These discrepancies could not be eliminated by variation in sample preparation. An interelement effect due to x-ray absorption and enhancement was found and was corrected to an accuracy of 0.2 percent by means of a mathematical treatment suggested by Lucas-Tooth and Price. The analysis by x-ray emission can be accomplished in approximately one-tenth of the time necessary for conventional wet chemical methods.

Key Words: Gold and platinum group alloys; noble metal alloys; x-ray emission.

Faison, T. K., Jr., Davis, J. E., and Achenbach, P. R., **Performance of square-edged orifices and orifice-target combinations as air mixers,** *Bldg. Sci. Series 12 (Nov. 24, 1967), 15 cents.*
A study was made at the National Bureau of Standards to determine the effectiveness of the square-edged orifice, or the orifice in combination with a target (circular baffle), for mixing an air stream which was initially nonuniform with respect to temperature. By achieving uniformity of temperature at all points within the cross section of an air stream, instrumentation for measurement might be simplified and a more representative temperature value obtained. Orifices having throat diameters of 8, 12, and 16 in were evaluated in a 24-in circular test duct to determine mixing effectiveness under selected test conditions of temperature distribution and flow rate. Targets of 8, 12, and 16 in in diameter in combination with a 12-in orifice were also investigated under similar conditions.
Graphic material is presented which illustrates how the orifice and orifice-target combinations perform as mixing devices under selected conditions. Results indicate that the 8-in (0.33 diam ratio) orifice effectively diminished the nonuniformity of temperature but only at a high pressure drop across the orifice and that a distance of 4.5 duct diameters was required for mixing.

Key Words: Diameter ratio; mixing effectiveness; square-edged orifice; temperature measurement; temperature pattern.

Faust, J. W., Jr., Ogburn, F., Kahan, D., and Ruff, A. W., Jr., **Twin configurations in FCC dendrites,** *J. Electrochem. Soc.: Solid State Science* **114,** *No. 12, 1211–1212 (Dec. 1967)*
The authors discuss possible configurations of intersections of twin planes which might be present in dendrites of diamond-type materials and fcc metals. They show that for dendrites growing in a [110] direction there will be a mismatch boundary wherever two or more twin planes intersect.
Experimental evidence is given for the existence of a configuration of two crossing twin lamellas with two mismatch boundaries in a silver dendrite.

Key Words: Dendrites; electrodeposition; growth twins; silver.

Fine, J., and Scheer, M. D., **Positive and negative self-surface ionization of molybdenum,** *J. Chem. Phys.* **47,** *No. 10, 4267–4268 (Nov. 15, 1967).*
The positive and negative self surface ionization of molybdenum has been observed in the 1800–2100 °K temperature range. The positive and negative ion sublimation energies were found to be 9.5 and 10 eV respectively. The electron affinity was determined as 1.0 ± 0.2 eV (estimated uncertainty).

Key Words: Electron affinity; ion sublimation energy; mass spectrometry; molybdenum; positive and negative ions; self-surface ionization.

Franklin, A. D., **Born model calculation of enthalpies of solution in CaF_2,** *J. Am. Ceramic Soc.* **50,** *No. 12, 648–652 (Dec. 1967).*
The Born model of ionic solids has been used to calculate the lattice energy, as an estimate of the enthalpy of solution, needed to dissolve NaF and YF_3 in CaF_2, in the limit of infinite dilution. For NaF, sufficient experimental data are available to provide reasonable estimates for the parameters describing the repulsive interactions between Na^+ and surrounding ions, and the calculated enthalpy of solution is in good agreement with the available experimental value, 1.4 ± 0.3 eV per NaF. For YF_3 the experimental data are not available and the estimated enthalpy of solution of about zero is subject to a large uncertainty. The results for NaF are consistent with the model normally assumed, in which each substitutional Na^+ ion is accompanied by and F^- vacancy, but do not rule out charge compensation by interstitial Na^+ ions as well. The calculations also yield an estimate for the lattice expansion.

Key Words: Born model calculation; CaF_2; enthalpies of solution; ionic solids; NaF; YF_3; point defects.

Freeman, D. H., Editor, **Separation and Purification Section: summary and initial activities February 1966 through June 1967,** *Tech. Note 429 (Feb. 1968), 35 cents.*
This Report describes the initial growth and research activities of the Separation and Purification Section since its formal organization in February, 1966.
A research capability for the study and refined adaptation of ion exchange materials is described. There are new activities reported for the areas of extreme purification, chemical reagents, organic chemicals, including the use of crystallization for the achievement, protection, and measurement of chemical purity. Specific studies have been conducted in the purification of mineral acids, nitrobenzene, and the development of zone refining methods.

Key Words: Ion exchange; purification; reagents; zone refining.

Frenkiel, F. N., and Klebanoff, P. S., **Correlation measurement in a turbulent flow using high-speed computing methods,** *Phys. Fluids* **10,** *No. 8, 1737–1747 (Aug. 1967).*
Third-order time-correlations downstream of a grid were measured with a hot-wire anemometer using high-speed computing methods. The nonlinear response of the hot-wire to the fluctuations of velocities is taken into account as well as the effect of transverse velocities. It is found that the third-order correlations are substantially different from previous results and demonstrate that the assumption of isotropy is not adequate for these correlations downstream of a grid. The nonlinear response does not significantly affect the difference $u_1^2u_2 - u_1u_2^2$. Since previous conclusions concerning the nature of third-order correlations were based on the measurements of such differences they masked the effects of nonlinearity on the individual correlations. Correlations of fifth-order are also presented and their relations to the third-order correlation are discussed. Although the nonlinear corrections are quite important for odd-order correlations they are negligible for correlations of even-order.

Key Words: Correlations; even-order; grid; hot-wire anemometer; isotropy; nonlinear response; odd-order; turbulence.

Goldstein, J. I., Majeske, F. J., and Yakowitz, H., **Preparation of electron probe microanalyzer standards using a rapid quench method,** *Advan. X-ray Anal.* **10,** *431–446 (1967).*
Standards for microprobe analysis can be made to serve two purposes: (1) Proposed correction models can be tested with them and (2) Analysis can be performed more accurately in the system which includes the standard. Few microprobe standards are presently available because they must be homogeneous on the micron scale and their composition must be known accurately. A modified Duwez splat cooling method is described which enables the investigator to prepare suitable standards in most cases. The apparatus which is relatively simple and inexpensive is described in detail. The systems Au-Si and Al-Mg were chosen as test cases. Suitable standards were prepared at different concentrations in each system. The analytical results for all compositions in Al-Mg are presented and discussed.

Key Words: Al-Mg; Au-Si; electron probe standards; quantitative microanalysis; splat cooling; standard preparation.

Gorden, R., Jr., and Ausloos, P., **Photolysis of ethylene at 1048–1067 Å. Reactions of $C_2H_4^+$ and fragmentation of the superexcited ethylene molecule,** *J. Chem. Phys.* **47,** *No. 5, 1799–1806 (Sept. 1, 1967).*
C_2H_4–NO, C_2H_4–O_2 and C_2H_4–$(CH_3)_2NH$–O_2 mixtures have been irradiated with an argon resonance lamp emitting only the 1048 and 1067 Å lines. The ionization efficiency ratios: $\eta_{C_2D_4}/\eta_{NO}$, $\eta_{C_2H_4}/\eta_{NO}$, $\eta_{C_2D_4}/\eta_{C_2H_4}$ were determined to be 0.30 ± 0.003, 0.27 ± 0.003 and 1.12 respectively. Trans-2-butene and cis-2-butene are major products when NO (I. P. = 9.25 eV) or $(CH_3)_3NH$ (I. P. = 8.24 eV) are added to C_2H_4. Radiation of pure C_2H_4 or of C_2H_4–O_2 mixtures yielded only minor traces of 2-C_4H_8. In accord with earlier radiolysis studies we ascribe the formation of 2-C_4H_8 to the charge transfer process:

$$C_4H_8^+ + NO \text{ (or } (CH_3)_2NH) \rightarrow C_4H_8 + NO^+ \text{ (or } (CH_3)_2NH^+)$$

where $C_4H_8^+$ may possess some excess internal energy carried over from the exothermic condensation reaction $(C_2H_4^*)^+ + C_2H_4 \rightarrow (C_4H_8^*)^+$. For a constant C_2H_4–NO mixutre $M(C_4H_8)/N$ increases drastically with an increase of the pressure of C_2H_4 from 0.1 to 6 torr. Also, in pure C_2H_4, $M(CH_3)/N$ which is close to unity at 0.5 torr is seen to diminish to 0.2 when the pressure is raised to 29.8 torr. These effects are largely ascribed to a competition between decomposition and stabilization of the $[C_4H_8^*]^+$ product ion.
A rate constant of 10^7 sec^{-1} is derived for the unimoleculat decomposition of $(C_4H_8^*)^+$ assuming that stabilization occurs at every collision with C_2H_4. It is shown that Ne is about 100 times less efficient than C_2H_4 in stabilizing $(C_4H_8^*)^+$.
The superexcited $C_2H_4^*$ dissociates as follows, $C_2H_4^* \rightarrow C_2H_2 + H_2$ and $C_2H_4^* \rightarrow C_2H_2 + 2H$. Isotopic analysis of the hydrogen formed in the photoionization of CH_2CD_2 shows that the relative probabilities for the elimination of H_2, HD and D_2 from $CH_2CD_2^*$ are the same for the superexcited molecule as for the excited molecule formed by absorption of 8.4 to 10 eV photons.

Key Words: Cis-2-butene; ethylene; hydrocarbons; photoionization; trans-2-butene.

Grosch, H. R. J., **The National Bureau of Standards program in computer sciences and technology,** *Stat. Reptr. 68–3, 37–41 (Superintendent of Documents, Government Printing Office, Washington, D. C. 20402, Sept. 1967, 20 cents).*
The NBS Center for Computer Sciences and Technology was established in 1965 to perform the Bureau's work in the field of computer technology—a broad program of standardization activities, applied research, and services to Federal agencies. Work on standards includes that on USASCII (for use in Federal procurement, under the terms of the Brooks Bill of October 1, 1965) and on optical character recognition. Services to other branches of government include providing data processing services, computational assistance, and consultation. The activities of the center's Technical Information Exchange and the continued experimentation with computers will have industry-wide benefits.

Key Words: Brooks Bill; computer standards; computer technology; data-processing; government.

Gross, D., Loftus, J. J., and Robertson, A. F., **Method for measuring smoke from burning materials,** *Am. Soc. Testing Mater. Spec. Tech. Publ. 422, 166–204 (1967).*
Based on a study of possible smoke-measuring methods, a laboratory test has been developed for the photometric measurement of smoke from burning materials. The method assumes the applicability of Bouguer's law to the attenuation of light by smoke, and smoke quantity is therefore reported in terms of optical density rather than light absorptance or transmittance. Optical density is the single measurement most characteristic of a "quantity of smoke" with regard to visual obscuration.
Experiments have been performed on a variety of building finish materials under both flaming and nonflaming (smoldering) conditions, and the results are reported in terms of (a) maximum smoke accumulation (b) maximum rate of smoke accumulation, and (c) the time period to reach an arbitrary "critical" smoke level.

Key Words: Aerosol; combustion; fire hazard; pyrolysis; smoke; smoke density; visual obscuration.

Haller, W., **Virus isolation with glass of controlled pore size: MS2 bacteriophage and kilham virus,** *Virology* **33,** *No. 4, 740–743 (Dec. 1967).*
MS2 bacteriophage and tritiated Kilham Rat virus have been isolated from natural lysates by restricted-diffusion chromatography on pore-controlled glass. Measurements of infectivity and hemagglutinating activity, as well as radioactivity and UV absorption, were used to determine recovery and purity of isolated viruses. The recoveries proved to be nearly 100 percent and the viruses were essentially host protein free.

Key Words: Chromatography; glass; kilham rat virus; MS2 virus; porous glass; virus.

Hamer, W. J., **Evaluation procedures and annual performance data for Leclanché cells,** *Electrochem. Technol.* **5,** *No. 11–12, 490–498 (Nov.–Dec. 1967).*
This paper deals with the development over the past 48 years of so-called "standardized tests" for the evaluation of Leclanché cells and batteries. Data covering this time period or a part of this time period are given for (1) general-purpose flashlight cells, (2) industrial flashlight cells, (3) railroad lantern batteries, (4) photoflash cells, (5) No. 6 cells for various end uses, (6) radio "A" batteries, (7) radio "B" batteries, (8) hearing-aid "A" batteries, (9) hearing-aid "B" batteries, and (10) transistor hearing-aid batteries. The presently used standard tests, 27 in number, are described. A history of the development of dry cells of the Leclanche type is also included.

Key Words: Advances in dry cells; battery nomenclature; dry cell specifications; dry cell standards; dry cell tests; International dry cell standards.

Hanley, H. J. M., and Klein, M., **On the selection of the intermolecular potential function: application of statistical mechanical theory to experiment,** *Tech. Note 360 (Nov. 20, 1967), 50 cents.*
We have developed a method here to evaluate quantitatively the relationship between model intermolecular potential functions and macroscopic experimental properties. Specifically, we have studied the function families: m–6, Kihara, exp:6, and Morse, and the properties: viscosity coefficient, diffusion coefficient, second virial, and Joule-Thomson coefficient. Our method is not restricted to these functions and properties; it is valid for any function and any property provided the appropriate theoretical expressions are available.
The principal conclusions from this work are: 1. A temperature range exists (around room temperature for most substances) in which data are completely insensitive to the potential function. This range makes it possible to quantitatively define what is meant by "high" or "low" temperatures. These definitions are most important when extrapolation of data arises. 2. The function families studied are essentially equivalent. 3. More than one function is required to represent data over a range of about 1000 °K. 4. We have estimated the experimental error which can be tolerated if experimental data are to be used to select a potential function. The conclusions are experimentally verified for both transport and equilibrium properties.

Key Words: Correlation; equilibrium properties; experimental data; intermolecular potential function; theory; transport properties.

Hayward, H. W., and Tauber, S. J., **The HAYSTAQ experiment,** *Proc. ICIREPAT Fifth Annual Meeting, London, England, Aug. 31–Sept. 10, 1965, Chapt. 26, pp. 337–350 (Thompson Book Co., Washington, D.C., 1967).*
The background of the Haystaq system is recapitulated. Shortcomings of an earlier chemical structure representation are reviewed; the scope and some advantages of the Hayward notation are stated. Suggestions are made for representing mixtures and classes of compounds. The scope is stated of notations for classes of reactions. The organization of files of chemical information and patterns of retrieval are discussed. Capabilities, limitations, and future implications of the techniques evolved are pointed out.

Key Words: Chemistry; compounds; computer; file organization; HAYSTAQ; Hayward; information retrieval; linear notation; Markush; mixtures; reactions; representations; screens; structures; topological codes.

Hollstein, M. G., and DeVoe, J. R., **Determination of medium-weight elements by gamma-excited x-ray fluorescence** (*Proc. Second Symp. on Low Energy X- and Gamma Sources and Applications, University of Texas, Austin, Texas, Mar. 27–29, 1967*), *ORNL-IIC-10, pp. 483–502 (1967).*
The application of gamma-excited x-ray fluorescence in the determination of medium weight elements has been studied. The pertinent components of the spectrometer are an ^{241}Am source and a solid state detector, with a low-noise preamplifier and multi-channel analyzer. The resolution of the system is between 1.2 and 1.3 keV (FWHM) for 8 to 45 keV photons. Three different techniques of sample mounting were investigated. For single elements in the range from Cu to Dy the estimated detection limits are 10–100 μg and 0.01–1 mg/ml, depending upon the sample mounting procedure. The corresponding K_α-peak intensities are $2\times10^4-3\times10^3$ cpm per mg and $4\times10^4-6\times10^2$ cpm per mg/ml, respectively. For testing the application of the method two series of NBS Standard Reference Materials were analyzed for Sn and Mo as minor constituents within a concentration range from about 0.04 to 9%. The best results were obtained by direct counting of the solid samples. Using this technique, a non-destructive analysis for Mo and Sn can be performed in a relatively short time with a precision of a few percent, a detection limit of about 100 ppm and a sensitivity of 6×10^3 to 1.4×10^4 cpm per percent concentration.

Key Words: Gamma-excitation; medium weight elements; molybdenum; quantitative analysis; tin; X-ray fluorescence.

Holt, H. K., **Frequency-correlation effects in cascade transitions involving stimulated emission,** *Phys. Rev. Letters* **19,** *No. 22, 1275–1277 (Nov. 27, 1967).*
The effect of the frequency correlation of photons emitted in an atomic cascade transition on the frequency profile of the light emitted in the second transition when the first transition is participating in laser action is examined.

Key Words: Laser; line profile; neon.

Hudson, R. P., **Generation of matrix elements of angular-momentum operators,** *J. Opt. Soc. Am.* **57,** *No. 12, 1552–1553 (Dec. 1967).*
A simple numerical array is shown to give the matrix elements of certain important angular momentum operators.

Key Words: Angular momentum operators; matrix elements.

Jenkins, W. D., and Willard, W. A., **Creep rupture properties of Ti-8Al-1Mo-1V alloy,** *J. Res. NBS* **72C** (*Eng. and Instr.*), *No. 2 (Apr.–June 1968).*
Creep tests were made at 600, 800, 1000 and 1200° F (588, 699, 811 and 921 °K) on duplex-annealed Ti-8Al-1Mo-1V alloy specimens. Creep-test conditions were selected to produce creep rates ranging from 0.1 to 50,000 percent per 1,000 hours and rupture times ranging from 0.1 to about 10,000 hours. Conformance of the test data to creep theories was obtained over a limited range of stress, strain, creep rate and temperature. Creep behavior was influenced by microstructural changes during creep and by prior thermal-mechanical treatment. Engineering-design curves are included in this paper.

Key Words: Creep; engineering-design; high temperatures; phase changes; rupture; titanium alloy.

Judd, D. B., **A flattery index for artificial illuminants,** *Illum. Eng.* **62,** *No. 10, 593–598 (Oct. 1967).*
Artificial illuminants are used for (1) light-dark discrimination of objects, (2) critical appraisal of colored objects, and (3) appreciative viewing of colored objects. A light source that renders object colors in accord with their preferred colors may be said to flatter those objects. A flattery index has been derived for light sources used for appreciative viewing of colored objects to measure the degree to which such sources render object colors as we would like to see them. This index is based solely on spectral distribution and is modeled after the index of color rendition recently recommended by the CIE. It uses 10 of the 14 test samples established for appraisal of color rendition, and it uses the same definition of reference illuminants. It is scaled so that the reference illuminant receives a flattery index of 90, and a test illuminant rendering object colors precisely in accord with the preferred colors of the test samples receives a flattery index of 100. The test sample representative of the human complexion receives about one-third of the total weight; the two test samples representative of food colors, about one-third; the seven other test samples, the remainder.

Key Words: Color; flattery; illuminants; preference; rendition of color.

Kneissl, G. J., and Richmond, J. C., **A laser-source integrating sphere reflectometer,** *Tech. Note 439* (*Feb. 1968*), *45 cents.*
A reflectometer was developed for measuring the absolute spectral reflectance of materials at temperatures up to 2500 °K. The equipment included (1) a helium-neon laser as the source, capable of operation at 0.6328, 1.15 or 3.99μm, (2) a 35 cm diameter integrating sphere coated with sodium chloride, (3) a lead sulfide detector, and (4) a radio frequency generator for heating the specimen by induction. A spike filter transmitting at the laser wavelength in front of the detector absorbed most of the background radiation from the hot specimen, and a chopped incident beam together with synchronous amplification of the signal from the detector was used to eliminate the effect of the remaining background radiation. The integrating sphere could be evacuated, or operated under a slight positive pressure of purified helium. An error analysis showed that the measured absolute reflectances are in error by less than one percent. Preliminary data are presented for thoria, tungsten and graphite. Graphite was found to be stable in reflectance on heating to 2150 °K in vacuum. Both thoria and tungsten were somewhat unstable in reflectance on heating in vacuum.

Key Words: Diffuse reflectance; graphite; high temperature reflectance; infrared reflectance; integrating sphere reflectometer; laser; reflectance; sodium chloride coating; synchronous amplification; thoria; tungsten.

Knight, J. M., O'Connell, J. S., and Prats, F., **Two- and three-body photodisintegration cross sections of ^3H and ^3He,** *Phys. Rev.* **164,** *No. 4, 1354–1359 (Dec. 20, 1967).*
Electric dipole photodisintegration cross sections of ^3H, ^3He into deuteron plus nucleon and into three nucleons are calculated using simple zero range forms for the initial and final state wave functions. Final state interaction between nucleon pairs in s-states are taken into account. Shape fits to the experimental data are obtained, but the required normalization of the ground state wave function is found to differ between two- and three-body breakup.

Key Words: Cross sections; dipole; final state interactions; helium 3; photodisintegration; tritium.

Kolbenstvedt, H., **Energy transfer in the collision of electron beams,** *Phys. Rev.* **163,** *No. 1, 112–114 (Nov. 5, 1967).*
The cross section for electron-electron scattering differential in energy transfer, is derived for the case that both electrons are in motion in the laboratory system. The result is valid for all electron energies much higher than the Rydberg energy. For the case in which both electrons are nonrelativistic and one of the electrons has an isotropic velocity-distribution, the cross section is averaged over the directions of motion of this electron.

Key Words: Average; cross-section; distribution; electrons; energy; isotropic; motion; scattering.

Koonce, C. S., Cohen, M. L., Schooley, J. F., Hosler, W. R., and Pfeiffer, E. R., **Superconducting transition temperatures of semiconducting $SrTiO_3$,** *Phys. Rev.* **163,** *No. 2, 380–390 (Nov. 10, 1967).*
The superconducting transition temperature T_c of $SrTiO_3$ has been measured for specimens having electron carrier concentrations n_c from 6.9×10^{18} cm^{-3} to 5.5×10^{20} cm^{-3}. The curve exhibits a maximum in T_c for n_c near 9×10^{19} cm^{-3}. The transition temperature has also been calculated using one adjustable parameter ξ, the intervalley deformation potential, in addition to the known normal-state properties of $SrTiO_3$. A good fit to the experimental curve is obtained.

Key Words: Semiconductors; $SrTiO_3$; superconductivity; transition temperatures.

Krauss, M., **Compendium of *ab inition* calculations of molecular energies and properties,** *Tech. Note 438 (Dec. 1967), 70 cents.*
The number of *ab initio* molecular electronic calculations has increased dramatically in the last few years. Both the practitioners and other interested students of the results of the calculations have found it increasingly difficult to determine the present status of these calculations. This compendium references the work from 1960 to the present and abstracts from the mass of data the best values for several observable properties including the total energy, dissociation energy, electron affinity, spectroscopic constants, electric moments, field gradients, polarizabilities, and magnetic constants. In order to provide an insight into molecular electronic structure tables of orbital energies are also included.
These tables are meant to direct attention to the successes and failures of the calculations by compiling a large percentage of the best results in a reasonably compact form. Its usefulness will be limited in time by rapid advance in the field.

Key Words: *ab initio* electronic calculation; molecular electronic structure; energy; dissociation energy; dipole moment; quadrupole moment; polarizability; electron affinity; field gradient; spectroscopic constants; magnetic constants; orbital energy.

Kruger, J., and Calvert, J., **Ellipsometric-potentiostatic studies of iron passivity, I. Anodic film growth in slightly basic solutions,** *J. Electrochem. Soc.* **114,** *No. 12, 1265–1267 (Dec. 1967).*
Cathodically reduced iron was anodically oxidized to potentials in the passive region of the anodic polarization curve at passive potentials in nearly neutral sodium borate-boric acid solutions by means of a potentiostat. The kinetics of film growth were studied using an ellipsometer coupled with a high speed recording technique, which enabled a determination of the rate of film formation for times less than one second. This study of the kinetics of film growth using a non-electrochemical technique agreed with kinetic results based on total charge measurements.
Three states of growth were detected: (1) *First Stage*—growth limited by the diffusion of oxidizing species thru solution. (2) *Second Stage*—start of limitation of growth of film. A combination of several processes difficult to characterize by any rate law. (3) *Third Stage*—growth obeying either a direct or indirect logarithmic rate law. The latter was found to imply that the passive film consisted of an outer layer poorly conductive for electrons.

Key Words: Anodic oxidation; ellipsometry; iron and passivity; iron oxide films; potentiostat.

Logan, H. L., **Some techniques used in the study of stress corrosion cracking,** *Am. Soc. Testing Mater. Stress Corrosion Testing Spec. Tech. Publ. 425, 127–144 (1967).*
Techniques used at the National Bureau of Standards in the study of stress-corrosion cracking of metals are described together with precautions taken in these investigations. Especially designed specimen of low carbon and stainless steels and a titanium alloy and supplementary techniques for obtaining data as to the mechanism of the stress-corrosion process are also described. A specimen and technique recently used to determine whether hydrogen plays a part in the delayed failures of high strength steels in chloride solutions is described.

Key Words: Experimental techniques for stress corrosion testing; high strength steels; hydrogen embrittlement; low carbon steels; stainless steels; stress-corrosion; titanium alloys.

Lovell, W. S., Anderson, M. M., and Seiller, F. E., **Laser harmonics useful for frequency translation,** *Appl. Opt.* **6,** *No. 8, 1430–1432 (Aug. 1967).*
Accidental coincidences between laser fundamental and harmonic frequencies usable (in principle) for frequency translation are tabulated.

Key Words: Accidental coincidences; frequency locking; frequency translation; laser harmonics.

Kuriyama, M., **Distortion correction in anomalous absorption coefficients,** *Phys. Stat. Sol.* **24,** *743–748 (1967).*
Based on the theory of X-ray diffraction by a distorted crystal which has recently been completed by the present author, the temperature- and distortion-correction in anomalous absorption coefficients has been studied in the case of a single symmetrical Bragg reflection (a symmetrical Laue case).
If the distribution of atomic displacements is given, then the anomalous absorption coefficient has the distortion correction of the same form, in terms of the second moment of the distribution, as the Debye-Waller factor. If the displacement of atoms in a distorted crystal is replaced by a proper time-average value of the thermal motion of atoms, then the temperature correction in the absorption coefficient is given by the Debye-Waller factor multiplied by the structure factor.

Key Words: Anomalous transmission; atomic displacement; Debye-Waller factor; distorted crystal; Laue case; photon Green's function; theory; x-ray diffraction.

Kuriyama, M., **Theory of X-ray diffraction by a distorted crystal,** *J. Phys. Soc. Japan* **23,** *No. 6, 1369–1379 (Dec. 1967).*
Based on the quantum theory of X-ray diffraction by a perfect crystal (M. Ashkin and M. Kuriyama, J. Phys. Soc. Japan **21** (1966), 1549), a diffraction theory for a distorted crystal has been developed. The scattering amplitude for the case of a single Bragg reflection has been obtained in terms of a lattice sum including the displacement of each atom. A basic assumption for this formulation is that there is no overlap of the electron wave functions of the displaced atoms. The existing basic assumption in the dynamical theory for a distorted crystal, that the local distortion in the crystal must change very slowly so that the local wave field can be described by the dynamical theory for a perfect crystal, has been successfully ruled out in the present formulation. A criticism has also been made to the so-called "Fourier" expansion of polarizability or electron distribution in the distorted crystal, which has been important for the dynamical theory.

Key Words: Atom; Bragg condition; displacement; distorted crystal; electron overlap; Green's Function; lattice; photon; theory; x-ray diffraction.

Madey, T. E., and Yates, J. T., Jr., **Work function studies: chemisorption of diatomic molecules on single-crystal tungsten,** *Nuovo Cimento Suppl. Series I, 5, No. 1, 483–505 (1967).*
The work function changes accompanying the chemisorption of diatomic molecules on single crystal (100) and (110) tungsten have been studied using a modification of Shelton's retarding potential method. Each crystal wafer was cut and polished to the desired orientation on both sides, suspended by fine W wires, and heated by electron bombardment. This mode of suspension and heating allowed measurements of surface coverage to be made with a minimum of error due to edge effects and desorption from support leads. The work function difference $\phi(110) - \phi(100) = 0.65$ eV was found to be independent of which crystal was used as emitter. The changes in work function and electron reflection upon chemisorption, as well as measurements of surface coverage and sticking coefficients have been made, where possible, for N_2, O_2, and CO on these two crystals.

Key Words: Adsorption; carbon monoxide; chemisorption; desorption; electron reflection; nitrogen; oxygen; single crystal; sticking coefficient; thermionic emission; work function.

Maki, A. G., Jr., and Lide, D. R., Jr., **Microwave and infrared measurements on HCN and DCN: observations on l-type resonance doublets,** *J. Chem. Phys.* **47,** *No. 9, 3206–3210 (Nov. 1, 1967).*
Microwave measurements have been made on the direct doublet splittings ($\Delta J = O$ transitions) of the $O1^1O$, $O2^2O$, $O3^1O$, and $O3^3O$ levels of DCN and the $O1^1O$ and $O2^2O$ levels of HCN. The sensitivity of the Δ and Φ level splittings to certain vibrational and rotational constants enables us to obtain new values for those constants. New infrared measurements are given for ν_1, $3\nu_2^1$, $4\nu_2^0 - \nu_2^1$ and $4\nu_2^2 - \nu_2^1$ of HCN.

Key Words: Deuterium cyanide; hydrogen cyanide; infrared spectra; microwave spectra; molecular constants; molecular structure; spectra.

May, L., and Snediker, D. K., **Criteria for selection of absorber mounting materials in Mössbauer spectroscopy,** *Nucl. Instr. Methods* **55,** *183–188 (1967).*
The criteria for the selection of materials for mounting absorbers include their mechanical and chemical properties and their attenuation of the γ-rays and X-rays emitted from the Mössbauer source. Attenuation of the 14.4-keV γ-ray and 6.3-keV X-ray associated with ^{57}Fe was measured for nine commercial materials including plastics and metals. The linear absorption coefficients and half-thicknesses for each material were measured. The usefulness and limitations of each material are discussed, along with three different absorber mounting techniques.

Key Words: Absorber mounting devices; absorption coefficients; gamma-rays and x-rays; half-thickness; Mössbauer spectroscopy; 14.4-keV.

Menos, O., **Analytical coordination chemistry: titrimetry, gravimetry, flame photometry, spectrophotometry, and gas evolution, July 1966 to June 1967,** *Tech. Note 424 (Jan. 1968), 55 cents.*
In the related areas of gravimetry, titrimetry, flame emission and atomic absorption spectroscopy, absorption and fluorescence spectrophotometry, and gases in metals, the versatile aspects of coordination chemistry have, in several instances, been uniquely exploited to yield either more precise and accurate results or lower detection limits. Fivefold improvement in the gravimetric analysis for beryllium has been obtained by means of an incomplete homogeneous precipitation followed by a selective spectrophotometric examination of the filtrate. In the field of thermal analysis a survey of fifteen compounds has revealed several promising, future standards for DTA studies covering the range of 75 to 900 °C. In the section on titrimetry highly precise procedures are described for the determination of boron and beryllium. Various instrumental parameters have been investigated in flame emission and atomic absorption spectroscopy in order to optimize such variables as nebulizer-burner and oxidant-fuel systems, elemination of interferences, and source difficulties. The use of chelate extraction systems has led to the extension of detection limits to the submicrogram level for impurities in zinc and selenium, while modified electronics has permitted the precise determination of 10 percent Li_2O in glass with a relative standard deviation of better than 0.2 percent. In absorption and fluorescence spectrophotometry the research aspect of ternary complexes or mixed chelates are described together with their potential use at the nanogram-picogram level. In the same area improvement in accuracy has been obtained by controlled dissolution of samples in closed systems with particular attention being given to the determination of arsenic in cast iron. Also described in this section is the differential spectrophotometric determination of dysprosium in a glass to be used as a neutron flux monitor, in which case the relative error was reduced to less than 0.25 percent. Finally, in the area of high vacuum fusion a new standard was certified for oxygen in titanium and in two titanium alloys. In addition, research in the use of the same technique for the determination of nitrogen has apparently eliminated the problem of low values that have in the past so frequently plagued the analyst.

Key Words: Absorption and fluorescence spectrophotometry; arsenic; atomic absorption; beryllium; DTA studies; dysprosium in a glass; flame emission; gases in metals; gravimetry; homogeneous precipitation; impurities in zinc and selenium; Li_2O in glass; nitrogen; oxygen in titanium; titrimetry.

Myers, V. W., **Inelastic scattering of cold neutrons in polycrystalline gray tin,** *J. Phys. Chem. Solids* **28,** *2207–2210 (1967).*
The inelastic scattering of cold neutrons by polycrystalline gray tin (diamond structure) at 0 °C has been investigated using the Brookhaven cold neutron facility. It is possible to obtain information on the phonon critical points. There is a narrow peak centered at about 7 meV phonon energy which is attributed to the transverse acoustic modes. A broad band centered around 23 meV is probably due to a combination of the longitudinal optic and acoustic modes. The results are consistent with single crystal dispersion measurements in Si and Ge when the frequencies are scaled inversely as the square root of the mass. This indicates that the force constants in Si, Ge, and Sn are of the same strength.

Key Words: Cold neutron scattering; force constants; gray tin; phonon energies.

Nimeroff, I., **Colorimetry,** *Mono. 104 (Jan. 1968), 35 cents. (Supersedes Circular 478.)*
The definition of color, as a characteristic of light, and the basic principles of its measurement are given. The reduction of spectrophotometric data to three chromaticity coordinates by means of the three-function CIE standard observer system for colorimetry is described. Various methods of direct colorimetry, and visual and photoelectric methods of colorimetry by differences from material standards are treated. The most useful collections of material color standards are described and the most widely used one-dimensional color scales are explained. The limitations of several colorimetric methods: spectrophotometric, photoelectric, and visual, are discussed.

Key Words: Color dictionaries; color vision; colorimeters; photoelectric tristimulus; spectrophotometric colorimetry; visual colorimetry.

Ohashi, M., Stanford, J. W., and Paffenbarger, G. C., **Pertinent data on some physical properties of different investments used in the casting of gold alloys,** *J. Nihon Univ. Sch. Dent.* **9,** *No. 3, 121–126 (Sept. 1967).*
Fineness, time of setting, compressive strength, linear thermal expansion, hydroscopic expansion, normal setting expansion, and surface defects of alloy castings were determined using casting investments of three types thermal inlay, hygroscopic inlay, and thermal partial denture. The use of the normal setting expansion combined with either the hygroscopic or thermal expansion to compensate for the shrinkage of casting gold alloys is discussed.

Key Words: Alloy castings; gold alloys; hygroscopic inlay; thermal inlay; thermal partial denture.

Popenoe, C. H., and Thompson, R. C., **Accessory equipment and teletypewriter modifications for remote computer consoles,** *Tech. Note 419 (Feb. 1968), 20 cents.*
Equipment auxiliary to, and simple modifications of a teletypewriter are described which enable it to be used more efficiently as a remote console of a computer. The descriptions and drawings are sufficiently detailed to enable one to duplicate the modifications or construct the auxiliary equipment with little or no design effort. Among the items treated are: pushbutton word generators, providing automatic typing of often used programming instructions; and option switches for full or half-duplex operation, for inserting the sixth bit for lower case letters, and the eighth bit for parity compatibility.

Key Words: Remote access; teletype; time-sharing.

Post, M. A., **Qualitative and quantitative determination of emulsion-polymerised binders in latex paints,** *J. Appl. Chem.* **17,** *315–320 (Nov. 1967).*
Methods for the separation and identification by infrared absorption spectroscopy of styrene-butadiene, acrylic, vinyl-acrylic and polyvinyl acetate homopolymer and dibutyl maleate copolymer in emulsion paints based on these materials are presented. Detailed procedures for their quantitative determination are discussed.

Key Words: Acrylic; identification; infrared spectroscopy; latex paints; polyvinyl acetate; separation; styrene-butadiene; vinyl-acrylic.

Preston, G. T., Chapman, T. W., and Prausnitz, J. M., **Transport properties of cryogenic liquids and their mixtures,** *Cryogenics* **7,** *No. 5, 274–279 (Oct. 1967).*
Based on the corresponding-states principle, a correlation is presented for the viscosities, thermal conductivities and self-diffusivities of nine cyrogenic liquids from the triple-point temperatures to temperatures close to the critical. Experimental data are reduced with two molecular parameters for each liquid: a characteristic energy and a characteristic size. The correlations are useful for predicting transport properties of pure liquids at temperatures where experimental data are not available; in addition, using reasonable mixing rules, the correlations may be used to estimate transport properties of liquid mixtures.

Key Words: Corresponding-states principle correlation, cryogenic liquids and liquid mixtures, mutual-diffusivity, self-diffusivity, thermal conductivity, viscosity.

Pytte, E., and Bennett, H. S., **Ultrasonic attenuation in the Heisenberg paramagnet. II. Antiferromagnets,** *Phys. Rev.* **164,** *No. 2, 712–715 (Dec. 10, 1967).*
The propagation of sound waves in antiferromagnetic insulators is studied within the framework of two models which describe the interaction between the spin system and the lattice. In particular, expressions for the ultrasonic attenuation coefficient near the Néel point are obtained in terms of time dependent correlation functions. The attenuation coefficient is found to be proportional to the square of the phonon frequency, to increase rapidly in the vicinity of the Néel point, and to be less singular than the attenuation coefficient for ferromagnetic insulators.

Key Words: Antiferromagnetic insulators; correlation function; ferromagnetic insulators; Heisenberg; Néel point; ultrasonic attenuation.

Rasberry, S. D., Margoshes, M., and Scribner, B. F., **Applications of a time-sharing computer in a spectrochemistry laboratory: optical emission and x-ray fluorescence,** *Tech. Note 407 (Feb. 1968), 40 cents.*
A time-sharing computer system employing the Dartmouth College Basic complier has been in use in this laboratory for more than two years, and it has been applied to both routine and non-routine calculations. Descriptions are given of the computer system and its associated programming language and commands. Typical applications and advantages and disadvantages of the system are discussed. An appendix contains descriptions of 13 programs thought to be of interest to other optical and x-ray spectrochemistry laboratories. Examples of input and output are given with each of these programs.

Key Words: Analytical chemistry; calculations; computers; emission spectroscopy; programming; spectrochemical analysis; time-sharing computer; x-ray spectroscopy.

Risley, A. S., **Parallel pump susceptibility of YIG under cw drive conditions,** *Physics Letters* **25A,** *No. 6, 471–472 (Sept. 25, 1967).*
The parallel pump susceptibility, χ'', has been measured versus the level and time duration of applied rf power. Unlike previously reported data taken by the pulse technique, χ'' increases at the higher drive levels.

Key Words: Parallel pump susceptibility; sample heating; saturation.

Rodriguez-Pasques, R. J., Mullen, P. A., George, G. A., and Harding, J. E., **Transmission through aluminum of beta-particles emitted by infinitely-thick sources,** *Intern. J. Appl. Radiation Isotopes* **18,** *No. 12, 835–847 (1967).*
The problem of determining the energy of beta particles emitted from sources containing low concentrations of radioactive substances is examined. Transmission curves of beta particles emitted by "infinitely-thick" disc-shaped sources were obtained with two different detectors and compared to the curves similarly obtained for beta particles coming from very thin "weightless" deposits on similar solid discs. Different matrix materials and beta-particle energies were used. The curves were studied for shape, secondary radiations and half-thickness. A series of curves were also obtained from four different potassium-salt thick sources, in order to investigate possible influences from variations of effective atomic number. No substantial difference was found between the curves corresponding to the three types of sources, in connection with half-thickness-maximum-energy relationship.
Guiding rules are proposed for the determination of maximum beta-ray energies by means of absorption studies and half-thickness determination.

Key Words: Beta absorption; beta-particle energy; beta-particle transmission; half thickness; infinitely-thick; low-level; synthetic beta sources; transmission curves.

Ronn, A. M., and Lide, D. R., Jr., **Infrared-microwave double resonance using a CO_2 Laser,** *J. Chem. Phys.* **47,** *No. 9, 3669–3670 (Nov. 1, 1967).*
A double resonance experiment is described in which a vibrational transition is pumped with a carbon dioxide laser and the effect of the pumping is detected through a rotational transition in the microwave region. Positive results have been found with methyl bromide. The interpretation of the results are discussed.

Key Words: Double resonance; infrared; laser; methyl bromide; microwave; pumping; saturation.

Ruegg, F. C., **Multiplex for dual-spectrum Mössbauer spectrometry** (*Proc. Second Symp. on Low Energy X- and Gamma Sources and Applications, University of Texas, Austin, Texas, Mar. 27–29, 1967*), *ORNL–IIC–10, pp. 157–175 (1967).*
It is often desirable to have the capability of accumulating two Mössbauer spectra simultaneously with both spectra having exactly the same Doppler velocity dependence. This is possible with a multiplexing system which allows accumulation of two spectra simultaneously and storing of each spectrum in a 200 channel subgroup of a multichannel analyzer. The memory of the analyzer which is operated in the time mode is used on a demand basis by the two detector systems, and the counts are routed to the proper subgroup in complementary channel locations, i.e., the channel location in the second subgroup is the channel number in the first subgroup plus 200. The logic, circuitry and performance are described.

Key Words: Dual spectra; Mössbauer; spectroscopy.

Rush, J. J., **Neutron-scattering study of hindered rotations in methylbenzenes,** *J. Chem. Phys.* **47,** *No. 10, 3936–3941 (Nov. 15, 1967).*
The low-frequency modes of a number of methylbenzenes in their solid and liquid phases have been investigated by the energy-gain scattering of cold neutrons. The compounds studied include benzene, o-xylene (1,2), hemimellitene (1,2,3), mesitylene (1,3,5), durene (1,2,4,5), prehnitene (1,2,3,4), and hexamethylbenzene. The neutron spectra for molecules with adjacent methyl groups (e.g. o-xylene) exhibit bands peaked near 170 cm^{-1}, which are assigned primarily to the $1 \rightarrow 0$ transitions of the torsional oscillations of the methyl groups. The hemimellitene and prehnitene spectra appear to show a second broad maximum in the region of 100 cm^{-1}, which is attributed to torsional modes due to methyl groups centered between two adjacent groups. Previous results on hexamethylbenzene show torsional bands peaked at 120 and 137 cm^{-1}, respectively, above and below the λ-transition near 115 °K. The mesitylene spectra indicate less hindrance to rotation of the methyl groups in this compound, with torsional frequencies less than 100 cm^{-1}. In addition, the results for all the compounds in their solid phases show broad bands below 90 cm^{-1}, which are assigned to whole-molecule librations and translations.
If simple threefold cosine potentials are assumed for all the methyl groups, "average" barriers to rotation 2 and ~0.7 kcal/mol are calculated from the average torsional peak frequencies of 170 and ~95 cm^{-1}, respectively. A comparison of these results indicates that methyl groups surrounded by two adjacent groups on the benzene ring experience a considerably different potential (and possibly a significantly lower barrier) than that experienced by methyl groups with one neighboring group. The neutron results are compared in detail with nmr and thermodynamic data.

Key Words: Barrier to rotation; cosine potential; frequency spectra; hindered rotation; internal rotation; methylbenzenes; methyl groups; neutron scattering; torsional modes.

Rush, J. J., **Neutron-scattering study of low-frequency modes in urea and ferroelectric thiourea,** *J. Chem. Phys.* **47,** *No. 10, 4278–4279 (Nov. 15, 1967).*
The low frequency modes in crystalline urea and three phases of thiourea have been investigated by the inelastic scattering of cold neutrons. The neutron spectra for thiourea in phases I, III and V exhibit bands peaked around 490, 110 and 46 cm^{-1} which are attributed, respectively, to NH_2 librations and whole-molecule librational and translational modes. The fact that there is little

change in these spectra in passing from phases I to V suggests little correlation between molecular motions and the ferroelectric transitions in this compound. The spectrum for urea at 295 °K shows bands peaked around 550, 168, 138 and 74 cm^{-1}, whose assignments are similar to those for thiourea. A comparison of the results for the two compounds suggests that hydrogen bonds in thiourea, if they exist, are much weaker than in urea and have little effect on the transition mechanisms.
Assuming twofold cosine potentials for the NH_2 groups, rotational barriers of 22 and 17.5 kcal/mol are calculated from the librational peaks in urea and thiourea.

Key Words: Ferroelectric; libration; molecular vibrations; neutron spectra; phase transitions; potential barrier; rotation; thiourea; urea.

Schneider, W. E., Stair, R., and Jackson, J. K., **Spectral irradiances as determined through the use of prism and filter spectroradiometric techniques,** *Appl. Opt.* **6,** *No. 9, 1479–1486 (Sept. 1967).*
Two spectroradiometers, one based on a conventional prism monochromator and the other on a system employing narrow band-pass interference filters, have been set-up and independently used in the determination of the spectral irradiances of a number of sources over the wavelength range 0.25 to 2.5 μm. Basically, the method of calibration for each system consists of comparing the spectral irradiance of the source under investigation to that of an NBS standard of spectral irradiance. The results obtained with each system on a number of "continuous" sources agree to about one percent whereas the differences in the spectral irradiances obtained with the two-set-ups on a number of line sources range up to several percent.

Key Words: Filter-spectroradiometer; measurements techniques; prism-spectroradiometer; radiometry; sources; spectral irradiance.

Scribner, B. F., Ed., **Activities of the NBS Spectrochemical Analysis Section, July 1966 through June 1967,** *Tech. Note 422 (Jan. 1968), 45 cents.*
A summary is given of activities of the NBS Spectrochemical Analysis Section for the year July 1966 through June 1967. In optical spectrometry, studies were made of (1) the effectiveness of a liquid Q-switch for laser pulse control and (2) the applicability of the high-frequency plasma torch in atomic emission and absorption spectroscopy. Two papers on laser probe spectrochemical analysis were published. In the electron probe microanalysis an alignment procedure was developed for the x-ray spectrometer, data on x-ray mass absorption coefficients were collected and critically evaluated, and a review of techniques for scanning microprobe analysis was published. The factors entering into quantitative electron probe analysis are being investigated. In x-ray spectrometry studies were made of interferences especially in the analysis of complex alloys. A combination of techniques involving enrichment by electro-deposition, stable isotope dilution, and determination by the spark source mass spectrometer has provided an accurate method for trace analysis. Improvements in the Section's equipment, including digital readout devices, and developments in computer applications are also discussed. Listings are given of 15 publications and 23 talks by members of the Section during the year.

Key Words: Computing; digital readout; electron probe; gold analysis; isotope dilution method; laser probe; liquid Q-switch; mass attenuation coefficients; microphotometer; optical spectrometry; plasma torch; platinum analysis; preconcentration; selenium analysis; spark source mass spectrometry; spectrochemical analysis; standard reference materials; sulfur analysis; time-shared computer; x-ray absorption coefficients; x-ray fluorescence analysis; vacuum spectrometer.

Shirley, J. H., **Effect of a sinusoidal excitation amplitude on the performance of an atomic-beam spectrometer,** *Phys. Rev.* **160,** *No. 1, 95–99 (Aug. 5, 1967).*
A theoretical analysis has been made of the transition probabilities for a Rabi-type atomic beam spectrometer in which the exciting field amplitude seen by the atoms has a sinusoidal rather than a rectangular envelope. The time-dependent Schrödinger equation was integrated numerically and a velocity average of the transition probabilities performed. The results indicate that the line width increases as the fourth root of the excitation power and that frequency shifts due to coupling of the exciting field with other atomic states can be reduced by an order of magnitude.

Key Words: Atomic beam; frequency shift; Rabi spectrometer; Schrödinger equation; transition probability; velocity average.

Shoub, H., and Ingberg, S. H., **Fire resistance of steel deck floor assemblies,** *Bldg. Sci. Series 11 (Dec. 1967), 25 cents.*
Tests were conducted to determine the resistance to fire of welded steel plate and beam floor assemblies with various conditions of floor covering on the plates, and ceiling protections beneath the beams. The trials included fire exposures from the burnout of combustible materials ranging from 10 to 40 lb/ft^2 on the floor surface as well as standard fire endurance tests in which the ceiling of the structure was exposed to fire.
The results of the tests indicated that the use of steel floor structures was practical from considerations of fire safety. For the test conditions established, fire exposure on top of the floor did not heat the structural steel supporting members sufficiently to cause load failure or collapse, and did not produce untenable conditions in the room below. In tests involving fire exposure to the underside of floors, the fire endurance times, based solely on heat transmission criteria, ranged from 1 hr 24 min to over 4 hr. Temperature levels attained by the structural members and deflection of the floor assemblies are also reported.

Key Words: Burnout tests; fire endurance; floor tests; steel plate floors.

Simpson, J. A., **Electron guns,** *Book, Methods of Experimental Physics, Chapter, Sources of Atomic Particles 4, 84–95 (Academic Press Inc., New York, N.Y., 1967).*
The physical limitations on electron beams are discussed. Design procedures for electron guns of optimum performance are given and illustrated by examples from the literature.

Key Words: Atomic source; electron gun; electron physics.

Smith, J. C., and Fenstermaker, C. A., **Strain-wave propagation in strips of natural rubber subjected to high-velocity transverse impact,** *J. Appl. Phys.* **38,** *No. 11, 4218–4224 (Oct. 1967).*
If a flexible filament, marked at intervals along its length is struck transversely by a flying projectile, high speed photography reveals a shifting of the marks caused by passage of a strain wave, and analysis of these shifts provides data on the strain and average strain velocity in the wave. Tests were performed on strips of lightly vulcanized natural rubber at transverse impact velocities up to 65 m/s, and the resulting strain-velocity distributions analyzed for viscoelastic effects. The analysis showed that although creep effects were small in the observation time interval of 1 msec to 8 msec after impact, significant creep must have occurred at the point of impact within the first millisecond, and additional significant creep occurs at times greater than 8 msec. The strain wave front velocity calculated from the quasi-static stress-strain curve was 35.2 m/s, but a value of approximately 60 m/s was observed in the tests. The strain at the wave front, however, tended to attenuate as the wave propagated causing a progressive decrease in the observed value of the strain wave front velocity.

Key Words: High-speed photography; impact testing; natural rubber; strain waves; viscoelasticity.

Sparks, L. L., and Powell, R. L., **Metals characterized by low-temperature thermoelectric methods,** *Meas. Data* **1,** *No. 5, 89–96 (Sept.–Oct. 1967).*
The thermoelectric properties of wire specimens provide a means of determining the effective electronic purity or homogeneity of metals and alloys. This characterization method is described in detail and examples are given of tests on commercial copper and high-purity platinum. The method involves use of a cryogenic liquid, usually liquid nitrogen or helium.

Key Words: Cryogenic tests; impurity characterization; metals; thermoelectric.

Spijkerman, J. J., **Application of Mössbauer spectroscopy to structure analysis** (*Proc. Second Symp. on Low Energy X- and Gamma Sources and Applications, University of Texas, Austin, Texas, Mar. 27–29, 1967*), *ORNL–IIC–10, pp. 85–100 (1967).*
A unique characteristic of the Mössbauer effect and its wide applicability to many scientific disciplines such as physics, chemistry, molecular biology and metallurgy. As a result of this versatility, Mössbauer spectroscopy becomes a very useful tool for structural analysis.
Furthermore it complements many of the physiochemical methods available by obtaining microscopic information, where macroscopic measurement have been made before.
The Mössbauer spectrum parameters of chemical shift, quadrupole splitting, magnetic hyperfine splitting and their temperature dependence uniquely characterize the material. The interpretation of these parameters in terms of structural analyses and their relation to other spectroscopic techniques will be discussed. A specific example is the determination of austenite and martensite in steel with particular emphasis on the dynamic equilibrium exhibited by these carbon impurity states.

Key Words: Applications; austenite; martensite; Mössbauer spectroscopy; structure analysis.

Stern, K. H., **Glass-membrane potentials in mixed anion melts,** *J. Electrochem. Soc.* **114,** *No. 12, 1257–1258 (Dec. 1967).*
The emf of the four-ion concentration cell with membrane

$$Ag|Ag^+, Na^+, Cl^-, Br^-|glass|Ag^+, Na^+, Cl^-, Br^-|Ag$$

is derived for the case $X_{Na^+} \ll X_{Ag^+}$ by assuming that the cationic chemical potentials are additive functions in the mole fractions of the thermodynamic components, e.g., $\mu_{Ag^+} = X_{AgCl}\mu_{AgCl} + X_{AgBr}\mu_{AgBr}$. For solutions very dilute in sodium, corrections for non-ideality are negligible. Experimental results agree satisfactorily with calculated ones.

Key Words: Galvanic cells; membrane potentials; molten salts.

Van Blerkom, D., and Hummer, D. G., **The ionization structure of planetary nebulae-VI. The Lyman continuum problem,** *Monthly Notices Roy. Astron. Soc.* **137,** *353–374 (1967).*
Because of the recent evidence that a planetary nebula does not completely agsorb Lyman continuum radiation for a substantial part of its life, we have used a generalized discrete-ordinate method to obtain accurate numerical solutions to the ionization balance problem in pure hydrogen, plane-parallel model nebulae of various optical thicknesses. The effects of incomplete absorption, interior boundary conditions and non-Planckian stellar fluxes are examined. We find that the density of neutral hydrogen in the nebula increases by less than a factor of two as the optical thickness varies from 0.5 to ∞, and is insensitive to large deviations in the stellar flux from the Planckian distribution, if the total number of Lyman photons is constant. The radius of the Strömgren sphere differs by about 5 percent for the two boundary conditions considered.
The accuracy of two simple approximations are assessed, and conditions for their validity are obtained.

Key Words: Ionization structure; Lyman continuum problem; Planetary nebulae; radiation.

Van Zyl, B., and Dunn, G. H., **Dissociation of N_2^+ and O_2^+ by electron impact,** *Phys. Rev.* **163,** *No. 1, 43–45 (Nov. 5, 1967).*
Cross sections for dissociation of N_2^+ and O_2^+ by electron impact were measured for interaction energies between 10 eV and 500 eV and between 15 eV and 500 eV respectively. The cross section versus interaction-energy curves exhibit maxima in the vicinity of 75 eV and decrease monotonically at higher energies with an $\frac{A}{E}\log BE$ dependence. Maximum cross section values are 4.3 πa_0^2 for N_2^+ and 4.1 πa_0^2 for O_2^+. The curves are remarkably similar at the higher interaction energies. The ion targets are typical of those formed by bombardment of gas by electrons of 150 eV and greater, and some may be in excited electronic states.

Key Words: Dissociation N_2^+; electron impact; interaction energies O_2^+.

Williams, G., Lauritzen, J. I., Jr., and Hoffman, J. D., **Effect of chain twisting on the effective barrier to reorientation for a hindered rotator,** *J. Appl. Phys.* **38,** *No. 11, 4203–4208 (Oct. 1967).*
The effective barrier to reorientation is calculated for a chain which may occupy two equivalent energy states, 180° apart for the case where the chain is allowed to twist during the reorientation process. Results are obtained for (I) a "Parabola-antiparabola" and (II) a cosine form for the intermolecular energy. The results for (I) and (II) are similar, but differ both in form and magnitude from that obtained earlier using a cusplike barrier. Both (I) and (II) lead to the conclusion that a chain will behave as a rigid rod up to a critical chain length, and then exhibit twisting for all lengths exceeding this critical value.

Key Words: Activation energy; chain twisting; hindered rotator; parabolic potential model; sinusoidal potential model; two-site model.

Yates, J. T., Jr., Madey, T. E., and Payn, J. K., **Desorption by electron impact: carbon monoxide, nitric oxide and oxygen on tungsten,** *Nuovo Cimento Suppl. Series I, 5, No. 2, 558–581 (1967).*
The interaction of low energy electrons with chemisorbed species has been employed as a tool for the characterization of various binding states for CO, NO, and Oxygen on a polycrystalline tungsten ribbon. The apparatus employed is similar to that of Redhead. Cross sections as a function of coverage for positive ion desorption, and average cross sections for neutral desorption have been measured. Threshold energies for ion production and ion energy distributions are compared for these three oxygen-bearing adsorbates. The electronic desorption phenomenon is shown to be useful for observing details of thermal interconversion and desorption from various binding states in the chemisorbed layer.

Key Words: Binding states; carbon monoxide; chemisorption; cross section; electronic desorption; electron impact; ion energy distribution; nitric oxide; oxygen; threshold voltage; tungsten.

Other NBS Publications

J. Res. NBS 72C (Eng. and Instr.), No. 2 (Apr.–June 1968), 75 cents.
Stonebraker, D. M., Analysis and design of an oscilloscope deflection system with a calculable transfer function.
Jarvis, S., Jr., and Adams, J. R., Calculation of substitution error in barretters.
Mitchell, R. A., Analysis of n-degree elliptical elastic rings of nonuniform cross section.
Homan, D. N., Applications of coaxial chokes to a-c bridge circuits.
Jenkins, W. D., and Willard, W. A., Creep rupture properties of Ti-8Al-1Mo-IV alloy. (See abstract.)

Chamberlain, G. E., Simpson, J. A., Mielczarek, S. R., and Kuyatt, C. E., Effect of double scattering on cross-section measurements at large momentum trnasfer, J. Chem. Phys. **47,** No. 10, 4266–4267 (Nov. 15, 1967).
Fatiadi, A. J., Acetic anhydride phosphoric acid as an acetylating agent, Carbohydrate Res. **6,** 237–240 (1968).
Haber, S., A theorem on arbitrary functions, Am. Math. Monthly **74,** Np. 8, 973–975 (Oct. 1967).
Haber, S., Midpoint quadrature formulas, Math. Compt. **21,** No. 100, 719–721 (Oct. 1967).
Hanley, H. J. M., Thermodynamics of transport phenomena in membrane systems, J. Chem. Educ. **44,** No. 12, 717–719 (Dec. 1967).
Johannesen, R. B., NMR studies of inorganic fluorides. IV. Relative signs of coupling constants in CH_3SiF_3, $HSiF_3$, and HPF_2, J. Chem. Phys. **47,** No. 8, 3088–3089 (Oct. 15, 1967).
Kolbenstvedt, H., Simple theory for K-ionization by relativistic electrons, J. Appl. Phys. **38,** No. 12, 4785–4787 (Nov. 1967).
Little, W. E., Ellerbruch, D. A., and Engen, G. F., An analysis of the "quarter-wave" technique of reducing the errors in UHF and microwave impedance measurement, IEEE Trans. Microwave Theory Tech. **MTT–15,** No. 9, 504–507 (Sept. 1967).

Mann, R. H., and Maryott, A. A., Dipole moment of $Co(CO)_3NO$ from the nonresonant microwave absorption of the vapor, J. Chem. Phys. **47,** No. 10, 4275–4276 (Nov. 15, 1967).

Moore, C. E., Annual report on spectroscopy, Astron. J. **72,** No. 9, 1117–1118 (1967).

Pierce, E. T., Price, O. W., Edelman, S. E., and Jones, E., Accelerometer resonances affect vibration measurement, J. Environ. Sci. **10,** No. 6, 17–21 (Dec. 1967).

Prince, E., and Rush, J. J., Many disciplines unit to study solid structure and dynamics, Phys. Today **21,** No. 2, 95–99 (Feb. 1968).

Tauber, S. J., Bolotsky, G. R., Fraction, G. F., Kirby, C. L., and Reed, G. R., Algorithms for utilizing Hayward chemical structure notations, Proc. ICIREPAT Fifth Annual Meeting, London, England, Aug. 31–Sept. 10, 1965, Chapt. 27, pp. 351–377 (Thompson Book Co., Washington, D.C., 1967).

Wegstein, J. H., A computer oriented single-fingerprint identification system, Tech. Note 443 (Mar. 1968), 25 cents.

Wilcox, R. M., Some thoughts on Fitzgerald's particle waves, J. Acoust. Soc. Am. **42,** No. 3, 678–679 (Sept. 1967).

**Publications for which a price is indicated are available by purchase from the Superintendent of Documents, U.S. Government Printing Office, Washington, D.C. 20402 (foreign postage, one-fourth additional). The NBS nonperiodical series are also available from the Clearinghouse for Federal Scientific and Technical Information, Springfield, Va. 22151. Reprints from outside journals and the NBS Journal of Research may often be obtained directly from the authors.*

U.S. GOVERNMENT PRINTING OFFICE : 1968 OL—299-547

JRA OCT 46129
UNIVERSITY MICROFILMS INC
ATTN SERIALS SECTION
300 NORTH ZEEB RD
ANN ARBOR MICH 48106

UNI
GOVERNMEN
DIVISION O
WASHING

OFFICIAL BUSINESS

POSTAGE AND FEES PAID
U.S. GOVERNMENT PRINTING OFFICE

JOURNAL OF RESEARCH of the National Bureau of Standards Vol. 72A, No. 4 July–August 1968
A. Physics and Chemistry

Contents

Page

Mass spectrometric study of photoionization. X. Hydrogen chloride and methyl halides. Morris Krauss, James A. Walker, and Vernon H. Dibeler. 281

The fourth and fifth spectra of vanadium (V IV and V V). Laura Iglesias. 295

Variation of absorptance-curve shape with changes in pigment concentration. Gerald L. Howett. 309

Periodic acid, a novel oxidant of polycyclic aromatic hydrocarbons. Alexander J. Fatiadi. 341

A galvanic cell with a low emf-temperature coefficient. Gerald N. Roberts and Walter J. Hamer. 351

Synthesis of cerite. Jun Ito. 355

Tables of collision integrals for the (m, 6) potential function for 10 values of m. Max Klein and Francis Smith. 359

Spectrum of relaxation times in GeO_2 glass. A. Napolitano and P. B. Macedo. 425

Resumé of values of the Faraday. Walter J. Hamer. 435

Publications of the National Bureau of Standards. 441

Library of Congress Catalog Card Number: 62–37059

For sale by the Superintendent of Documents, U.S. Government Printing Office, Washington, D.C. 20402. Price $1 (single copy). Subscription price: $5 a year; $1.00 additional for foreign mailing.
UNITED STATES GOVERNMENT PRINTING OFFICE, WASHINGTON : 1968